TECHNICAL REPORT
NATICK/TR-12/023

AD _____

LIGHTWEIGHT AND COMPOSTABLE FIBERBOARD FOR THE MILITARY

by
Jo Ann Ratto
Richard Farrell*
Nandika D'Souza**
Koffi Dagnon**
Susan Sun***
Jason Niedzwiecki
and
Jeanne Lucciarini

***University of Saskatchewan**
Saskatoon, SK S7N 5A2, Canada

****University of North Texas**
Denton, TX 76203

*****Kansas State University**
Manhattan, KS 66502

August 2012

Final Report
October 2007 – December 2010

Approved for public release; distribution is unlimited

U.S. Army Natick Soldier Research, Development and Engineering Center
Natick, Massachusetts 01760-5018

UNCLASSIFIED

DISCLAIMERS

The findings contained in this report are not to be construed as an official Department of the Army position unless so designated by other authorized documents.

Citation of trade names in this report does not constitute an official endorsement or approval of the use of such items.

DESTRUCTION NOTICE

For Classified Documents:

Follow the procedures in DoD 5200.22-M, Industrial Security Manual, Section II-19 or DoD 5200.1-R, Information Security Program Regulation, Chapter IX.

For Unclassified/Limited Distribution Documents:

Destroy by any method that prevents disclosure of contents or reconstruction of the document.

REPORT DOCUMENTATION PAGE

Form Approved
OMB No. 0704-0188

PLEASE DO NOT RETURN YOUR FORM TO THE ABOVE ADDRESS.

1. REPORT DATE *(DD-MM-YYYY)*	2. REPORT TYPE	3. DATES COVERED *(From - To)*
8-8-2012	Final	October 2007- December 2010

4. TITLE AND SUBTITLE

LIGHTWEIGHT AND COMPOSTABLE FIBERBOARD FOR THE MILITARY

5a. CONTRACT NUMBER

5b. GRANT NUMBER

5c. PROGRAM ELEMENT NUMBER

6. AUTHOR(S):

Jo Ann Ratto, Richard Farrell*, Nandika D'Souza**, Koffi Dagnon**, Susan Sun***, Jason Niedzwiecki, and Jeanne Lucciarini

5d. PROJECT NUMBER
SI-1479

5e. TASK NUMBER

5f. WORK UNIT NUMBER

7. PERFORMING ORGANIZATION NAME(S) AND ADDRESS(ES)
Natick Soldier Research, Development and Engineering Center
ATTN: RDNS- CFA
Kansas Street, Natick, MA 01760-5018

8. PERFORMING ORGANIZATION REPORT NUMBER
NATICK/TR-12/023

9. SPONSORING / MONITORING AGENCY NAME(S) AND ADDRESS(ES)
US Department of Defense
Strategic Environmental Research and Development Program
901 North Stuart Street, Suite 303
Arlington, VA 22203

10. SPONSOR/MONITOR'S ACRONYM(S)
SERDP

11. SPONSOR/MONITOR'S REPORT NUMBER(S)
WP-1479

12. DISTRIBUTION / AVAILABILITY STATEMENT
Approved for public release; distribution is unlimited.

13. SUPPLEMENTARY NOTES
*University of Saskatchewan, ** University of North Texas, *** Kansas State University

14. ABSTRACT

Novel lightweight fiberboard structures have been researched and developed to replace the existing military fiberboard containers with the ultimate goal to reduce the amount of solid waste for the military. The research effort utilized a three prong approach to create more sustainable ration packages that offer performance, recyclability, biodegradability and compostability. The first approach explored a biobased fiberboard comprised of a soy protein adhesive with either wood or pulped fibers to produce mechanically competitive fiberboard with water resistance properties. The obstacle for this approach was that prototypes or scale up could not be performed by preparing individual sheets with compression molding methods. The second approach examined different biodegradable coatings for paper formation which enhanced wet strength properties of paper based products. The third approach identified effective coated corrugated alternatives that exhibited comparable performance under adverse environmental conditions to the existing containers. Compression studies were performed on prototypes after exposing the fiberboard containers to different environmental conditions. Analysis of variance of compression data as a function of moisture, insert design and paper weight determined optimal design structures that will be used in transitioning this research. The optimal corrugated container consists of a wax alternative medium (WAM), a corrugated insert in the container and a paper weight of 69 lb. In addition, laboratory and full scale compost tests assessed the bio-environmental degradability (compostability) of various fiberboard containers under controlled aerobic composting conditions. This fiberboard waste was also used with military food waste and grass clippings to produce a valuable form of compost. Overall, this research developed novel lightweight secondary packaging that has reduced fiber, has improved functionality, is compostable, and is repulpable.

15. SUBJECT TERMS

PAPER	DISPOSAL	REDUCTION	SOLID WASTES	COMPRESSION MOLDING
WASTE	COMPOSTING	FIBERBOARD	BIOBASED PRODUCTS	WASTE MANAGEMENT
SOLIDS	COATINGS	SOY PROTEIN	WASTE RECYCLING	RECYCLED MATERIALS
SHIPPING	ADHESIVES	SUSTAINABLE	WATER RESISTANT	CORRUGATED BOARD
POST-USE	FIBER WASTE	LIGHTWEIGHT	BIODEGRADABILITY	ENVIRONMENTAL CONDITIONS

16. SECURITY CLASSIFICATION OF:			17. LIMITATION OF ABSTRACT	18. NUMBER OF PAGES	19a. NAME OF RESPONSIBLE PERSON
a. REPORT	b. ABSTRACT	c. THIS PAGE			Jo Ann Ratto
U	U	U	SAR	156	19b. TELEPHONE NUMBER *(include area code)* 508-233-5315

Standard Form 298 (Rev. 8-98)
Prescribed by ANSI Std. Z39.18

This page intentionally left blank

Table of Contents

List of Figures

List of Tables

Acknowledgements

The Principal Investigator (Dr. Jo Ann Ratto) and Co-Investigator (Ms. Jeanne Lucciarini) gratefully acknowledge the Strategic Environmental Research and Development Program (SERDP), especially Dr. John Hall, Dr. Jeff Marquese, Ms. Carrie Wood, Mr. John Thigpen and Ms. Kristen Lau, for their technical and financial support for this project. This has been an innovative program for the Natick Soldier Research, Development and Engineering Center (NSRDEC) and all the collaborators. NSRDEC thanks the collaborators as well as the Advanced Materials Engineering Team (AMET) members, Christopher Hope, Danielle Froio, Jason Niedzwiecki, Sarah Schirmer, and Christopher Thellen who have all assisted with this fiberboard project. NSRDEC appreciates all the technical progress that the team has made during this program. NSRDEC is grateful to: Dr. Susan Sun, and Dr. Wang of Kansas State University who worked on the soy protein fiberboard structures. NSRDEC thanks Dr. Nandika D'Souza and Dr. Koffi Dagnon of University of North Texas for the coated paper research. The corrugated structures and containers were produced by Interstate Containers and NSRDEC is most thankful to Mr. Larry Nykwest, Mr. Terry Moore and Mr. Keith Gray of Interstate Containers. NSRDEC is also grateful to Dr. Richard Farrell of the University of Saskatchewan for the composting efforts. Most importantly, Dr. Jo Ann Ratto is indebted to Mr. Jason Niedzwiecki of NSRDEC who has been dedicated to this entire project. He has been the fiberboard expert on this project and responsible for the execution of the environmental testing and characterization of the fiberboard prototype containers. Also, NSRDEC is grateful to Toledo Forest Laboratory which was an outside laboratory that confirmed compression results and also did the cold weather study. NSRDEC acknowledges Dr. Robert Whitehouse of Metabolix Inc for the paper coating trials and Massoud Mollaghaffari and Portco Packaging for the paper bag trials. Dr. Susan Sun, Dr. Nandika D'Souza, Dr. Koffi Dagnon, Dr. Richard Farrell and Mr. Jason Niedzwiecki also are acknowledged for being co-authors of this report. Also, Sarah Schirmer is gratefully acknowledged for reviewing every word of this manuscript!

Executive Summary

Novel lightweight fiberboard structures have been researched and developed to replace the existing military fiberboard containers with the ultimate goal to reduce the amount of solid waste for the military. A research effort was conducted by the Natick Soldier Research, Development and Engineering Center (NSRDEC) and sponsored by the US Department of Defense through the Strategic Environmental Research and Development Program (SERDP) during the period of October, 2007 to December, 2010 that utilized a three-prong approach to create more sustainable ration packages that offer performance, recyclability, biodegradability' and compostability. The first approach explored a bio-based fiberboard comprised of a soy protein adhesive with either wood or pulped fibers to produce mechanically competitive fiberboard with water resistance properties. The obstacle for this approach was that prototypes or scale up could not be performed by preparing individual sheets with compression molding methods. The second approach examined different biodegradable coatings for paper formation, which enhanced wet strength properties of paper based products. The third approach identified effective coated corrugated alternatives that exhibited comparable performance under adverse environmental conditions to the existing containers. Compression studies were performed on prototypes after exposing the fiberboard containers to different environmental conditions. Analysis of variance of compression data as a function of moisture, insert design, and paper weight determined optimal design structures that will be used in transitioning this research. The optimal corrugated container consists of a wax alternative medium (WAM™), a corrugated insert in the container and a paper weight of 69 lb. In addition, laboratory and full scale compost tests assessed the bio-environmental degradability (compostability) of various fiberboard containers under controlled aerobic composting conditions. This fiberboard waste was also used with military food waste and grass clippings to produce a valuable form of compost. Overall, this research developed novel lightweight secondary packaging that has reduced fiber and has improved functionality and is compostable and repulpable.

This page intentionally left blank

LIGHTWEIGHT AND COMPOSTABLE FIBERBOARD FOR THE MILITARY

1.0 Introduction

The study described in this report was sponsored by the US Department of Defense through the Strategic Environmental Research and Development Program (SERDP) from October, 2007 to December, 2010. The Natick Soldier Research, Development and Engineering Center (NSRDEC) was the lead organization for this effort. Other partners included Kansas State University for soy protein fiberboard research, University of North Texas for paper coating development and University of Saskatchewan for the evaluation of fiberboard in compost. SERDP produced and optimized formulations for new biodegradable, lightweight and compostable containers, used to package the Meal, Ready-To-Eat (MRE™) and Unitized Group Ration (UGR™). The objectives were to; 1) investigate fiberboard formulations consisting of soy protein adhesives and raw materials, 2) study polymeric coatings on paper that could be utilized in fiberboard structures, 3) formulate coated corrugated containers and produce prototypes and 4) evaluate the biodegradation properties in compost and convert fiberboard along with military waste to compost. These environmentally friendly materials were expected to meet the operational and performance requirements of combat ration packaging.

2.0 Background

The Army, Air Force, and Marine Corps consume approximately 46.6 million operational rations each year generating 14,117 tons of packaging waste [1]. Due to the operational requirements for combat rations (i.e. air-droppable, minimum 3-year shelf life at 80°F, six months at 100°F); the rations must be packaged appropriately to meet these requirements. Shipping containers fabricated from fiberboard and coated paper are necessary to safely transport and store food and other military items for all Warfighters including sailors on Navy vessels. Paper and fiberboard production is a costly process which uses cellulose and hazardous chemicals, depletes natural resources in our environment, and creates hazardous waste. The existing fiberboard is not repulpable due to the wet strength additives.

The MRE™ and UGR™ containers are self contained combat ration systems that are used to sustain military personnel during worldwide operations and military training when normal food service facilities are not available. They must overcome many hazards in the distribution environment and at the same time protect their contents to the conclusion of their extended shelf life. Each container must meet operational requirements for combat ration packaging that overcome varying levels of shock, vibration, compression, puncture and diverse environmental conditions that ultimately degrade and damage the food rations and their packaging components. Current research and development efforts through SERDP have focused on lightweight and compostable materials that are capable of meeting current operational demands.

The current MRE™ container consists of a solid fiberboard with a C flute corrugated insert with 3 ply constructions. The paper weight is 90 lb and uses a waterproof chemical. The liner that is currently used is a C flute with 56 lb single liner, 36 lb medium, and 56 lb double liner.

Three approaches are described below to develop new packaging materials to replace the existing fiberboard: 1) produce a new fiberboard from biodegradable soy protein adhesives and raw materials; 2) coat paper with an environmentally friendly plastic which allows the use of thinner fiberboard packaging and improved water and puncture resistant paper; and 3) utilize coated corrugated structures to produce prototypes for evaluation. The structures or prototypes from these approaches were evaluated for biodegradation, as well as preparation of compost from these new fiberboard materials when combined with food waste, grass, and leaves.

In recent years, a great deal of research has shown that the first approach of modified soy protein-based adhesives have high adhesive strength and water resistance [2,6,7,5], to potentially produce fiberboard [3,15,16].

Fiberboard is a panel product made from cellulosic fibers combined with a suitable adhesive binder. A newly developed, biodegradable soy-based adhesive is being used as a binder for this replacement fiberboard. The soy-based adhesive enhances degradability of the fiber by providing a nitrogen source for bacteria and other microorganisms involved in the composting process. Another advantage to substituting existing synthetic adhesives with the soy-based adhesives is to reduce petroleum dependence which is a major goal of the US energy strategy. The soybean is an agricultural product available as an abundant resource with significant potential applications as biofuels.

The soy-based adhesive would also be competitive in cost. Material cost based on food-grade soy protein isolate is around $0.20/lb. Cost of commercial phenol formaldehyde (PF) resin is approximately $0.14 ~ $0.17/lb. Price of hot-melt adhesive for fiberboard is around $6/lb.

The soy-based adhesive has the functional component, soy protein, which is made of 20 amino acids with various side groups. The soy protein is hydrophilic globular protein with hydrophilic groups exposed outside and hydrophobic groups embedded inside. The hydrophilic nature of the soy protein makes it a good candidate to form interactions with the cellulosic fibers. However, the globular structure results in the native soy protein having poor adhesion strength and water resistance. The key approach to successfully utilize soy protein is to achieve chemical, physical, and enzymatic modifications. Modification methodology has been shown to significantly improve both strength and water resistance of soy protein adhesives [4]. Once this adhesive is chemically optimized, it will be combined with biodegradable materials to produce a novel biodegradable fiberboard.

Native soybean proteins have a highly ordered global structure with hydrophilic groups exposed outside and hydrophobic groups buried inside. When the internal bonds are broken by chemical modification, protein molecules unfold, promoting the adhesion potential of the protein complex and making reactive groups available to interact with cellulosic materials [5]. Alkaline [6], urea [7], guanidine hydrochloride [8], Sodium dodecylbenzene sulfonate [9] (SDS), polyamide-epichlorohydrin [10], etherification by ethanol and HCL solution [11], Phytagel [12], and stearic acid [13] have been used to modify soybean protein and improve the properties of bonding strength and water resistance. Huang and Sun showed that 1% SDS modification had significantly enhanced adhesive strength as well as water resistance [9]. SDS was used as a denaturation agent to bind proteins and induce a conformation change to promote a water resistant fiberboard [14]. However, this type of research is currently limited to the scale up or manufacturing of this type of fiberboard.

Soybean protein adhesives have been used for wood board preparation such as fiberboard [15], oriented strand board [16], wheat straw particleboard, [17, 18, 19] and low density particleboard from wheat straw and corn pith [20]. Kuo et al. [21] prepared wood fiberboards that had no moisture resistance. Ye et al. [22] stated that the hot press process might play an important role in fiberboard preparation in terms of mechanical properties.

The second approach utilizes paper coated with polymers to enhance water-repellency and wet strength. Polymeric coatings are useful for a wide range of industries including packaging. Coatings are used for protective, decorative, and functional purposes on many kinds of surfaces [23]. Current technology uses materials such as polyethylene as the primary coating material. While effective in preventing water damage, these hydrocarbon coatings do not biodegrade and exclude them from being repulped.

The application of a biodegradable polymer as a moisture barrier for paper and fiberboard solves these shortcomings. Examples of such polymers include aliphatic polyesters. Levit, et al. reported using poly(lactic acid) (PLA) as a coating on fiberboard [24]. They found the tensile strength of the coated material was higher than that of the uncoated fiberboard, particularly when wet. They also reported the biodegradation rate of the coated material was faster than that of pure PLA and was independent of the PLA coating thickness. A number of researchers have investigated biodegradable polymers as water-resistant coatings for paper. Most researchers have employed poly(lactic acid) as either a melt [25,26] or as an aqueous dispersion, i.e. a latex [27,28,29,30,31,32,33,34]. Poly(lactic acid) has also been coated on paper from an organic solvent solution [35]. Biodegradable polymers have also been applied as dry particles to the paper surface and subsequently melted with a hot roller [36]. Other materials used as a latex or melt include esterized starch [37,38], Bionolle 1903 poly(butylenes succinate) [39], polysaccharides mixed with silica [40], polycaprolactone [41,42], adipic acid-1,4-butanediol-

terephthalic acid copolymer [43], blends of starch and polyolefins [44], talc-filled systems [45], cellulose and hydrophobic polymer latex [46], starch acetate [47], 3-hydroxybutyrate-3-hydroxyvalerate copolymer [48], poly(ethylene vinyl alcohol) blended with starch [49], and poly(β-hydroxyalkanoate) latex [50]. A latex can be made from aliphatic polyesters by compounding with poly(vinyl alcohol) in a twin screw extruder at low temperature [51]. Monsanto has demonstrated polyhydroxyalkanoate (PHA) to be useful as a heat-sealable coating on paper [52]. PHAs such as poly-3- hydroxybutyrate (PHB) produced in nature by bacterial fermentation of sugar or lipids are biodegradable and biocompatible thermoplastic polyesters. It is expected that much of this knowledge can be extended to fiberboard. The focus is on using an optimized formulation using PHA and perhaps other biodegradable polymers and/or fillers to compare the effectiveness of the coatings on mechanical properties.

Coating of polymeric materials can be conducted on a variety of substrates using a number of different techniques such as melt-extrusion, dispersion coating and solution methods. These techniques give vast opportunities to form coated, multilayer and laminated structures. Most coatings are the result of the intimate interaction between two different materials–an organic/inorganic substrate and a polymeric resin that form adhesive bonds with each other. The quality and durability of the coating is directly related to the level of adhesion [53]. By utilizing a biocompostable polymer and paper, a potential biocompostable package can be realized for the military. In addition, the US Navy utilizes a 30-gal bag on board ship for food waste and the current bags have insufficient water barrier and strength properties that can lead to sanitation issues. A high strength, lightweight, water-proof, marine biodegradable, non-toxic bag was developed in this project as an alternative to the existing bag. This bag must also be capable of being processed though the existing shipboard equipment and passing the military specifications.

Kraft paper is a universal material made essentially from wood pulp that is produced by a modified sulfate pulping process (Kraft Process). It comprises a matrix of long cellulose fibers held together by hydrogen bonding between hydroxyl groups. Cellulose is an environmentally friendly and renewable biomaterial [54]. It is a linear polysaccharide of D-glucose units ($C_6H_{10}O_5$) linked by β-1, 4-glycosidic bonds. Kraft paper is widely used in packaging applications for both food and non-food materials due to its high mechanical resistance to tearing and to tensile forces. These properties are due to the long fibers used in the manufacture of Kraft paper and its basis weight of 30-150 g/m^2[55]. In addition, its environmentally friendly nature has helped the material to resist substitution by petroleum-based plastics. However, due to its hygroscopic properties and poor barrier to water and water vapor, Kraft paper is not suitable for long-term storage of dehydrated products, whose shelf life would be reduced.[55,56]

PHAs have occupied a special position among biodegradable green polyesters. PHAs are a family of natural, biodegradable polyesters which are intracellularly synthesized as a carbon and an energy reserve material by various microorganisms such as alcaligenes eutrophus and pseudomonas oleovorans [57]. PHAs have been recognized as a potential environmentally-friendly substitute for fossil based plastics such as polyethylene, polystyrene, and other consumer plastics. They are fully biodegradable, thermoplastic polyesters and their applications can be found in the food industry (as packaging and antioxidant materials), agriculture (as coating material for seeds, fertilizers and pesticides), medicine and pharmacology. Their physico-chemical properties, diversity and the feasibility of producing PHA-based composites with various materials make them the materials of the 21st century. Poly (3-hydroxybutyrate) (PHB), poly(3-hydroxybutyrate-*co*-4-hydroxybutyrate) [P(3HB-*co*-4HB)] and poly(3-hydroxybutyrate-*co*-3-hydroxyvalerate) [P(3HB-*co*-3HV)] are representatives of the PHAs family.

In an effort to produce more environmentally friendly materials, PHAs have been investigated as paper coating materials. PHAs possess excellent film-forming and coating properties and are water resistant due to their high hydrophobicity [58,59]. For example, PHB-coated paperboard has been used for packaging of ready meals, while P(3HB-*co*-3HV) coated board has been used for dry products, dairy products and beverages [58,60]. The US Patent and Trademark Office awarded Metabolix, Cambridge, MA the US Patent 7,094,840 covering low molecular weight PHAs for use as hot melt adhesives, waxes and protective coatings [61]. Coating compositions include a PHA oligomer and also stabilizers, plasticizers, dyers, emulsifiers, thickening agents, antioxidants, preservatives, cross-linking agents, other biologically degradable polymers, and anti-fungal agents. The coatings are used in coating cheese and other food products [61]. Lim et al. [62] prepared solution-based PHB coating obtained by PHB penetration into and adhesion onto cellulose paper. The coating efficiency index of PHB-coated paper was investigated through solution enzymatic degradation. The results indicated that PHB-coated paper exhibited the lowest degradability by cellulases (enzymes that degrade cellulose paper) with respect to pure cellulose paper. Kuusipalo [63,64] investigated coatings obtained by P(3HB-*co*-3HV) extrusion coated onto a series of paper and paperboard substrates. The physical properties of the coatings showed that the adhesion between the biopolymer and the substrate was poor when corona and flame pretreatments were used. Conversely, the adhesion was sufficient when the substrate was primed with an acrylic-based primer [63]. The results of the heat sealability of P(3HB-*co*-3HV) extrusion coatings show that the sealing temperature increased with increased substrate basis weight. The water vapor barrier of the coatings can be further lowered by incorporation of wax or tall oil rosin. Krook et al. [65] investigated the creasability of P(3HB-*co*-3HV) compression molded onto paperboard. Their results showed that upon application of creasing and bending stresses, P(3HB-*co*-3HV) coating showed no evidence of cracks, and the delamination was observed to decrease with increased molding temperature due to improved paperboard-coating adhesion.

This part of the project investigates the structure and performance of Kraft paper coated with P(3HB-*co*-4HB). Solvent and non-solvent (melt) methods are employed to manufacture the coating. Solvent-based approaches included a dip coating method and the deposition of a solution between the nips of a two roll coating system (roll coating method). The non-solvent based approach was the application of the compression molded P(3HB-*co*-4HB) films to the Kraft paper. In addition, for the US Navy bags, extrusion coating of PHA onto Kraft paper trials was performed.

The coating structure and quality were examined using environmental scanning microscopy (ESEM), Fourier transform infrared spectroscopy (FTIR) and wide angle X-ray diffraction (WAXD) while the mechanical properties were examined using dynamic mechanical analysis (DMA) and impact testing. The coated bags for the US Navy were characterized for water vapor transmission rates, performance and biodegradation.

The third approach of corrugated fiberboard structures have been investigated by the NSRDEC as viable replacements for military grade secondary packaging in the MRE™ and UGR™ packaging systems.

Corrugated fiberboard or "combined board" has two main components: the liner and the medium. Both are made of a special kind of heavy paper called containerboard. Linerboard is the flat facing that adheres to the medium. The medium is the wavy or fluted paper in between the two liners as shown in Figure 1. A critical packaging characteristic investigated in this study is the wet strength property of the fiberboard containers. As corrugated board absorbs water the

fiberboard structure degrades, which diminishes the strength characteristics of the container. Wet strength means that the board is "strong when wet" and is different from being water-resistant or waterproof, which imply that the corrugated board itself holds out water and helps prevent water from penetrating the container. Wet strength linerboards also provide additional strength under conditions of high humidity.

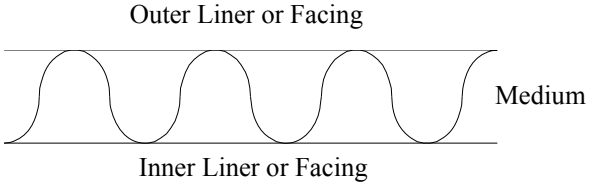

Figure 1. Combined board structure for single-wall fiberboard

The prototype fiberboard containers that have been developed and tested utilize lightweight fiberboard material with commercial coatings that offer wet strength performance in high moisture or wet environments. The ability of a container to perform in distribution and storage is significantly impacted by the conditions it encounters throughout its lifetime. Factors that diminish compression performance include environmental factors such as relative humidity, temperature extremes and cyclic environmental conditions as discussed in the Fibre Box Handbook [66]. In addition to these conditions, other factors such as material degradation, material/container creep, storage time, unitizing patterns and processes and handling operations may also work to reduce the compression performance of the fiberboard containers. These strength diminishing factors are observed values for RSC containers and may vary based on overall design and material grade.

The most significant factor that weakens the structural integrity of a fiberboard container is humidity. Humidity affects not only the paper, but also the overall structure, since the board, joint and closures are usually bonded with water-soluble adhesive [67]. High humidity storage conditions can severely degrade the strength of a stack of corrugated boxes in a matter of hours, for instance at 90% RH, a container can lose over 50% of its original compression strength.

Water-resistant coated containers have been developed to meet existing military requirements during handling, transport and storage while dramatically reducing material needs. The prototype packaging is designed to meet critical performance requirements for rough handling encountered during transportation by air drop, material handling and long term storage and also to maintain performance during exposure to adverse environmental conditions. In addition to meeting these challenges, the focus of this study is to determine the compression strength of the prototype containers and compare them to the existing ration containers. The test containers were exposed to multiple environmental conditions to obtain an overall level of compression performance within each environment.

In most industrialized countries, landfill space is rapidly becoming depleted; hence, there is a growing need to either develop new landfills or extend the life of current landfills. Paper and fiberboard packaging materials make up an estimated 30–40% of all municipal solid waste in the United States [68,69]. Most of these fiberboard materials are disposed of in municipal landfills. The need to increase the recovery of organic wastes—diverting them from landfills—has made composting a popular and growing choice for inclusion in municipal waste management programs. Indeed, composting continues to gain momentum as a cost-effective and environmentally acceptable alternative to the land filling of organic wastes, as well as the

preferred method for disposing/recycling of yard wastes. Nevertheless, composting is generally considered a viable option only as long as collection and handling are convenient and the end-product is of high quality. For the military, composting is also an attractive alternative to recycling—largely because it reduces the costs of storing and then shipping these 'waste' materials back to the United States. Indeed, in 2005 Bost et al. [70] reported that composting had the ability to "successfully treat large amounts of solid waste (including paper and fiberboard products) on-site within a short time period" in military contingency operations.

Over the past two decades, considerable research has focused on the development of biodegradable (compostable) plastics and hybrid paper/biodegradable polymer composites as replacements for traditional paper-based packaging materials. Moreover, an understanding of the bio-environmental degradability of these materials has been considered critical to assessing the environmental footprint of the material. Oddly, however, whereas there have been intensive efforts to evaluate the biodegradability of these new biopolymers and bioplastics, relatively little attention has been focused on the biodegradability of paper and fiberboard products themselves [71]. Thus, the goal of this study was to demonstrate the bio-environmental degradability of new "biodegradable" fiberboard and paperboard products that incorporate biodegradable polymer coatings (e.g., PHA) and recently developed bioadhesives along with materials such as wood fibers, chicken feather fibers, cheese cloth, straw fibers, cotton and kenaf fibers.

The bio-environmental degradability (i.e. compostability) of these new, lightweight fiberboard and paperboard materials was assessed using a three-tiered testing scheme involving both laboratory and field components. Laboratory and bench-scale reactors were used to simulate bioactive disposal sites in which the biodegradability of the test materials could be evaluated under controlled aerobic composting conditions. As much as possible, these tests were conducted in accordance with the protocols described in ASTM D6002 Standard Guide for Assessing the Compostability of Environmentally Degradable Plastics [72] and D6400 Standard Specification for Compostable Plastics [73]. Initial testing involved the use of laboratory-scale reactors to investigate the inherent biodegradability (i.e., mineralization: the conversion of polymer-C into CO2; Tier I test) of the test materials. At the same time, a bench-scale compost reactor was constructed to assess the degradation/disintegration (measured as weight loss; Tier II test) of the test materials. The last phase of the testing program involved a field trial (Tier III tests) to demonstrate the compostability of the test materials under field conditions and assess the impact of the test materials on the quality of the final compost product in accordance with US Composting Council standards.

3.0 Soy Protein Adhesive Fiberboard with Wood Fiber or Pulped Fiber

3.1 Materials and Methods

3.1.1 Wood Fiber Materials

3.1.1.1 Preparation of soybean protein adhesive

Soybean protein was extracted from defatted soybean flour purchased from Cargill Inc., Minneapolis, MN following the procedure described by Huang and Sun [8]. The soy flour contained 88% protein (dry basis) with 90% of particles passing through a 150 μm sieve opening. Soybean protein (64.5 g) was gradually added to 1% SDS solution (365.5 g) with stirring. The SDS was supplied from Sigma Chemical Company in St. Louis, MO. The slurry was stirred for 3 h at room temperature before coating onto the wood fiber.

3.1.1.2 Medium density fiberboard (MDF) panel preparation

Southern yellow pine wood fibers (length= 2-5 mm, diameter= 25-70 μm) with approximately 10% moisture content were provided by the fiberboard division of Georgia-Pacific Company in Holly Hill, SC. These wood fibers (300 g) were coated with 430 g of the modified soybean protein slurry in a rotary blender (Patterson-Kelly Co., East Stroudsburg, PA) for 12 min, then the fiber was dried with an air aeration dryer at room temperature to adjust the initial moisture content (IMC) of the coated fiber. The IMC of the coated fiber was determined with the air oven method at 130 ºC for 1 h. Coated fibers with different IMC (52 g, dry basis) were manually loaded into a single fiber mat using a 152.4 mm x 152.4 mm aluminum mold. Then, the coated fibers were pressed into fiberboard using a Hot-Press (Model 3890 Auto "M", Carver Inc, Wabash, IN) at force of 116.6 KN. A programmed hot-pressing schedule was used to control the press time and temperature. In this process, the aluminum mold was equipped with stops so that a constant gap was always achieved to control the thickness of the board. The final thickness of the fiberboard was approximately 3.2 mm. The fiberboard was placed in a constant humidity chamber at 50% relative humidity (RH) and 23ºC for 2 days for further analysis.

3.1.2 Wood Fiber Methods of Characterization

3.1.2.1 Density

The density of each fiberboard panel was obtained by dividing the fiberboard mass (wet basis) by its volume, giving an average bulk density of 0.74 g/cm^3. Each MDF panel was cut into five 25.4 mm square specimens and four 25.4 mm x 127 mm rectangular testing specimens for evaluation as seen in Figure 2.

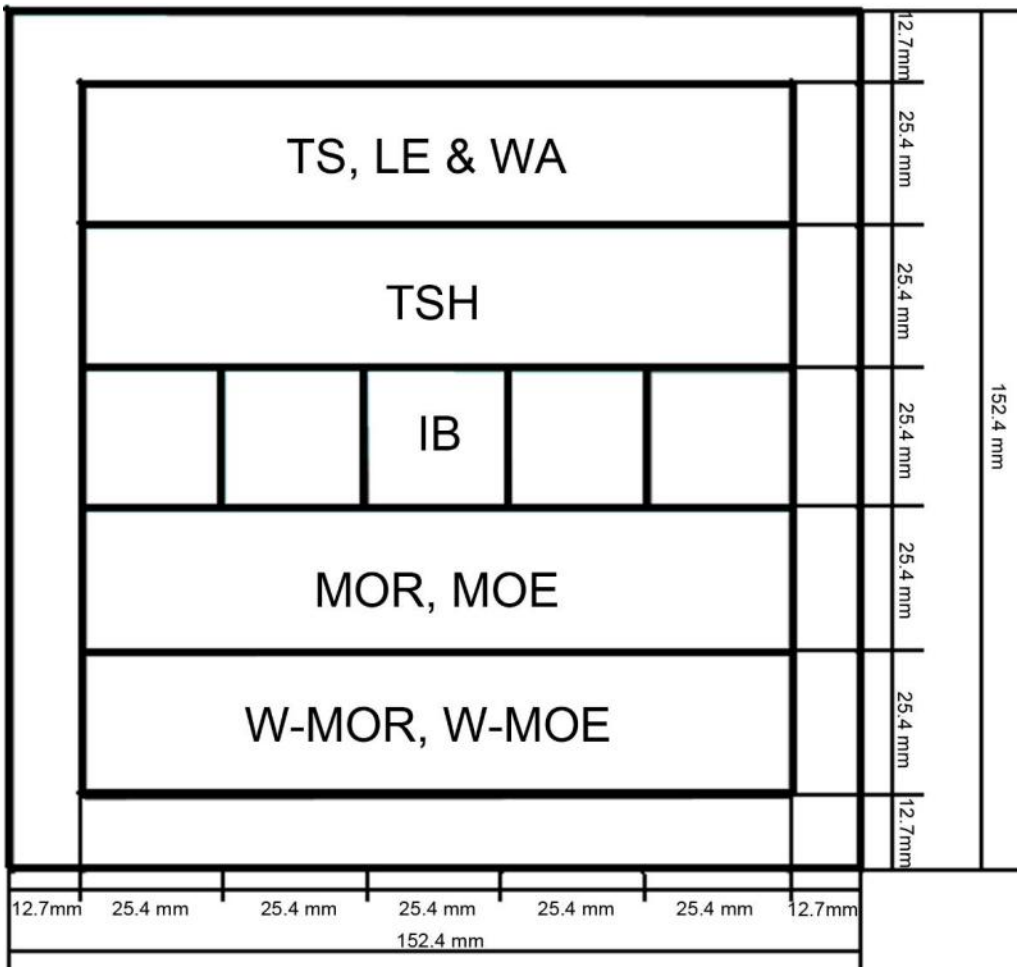

Figure 2. Dimensions of the test specimens for the medium density fiberboard panel

3.1.2.2 Mechanical properties

The mechanical properties were determined following ASTM D1037-99, Standard Test Methods for Evaluating Properties of Wood-Base Fiber and Particle Panel Materials[74] using an Instron testing machine (Model 4466, Canton, MA). Tensile strength (TSH) was obtained by tensioning the specimen (25.4 mm x 127 mm) at a crosshead speed of 4 mm/min. Internal bonding strength (IB) was measured by pulling the specimen (25.4 mm x 25.4 mm) apart in the cross section direction at a crosshead speed of 0.5 mm/min; both side surfaces of the specimen panel were mounted onto the testing accessory with Speed Bond #1 glue (Prime Resins Inc., Conyers, GA). Wet modulus of rupture (MOR) and modulus of elasticity (MOE) of the fiberboard (25.4 mm x 127 mm) were obtained by performing the three-point flex test at a crosshead speed of 3 mm/min.

3.1.2.3 Water soaking properties

Thickness swell (TS), linear expansion (LE) and water absorption (WA) were measured according to ASTM D1037-99 [74] as well. The 25.4 mm x 127 mm specimens were soaked in water for 24 ± 1 h at room temperature. Thickness, length and weight were measured before and

immediately after soaking. The dimensional size and weight measured before and after soaking were used to calculate TS, LE and WA, which were expressed as percentages of the data after soaking to data before soaking. Wet modulus of rupture (W-MOR) and wet modulus of elasticity (W-MOE) after soaking were measured using the same three-point flex test as was used for the dry fiberboard samples.

3.1.2.4 Microscope images

The microstructures of the fractured surface of MDF were observed with scanning electron microscopy (SEM) (Hitachi S – 3500N, Hitachi Science Systems, Ltd., Ibaraki, Japan). The specimens were first mounted on aluminum stubs, and then the fractured surfaces were coated with a mixture of 60% gold and 40% palladium with a sputter coater (Desk II sputter/etch unit, Denton Vacuum, Moorestown, NJ) before analysis.

3.1.2.5 Experimental design

Response surface methodology (RSM) was used to study the influence of IMC of coated fiber, press time (PT), and press temperature (PTT) on properties of MDF. The second order model used in this research is:

$$Y = a_0+a_1X_{IMC}+a_2X_{PT}+a_3X_{PTT}+a_{11}X_{IMC}^2+a_{22}X_{PT}^2+a_{33}X_{PTT}^2+a_{12}X_{IMC}X_{PT}+a_{13}X_{IMC}X_{PTT}+a_{23}X_{PT}X_{PTT} \quad (1)$$

Where *a* is a constant, X represents all the variables, and the subscribed acronym of the X is the variable name: IMC of the coated fiber (%), PT (min), PTT (ºC), and Y represents the response variables including TSH (MPa), MOR (MPa), MOE (MPa), IB (MPa), TS (%), LE (%), WA (%), W-MOR (MPa) and W-MOE (MPa).

A central composite design was applied as an approach to analyze the effects of three variables on mechanical and water soaking properties. Each of the five levels of the variable was scaled separately to -1.68, -1, 0, 1, and 1.68.

According to preliminary experiments and previous research results [75,18], the zero level of IMC was defined as 22.5%, at a press time of 10 min, and press temperature of 170 ºC. The hot–pressing variables and experimental design are shown in Table 1. All data reported was completed in quintuplicate. Processing parameters include IMC of wood fiber coated with soybean protein adhesives, press time and temperature. The standard error and significance of coefficients obtained were based on the six replicated runs conducted at center points (zero level). Statistical software (Minitab of Minitab Inc.) was used to analyze the experimental data.

Table 1. Surface Response Experimental Design for MDF

Run Order	IMC (%)	Temperature (°C)	Time (min)	Density (g/cm^3)	TSH (MPa)	IB (MPa)	MOR (MPa)	MOE (MPa)	LE (%)	TS (%)	WA (%)	MOR-W (MPa)	MOE-W (MPa)
1	22.5	170	18.4	0.792	10.301	0.49	14.403	1532.92	0.703	47.037	150.473	1.307	67.333
2	30	190	15	0.722	10.985	0.577	15.495	1538.76	0.611	33.759	131.566	2.016	88.48
3	30	150	5	0.756	8.774	0.419	17.552	2252.82	0.98	43.093	132.861	1.303	64.733
4	22.5	203.6	10	0.758	7.465	0.307	11.153	1163.09	0.844	46.857	160.333	0.93	47.163
5	15	190	15	0.716	5.947	0.101	8.667	946.66	0.737	48.755	207.639	0.604	40.249
6	22.5	136.4	10	0.796	6.181	0.154	11.81	1555.19	1.091	61.854	167.861	0.537	38.325
7	15	190	5	0.672	5.461	0.058	6.196	570.78	1	93.582	264.082	0.341	7.766
8	22.5	170	10	0.738	8.282	0.153	11.701	1182.57	0.82	60.277	170.567	0.842	30.211
9	15	150	5	0.705	4.873	0.076	6.373	829.75	1.213	90.977	236.234	0.218	11.144
10	22.5	170	10	0.736	9.154	0.155	12.089	1159.06	0.832	50.513	169.314	0.737	32.443
11	22.5	170	1.6	0.725	6.489	0.288	7.866	943.86	1.426	63.574	184.286	0.454	17.621
12	22.5	170	10	0.718	7.551	0.285	10.784	957.38	0.889	32.664	149.368	1.213	48.629
13	30	190	5	0.758	11.508	0.659	18.376	1745.91	0.986	34.101	129.052	1.765	67.666
14	9.9	170	10	0.643	2.993	0.01	3.627	428.66	1.487	115.313	296.52	0.172	4.127
15	15	150	15	0.714	5.464	0.075	5.919	669.01	1.151	78.002	203.403	0.483	13.568
16	35.1	170	10	0.776	14.457	0.866	29.656	2992.11	0.705	28.432	101.272	3.536	162.311
17	22.5	170	10	0.73	7.03	0.192	12.178	1248.89	0.861	44.647	154.975	1.194	44.535
18	22.5	170	10	0.726	7.848	0.267	10.381	1073.09	0.76	46.311	144.893	1.209	48.094
19	22.5	170	10	0.726	7.54	0.278	10.715	1082.04	0.811	49.159	143.077	0.977	48.517
20	30	150	15	0.778	11.786	0.707	19.317	2113.81	0.854	37.089	111.12	2.43	81.985

3.1.3 Pulped Fiber Materials

3.1.3.1 Chemicals

One hundred percent virgin pine pulp (made through an unbleached Kraft process) with 88% moisture content was provided by Interstate Paper LLC (Riceboro, GA). Defatted soy flour, containing 48.5% (dry basis) protein and 4.6% moisture was provided by Cargill Inc. (Minneapolis, MN). Sodium hydroxide, hydrochloric acid, and SDS were all purchased from Sigma Chemical Co (St. Louis, MO).

3.1.3.2 Soy Protein-based Adhesives Preparation

Five soy protein-based adhesives (SPA) were prepared from defatted soy flour with and without SDS modifications. Table 2 shows the SPA concentrations for preparing the paper sheets. SPA-I was prepared with SDS pre-modified soy flour powder containing 47.7% (dry basis) protein. This was gradually added to distilled water at 5% solid content and stirred for 1 h at room temperature (pH ≈ 7.1). SPA-II was prepared with defatted SDS modified soy flour and gradually added to 1% SDS solution at 5% solid content and stirred for 3 h at room temperature (pH ≈ 6.9). SPA-III was prepared with defatted soy flour and gradually added to distilled water at 5% solid content and stirred for 30 min at room temperature (pH ≈ 6.5). SPA-IV was prepared with SDS-modified soy protein isolates (SPI), which was extracted from defatted soy flour following the procedure described by Huang and Sun [8], containing 88% protein (dry basis). SPI was gradually added to 1% SDS solution at 5% solid content and stirred for 3 h at room temperature (pH ≈ 7.7). SPA-V was prepared with SPI directly and was added to distilled water at 5% solid content and stirred for 30 min at room temperature (pH ≈ 7.4).

Table 2. SPA concentration for preparing paper sheet

SPA slurry (wet base, %)	SPA content (dry base, %)	Pulp fiber slurry (wet base, %)	Pulp fiber solid (dry base, %)
0	0	4.00	0.48
1.0	0.050	3.67	0.44
1.5	0.075	3.50	0.42
2.0	0.100	3.33	0.40

3.1.3.3 Bio-based Fiberboard Panel Preparation

The paper sheet was used to prepare the fiberboard panel in a pair of specially designed molds. The sample holder is a female mold as shown in Figure 3, while the cover is a male mold as shown in Figure 4. This mold can prepare a 152.4 mm by 152.4 mm panel board. Figure 3, enlargements A and B illustrate vertical and horizontal notches, which allow for the evaporation of water vapor. Figure 3 Enlargement A shows nine round holes that were specifically designed at each cross point on the mold.

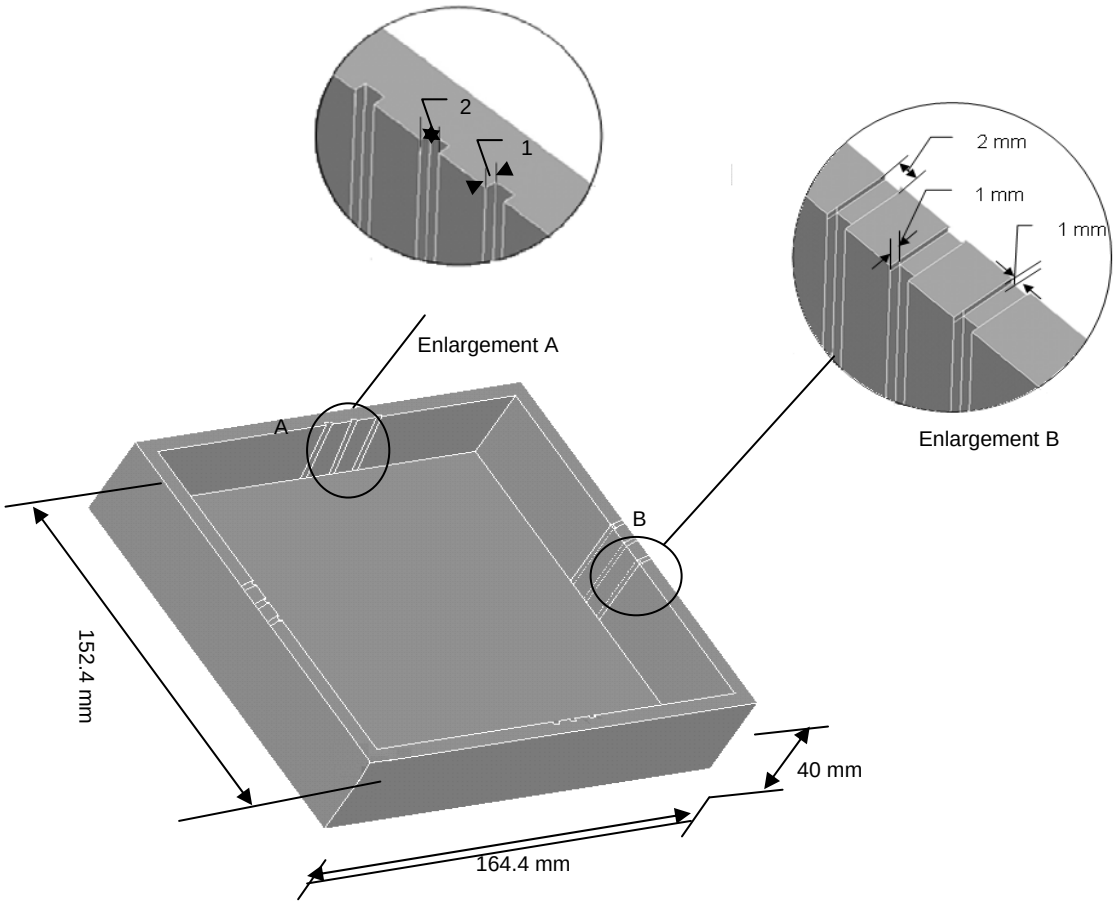

Figure 3. Pair of specially designed molds: (female mold)

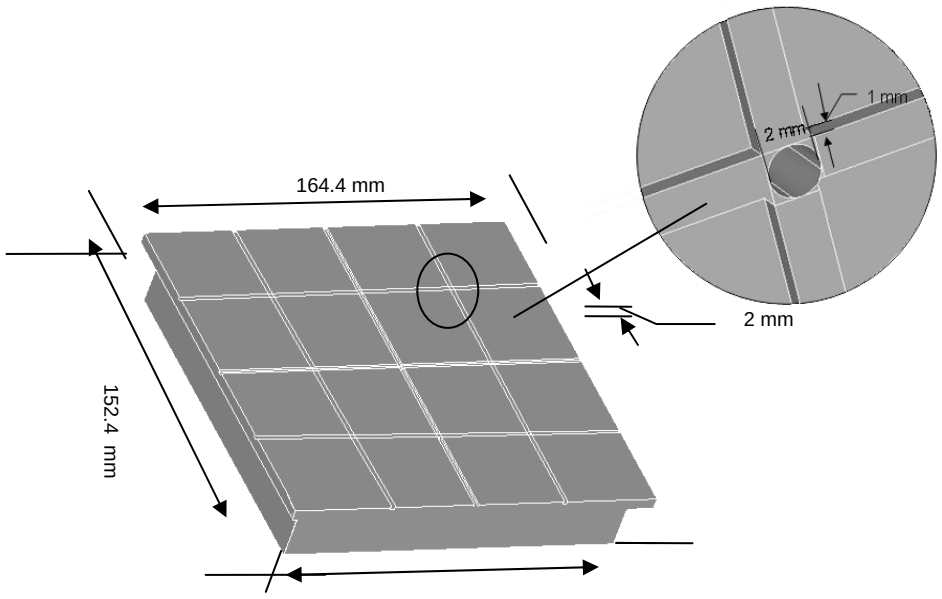

Figure 4. Pair of specially designed molds: (male mold)

The paper sheets were layered together using five to eight sheets depending on the desired thickness of the board. Table 3 shows the thickness of the panel in relation to paper sheet (weight and number) and press time and temperature. To prepare a sample, 1.75 ± 0.25 g of water was added to the female mold between two sheets of fiber. The male mold was placed over the female mold and then the layered paper sheets were pressed using a Hot-Press (Model 3890 Auto "M", Carver Inc, Wabash, IN) with 66.7 KN. The thickness of fiberboard was controlled by the gap adjustment in the mold using metal sheets of known thickness. The density of the board was controlled by the amount of fiber and the thickness of board. The panels were conditioned in a humidity chamber at 23 ºC and 50% RH for 5 days to equilibrate before characterization.

Table 3. Method for Controlling the Thickness of the Fiberboard Panel

Target thickness of fiberboard (mm)	Weight of total paper sheets (g)	No. of paper sheets	Hot Press	
			Time (min)	Temperature (ºC)
0.6	14±0.5	5	3	160
1.2	23±0.5	8	3.5	160

3.1.4 Pulped Fiber Methods of Characterization

3.1.4.1 SPA Viscosity measurement

The rheological properties of the SPAs were determined using a Brookfield DV-III^{+} Programmable Rheometer (Brookfield Engineering Laboratories, Inc., Middleboro, MA) equipped with a small sample adapter (SC4-21). The SPA slurry was transferred into the sample holder of the rheometer, and its viscosity was recorded every 60 s, from 80 s to 680 s at a shear rate of 93.0 s^{-1} and at room temperature.

3.1.4.2 Contact angle measurement

The contact angle was monitored by an optical contact angle meter (CAM 100, KSV Instruments, Helsinki, Finland). Contact angle was measured immediately after a droplet (about 2 μL) of supernatant of SPA slurry dropped on the surface of the substrate. The substrate was prepared by pressing three pieces of paper sheet, (0% SPA content), using a Hot Press (Model 3890 Auto "M", Carver Inc, Wabash, IN) at 66.7KN and 105 ºC for 5 min. The values reported were averages of the five replications.

3.1.4.3 Thermal property

Protein heat denaturation was carried out on a differential scanning calorimeter (DSC, Pyris-1, Perkin-Elmer, Norwalk, CT). The instrument was calibrated with indium and zinc standards and all measurements were conducted under a nitrogen atmosphere. About 35 mg of SPA slurry with 10% solid content was sealed in a large-volume DSC pan. All samples were held at 30 °C for 1 min and then were scanned to 150 °C at a heating rate of 10 °C/min. The enthalpy of denaturation (ΔH_d) was determined in duplicate by integrating the area under the endothermic peak.

3.1.4.4 Properties Characterization of Fiberboard Panel

Mechanical properties were determined following ASTM Standard Method D1037-99 [74] using an Instron testing machine (Model 4466, Canton, MA). TSH was obtained by tensioning the specimen (25.4 mm × 127.0 mm) at crosshead speed of 4 mm/min. MORs of the fiberboard samples were obtained by performing three-point bending tests at crosshead speed of 3 mm/min. The wet TSH (W-TSH) and wet MOR (W-MOR) were obtained after 24±1 h of water soaking.

Burst strength was determined following the Technical Association of the Pulp and Paper Industry (TAPPI) method T 810 om-06 [76] using a Burst Tester (MTA 2000, West Berlin, NJ). A specimen (152.4 mm x 152.4 mm) was clamped in a pair of circular plates with a pneumatic system, then a constantly increasing pressure acted on the unsupported area of specimen until the specimen was burst, and the force required to burst the specimen was displayed. The hydraulic system rate of flow was 170 ± 15 mL/min. The burst index (BI) was obtained by dividing burst strength by its grammage. The values reported were averages of three replications.

3.1.4.5 Dimension stability

TS, LE and WA were measured according to ASTM standard method D1037-99 [74]. The 25.4 mm × 127 mm specimens were soaked in water for 24±1 h at room temperature. The dimensional size and weight before and after soaking were measured to calculate the values of TS, LE and WA, which were expressed as percentages, comparing the before and after soaking values.

3.2 Results and Discussion

3.2.1 Wood Fiber

3.2.1.1 Experimental Design

Processing variables and their interactions on mechanical and water soaking properties of MDF were empirically expressed with statistical equations. After adjusting the model (Eq. 1) using a significance test and lack-of-fit values, all variables in the final models were required or significant at the level of 0.1. These equations and their R^2 values and standard deviation (S) values were as follows:

$$TSH = -34.841+0.398X_{IMC}+0.143X_{PT}+0.367X_{PTT}-0.001X_{PTT}^2 \quad (2)$$
R^2: 0.920; S: 0.739

$$MOR = 6.556-0.525X_{IMC}+0.174X_{PT}-0.006X_{PTT}+0.031X_{IMC}^2 \quad (3)$$
R^2: 0.927; S: 0.775

$$MOE = -1752.9+101.4X_{IMC}+12.6X_{PT}+14.3X_{PTT}+3.2X_{IMC}^2-0.92X_{IMC\cdot PTT} \quad (4)$$
R^2: 0.931; S: 102.07

$$IB = -0.703-0.023X_{IMC}+0.035X_{PT}+0.005X_{PTT}+0.001X_{IMC}^2+0.002X_{PT}^2-0.0004X_{PT\cdot PTT} \quad (5)$$
R^2: 0.951; S: 0.062

$$LE = 2.993-0.0697X_{IMC}-0.0299X_{PT}-0.0047X_{PT}T+0.001X_{IMC}^2 \quad (6)$$
R^2: 0.737; S: 0.044

$$TS = 278.18-10.78X_{IMC}-5.207X_{PT}-0.235X_{PT}T+0.134X_{IMC}^2+0.172X_{IMC\cdot PT} \quad (7)$$
R^2: 0.904; S: 7.834

$$WA = 507.45-21.169X_{IMC}-7.677X_{PT}+0.132X_{PTT}+0.259X_{IMC}^2+0.234X_{IMC\cdot PT} \quad (8)$$
R^2: 0.962 S: 11.03

$$W\text{-}MOR = 0.0198-0.1300X_{IMC}+0.0489X_{PT}+0.0035X_{PTT}+0.0054X_{IMC}^2 \quad (9)$$
R^2: 0.925; S: 0.208

$$W\text{-}MOE = -6.960-5.388X_{IMC}+2.294X_{PT}+0.174X_{PTT}+0.227X_{IMC}^2 \quad (10)$$
R^2: 0.908; S: 8.488

The R^2 values for each equation indicate how well the models fit experimental data. Almost all R^2 values were higher than 0.9, except for LE ($R^2 = 0.74$), which was caused by board density effect on the LE [77]. These models were then used to predict mechanical and water soaking properties as functions of the three processing variables. To show the main effect and interaction of processing parameters on mechanical and water soaking properties, the curves were plotted for each responsive property as a function of variables.

3.2.1.2 Effect of IMC on mechanical and water soaking properties

For hot press processing, if the IMC of coated fiber approaches 40%, the board will crack in the middle layer because of the higher water vapor pressure produced [17] ; this was observed in initial experiments as seen in Figure 5. To avoid cracking of the board, the IMC of the coated fiber had to be lower than 36%. The regression models (2 - 10) indicated that the influence of IMC on mechanical and water soaking properties was largest, except for IB. In the variable range of this experiment, as IMC increased, TSH, MOR and MOE increased significantly, and IB also increased from 0 to 0.44 MPa. Figure 5 shows the following: a) TSH, IB, MOR and MOE; b) W-MOR and W-MOE after 24 h of water soaking; c) LE, TS and WA of wood MDF (ρ = 0.74 g/cm3), all made at a press temperature of 170 ºC and a press time of 10 min.

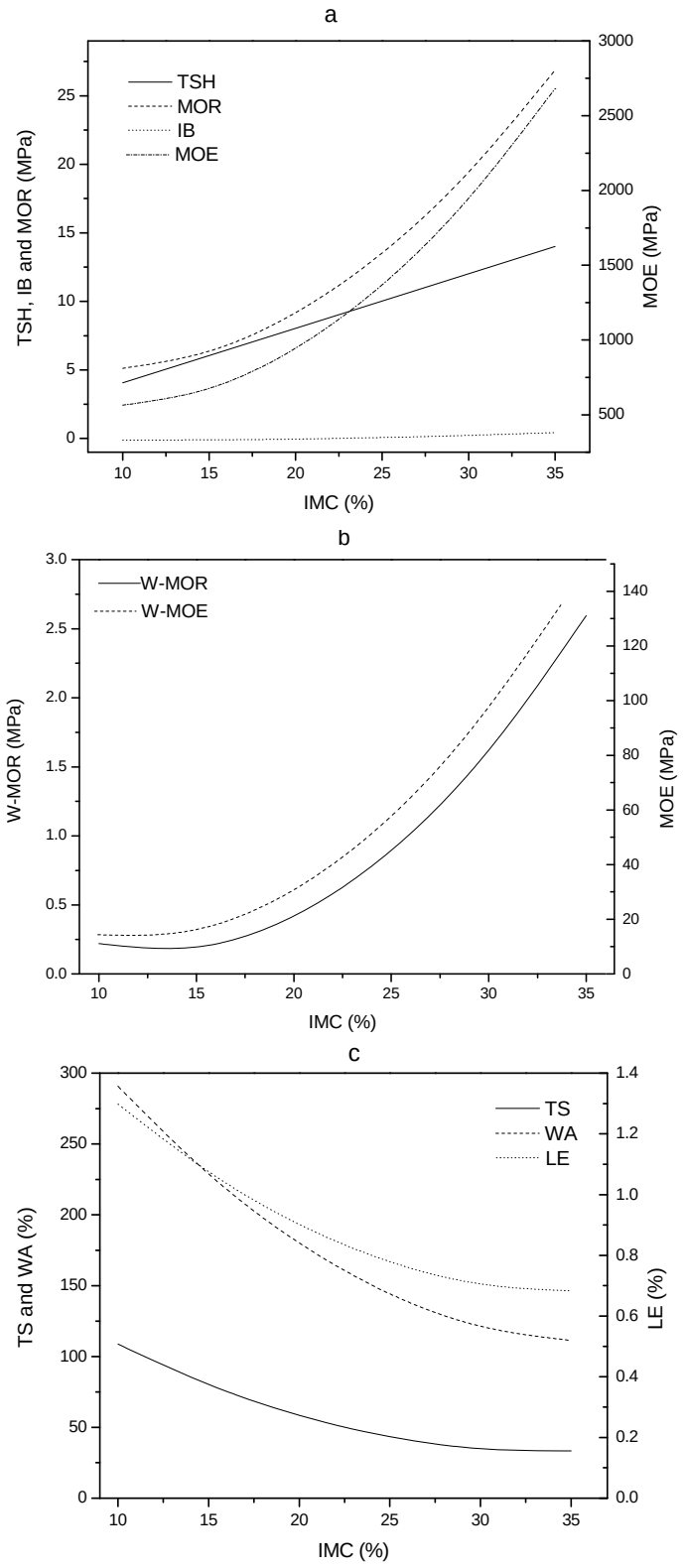

Figure 5. Mechanical Properties: (a) TSH, IB, MOR, and MOE; (b) W-MOR and W-MOE; (c) TS, WA and LE of initial moisture content of 1% SDS modified soybean protein adhesive coated wood fiber

Figure 5a. showed that the W-MOR and W-MOE followed the same trends as MOR and MOE in Figure 5b. The water soaking properties of MDF improved as IMC of soybean protein adhesive coated fiber increased as shown in Figure 5c. All mechanical and water soaking properties reached the optimum values at 35% IMC.

In the soybean protein system, water acts as a plasticizer, which reduces protein exothermic temperature [75] and improves mobility of soybean protein polypeptide chains, which might then interact easily with other polymers. Compared with the round and curly shape of the fracture structure with low IMC (10%), Figure 6a, SEM images showed that after hot press, the shape of the fiber with a high IMC (35%), Figure 6b, was flat and straight, and the adhesion between coated fibers with high IMC was significantly stronger than between coated fibers with low IMC. Moisture was a promoter for the adhesion behavior of soybean adhesive and fiber in hot press processing and led to better entanglements at higher IMC.

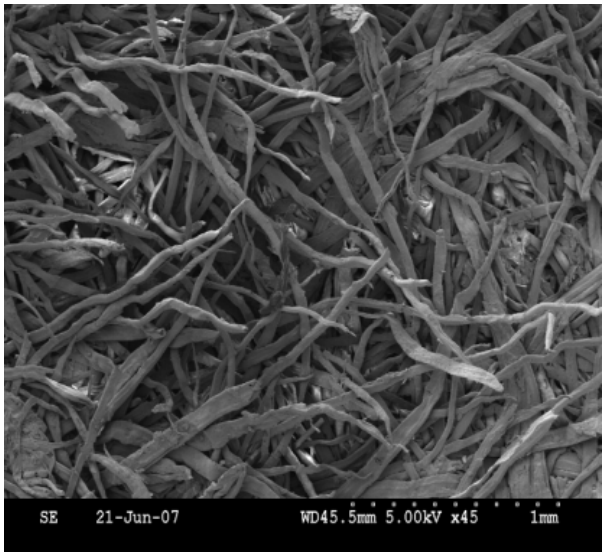

(a)

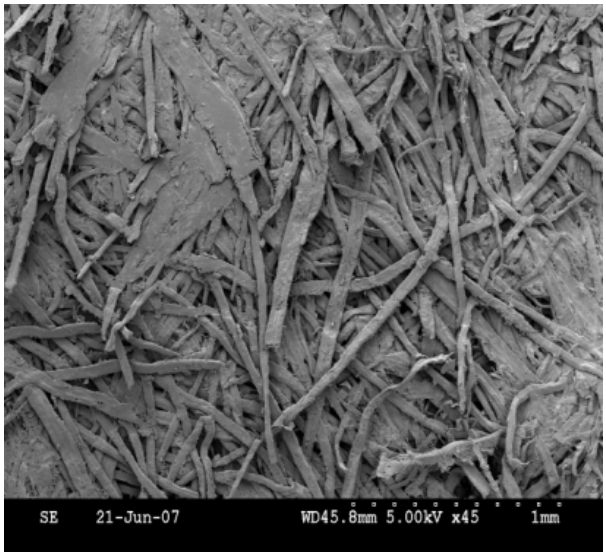

(b)

Figure 6. SEM of the fractured surface of the wood fiberboards pressed at 170 ºC for 10 min: (a) 10% IMC of coated wood fiber; (b) 35% IMC of coated wood fiber

3.2.1.3 Effect of PTT and PT on mechanical and water soaking properties

The denaturation temperature of SDS-modified soybean protein is 73 ºC and 90 ºC caused by conglycinin (7S) and glycinin (11S) components, respectively. During thermal denaturation, the ordered structure of soybean protein is changed to a relatively loose and random structure [78], which improves interactions between protein adhesive and fiber. However, when the temperature of the soybean protein increases to 200 ºC, which is above the protein exothermic temperature of 192 ºC, the protein becomes overheated and degraded, resulting in some small fragments and voids in the protein phase [75]. In this study, soybean protein demonstrated strong adhesive strength in the temperature range between the denaturation and exothermic point. In this study, a press temperature from 130 ºC to 200 ºC and press time from 1.6 min to 18 min was used. Optimum strength occurred at 35% IMC; therefore, the effects of press time and temperature on properties of MDF prepared with 35% IMC are discussed.

In the temperature range between denaturation and the exothermic point, press temperature and press time had significant effects on properties of MDF. In general, a long press time promoted the interaction between protein polymer and fiber surface and led to higher mechanical strength as shown in Figure 7. A longer press time allowed the water residues to evaporate from the board, which also improved the mechanical strength. At a press time of 2 min, water vapor could not completely evaporate from the surface of the panel, but instead coagulated and assembled inside the panel, thus reducing mechanical and soaking properties.

No interactive effects of press time and temperature were observed on TSH which is shown in Figure 7a, MOR which is shown in Figure 7b and MOE which is shown in Figure 7c. TSH, MOR and MOE all increased as press time increased. TSH reached its highest value at a press temperature of approximately 180 ºC and then leveled off in the press time range of 2-18 min (Figure 7a). As mentioned previously, press temperature promoted soybean protein entanglements that enhanced adhesion strength. At press temperatures above 180 ºC, the protein became partially denatured, resulting in no increase in adhesion strength. It was predicted that TSH would decrease at press temperatures above 200 ºC. Press temperature had no significant effect on MOR as shown in Figure 7b, but had a negative proportional effect on MOE as shown in Figure 7c. As press temperature increased, adhesion strength was enhanced by the higher degree of entanglement of the soybean proteins. The morphology of fiberboard at higher press temperatures is similar to that at higher moisture content as shown in Figure 6b. The improved adhesion resulted in a tougher material, because the MOE is the ratio of stress (σ) and strain (ε) at proportional limit, therefore MOE could be different when the MOR remains the same. For example, as shown in Figure 8, both Samples a and b had 30% moisture content, but Sample a was pressed at 190 ºC for 5 min and Sample b was pressed at 150 ºC for 5 min. The area under the curve of Sample a was bigger than that of sample (b), which means that Sample a is tougher than Sample b. In this case, Sample b had a larger MOE of 2275 MPa, as compared to Sample a which had a MOE of 1745 MPa. Similar trends were observed for all the other samples. Press time and temperature had interactive effects on IB as shown in Figure 7d. At low temperature (i.e., 140 ºC), IB increased as press time increased. At high temperature (i.e., 200 ºC), IB decreased as press time increased and then increased slowly at press times of about 12 min and beyond. At lower temperatures, a longer press time promoted soy protein entanglements, leading to higher adhesion, which had morphology similar to that shown in Figure 6b. In addition, water vapor pressure was lower at the lower temperature, and water vapor could appropriately evaporate with a longer press time, which also resulted in higher IB.

At higher temperatures, soy protein became denatured at longer press times, decreasing adhesion. At press times of 12 min and longer, water vapor was completely evaporated; therefore, IB slightly increased.

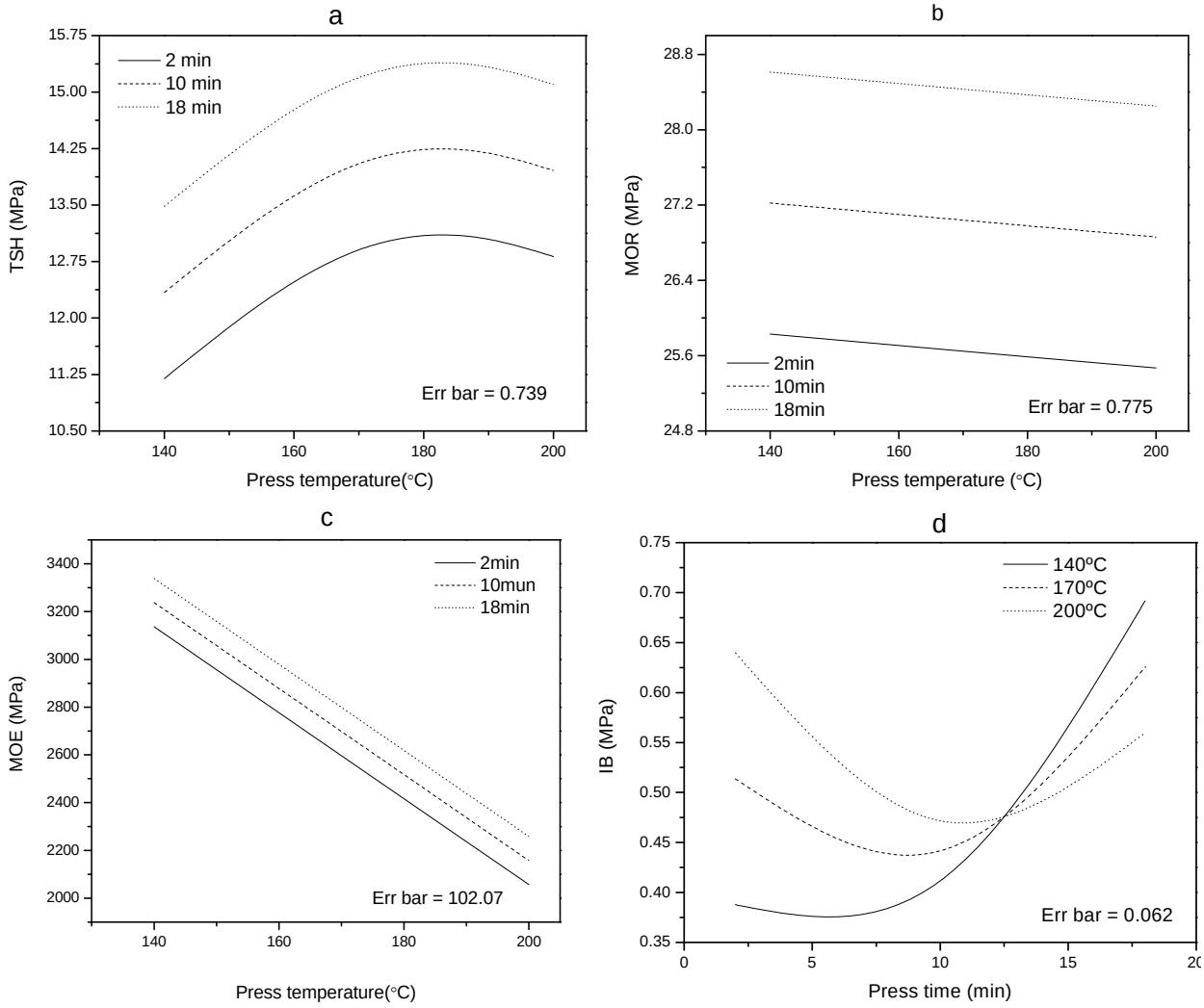

Figure 7. Interactive effects of press time and temperature on different strengths with 35% IMC of coated wood fiber: (a) TSH, (b) MOR, (c) MOE, (d) IB

Both W-MOR and W-MOE of the MDF proportionally increased as press time and temperature increased after 24 h of water soaking as shown in Figure 9. As discussed previously, longer press times and higher temperatures promoted protein molecular entanglements; this improved water resistance and, in turn, wet mechanical strength.

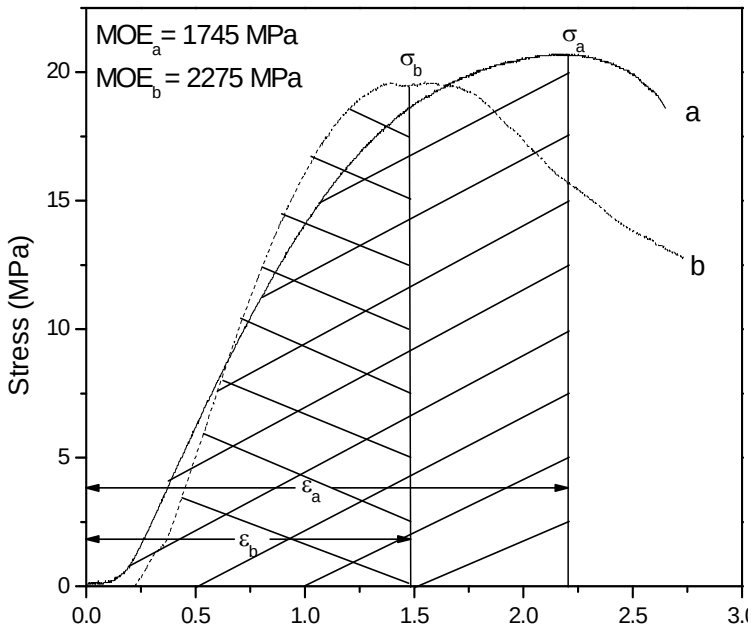

Figure 8. Strain curves of wood fiberboards recorded during three-point bending test of samples with 30% IMC pressed for 5 min: (a) 190 °C, (b) 150 °C

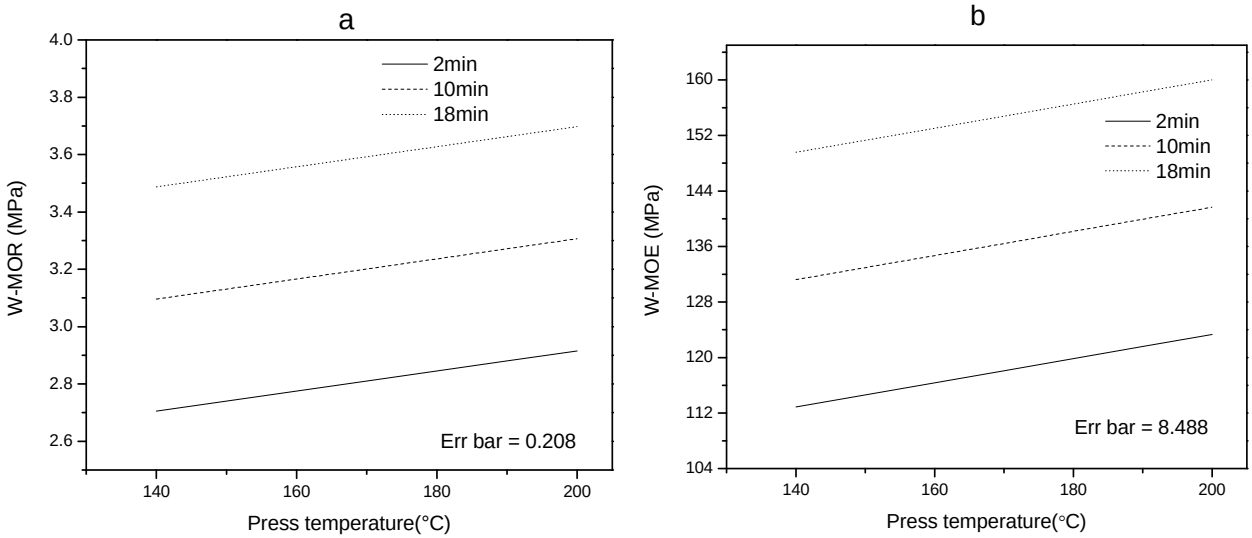

Figure 9. Interactive effect of press time and temperature after 24 h of water soaking with 35% IMC of coated wood fiber: (a) W-MOR, (b) W-MOE

LE was significantly reduced with press time and temperature as shown in Figure 10a. The degree of crosslinking between the soybean proteins and the wood fibers was improved at longer press times and higher press temperatures. TS and WA of the MDF were not significantly affected by press time and temperature as shown in Figure 10b and 10c, respectively.

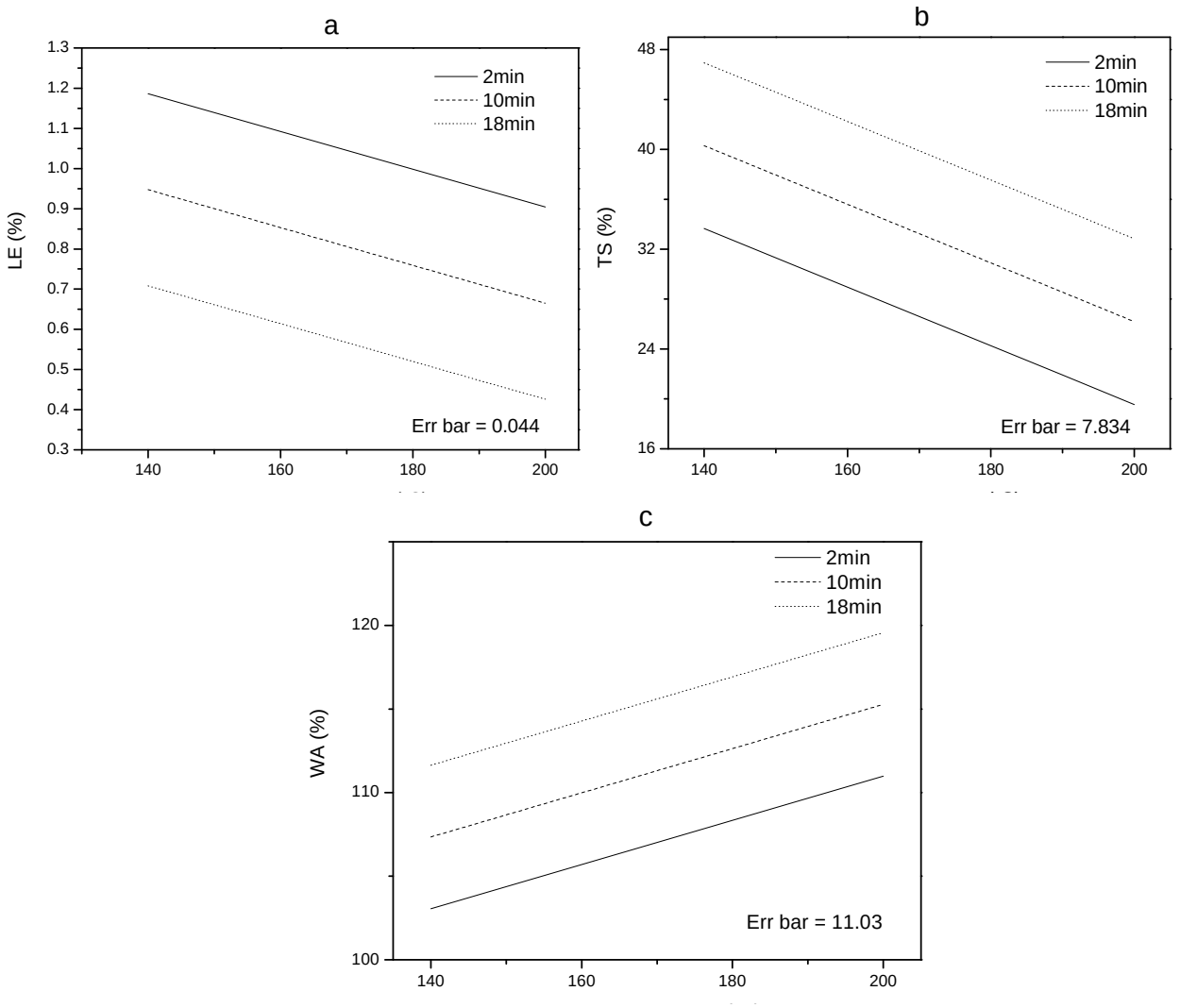

Figure 10. Interactive effect of press time and temperature on dimension stability on different conditions after 24 h of water soaking with 35% IMC of coated wood fiber: (a) LE, (b) TS, (c) WA

3.2.1.4 Optimum MDF processing parameters

Optimum processing parameter ranges for MDF were obtained using Equations 2–10 derived from surface response experiments at 35% IMC with Minitab statistics software. The optimum operation zone was a narrow irregular shape with press temperatures ranging from 192 to 200 ºC and press times from 13.0 to 14.5 min. The values of mechanical and water soaking properties predicted from the optimum zone are summarized in Table 4. The predicted data uses the Minitab statistical software at the optimum condition of 35% IMC, 195 ºC press temperature and 13 min press time. To verify the predicted optimum point, MDF panels were prepared using the parameters from the optimum zone: IMC was 35%, press temperature was 195 ºC and press time was 13 min. The experimental data of mechanical and water soaking properties of the MDF had good agreement with the predicted properties, which is shown in Table 4, indicating these models can be used to predict the properties of MDF as functions of IMC, press time and temperature in the variable range tested in this research. Compared with the commercial MDF

standard [79], MDF made with soybean protein adhesive has IB and MOR values that are significantly stronger than Grade 210 and the same as Grade 230, which are shown in Table 5. The MDF with soybean protein adhesive has great potential as an alternative to current commercial board.

Table 4. Comparison of Actual and Predicted Results of Mechanical and Water Soaking Properties of MDF

	Experimental data	Predicted data
Density, g/cm^2	0.80 ±0.05	---
Tensile strength, MPa	22.8 ±2.0	>15
Internal bonding strength, MPa	1.03 ±0.43	>0.8
Modulus of rupture (MOR), MPa	33.7 ±7.4	>25
Modulus of elasticity (MOE), MPa	2847 ±654	>2300
Thickness swell, %	23.9 ±2.8	<30
Linear expansion , %	0.95 ± 0.23	< 1.1
Water absorption, %	64.3 ± 9.6	<80
MOR after soaking, MPa	7.87±0.68	>3.0
MOE after soaking, MPa	380.3 ± 58.7	>155

Table 5. Mechanical Properties of MDF at 35% IMC

		ANSI A208.2		
Mechanical properties	Experimental data	210	220	230
Internal bonding strength, MPa	1.03 ±0.43	0.4	0.6	1
Modulus of rupture (MOR), MPa	33.7 ±7.4	21	31	31

These measurements were obtained at a press temperature of 195 ºC and a press time of 13 min which meet or exceed the properties required by the American National Standards Institute (ANSI A208.2-2002) for Grades 210, 220, and 230.

Processing parameters influenced the mechanical and water soaking properties of the fiberboard samples. The effect of IMC was significant because moisture was a promoter for the adhesion behavior of soybean protein adhesive and wood fiber. Press temperature and press time were also found to have effects on properties. In general, a long press time promoted the interaction between protein polymer and fiber surface leading to higher mechanical strength. Overall, MDF with wood fiber and soybean protein adhesive gave high mechanical and water soaking performance and are attractive for military applications. Replacing petroleum-based

resin with soybean protein adhesive in MDF applications would also solve problems related to the emission of toxic chemicals.

3.2.2 Pulped Fiber

3.2.2.1 Properties of different soy protein-based adhesives

In order to investigate the influence of soy protein-based adhesives on fiberboard preparation and performance, the viscosity, contact angle and enthalpy of denaturation of five types of SPAs were tested as shown in Table 6.

Table 6. Properties of Different SPAs[1]

Formula	Viscosity at 93/s of shear rate (mPa s, 5 % solution)	Contact angle on wood fiber sheet (°, 5 % solution)	Enthalpy of denaturation (J/g SPA, 10 % slurry)
SPA-I	3.59±0.54$^{c, d}$	49.47±4.78^{c}	2.78±0.26^{d}
SPA-II	3.77±0.41^{c}	45.59±3.57$^{c, d}$	2.03±0.11^{e}
SPA-III	3.41±0.38^{d}	78.46±4.72^{a}	4.04±0.03^{c}
SPA-IV	6.82±0.40^{a}	41.36±5.11^{d}	6.03±0.04^{b}
SPA-V	6.27±0.26^{b}	62.99±3.09^{b}	7.97±0.04^{a}
Water		41.40±2.78^{d}	---

[1]Analysis of Variance (ANOVA) and LSD tests were performed using SAS. Means in the same column followed by different superscript letters are significantly different and the probability level of $\alpha = 0.05$.

The viscosities of SPA-IV and SPA-V were higher than other formulations because they were derived from SPI with a protein content of 88% which is significantly higher than defatted soy flour (48.5%). Furthermore, the viscosity values of all five SPAs were very low, therefore there was no difficulty mixing with the wood pulp fibers. During the heating period, protein is denatured, and the structure of protein is unfolded. Enthalpy of denaturation of SPI-based adhesives (SPA-IV, and SPA-V) was significantly higher than other formulations due to the higher protein content of SPI (88%). Comparing the enthalpy of denaturation with and without SDS-modified SPAs, the enthalpy of denaturation significantly decreased after SDS modification. This suggests that the soy protein native structure partly unfolded during SDS modification and the pre-modified SPA (SPA-I) was unfolded slightly less than modified SPA (SPA-II) [13].

Contact angle is an index which reveals the wetting property on the surface of wood fiber. Lower values of contact angle indicate that the liquid wets the surface well. SPA-IV had the best wetting property which equaled the value of water. The native soy protein (SPA-V and SPA-III) wets the wood fiber surface poorly; however, after being modified by SDS, the wetting property of SPAs on the surface of wood fiber was significantly improved, reaching the value of water. SDS modification enhances the soy protein wetting on wood fiber. At 5% SPA, the native protein content affects the contact angle with more protein quantity, giving the lowest value (SPA-V and SPA-III). After modification by SDS, the effect of different protein content was minimized for the sample analysis (SPA-II and SPA-I).

3.2.2.2 Effect of concentration of soy protein-based adhesive on mechanical properties of BBF

The bio-based fiberboards (BBF) were prepared with concentrations ranging from 0% to 0.15% of SPA-I (Figure 11). TSH and MOR showed an improvement as the adhesive concentration in the pulp slurry increased from 0 to 0.1%. However, there was a slight decrease when the adhesive concentration in the pulp slurry increased to 0.15%. MOE showed an increase as the adhesive concentration in the pulp slurry increased from 0% to 0.05%, and it was determined that formulations incorporating 0.05% of soy protein-based adhesive were preferred.

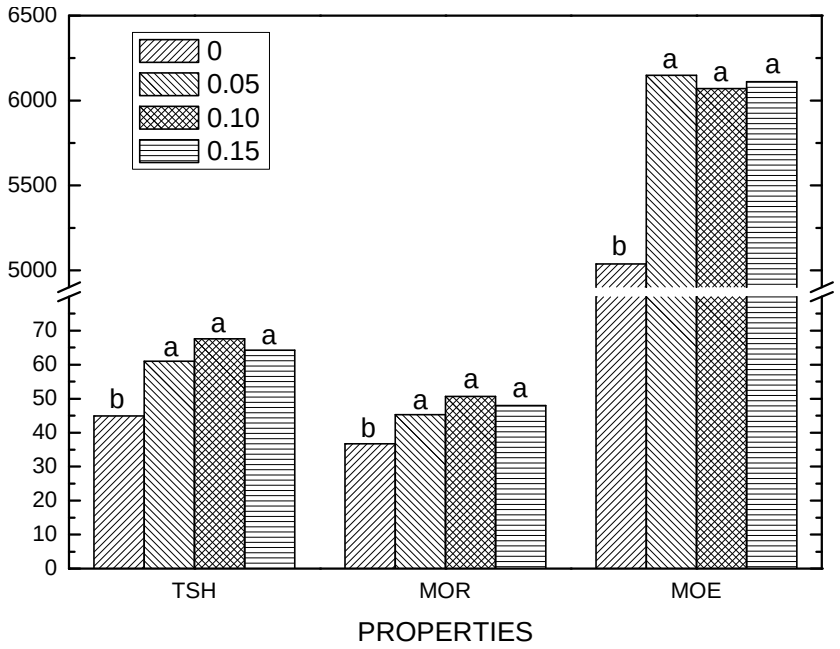

Figure 11. Mechanical properties of BBF made at 66.7 KN forces, 160 °C for 3.5 min, with 1.0 g/cm^2 of area density and 1.2 mm of thickness, prepared by different concentrations of SPA-I, from 0% to 0.15%

3.2.2.3 Effect of press time on tensile strength of BBF

Table 7 shows the TSH of fiberboard prepared by different press times at a force of 66.7 KN, 160 °C press temperature with 0.05% of SPA-1. The board panels with a press time of 1.5 min and 2.0 min were wet after hot pressing and needed continuous evaporation of moisture during the conditioning period. After 5 days of controlled conditioning, TSH showed similar results despite increasing the press time from 1.5 min to 5.0 min. Due to the quality of the fiberboard, the press time needed to be at least 3 min.

Table 7. Press Time on TSH of Fiberboard Samples with 0.05% of SPA-I, pressed at 66.7 KN of force and 160 °C

Press time Min	Area density (g/mm^2)	Thickness (mm)	Tensile strength (MPa)
1.5	1.07	0.57	66.0
2.0	1.04	0.56	68.0
3.0	1.00	0.59	65.9
4.0	1.06	0.60	60.0
5.0	1.08	0.50	62.2

3.2.2.4 Different soy protein-based adhesives on BBF properties

Table 8 shows the influence of different SPAs on mechanical properties for fiberboard before and after water soaking. At a thickness of 1.15 mm and a density of 0.09 g/mm², the SPA-I and SPA-III samples had the strongest TSH. The TSH of the other three SPA sample boards performed at a range in between the SPA-I and SPA-III samples. The MOR of the other SPA samples was significantly stronger than that of the control. All the SPA samples except for SPA-III, showed an increase in the mechanical properties of bio-based fiberboard. After water soaking, the five different SPA samples showed improvements in both TSH and MOR. As an adhesive, defatted soy flour could enhance water resistance of bio-based fiberboard, but there was no significant effect on mechanical properties of the board. SDS-modified soy protein increased both mechanical properties and water resistance, because SDS modification partly unfolds the soy protein structure to promote adhesion action on the wood fiber [78]. The properties were improved for SPI which was essentially due to the sensitivity of the pH level [80,81].

Table 8. SPA Fiberboard Preparation[1]

Formula	Area density (g/cm^2)	Thickness (mm)	TSH (MPa)	MOR (MPa)	Wet TSH (MPa)	Wet MOR (MPa)
SPA-I	0.090	1.10	61.0^a	46.7^a	4.12^a	3.53^a
SPA-II	0.090	1.18	51.7^b	45.2^a	3.73^a	3.28^a
SPA-III	0.088	1.15	39.9^c	37.9^b	4.14^a	3.17^a
SPA-IV	0.094	1.13	54.2^b	47.5^a	3.81^a	3.34^a
SPA-V	0.089	1.13	51.9^b	48.0^a	4.23^a	3.30^a
Control	0.090	1.21	42.8^c	36.7^b	2.60^b	2.10^b

[1]ANOVA and LSD tests were performed using SAS. Means in the same column followed by different superscript letters are significantly different and at a probability level of $\alpha = 0.05$.

3.2.2.5 Comparison of BBF with commercial solid fiberboard (SF)

The two low weight BBFs (0.09 g/cm^2 and 0.05 g/cm^2 area density, 1.1 mm and 0.6 mm thickness) in comparison to SF are shown in Table 9. The TSH of the low weight BBFs was stronger than the TSH of the MRE™ SF. The BBFs had a high burst index, indicating that the

multi-directional TSH of the low weight BBFs was as strong as the SF. The two low area density fiberboards showed lower TS and LE in comparison to the MRE™ SF.

Table 9. Comparison of Mechanical Properties and Dimensional Stability of BBFs with Commercial SF

	Area density (g/cm2)	Thickness (mm)	Tensile strength (MPa)	Burst Index (KPa m^2/g)	Tensile strength after soaking (MPa)	Linear expansion (%)	Thickness swell (%)
BBF 1	0.09	1.1	65	2.8	3.1	0.6	60.0
BBF 2	0.05	0.6	68	2	5.5	0.4	69.3
MRE™ SF (perpendicular)	1.24	1.7	23	2.8	2.5	2.5	55.6
MRE™ SF (Parallel)	1.24	1.7	50	2.8	3.5	0.1	56.3

Most of SPAs had a good influence on the low weight BBF except for SPA-III. Overall, the SDS-modified soy flour adhesive is the optimal candidate for the continuation of this work. However, the Go/No Go decision was made to stop this approach for the manufacturing of the fiberboard as it would be hard to transition.

An optimal concentration of 1% SDS-modified soy flour adhesive, in pulp slurry was determined to be 0.05% to 0.1%. Compared to commercial MRE™ SF, the low weight BBF had a similar burst index, significantly stronger TSH, and stronger TSH after 24 h of soaking; lower or similar linear expansion and thickness swell were also found. This research suggests that the BBF with soy flour adhesive has great potential as an alternative to the current commercial fiberboard.

4.0 Biodegradable Coatings for Kraft Paper

4.1 Materials and Methods

4.1.1 Materials

4.1.1.1 Paper and Polymer

Brown Kraft paper was supplied by NSRDEC. The Kraft papers used for the coating had weights of 60 and 75 lb and a thickness of 0.20 and 0.22 mm (±0.01), respectively. P(3HB-*co*-4HB) (Lot # MBX CS06082205; M_w = 437,084 $gmol^{-1}$; M_n = 189,902 $gmol^{-1}$; PDI = 2.3) was supplied by Metabolix (Cambridge, MA). P(3HB-*co*-4HB) pellets were dried in an oven for 48 h at 40 °C before use. The biopolymer chemical structure is illustrated in Figure 12, and its thermal properties obtained by differential scanning calorimetry (DSC) and thermogravimetric analysis (TGA) are summarized in Table 10. The biopolymer displayed two endotherm peaks T_{m1} at 148 °C and T_{m2} at 162 °C, indicating the presence of two crystalline phases in the sample and the two ΔH_m values reflect the relative amount of the crystalline phases. T_{m1} is related to the melting of crystals formed during non-isothermal crystallization whereas T_{m2} is due to the melting of crystals that are recrystallized during the heating of the biopolymer sample in the DSC pan [82]. A melt crystallization peak T_{mc} is obtained at 105 °C. The biopolymer displayed a maximum decomposition temperature T_p at 299 °C obtained by TGA. Analytical grade dichloromethane (>99.8% purity, EMD Chemicals: Gibbstown, NJ) was used as the biopolymer solvent.

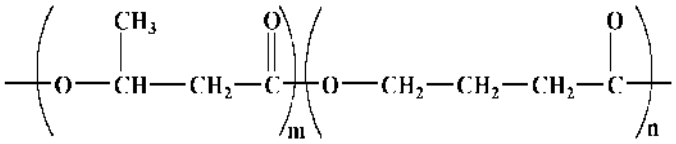

Figure 12. Chemical structure of P(3HB-co-4HB)

Table 10. Thermal properties of P(3HB-co-4HB)

Sample	[a] T_{m1} (°C)	[a] T_{m2} (°C)	[b] ΔH_{m1} (J/g)	[b] ΔH_{m2} (J/g)	[c] T_{mc} (°C)	[d] ΔH_{mc} (J/g)	[e] T_p (°C)
P(3HB-*co*-4HB)	148	162	12.7	37.7	105	47.5	299

[a] Melting (T_m)

[b] Enthalpy of melting (ΔH_m) obtained from second heating differential scanning calorimetry (DSC) at 10 °C/min

[c] Melt crystallization (T_{mc})

[d] Enthalpy of melt crystallization (ΔH_{mc}) obtained from the cooling differential scanning calorimetry at 10 °C/min

[e] Temperature at which the weight loss rate is maximum (Tp): obtained from thermogravimetric analysis (TGA) at 20 °C/min

4.1.1.2 Solution Coatings

10 g of (P3HB-*co*-4HB) were stirred in 200 mL of dichloromethane. The solution was heated to 50 °C overnight to obtain complete dissolution of the biopolymer. Roll and dip coating techniques were used for solution coating. For the roll coating, the solution of (P3HB-*co*-4HB) was poured uniformly onto the substrate which was then rolled between two cylindrical bars. Both sides of the substrate were coated. Controlled thickness can be obtained by adjusting the gap between the two cylindrical bars. In the case of dip coating, a solution bath of $30\times20cm^2$ was used. The paper substrates were immersed with the aid of a weighted screen (3 kg) to prevent them from floating and withdrawn from the solution bath after 10 min. In both cases, the liquid film formation of the biopolymer on the paper was obtained by evaporation of the solvent. The coated papers were dried at ambient conditions for 48 h with a total pressure of 2 MPa. Only one side of the Kraft paper substrate was coated. However, it was observed that diffusion of the biopolymer occurred on the second side. Compression molded biopolymer film with thickness of 0.12 (±0.02) mm was also made and used as control sample for different characterizations.

All the samples were sectioned for characterization. Sample nomenclature employed in describing the results is the Kraft paper weight followed by manufacturing process.

4.1.2 Methods of Characterization

4.1.2.1 Environmental scanning electron microscopy (ESEM):

The surface and the cross section structures of the uncoated and coated Kraft paper samples were observed using a FEI Quanta 2000 ESEM (Hillsboro, OR). Cross section samples were immersed in liquid nitrogen before fracture. All samples were coated with gold before imaging and were examined using an accelerating voltage of 12.5 to 20 kV.

4.1.2.2 Attenuated total reflectance-Fourier transform infrared spectroscopy (ATR FTIR):

ATR FTIR measurements of neat Kraft paper, neat biopolymer and the coated samples were performed using a Nicolet Nexus 6700 FT-IR spectrometer (Thermo Fisher Scientific Inc, Waltham, MA) having a resolution of 4 cm^{-1}, a scan range of 4000 to 400 cm^{-1}. A total of 64 scans per sample were performed. The Germanium crystal was used for ATR FT-IR measurements

4.1.2.3 Wide angle X-ray diffraction (WAXD):

The existence of crystallinity in the neat P(3HB-*co*-4HB), Kraft papers and the coated samples was observed using a wide angle XRD (Rigaku model D/Max -2000 / PC series: The Woodlands, TX). An angular range of 10° to 50° with a Cu-Kα wavelength of 1.542 A°, generated at 44 mA and 40 kV, and a scanning rate of 0.02°/s were used.

4.1.2.4 Dynamic mechanical analysis (DMA):

The thermomechanical properties of the pure P(3HB-*co*-4HB), uncoated and coated Kraft paper samples were measured by means of a dynamic mechanical analyzer RSA III (TA

Instruments, New Castle, DE) operating in the tension mode. For the DMA measurements, the pure biopolymer film, uncoated and coated Kraft papers were cut into bars with dimensions of 30 x 10 mm^2. A single frequency temperature scan was used for the measurement. The specimens were heated at 2 °C/min from -50 °C to 50 °C under an oscillatory strain of 0.3% and a force of 250 gm (previously determined from a separate strain amplitude sweep of the biopolymer at 1 Hz to establish the linear viscoelastic region) at a frequency of 1 Hz. All DMA measurements were done in triplicate.

4.1.2.5 Impact testing

Instrumented impact testing was conducted on an Instron instrumented tester 9250 (Norwood, MA) connected to a piezotup unit capable of measuring up to 500 lb of load. An impact weight of 8.5 kg was used at a height of 0.4 m. The velocity of the impact is 2.80 m/s and the tests were measured under ambient conditions. Pieces (10 cm x 10 cm) of uncoated and coated Kraft papers were used for the instrumented impact testing.

4.2 Results and Discussion

4.2.1 Coating cross-sections and surfaces analyzed by ESEM

Figures 13 to 19 show the representative ESEM micrographs of the cryo-fractured surfaces. Figure 20 shows the surfaces of the uncoated 60 lb Kraft paper, and Figures 21 to 23 show the coated 60 lb Kraft paper.

The cryo-fractured surface of the uncoated paper in Figure 13 exhibited heterogeneous fibrous structure. After the impregnation of the Kraft paper with P(3HB-*co*-4HB), it appeared as if the coating was in close contact with the base paper and filled out the irregularities of the substrate cross-section surface as shown in Figure 14, Figure 16 and Figure 18. The cross-sectional morphology of the coated paper samples showed a layer-by-layer structure. Figure 15, Figure 17, and Figure 19 show the penetration of the biopolymer into the cellulose structure of paper. This suggests that the biopolymer interfered with fiber-to-fiber interaction, causing an increase of interaction force between the fibers of coated paper substrates. However, the presence of more voids in the Figure 17 micrograph of 60Roll with respect to those of 60Dip (Figure 15) and 60Melt (Figure 19) could have indicated lower penetration of the biopolymer in the 60Roll sample. The coating film seemed to be continuous and homogenous as can be seen in the cross section micrographs in Figure 14 and Figure 18 for 60Dip and 75Melt samples, respectively. This result could have implied that the interface region between the biopolymer coating and the paper surface contained many contact points. Thus, this type of composite could have been characterized as having many sites of interaction between the biopolymer and the paper substrate, which could have implied a good adhesion between the biopolymer and the paper substrate. However, the examination of the cross-section of 60Roll sample, Figure 16, showed that this latter lacked a defined boundary as for 60Dip and 60Melt samples. This observation could have been due to the fact that 60Roll sample was compressed between the nips of a two roll coating system. As a result of this, there was no clearly defined boundary between the coating and the base paper. Furthermore, the coating film for 60Roll sample seemed to be very thin and discontinuous; and the fibers shape could be distinguished throughout the biopolymer layer. This result could have indicated that the interface region between the thin coating and the paper surface contained irregularities such as voids (the biopolymer bonding to

the paper substrate appeared to be low) as a result of few contact points between the biopolymer and the paper substrate. Thus, this type of composite could have been characterized as having limited sites of interaction between the biopolymer and the paper substrate, which could have indicated a restricted adhesion between the biopolymer and the paper substrate.

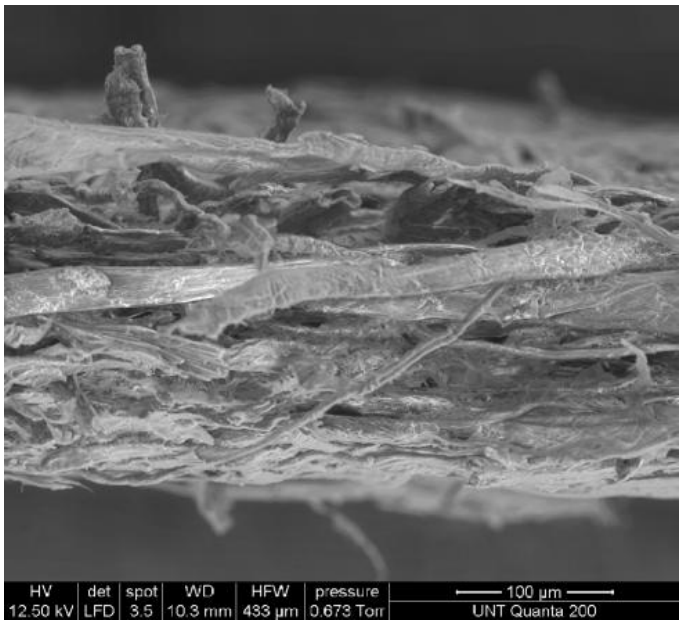

Figure 13. ESEM micrograph of a cross-section of Kraft paper 60 lb showing fibrous structure

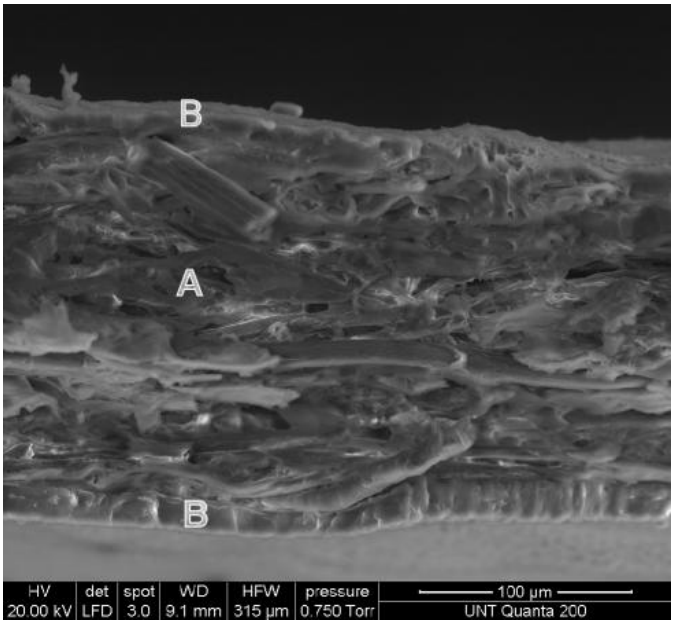

Figure 14. ESEM micrograph of a cross-section of 60Dip: (a) Kraft paper and biopolymer; (b) biopolymer layer

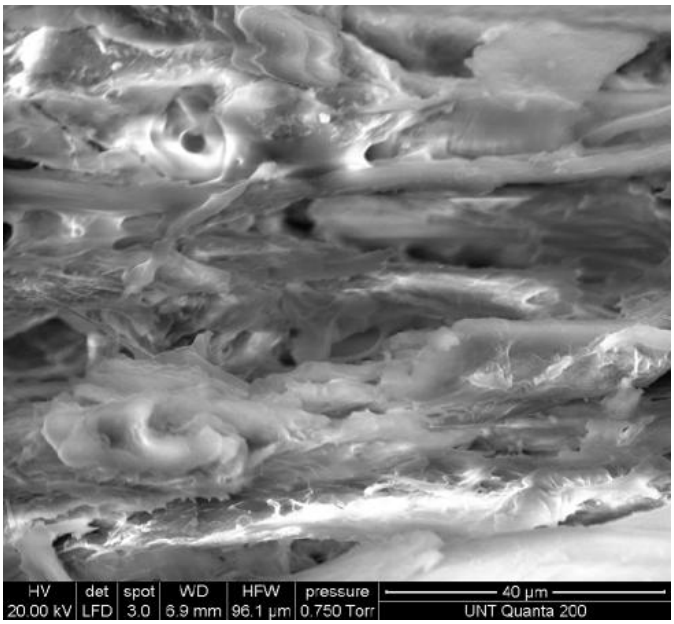

Figure 15. ESEM micrograph of the A region for 60Dip sample showing the penetration of the biopolymer into Kraft paper

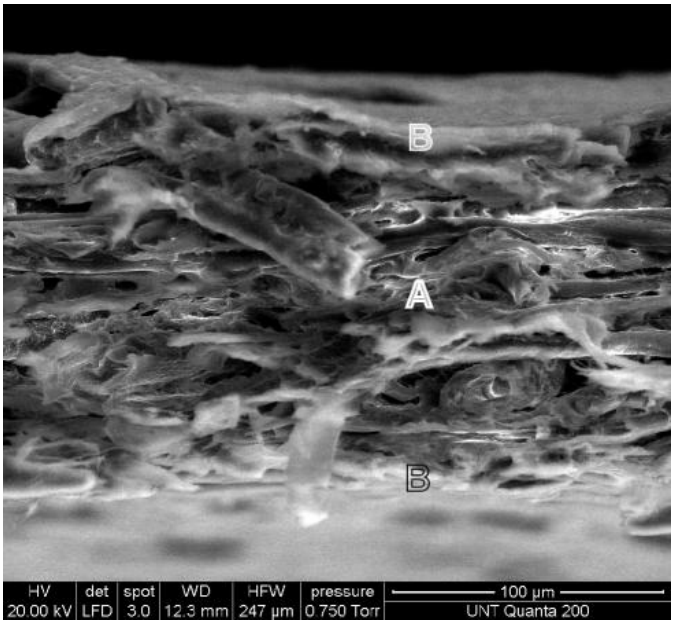

Figure 16. ESEM micrograph of a cross-section of 60Roll: (a) Kraft paper and biopolymer; (b) biopolymer layer

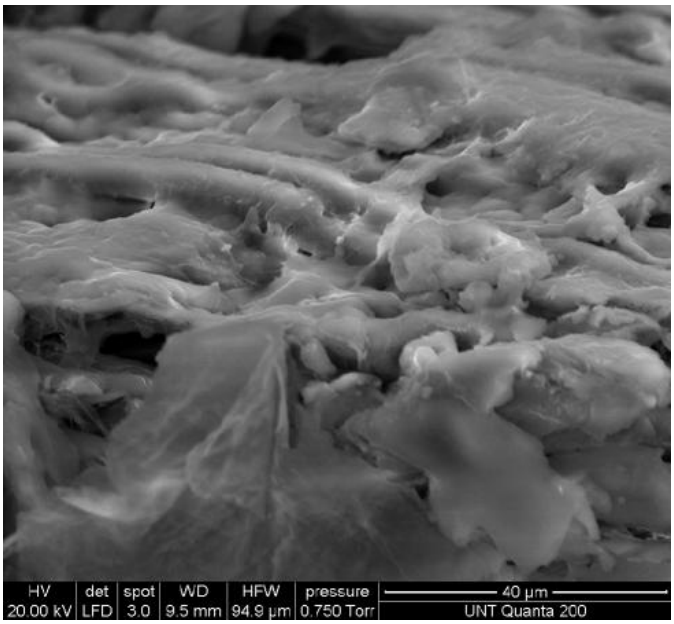

Figure 17. ESEM micrograph of the A region for 60Roll sample showing the penetration of the biopolymer into Kraft paper

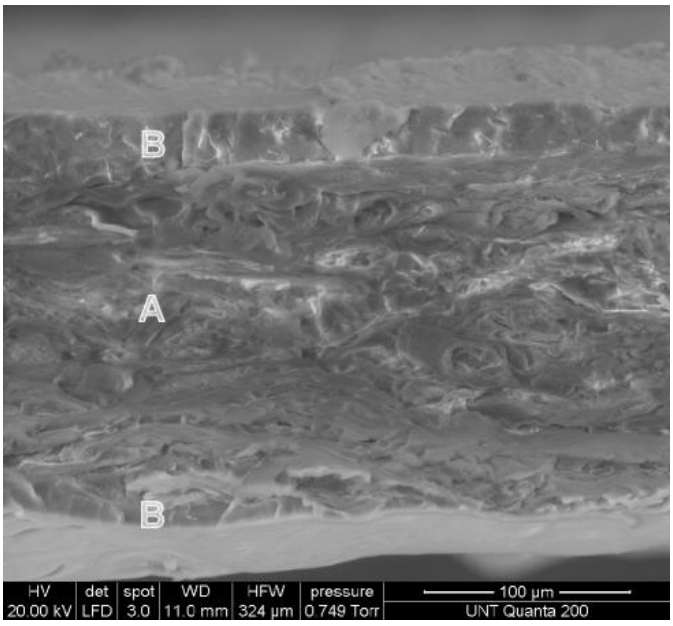

Figure 18. ESEM micrograph of a cross-section of 60Melt: (a) Kraft paper and biopolymer; (b) biopolymer layer

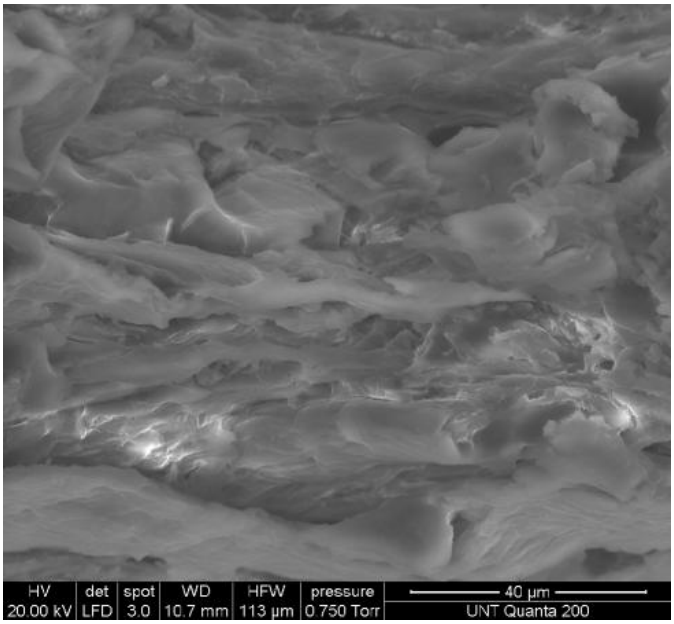

Figure 19. ESEM micrograph of the A region for 60Melt sample showing the penetration of the biopolymer into Kraft paper

Figure 20 displays the surface of the Kraft paper forming a heterogeneous porous material. The impregnation with the biopolyester notably modified the surface of the material. The micrographs of the coated samples in Figure 21 to Figure 23 indicate a biopolymer layer was formed on the surface of the Kraft paper. The porous fibrous structure was covered and filled with P(3HB-*co*-4HB). The coating material acted in a similar manner to fillers, like clay. Fillers fill in the void areas on the surface of the Kraft paper. However, the coating surface was rather rough with the presence of the some irregularities, which most likely could have been the result of an incomplete dispersion of the biopolymer and insufficient homogenization of the coating film in some areas. Furthermore, the roughness of the paper substrate can be seen (the shapes of the fibers can be observed) throughout the coating layer of the solution-based coating samples due to the low coat weight as displayed in Figure 21 and Figure 22. The formation of the P(3HB-*co*-4HB) layer on the surface of the base paper suggested that the coated samples will have decreased hygroscopicities, because the biopolyester is less hygroscopic than Kraft paper. Furthermore, if the biopolyester penetrated into the internal paper pores, it is expected that water movement would be more difficult, decreasing the permeability of the paper.

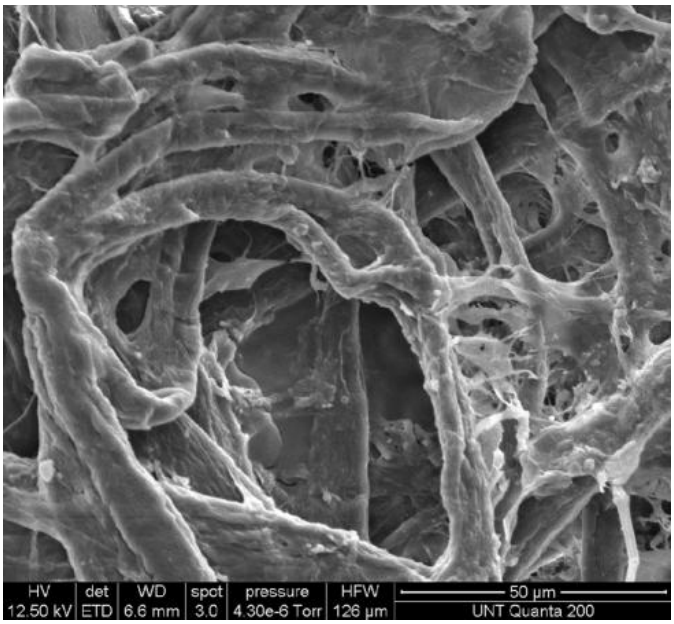

Figure 20. ESEM micrograph of the surface of Kraft paper 60 lb showing porous and fibrous structure

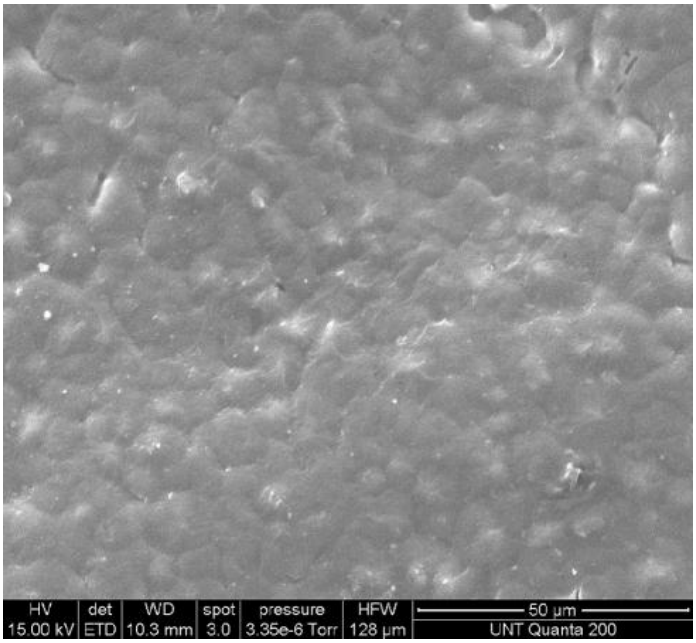

Figure 21. ESEM micrograph of the surface of 60Dip coating

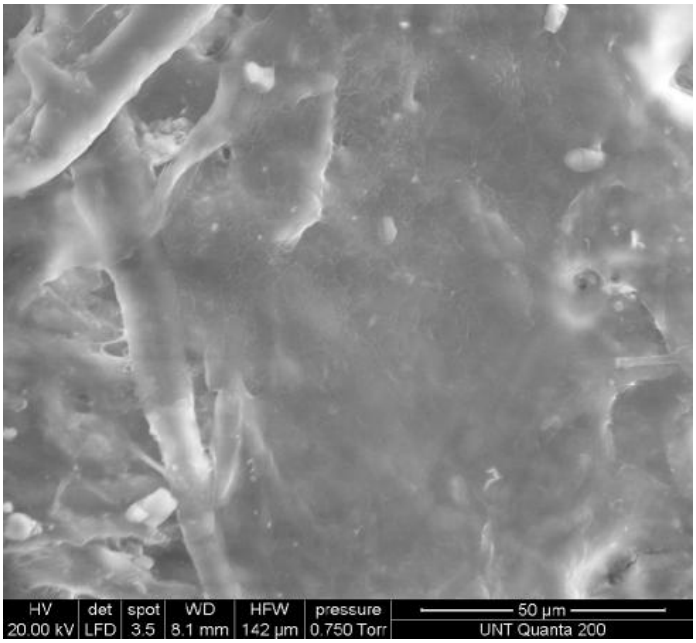

Figure 22. ESEM micrograph of the surface of 60Roll coating

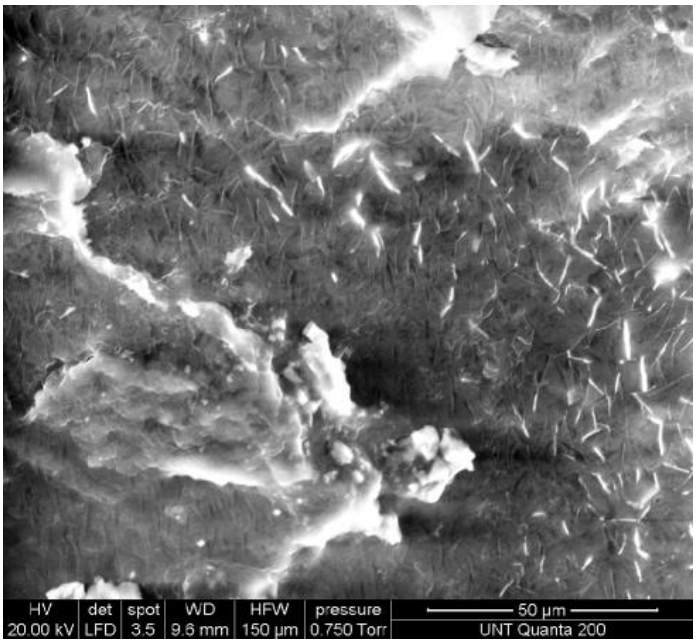

Figure 23. ESEM micrograph of the surface of 60Melt coating

4.2.2 Thickness and coating weight of the samples

The influences of the impregnation with the biopolymer on the thickness and the weight of the uncoated Kraft paper sample are presented in Table 11. The average thickness values for all the samples are shown in Table 11. For the coated samples the average coating thickness is reported. The coating thickness for the solution-based approaches was determined by first conducting the dip coating method with a range of concentrations to achieve a uniform coating. The gap of the rolls was then set to manufacture a coated paper that matched the thickness of the

dip coated sample. The thickness of the melt coated sample was set to correspond to the solution-based coating approach. However, due to the variability involved in making a film and applying pressure over a small gap in the compression molding on one hand, and compressing the coated paper between the nips of a two roll coating system on the other hand, variation in both techniques persisted. The melt-processed samples have the highest coating thickness, while the roll coated samples have the lowest. This result is consistent with the cross-sectional ESEM micrographs.

The average coating weight values determined by comparing five coated and uncoated weights of the same area of each sample are also reported in Table 11. Melt-coated samples showed the highest values whereas roll-coated samples showed the lowest values. This result is consistent with the variation in thickness of the different samples.

Table 11. Thickness measurements of Kraft paper 60 and 75 lb and their coating samples

	60Melt	60Dip	60Roll	75Melt	75Dip	75Roll
Thickness (μm)	45 [a] (±5)	35 [a] (±2)	20 [a] (±2)	55 [a] (±5)	45 [a] (±2)	30 [a] (±2)
Coating weight (g/m^2)	35.50 [b] (±0.56)	22.07 [b] (±0.85)	10.75 [b] (±0.48)	37.43 [b] (±0.67)	25.85 [b] (±0.55)	12.85 [b] (±0.42)

[a] Average coating thickness values determined by comparing the thickness of coated and uncoated sample.

[b] Average coating weight values determined by comparing five coated and uncoated weights of the same area of each sample. Analysis of the coating by ATR FTIR and WAXD

Since the coated samples were not infrared transparent, an ATR method was employed to evaluate the coatings by FTIR. Good contact between the sample and the crystal is essential to record a good qualitative and quantitative ATR spectrum. The representative spectra of the pure components (biopolymer and paper 75 lb) and their coatings are shown in Figure 24. Luo et al.[83] and Xu et al. [84] reported on the characteristic bands of P(3HB-*co*-4HB) and other PHAs, respectively. The bands at 980, 1227, 1279 and 1722 cm^{-1}, respectively, are characteristic of the crystalline phase in the biopolymer while that at 1181 cm^{-1} is characteristic of the amorphous phase. The band at 1722 cm^{-1} represents the stretching vibration of carbonyl groups (C=O) in the crystalline phase. The band at 1279 cm^{-1} corresponds to the symmetric CH_2 stretching. The band at 1227 cm^{-1} was proposed as the conformational band of the helical chains. The bands at 1181 and 1133 cm^{-1} are characteristic of the asymmetric and the symmetric stretching vibration of the C–O–C group, respectively. The characteristic bands of Kraft paper were reported elsewhere [85]. In the spectrum of Kraft paper, a broad band at 3350 cm^{-1} is attributed to O-H stretching vibrations. The band at 2875 cm^{-1} represents the aliphatic C–H stretching vibration. The band observed at 1050 cm^{-1} is due to skeletal vibration involving C-O stretching.

FTIR measurements on variable points of the sample surface were performed and it was observed, by comparing the coated Kraft papers and P(3HB-*co*-4HB) spectra, that the biopolymer crystalline phase absorptions are predominant on the coatings. This could imply a certain degree of the biopolymer bonding to the paper substrate as shown in the ESEM analysis. As proposed by Xu et al. [84], a crystallinity index (CI) defined as the ratio of the intensity of a band at 1453 cm^{-1} which is insensitive to the crystallinity and composition to that of the band at

1181 cm^{-1}, was used to quantitatively measure the crystallinity of the biopolymer since the coatings were obtained though solution and melt processed techniques. The CI is not an absolute measure of the degree of crystallinity but is useful as a comparison criterion. The results for the P(3HB-*co*-4HB) and coatings on 60 and 75 lb paper are shown in Table 12. It can be observed that CI does not change for the melt-processed coating while it decreases for the solution-processed coating (both roll and dip coated samples), reflecting the decreased crystallinity of the biopolymer during solution coating. These types of composites (melt and solution processed) could be useful in decreasing the hygroscopic and the permeability properties of the paper substrate, with melt-processed coating samples having better properties than solution-processed coatings. Furthermore, the mechanical properties of the paper substrate could also be improved through interaction between the biopolymer and the paper substrate.

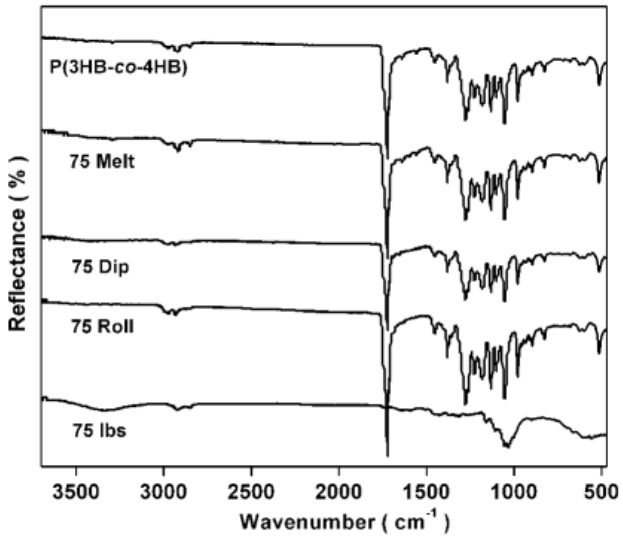

Figure 24. ATR FTIR spectrum of P(3HB-co-4HB), Kraft paper 75 lb and their coatings

Table 12. The CI defined as the ratio of the intensities of 1453 cm^{-1} peak and that of 1181 cm^{-1} peak in the FTIR spectra of P(3HB-co-4HB) and its coating samples

	P(3HB-*co*-4HB)	60Melt	60Dip	60Roll	75Melt	75Dip	75Roll
CI	0.34	0.34	0.26	0.22	0.34	0.26	0.22

The representative X-ray diffractogram of the pure components (biopolymer and paper 75 lb) and their coatings are shown in Figure 25. The X-ray diffractogram of the pure biopolymer showed that the copolyester is a semicrystalline material. Its characteristic reflections have been reported in the literature [86,87,88], and these reflections correspond to a rhombic cell. Since Kraft paper comprises a matrix of long cellulose fibers held together by hydrogen bonding between hydroxyl groups, its crystalline structure might be derived from these fibers. The crystalline structure of cellulose has been well studied [54, 89]. The diffractogram of the Kraft paper shows a well-defined principal peak at $2\theta = 22.5°$ and a secondary peak at $2\theta = 15.5°$. This diffractogram is characteristic of cellulose I [89]. The diffractogram of all the coatings samples showed different characteristics in terms of peak reflections and intensity. It

was observed that the crystalline phase of the biopolymer was present in the melt processed coating samples (75Melt). This behavior could be due to the thick biopolymer layer of this composite. However, a small decrease in the intensity can be observed in the reflection peaks of the coatings with respect to that of pure P(3HB-*co*-4HB). An overview of the diffractogram of the solution processed coating samples (75Dip and 75Roll) indicated few reflection peaks with low intensity of the biopolymer, reflection peaks which could have been masked by the broad amorphous reflection peaks of the paper substrate. These results are consistent with the results of the CI. Roll-coated samples (75Roll) exhibited the poorest characteristic in terms of biopolymer reflection peaks, characteristic which can be due to the thin thickness of the biopolymer layer. Based on the above observation, we can conclude that the different types of composites (melt coating, dip coating and roll coating) showed different structures; therefore they might behave differently in terms of properties.

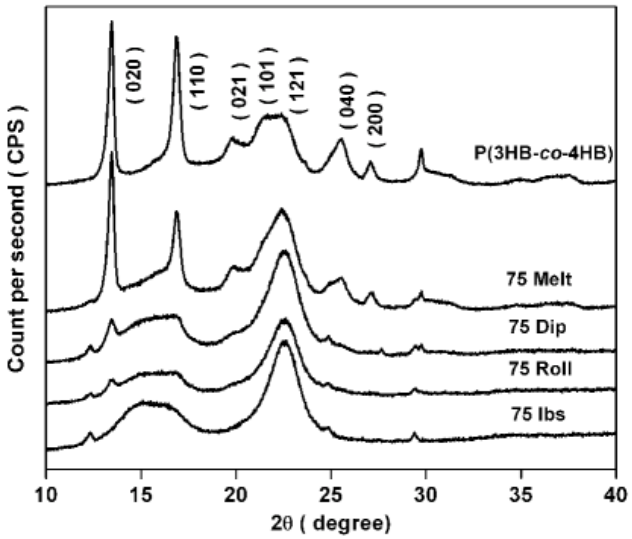

Figure 25. WAXD diffractogram of P(3HB-co-4HB), Kraft paper 75 lb and their coatings

4.2.3 Effect of coatings on the viscoelastic and mechanical properties

Figure 26 and Figure 27 are representative data and illustrate the trends of the dynamic storage modulus (E') and the loss tangent (tan δ), respectively, as a function of temperature for all the samples for pure components (Kraft paper 60 lb and biopolymer) and their coating. E' represents the stiffness of a viscoelastic material and is proportional to the energy stored during a loading cycle. Tan δ is the ratio of loss modulus (E") to storage modulus (E'). It is a measure of the energy lost, expressed in terms of recoverable energy, and represents mechanical damping or internal friction in a viscoelastic region. Table 13 summarizes the glass transition temperature (T_g: temperature at tan δ_{max}) and the dynamic tensile modulus of the samples at various temperatures (-40, 0, 25 and 40 °C).

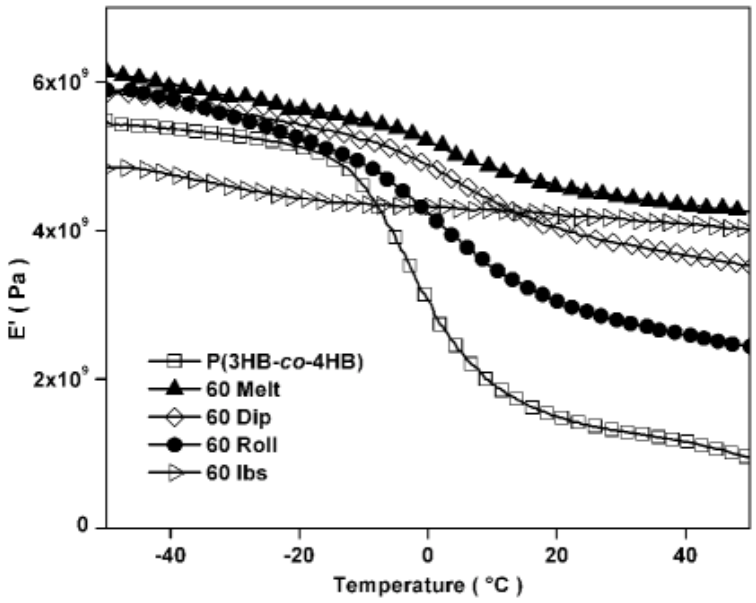

Figure 26. Characteristics of E' of P(3HB-co-4HB), Paper 60 lb and their coatings

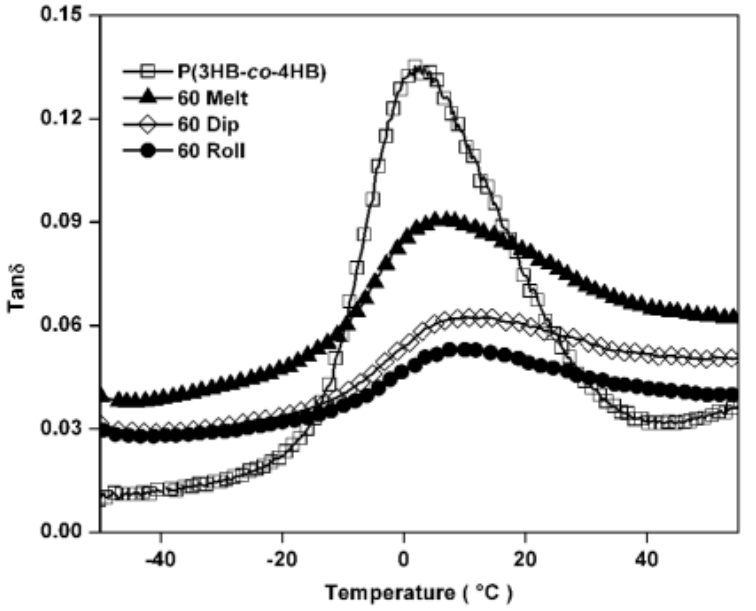

Figure 27. Characteristics of Tan δ of P(3HB-co-4HB) and 60 lb coatings

Table 13. Dynamic mechanical summary for P(3HB-co-4HB), Kraft paper 60 lb, Kraft paper 75 lb, and the coatings

Sample	E'(GPa) -40 °C	E'(GPa) 0 °C	E'(GPa) 25°C	E'(GPa) 40 °C	T_g(°C)
P(3HB-*co*-4HB)	5.40 ±(0.15)	3.20 ±(0.13)	1.39 ±(0.15)	1.20 ±(0.16)	2.00 ±(0.2)
60 lb	4.75 ±(0.20)	4.32 ±(0.20)	4.19 ±(0.18)	4.09 ±(0.20)	-
60Melt	5.95 ±(0.35)	5.18 ±(0.33)	4.51 ±(0.30)	4.33 ±(0.29)	5.20 ±(0.3)
60Dip	5.75 ±(0.18)	4.89 ±(0.15)	3.92 ±(0.19)	3.67 ±(0.15)	9.40 ±(0.3)
60Roll	5.75 ±(0.23)	4.22 ±(0.21)	2.89 ±(0.18)	2.60 ±(0.20)	11.20 ±(0.2)
75 lb	4.95 ±(0.20)	4.55 ±(0.19)	4.48 ±(0.20)	4.43 ±(0.20)	-
75Melt	7.70 ±(0.17)	5.90 ±(0.16)	4.55 ±(0.15)	4.42 ±(0.16)	4.50 ±(0.5)
75Dip	6.41 ±(0.22)	5.44 ±(0.20)	4.37 ±(0.19)	4.40 ±(0.20)	6.90 ±(0.3)
75Roll	5.73 ±(0.15)	5.06 ±(0.14)	4.19 ±(0.17)	3.91 ±(0.15)	10.80 ±(0.4)

The glass transition of the pure biopolymer was 2 °C. As can be observed from the maxima of the tan δ (Figure 27, Table 13), the glass transition temperature shifted to significantly higher temperatures for the coated samples. For 60 lb paper-coated samples, T_g shifted from 2 °C for the neat biopolymer to 5.2, 9.4 and 11.20 °C for 60Melt, 60Dip and 60Roll, respectively. Likewise, for 75 lb paper-coated samples, T_g shifted from 2 °C for the neat biopolymer to 4.5, 6.90 and 10.80 °C for 75Melt, 75Dip and 75Roll, respectively. The shift to high temperature could have indicated favorable attractive interaction at the interface between the biopolymer and the paper substrate. Furthermore, the decrease in the T_g peak intensity for the coated samples could have indicated a modification in the relaxation time of the biopolymer as a result of positive interaction between this latter and the paper substrate. Since the glass transition process is related to the molecular motion, the T_g is considered to be affected by molecular packing, chain rigidity and linearity. For both paper weights, the glass transition temperature was significantly higher in the solvent-based coating than in the melt-based coating. Between the dip and roll coated samples, the roll-coated samples showed higher glass transition temperatures than the dip-coated samples.

In sub-ambient conditions, the dynamic storage modulus (E') of the coatings is higher than that of the biopolymer and the uncoated Kraft papers (Figure 26, Table 13). Over the temperature range, E' of uncoated Kraft papers showed insignificant change. As the temperature increased, E' of coated samples and pure P(3HB-*co*-4HB) decreased. However the decrease is higher for the neat biopolymer than for the coated samples. An overview of Table 13 showed that for both coated paper weights, E' was significantly higher in the melt-based coating than in the solvent-based coating. Also, with respect to the uncoated paper weight (60 lb and 75 lb), an increase in E' of the coated paper weights is noticeable in sub-ambient. For example at -40 °C E' for 60 lb paper coated samples increased to 25.3, 21 and 21% for 60Melt, 60Dip and 60Roll sample, respectively. Similarly, E' for 75 lb paper coated samples increased to 55.6, 29.5 and 15.8% for 75Melt, 75Dip and 75Roll samples, respectively. The increase in E' reflected the

coating structure results obtained by ESEM, FTIR and WAXD for each coated sample. The increase in the T_gs and the E' of the coated samples in comparison with the P(3HB-*co*-4HB) can be due to good adhesion between the biopolymer and the uncoated Kraft papers. A micromechanical model was utilized for predicting the coating properties from its pure components to that obtained experimentally.

$$E_{coating} \times A_{coating} = E_{paper} \times A_{paper} + E_{biopolymer} \times A_{biopolymer}$$

Where E is the modulus and A the area. Using this, it was found that the experimentally obtained values of E' are significantly greater than the predicted composite values (Table 14). This indicated that the coating interaction with the paper significantly enhances its own mechanical contributions to the coated paper. Furthermore, we noticed that the reinforcement potential is more effective in melt-processed coating samples than solution-processed coating samples, with roll coating samples displaying less reinforcement.

Table 14. Dynamic mechanical advantage of composite over the pure components

Sample	-40 °C	0 °C	25°C	40 °C
60Melt	22.41%	25.45%	21.41%	20.30%
60Dip	18.82%	17.37%	03.80%	02.75%
60Roll	19.70%	09.6%	03.10%	01.40%
75Melt	52.77%	37.85%	13.15%	09.80%
75Dip	27.52%	25.90%	10.72%	08.84%
75Roll	16.90%	15.31%	05.94%	01.93%

Damage resistance and damage tolerance under impact loading are important composite materials characteristics because the military packaging is often susceptible to impact. Velocity impact can introduce severe internal damages to composite structures and significantly reduce their load-carrying capacity [90]. Velocity impact damages may consist of cracks, delamination, and fiber breakage in a zone surrounding the impact point. When a foreign object impacts on a composite material, the impact energy is absorbed by the composite and damages such as delamination, fiber breakage, and cracks occur in the composite structure. The mechanical properties of the specimens were evaluated and are shown in Figure 28. Figure 29 illustrates the representative data of load as a function of deflection and time, respectively, for Kraft paper 75 lb and their coating. Four tests were run on each specimen. The average maximum load, total energy for the Kraft papers and the coatings were recorded in Table 15. From Figure 28, it is clear that the 75Melt samples showed more elastic features than other specimens since the 75Melt samples responded more quickly upon impact loading. After the impact, it was observed that the melt-processed samples showed large crack lines whereas the solution-processed ones exhibited medium crack lines, with respect to the pure Kraft paper samples as shown by the representative data in Figure 30, Figure 31, Figure 32, and Figure 33. These different characteristics of the coatings can be related to the difference in the coating texture which plays an important role in coating performance.

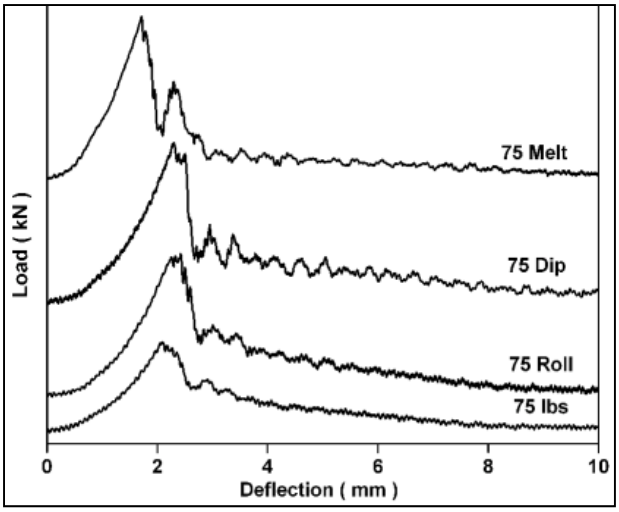

Figure 28. Load versus deflection plots of Kraft paper 75 lb and the coatings

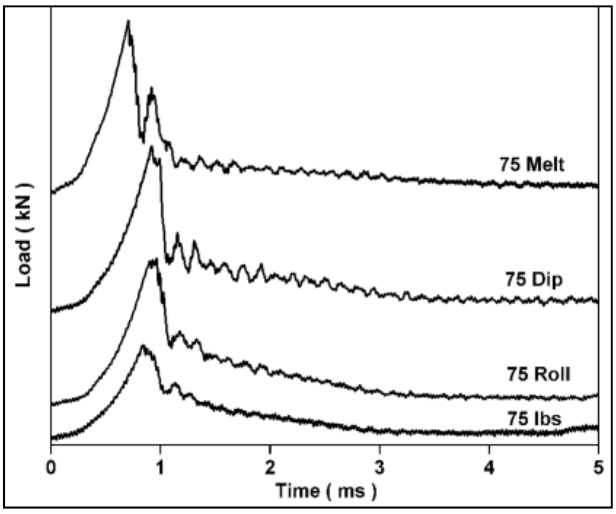

Figure 29. Load versus time plots of Kraft paper 75 lb and the coatings

Under high impact, the coated papers indicated better resistance than uncoated paper. However, melt- applied biopolymer samples showed enhanced adhesion and the delamination occurred in multiple stages resulting in enhanced fracture toughness. Table 15 indicated that both 60 and 75 lbs papers showed similar trends in impact performance. The total energy was higher for the melt- processed samples compared to the solvent- processed samples. Improvements of approximately 45% were observed for the melt- processed samples while solvent- based samples showed approximately 30% improvement in energy absorption capability**.** The maximum load followed the same trend and improvements of around 85% were observed for the melt- processed samples while solvent- based samples showed around 75%.

Table 15. Average maximum load and the total energy for Kraft papers and the coatings

Sample	Max. load ($kNx10^{-3}$)	Total energy (mJ)
60 lb	19 (±0.8)	20 (±0.5)
60Melt	31 (±1.5)	29 (±2.0)
60Dip	29 (±0.7)	26 (±1.0)
60Roll	27 (±2.2)	24 (±1.0)
75 lb	20 (±1.2)	22 (±0.5)
75Melt	37 (±1.8)	31 (±2.5)
75Dip	35 (±0.6)	28 (±1.0)
75Roll	31 (±2.4)	25 (±1.0)

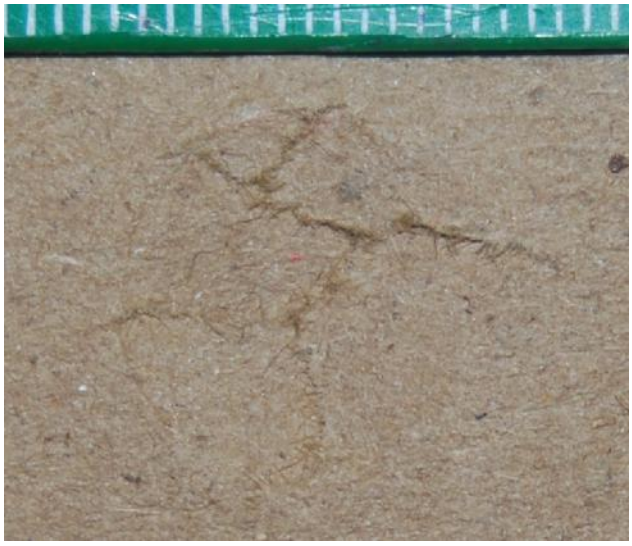

Figure 30. Fractured surface of 75 lb paper after impact test

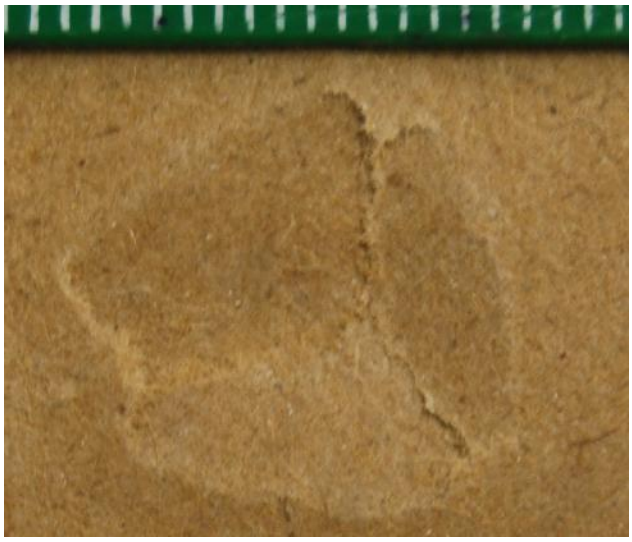

Figure 31. Fractured surface of 75Roll sample after impact test

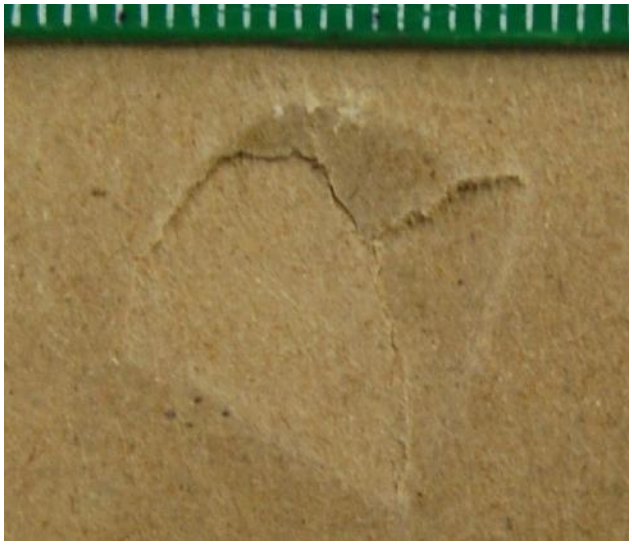

Figure 32. Fractured surface of 75Dip sample after impact test

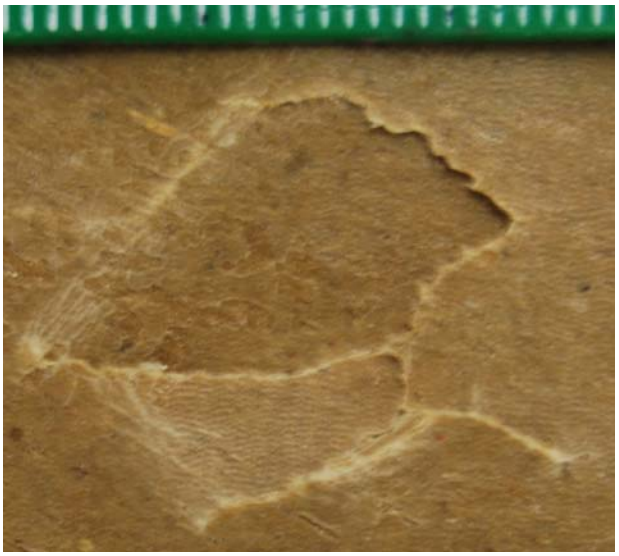

Figure 33. Fractured surface of 75Melt sample after impact test

This study has shown that P(3HB-*co*-4HB) coated paper can be obtained through solution and melt processed techniques. ESEM results indicated the formation of biopolymer layers with variable thickness on the paper substrate, depending on the type of coating technique used. FTIR results showed that the reflectance peaks were from the biopolymer, indicating retention of the chemical structure of the pure P(3HB-*co*-4HB) in the coatings. WAXD results indicated that the coatings samples showed different characteristics in terms of peak reflections and intensity, with the melt-processed coated samples showing most of the crystalline structure of the biopolymer. DMA results showed that the melt-processed samples exhibited better storage modulus in subambient conditions and that the improvement in storage modulus was higher for the higher weight Kraft paper. At room temperature and above, the coatings showed values of the storage modulus close to those of Kraft paper but higher than those of the biopolymer. Impact results conducted at room temperature showed that the melt-based samples had a higher total energy absorption capability indicating superior adhesion to the solution-processed samples.

5.0 Corrugated Coated Structures

5.1 Materials and Methods

5.1.1 Fiberboard Materials

The corrugating and manufacturing trials for all the corrugated prototypes were conducted at Interstate Containers at the Lowell, MA and Cambridge, MD plants. During the study, several container designs, fiberboard grades, and functional coatings were used during combined board manufacture and subsequent conversion to the finished containers.

The fiber materials used to create initial fiberboard structures are listed in Table 16. They included 90 lb paper for both the single and double liner with 36 lb treated medium with an EvCo (from EvCo Research, LLC.; Pendergrass, GA) wax alternative medium (WAM™) as shown in Table 16. In addition, 56 lb liners (both single and double) which were two-stage coated with Spectra-Kote (from Spectra-Kote Corp., Gettysburg, PA) were used with a 36 lb medium. Typical processing parameters for corrugators are shown in Appendix A.

Table 16. Interstate trial for prototype fiberboard

Trial	Single Face liner (lb)	Double face liner (lb)	Medium weight (lb)	Total weight (lb/1000 ft^2*)
1	90	90	36 with EvCo	216
2	90	90	36 with EvCo	216
3	56	56	36 with EvCo	148
MRE™ -SF	90	90	Liner Control	397

*For corrugating manufacturing

Note: All weights include the liners.

The fiberboard was then inspected for warp or any visual defects such as blisters, puckers, washboard, or brittle bond. Stacks of combined board were allowed to cure for 18-20 h prior to sample collection.

The fiberboard structures were downselected to create the combined board structures for the prototype fiberboard containers which consisted of coated 69 lb inner and external liner, a 36 lb medium with a C-flute profile and two coating alternatives within the medium. In the corrugated industry the units of measurement are English, rather than SI, and are reported here as such. The medium incorporated either a WAM™ or Tallow coated medium to improve water resistance within the structure. The combined board formed a single-wall structure, utilizing two coated liners and a coated medium which utilized commercial Spectra-Kote coatings from Spectra-Kote Corporation. The Spectra-Kote (sg 48m) coating is an aqueous based multi-functional barrier designed to provide superior water resistance. The barrier provides an enhanced paper capable of enduring humid environments. The coating is a non-hazardous water-based polymer coating that is Food and Drug Administration (FDA) compliant and is used in several commercial applications involving produce and poultry box designs [91].

The materials/structures that were used during testing were from three corrugated grades which utilized 55 lb, 69 lb and 72 lb liners and coated 30 and 36 lb mediums. The corrugated samples utilized a 30 lb C-flute WAM™ and also a Tallow coated medium in each design. An antiskid coating was also applied to the liners to enhance stacking performance of the finished

containers. The structures that were tested initially consisted of four distinct corrugated design styles and were later downselected to two corrugated regular slotted container (RSC) design structures: an RSC with an insert (RSC IN) and an RSC with an internal width divider (RSC WD). The current MRE™ solid fiberboard container and UGR™ A Version containers from Temple Inland were used as the control throughout the study and laboratory trials. All adhesives for the trials employed a WAM™ starch formula adhesive which incorporates 30% solids with a Harper Love resin to make the adhesive waterproof. Initial trials were run with a water resistant formulation and then changed to a water proof formulation. No issues with rheology that would indicate either abnormal viscosity or "fish eye" (uncooked starch) were observed.

5.1.2 Designs for the Military Containers

The two prototype MRE™ designs are shown in Figure 34. The first design (RSC-IN, Figure 34a) was constructed into an industry standard RSC with internal dimensions of 17 x 10.5 x 8.875 in. The corrugated insert wraps around the perimeter of the container's footprint to provide additional support (i.e., added stacking strength) under load and to improve puncture resistance along the side panels of the container. The second design (RSC WD, Figure 34b) consists of a one-piece RSC design with the internal divider built into the end panel. This RSC WD design is commonly referred to as a center support bridge container which has regular slotted flaps on top and bottom for normal closure and an added panel in center of box for stacking strength. The additional panel also provides two separate compartments for the UGR™ components and MRE™ rations. The prototype UGR™ design, shown in Figure 35, also incorporated the RSC WD design with internal dimensions of 23.25 in long, 13 in wide and 8.4375 in deep.

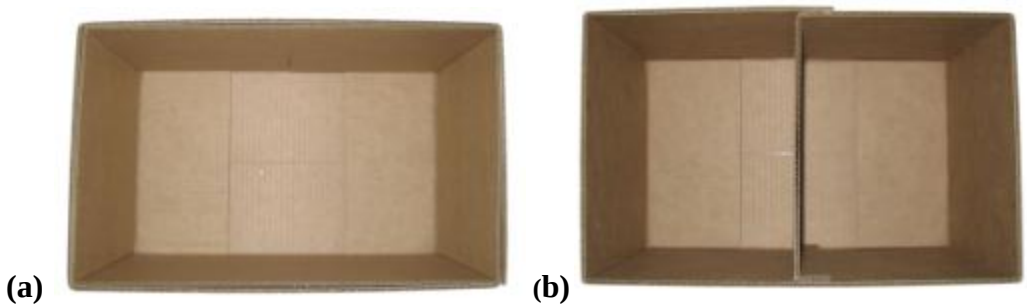

Figure 34. Prototype MRE™ designs constructed from corrugated fiberboard: (a) RSC IN; (b) One-piece RSC WD

Figure 35. UGR™ WD design used to hold UGR™ A ration components

The existing SF container (MRE™ SF) consisted of a die cut regular slotted container from solid fiberboard material and a corrugated insert for added compression support. The fiberboard box was constructed according to RSC-L, of ASTM D 5118/D 5118M, Standard Practice for Fabrication of Fiberboard Shipping Boxes, and grade V2s of ASTM D 4727/D 4727M Standard Specification for Corrugated and Solid Fiberboard Sheet Stock (Container Grade) and Cut Shapes [92,93]. The solid fiberboard material consisted of two outer facings of 90# wet strength linerboard and an inner ply of 69# linerboard. The box liner is a full inside width box liner fabricated from grade W5c fiberboard in accordance with ASTM D 5118/D 5118M, except the terminal ends of the liner overlap a minimum of 2 in. The inside dimensions of the MRE™ container are 16.6875 in long, 9.125 in wide and 10.25 in deep [94].

The existing UGR™ A container was constructed into a RSC from fiberboard grade V3c of ASTM D 5118/5118M. The RSC material is a water resistant single-wall (B-flute) container with a minimum bursting strength of not less than 400 psi. The UGR™ A design also incorporated two corrugated inserts within the container to provide additional support under load and to make two equal compartments for the UGR™ items. The inside dimensions of the UGR™ A container are 23.75 in long, 13.1875 in wide, and 8.75 in deep.

5.1.3 Procedure --Cobb Evaluation of Fiberboard Material

This test will compare the water resistance of existing fiberboard materials used in the MRE™ and UGR™ systems to prototype materials that utilize Spectra-Kote coatings on the internal and external facings and fluted mediums of corrugated fiberboard.

The Cobb Test Method, T 441 om-04 Water absorptiveness of sized (non-bibulous) paper, paperboard, and corrugated fiberboard [95] from TAPPI was used to determine the amount of water absorbed after 30 m by the surface of a 100 cm² test sample under controlled conditions.

The test measures paper's water absorption rate and is expressed as the amount of water pick-up per unit surface area of paper. The United Nations (UN) and Code of Federal Regulations require that the 30-min pick-up must be 155 g per square meter or less for containerboard used in hazardous material transport and were used as a benchmark for military ration containers. The Cobb test is an economical and practical means of determining liquid absorptiveness or resilience of treated and untreated papers, boards, fabrics and other sheet materials.

The water absorption apparatus or Cobb tester permits one side of the specimen to be wetted uniformly throughout the duration of the test period. The Cobb tester as shown in Figure 36 comprises of a metal cylinder with an 11.28 ± 0.02 cm inside diameter that is clamped to a flat base plate. The test also requires blotting paper, 200-250 g/m^2 with a capillary rise of 50-100 mm of water as measured by the Klemm method and distilled or deionized water to wet the sample surface.

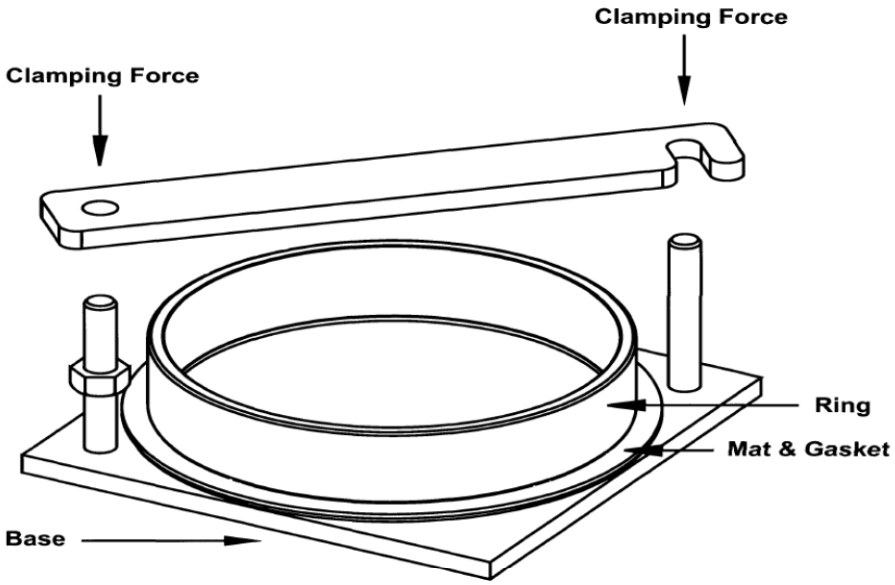

Figure 36. Water absorption apparatus or Cobb tester

The test samples were subject to standard conditions at 23 °C and 50% RH for a period of 24 h prior to testing in accordance with TAPPI T 402 Standard Conditioning and Testing Atmospheres for Paper, Pulp Handsheets, and Related Products [96]. Prior to testing, each specimen was weighed to the nearest 0.01 g. Each side of the sample was tested, which included the single face liner, which is the inner liner, and the double back liner, which makes up the outer liner of the combined board. Three samples from each set were tested. Once the sample was secured, 100 mL of distilled or deionized water (23 ± 1 °C) was poured into the ring as rapidly as possible thus giving a head of 1.0 cm, then the timer was started immediately and ran for the 30-min test duration.

Weight of water, g/m^2 = [Final weight, g – Conditioned weight, g] × 100. The Cobb value was calculated as the average weight of the water absorbed in g/m^2 by the three samples, for each side. Test materials included prototype fiberboard of two distinct grades with 55 lb and 69 lb liner facings and a 30 lb fluted medium with a C-flute profile. In addition to the fiberboard grades, two medium coatings were also used to treat the fluted material of the structure. These coatings included the WAM™ coating and the Tallow coating from Spectra-Kote Corporation. The prototype materials were directly compared to existing fiberboard grades for the MRE™ and UGR™ systems, as shown in Table 17.

Table 17. Sample material for 30-min Cobb test

Material Description	Sample I.D.
55# sg48m / 30# WAM / 55# sg48m	1
69# sg48m / 30# WAM / 69# sg48m	2
55# sg48m / 30# Tallow / 55# sg48m	3
69# sg48m / 30# Tallow / 69# sg48m	4
45# / 30#B / 45# Liner	5
45# / 30#B / 45# Liner Coated	6
69# sg48m / 30#WAM / 42#kraft / 30#sc / 69# sg48m	7
UGR WD 69# sg48m / 30# WAM / 69# sg48m	8
MRE SF™ Solid Fiberboard (AmeriQual)	9
MRE SF™ Liner	10
V3c	11
UGR A	12
UGR A Liner	13

5.1.4 Cold Weather Testing of Corrugated/Solid Fiberboard Containers

In February 2008, NSRDEC partnered with Toledo Forest Products Labs to evaluate weathered fiberboard containers for the MRE™ fiberboard containers. The environmental test exposed the containers to high winds and freezing conditions on the Bass Islands near Toledo, Ohio. Material inspections took place at the end of the test period and lasted for 1 month. The test samples were placed directly on the ice/ground for the duration of testing and at times of high precipitation were in snow, as shown in Figure 37a. At times, they were covered by snow. Figure 37b shows the set of containers after snow was cleared.

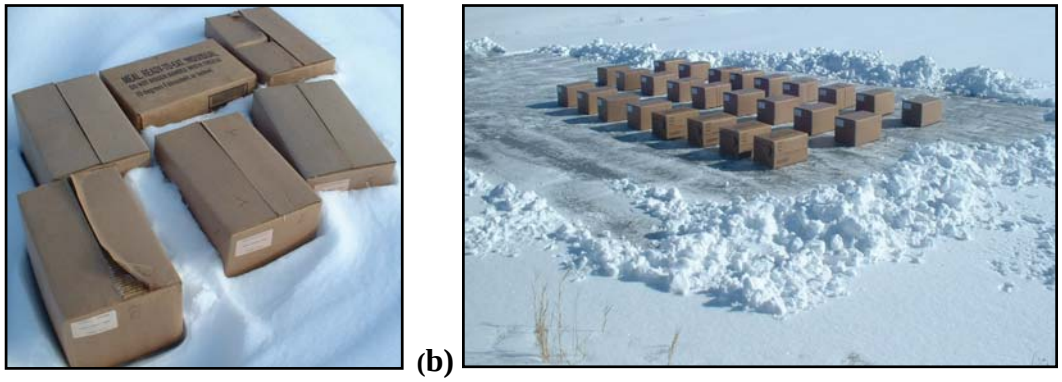

Figure 37. Corrugated/solid fiberboard test samples during cold weather testing:
(a) Small set of samples in snow; (b) Large set of samples with snow cleared for testing

The sample set of weathered containers were all constructed from the prototype corrugated fiberboard, manufactured by Interstate Container in January 2008. The test material features a water resistant WAM™ coating from Spectra-Kote Corporation, which can be repulped and recycled. Two corrugated grades which utilized 55# and 72# facings and a coated

30# C flute medium with WAM™ were used. The existing solid fiberboard (MRE™ SF) container from Temple-Inland was also tested as the control.

During the cold weather study, 18 samples (15 corrugated and 3 solid fiberboard samples) were used and evaluated. Nine additional samples (eight corrugated and one solid fiberboard) also had a 66 lb steel weight on the top of the container to simulate the weight of three additional boxes. This stacking arrangement is the typical stacking pattern for the MRE™ ration when configured in a unit load.

The sample containers were taken out of the elements twice during the test, once to weigh and move the containers to Bass Islands and once to remove the containers from a prolonged period of freezing rain. The samples were placed in direct contact with the ground/ice for the duration of the cold weather test. The containers were exposed to conditions of high moisture and at times were in snow (Figure 37) after long periods of precipitation. During the 27 test days, they were subjected to an average low temperature of 18 °F and an average high of 34 °F (based on weather.com for Toledo, OH – February 13 to March 10), as shown in Figure 38.

The test samples were inspected for physical damage and wear of the container surface. Any notable failures such as delamination, joint failure, and excessive wear were noted at the container edges, corners, slots, folds and glue joints.

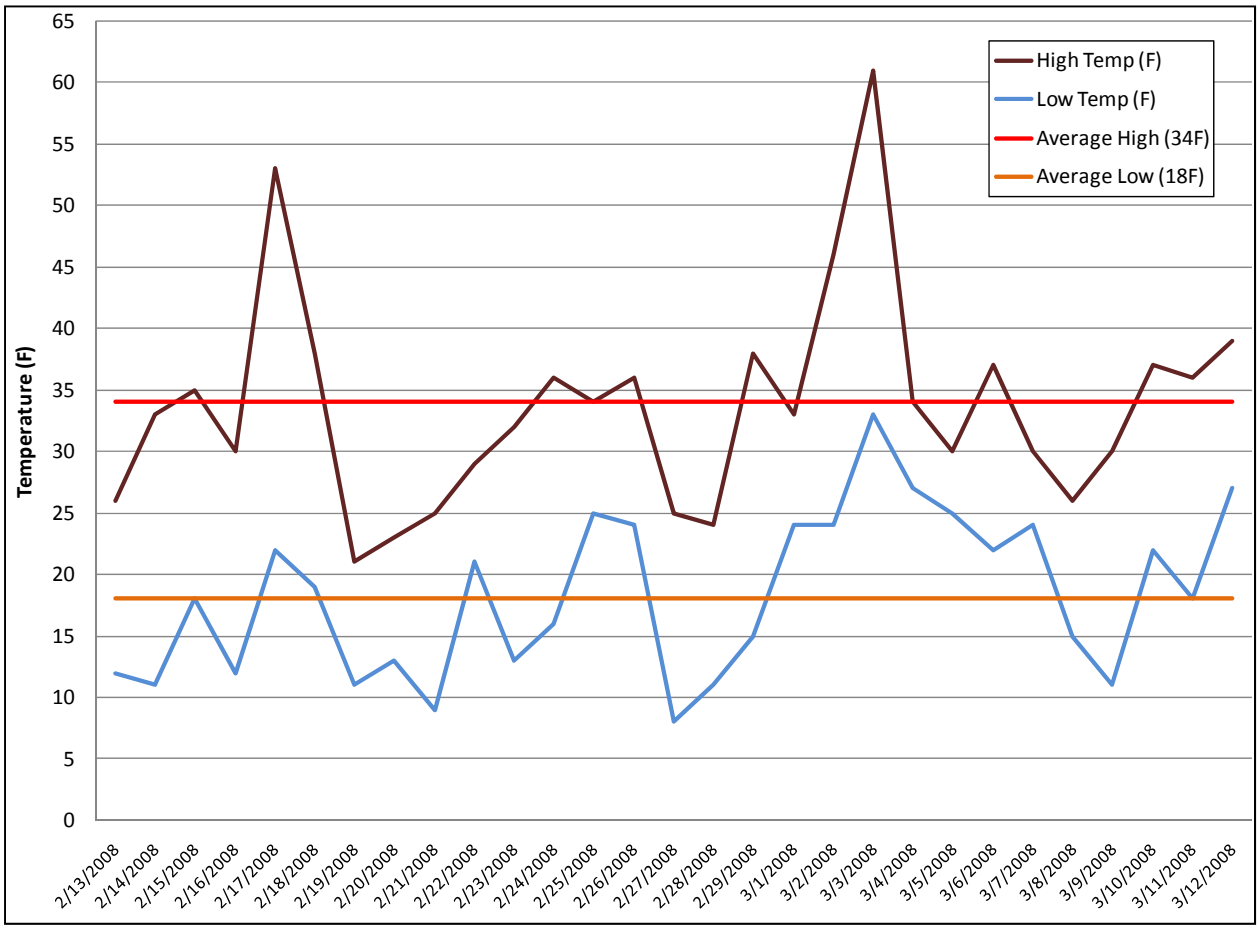

Figure 38. Average high and low temperature for the Toledo area, taken from weather.com

An inspection was also conducted on weathered containers that were exposed to high winds and freezing conditions for nearly a month. In general the coatings, joint adhesive and corrugated structures remained intact with some samples having only minor delamination at the top or bottom flaps.

5.1.5 Compression Testing

The box compression test is a dynamic measurement of the momentary force necessary to cause a box to fail or crush. It is normally conducted under standard laboratory conditions, 23 °C, and 50% RH and provides results in force and deflection. Box compression strength is the primary characteristic used to define fiberboard container performance and is one of the key properties used to evaluate the ability of a shipping container, component, or unit load to successfully endure compressive loads during transportation, storage and handling operations. Two categories of loading conditions exist which include dynamic loading during handling and transport and static loading which takes place during long term storage or stacking situations. In this study, the effects of dynamic loading on prototype corrugated containers and existing rations containers was investigated.

The first materials used to create some fiberboard structures were 90 lb paper for both the single and double liner with 36 lb treated medium with an EVCO (WAM™) as shown in Table 16. In addition, 56 lb liners (both single and double) which were two-stage coated with Spectra-Kote were used with a 36 lb medium. Typical processing parameters for corrugators are shown in Appendix A.

5.1.6 Rain Compression Testing

Stacked columns of MRE™ rations of 63 lb were arranged into a column stack of four containers, simulating the stack height of one unit load of MRE™ rations. Two columns of each sample set were exposed to high intensity rain and the resulting deflection values were recorded. The columns, as shown in Figure 39, were exposed to high intensity rain conditions which ranged from 3.1 to 5.4 in/h with a room temperature 37.8 °C. The performance of each container was measured by recording the overall deflection within the column stack, measuring from the top corner of the highest container to the base of the stack. The deflection values were recorded hourly over the 8 h rain test and also after 93 h from the beginning of the test.

The MRE™ compression study focused on individual compression strength of fiberboard containers filled with MRE™ ration components and were exposed to standard conditions (50% RH, 23 °C), high humidity (85% RH, 37.8 °C) and two independent studies at 4 and 8 h of high intensity rain conditions at 37.8 °C to simulate extreme tropical climates.

The prototype corrugated containers and control samples were subjected to high intensity rain conditions followed by compression testing of the filled fiberboard containers. The duration of rain exposure and recovery time varied during testing to analyze the combining effects that water exposure and recovery had on the fiberboard containers. The information presented will highlight several studies investigating the compression strength and coating performance of corrugated containers under adverse environmental conditions.

A summary of the test samples tested for compression can found in

Table 18, which lists the containers and their board descriptions. Overall the study analyzed two prototype designs that utilized four different combined board structures as shown above.

Table 18. Test matrix for rain study and compression analysis

Container	Board description
RSC IN	69# sg48m / 30# WAM™ / 69# sg48m
RSC WD	69# sg48m / 30# WAM™ / 69# sg48m
RSC IN	69# sg48m / 30# Tallow / 69# sg48m
RSC WD	69# sg48m / 30# Tallow / 69# sg48m
MRE SF	MRE solid fiberboard container†
UGR WD	69# sg48m / 30# WAM™ / 69# sg48m
UGR A	Unitized group ration container†

†See container †specifications in NSRDEC specification sheets.

The primary objective of the study was to expose prototype corrugated samples and existing fiberboard containers used for UGR™ and MRE™ rations to wet environments and evaluate the coating performance and mechanical properties under a dynamic compressive load.

Prior to environmental exposure and compression testing the MRE™ ration containers were packed with 12 standard MRE™ rations in a standard configuration of two vertical rows of six rations to simulate actual packing conditions and were free of any damage or defects (abrasions, punctures, etc.) that may accelerate water absorption or alter compression performance. The packed containers were then sealed with hot melt adhesive and strapped with two girthwise nonmetallic straps. The UGR™ containers were tested without ration components as the items do not help support any externally applied load.

The existing solid fiberboard containers and prototype designs were subjected to wet environmental conditions followed by laboratory compression testing of the fiberboard containers. The test samples were exposed to high intensity rain conditions from four to eight hours in order to investigate the relationship between increased rain exposure and the resulting failure modes of the fiberboard containers. The recovery time was set at 48 h as the containers were allowed to recover or dry prior to individual container compression testing. An additional test investigated the structural integrity of the containers under load within adverse environments. This 8 h stack test, as shown in Figure 39, measured the overall deflection within each column stack over specified time periods.

Figure 39. MRE™ test samples during 8 h stack rain test

The spray test method, ASTM D 951-04 *Water Resistance of Shipping Containers by Spray Method*, was used to determine the ability of the container to resist deterioration caused by water or the ability of the container to protect the contents from water [97]. The test was used in combination with standard compression testing following ASTM D 642-05 *Determining Compressive Resistance of Shipping Containers, Components, and Unit Loads* [98]. The compression test method, TAPPI T 804-06 Compression test of fiberboard shipping containers, was also used as a reference during the 4 h and 8 h spray test [99].

The spray test was conducted at the Doriot Climatic Chambers at the NSRDEC and followed ASTM D951-04 to perform the four hour, eight hour and eight hour stack test in adverse weather environments. The testing area included a bottom that was covered with a false floor of wooden pallets to reduce water pooling as shown in Figure 40. The design of the spray nozzles were of ideal size and spaced so that the specified intensity of spray fell uniformly over the test area. In two specific areas where the rain droplets hit the exposed copper piping there were higher intensities of rain as it dripped from the piping, these areas were excluded from testing as the samples were moved to an area not directly below the copper pipes. The nozzles were located within the testing chamber so that the droplets fell from gravitational force only when they struck the test specimens. Flow control valves were used to control the intensity (flow rate and droplet size) of the spray as required. The spray intensity as shown in Table 19 was controlled during testing with headers “one” and “two” of the rain chamber open and the flow control valve set at 35%. For this study, the water remained at standard temperatures with the temperature of the room maintained at 37.8 °C to simulate a tropical environment or worst case scenario. This study measured the overall deflection within each stacked column over specified time intervals.

Figure 40. MRE™ test samples during 8 h high intensity rain exposure

Table 19. Summary of averaged conditions during the 4 h/8 h rain exposure

	% RH	Temp (°C)	Wind speed (mph)	Rain intensity (cm/h)*
4 h MRE rain test	45.7	38.0	3.5	12.2 - 14.2
8 h MRE rain test	49.2	37.7	3.4	8.9 - 14.7
8 h MRE stack test	46.2	37.9	3.3	7.9 - 13.7
4 h UGR rain test	56.5	38.0	3.2	7.6 - 12.2
8 h UGR rain test	55.5	38.2	3.2	7.6 - 12.2

Note: Values recorded every hour during testing. *Intensity of rain may have varied by location..

The fiberboard structures as shown in Figure 40 were exposed to 4 and 8 h time intervals of the prescribed climatic conditions. Ten samples of each set were inspected and tested after 4/8 h of high intensity rain exposure. The samples remained in the climatic testing chamber for a period of 48 h prior to compression testing. Additional sets were tested at 50% RH/23 °C and 85% RH/37.8 °C to further analyze compression performance in specified environments with a summary of all the conditions as shown in Table 19. The baseline test at 50% RH and 23 °C was used to compare to the three other tests at elevated humidity levels.

Measurements of top-to-bottom compression strength and the container's load-deflection behavior were analyzed during the study and compared directly to existing ration containers. The applied load was applied at a constant rate until the container failed catastrophically. The value obtained from this test is referred to as the ultimate yield strength of the box. This is the maximum value that the container can withstand during top loading. In actuality, the maximum top load applied to the container can be only a fraction of this amount as many events and conditions combine to reduce the ultimate yield strength of the containers. Some specific examples that reduce compression performance of ration containers include: adverse weather

environments and storage conditions, rough handling, long term storage, pallet overhang, internal pallet overhang, misaligned columns and bulging of secondary containers as mentioned in the background section of this report.

The container compression strength was measured on a fixed platen, L.A.B. Validator Two, compression tester utilizing Lynx ValViewPRO v2.1 compression software. Measurements of compression strength and the container's load-deflection behavior were recorded for top-to-bottom strength and tested in normal stacking arrangements with the applied load traveling perpendicular to the opening plane. In contrast, the current solid fiberboard containers are stacked on the side panels with the applied load traveling parallel with the opening plane. Top-to-bottom compression occurs when the container is in a stack or part of a palletized system of containers with pallets loaded on top of other unit loads. The compressive load started at a preload of 50 lb with the exception of the UGR™ A containers which started at a preload of 100 lb. Each sample was tested at a constant rate of 0.5 in/min until the critical or catastrophic failure occurred or the onset of product support.

5.1.7 Airdrop Procedure for Fiberboard Containers

Combat rations must also be able to be delivered through aerial transport. The following samples shown in Table 20 were used for an initial air drop evaluation of the fiberboard containers. Aerial delivery trials were conducted at the Yuma Proving Grounds to evaluate the package integrity and survivability of prototype MRE™ containers using low cost aerial delivery systems. The type of aerial delivery system, total weight, dimensions and altitude were all reported. After the airdrop test, samples were analyzed for glue joint failures, compression marks and other material failures.

Table 20. Fiberboard containers for air drop

Container	Board description	Quantity	Load #
MRE SF (Control)	90#WS / 69# / 90# WS	9	1
RSC IN[1]	55# sg48m / 30# WAM™ / 55# sg48m	9	2
RSC WD	55# sg48m / 30# WAM™ / 55# sg48m	9	3
RSC IN[1]	69# sg48m / 30# Tallow / 69# sg48m	9	4
RSC WD	69# sg48m / 30# Tallow / 69# sg48m	9	5
RSC DW	69# sg48m / 30# WAM™ / 42# / 30# SC / 69# sg48m	9	6

[1]Corrugated insert - 45# / 30# Medium / 45#

5.2 Results and Discussion

5.2.1 Cobb Test Results

Test results from the two independent studies as shown in Table 21 have demonstrated that the prototype coated material has improved water resistance over the existing fiberboard material when exposed to 30 min of continuous water contact. NSRDEC results show in Figure 41 that the WAM™-coated material for the 55 lb and 69 lb fiberboard exhibited a 94% and 89% reduction, respectively, in Cobb value when compared to the MRE™ solid fiberboard. The Tallow-coated material for the 55 lb and 69 lb fiberboard exhibited an 82% and 86% reduction

respectively in Cobb value when compared to the MRE™ solid fiberboard. When comparing the prototype fiberboard to the UGR™ fiberboard material, the WAM™-coated material for the 55 lb and 69 lb fiberboard exhibited a 93% and 88% reduction, respectively, in Cobb value and the Tallow-coated material for the 55 lb and 69 lb fiberboard structures exhibited an 80% and 85% reduction respectively in Cobb value when compared to the UGR™ fiberboard material. The Spectra-Kote assessment, as shown in Figure 42, had higher levels of variation and in general higher Cobb values. When comparing results from the independent studies as shown in Figure 43 and Figure 44, the Spectra-Kote results for the military grade fiberboard (Samples 9-13) had consistently higher Cobb values when compared to the NSRDEC study. The results from the prototype materials (Samples 1-8) were comparable to each other as most were within the standard deviation.

Table 21. 30 min Cobb test results -NSRDEC and Spectra-Kote Corporation

Container		Double back (outside				Single face (inside			
		NSRDEC		Spectra-Kote		NSRDEC		Spectra-Kote	
Material description	Sample ID	AVG	S.D	AVG	S.D.	AVG	S.D.	AV	S.D.
55# / 30# W / 55#	ID 1	5.8	0.3	9.0	1.7	5.1	1.6	9.0	1.0
69# / 30# W / 69#	ID 2	11.0	1.9	12.0	1.0	14.3	1.1	16.7	6.4
55# / 30# T / 55#	ID 3	17.3	0.8	18.0	2.0	17.3	1.1	16.3	1.2
69# / 30# T / 69#	ID 4	13.4	0.5	12.7	4.7	18.8	1.9	21.0	3.6
45# / 30#B / 45# liner	ID 5	103.4	1.4	150.3	6.4	103.7	1.9	184.0	66.7
45# / 30#B / 45# liner coated	ID 6	41.3	3.4	44.7	8.4	8.1	0.5	10.7	0.6
69# / 30#W / 42#kr / 30#sc / 69#	ID 7	11.2	0.6	14.0	3.5	10.4	0.6	20.0	9.6
UGR WD 69# / 30# W / 69#	ID 8	7.5	1.5	18.7	4.6	8.9	1.3	22.0	1.7
MRE SF solid	ID 9	96.6	1.3	126.0	7.9	96.8	0.3	131.0	9.8
MRE SF	ID 10	89.5	10.2	125.0	8.9	93.6	1.8	123.3	5.1
V3C	ID 11	102.0	1.3	126.7	17.0	102.1	0.1	131.7	9.1
UGR A	ID 12	88.7	1.1	122.0	25.9	85.6	2.1	136.7	15.5
UGR A liner	ID 13	85.8	3.8	116.3	5.5	90.0	0.7	124.0	13.7

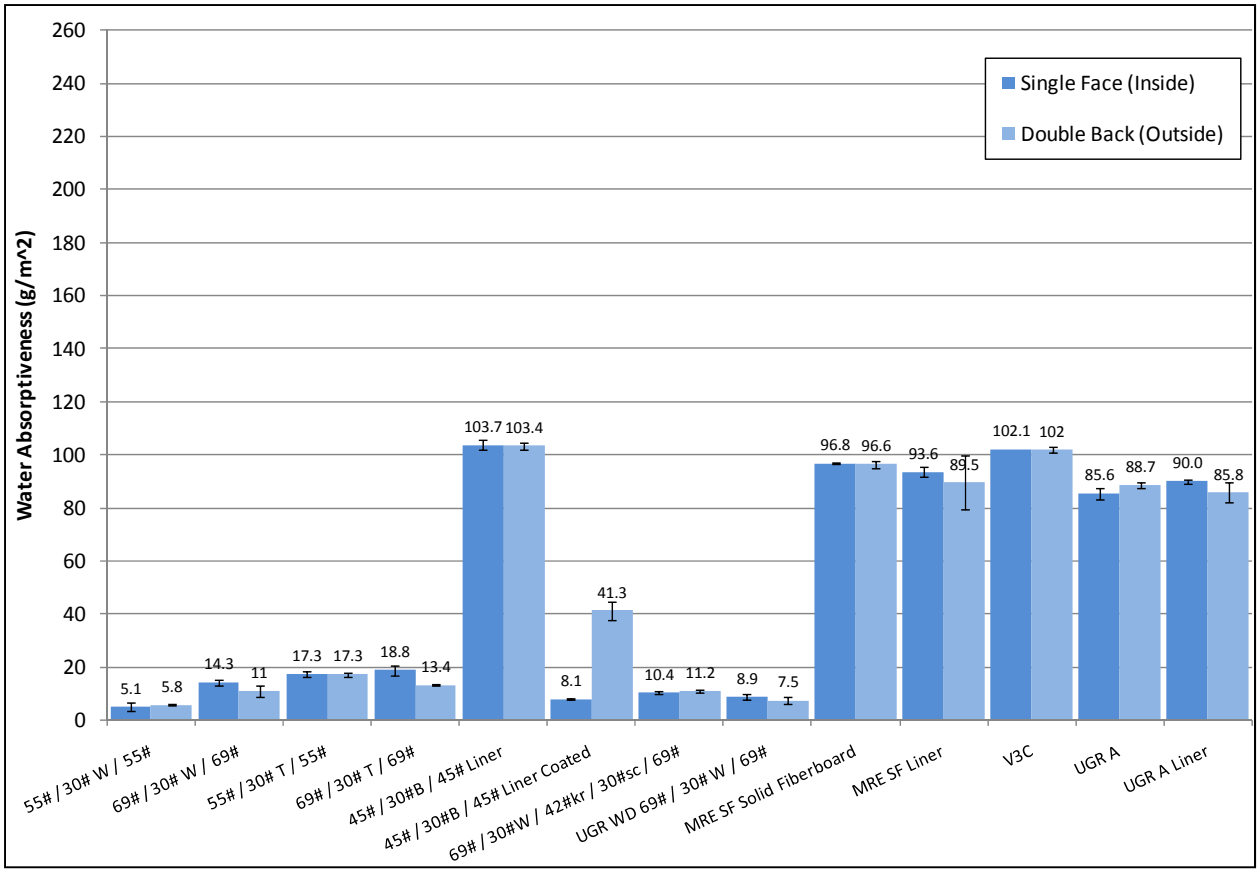

W – WAM™-coated medium

T – Tallow-coated medium

Figure 41. 30 min Cobb test results performed by NSRDEC

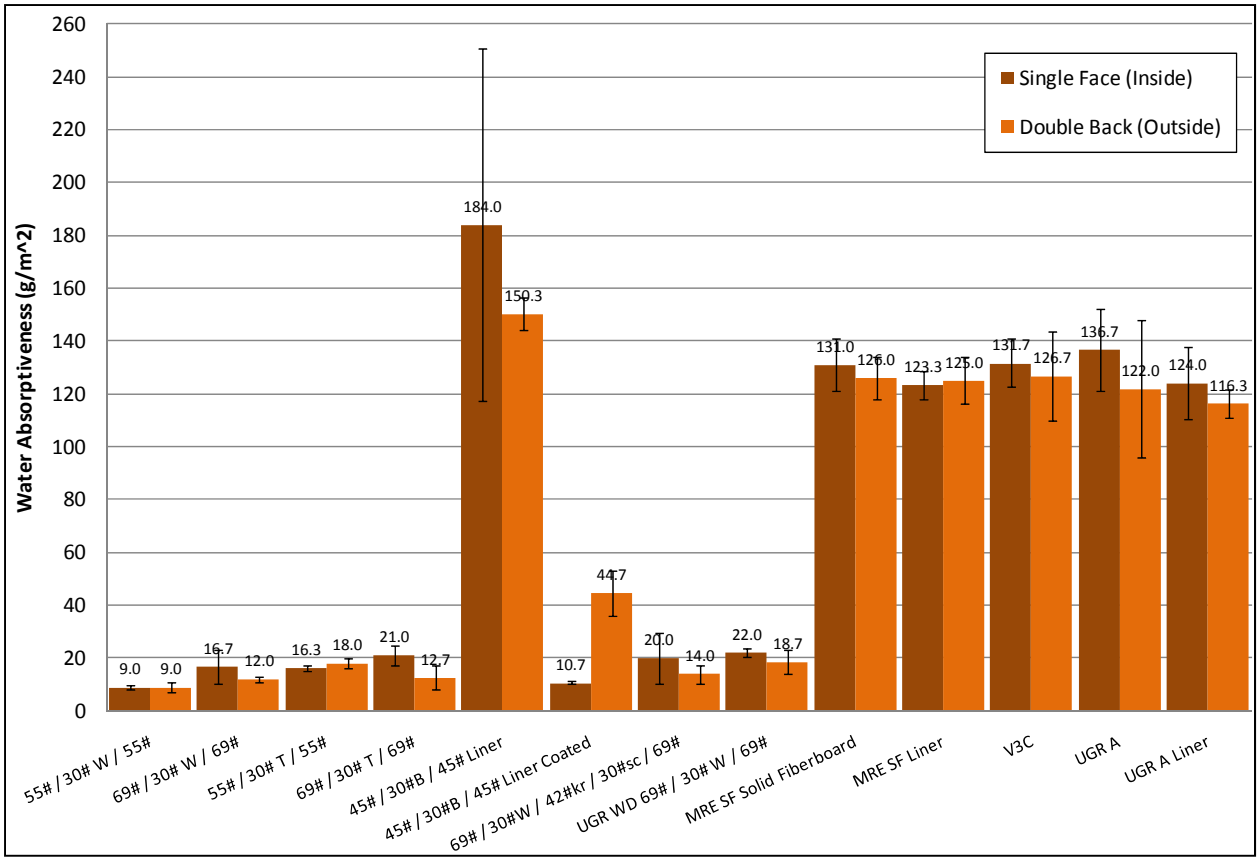

W – WAM™-coated medium

T – Tallow-coated medium

Figure 42. 30 min Cobb test results performed by Spectra-Kote Corporation

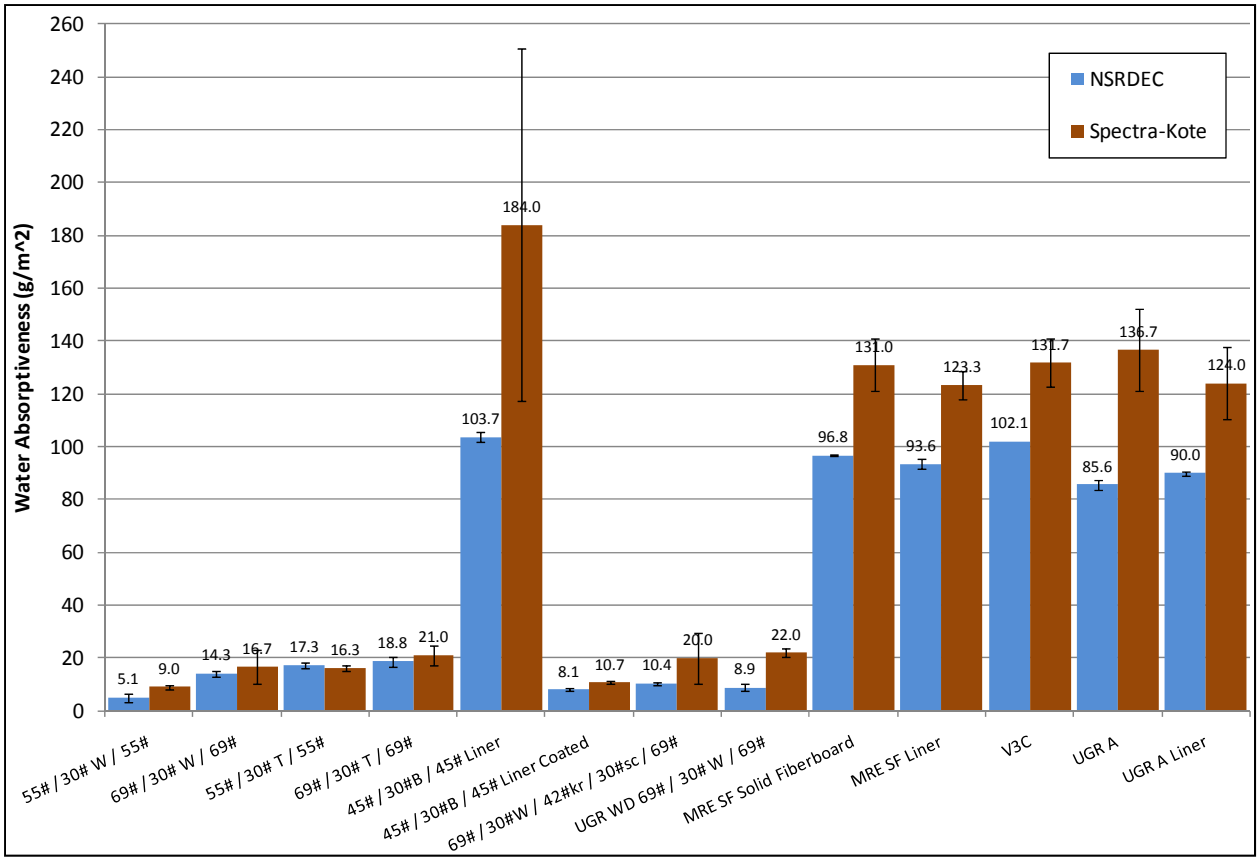

Results are stated as an average of three test samples.

Two independent tests were performed by NSRDEC and Spectra-Kote Corporation.

W – WAM™-coated medium

T – Tallow-coated medium

Figure 43. 30 min Cobb test results for the single face liner of the combined board

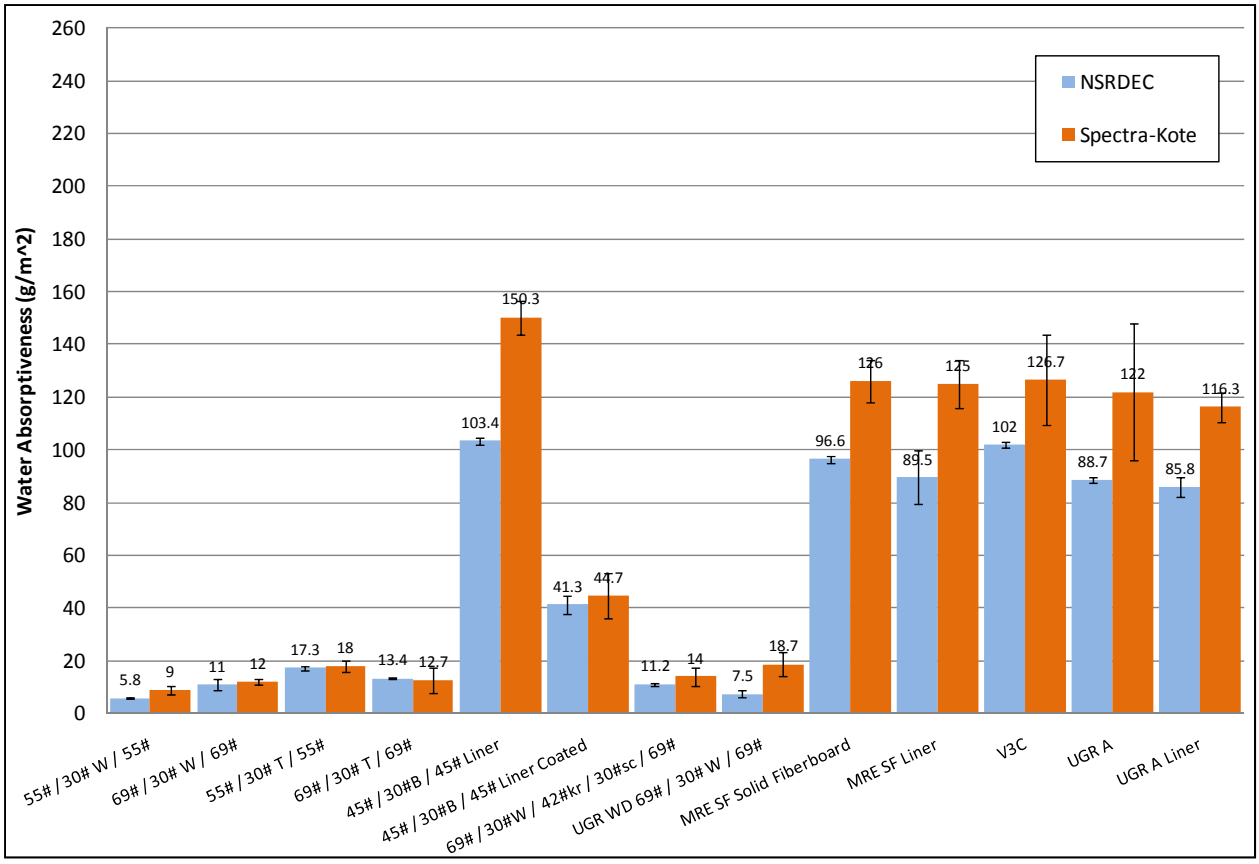

Results are stated as an average of three test samples.

Two independent tests were performed by NSRDEC and Spectra-Kote Corporation.

W – WAM™coated medium

T – Tallow-coated medium

Figure 44. 30 min Cobb test results for the double back liner or outer facing.

The results from these studies show that the commercially-coated materials from Spectra-Kote Corporation have improved resistance to water pentration over the existing milatary grade fiberboard for the UGR™ and MRE™ rations. The low results indicate that the coated fiberboard actively repelled moisture intrusion into the fiberboard structure. While this test does not determine the overall performance of containers in adverse climates it does predict the water resistance of the combined material and will help in the design and development of secondary packaging for military rations. Further analysis of the commercial coatings was investigated during the environmental/compression studies at the NSRDEC which also demonstrated that the commercial coatings provided wet strength properties to the combined board under wet or moist conditions.

5.2.2 Rain Test and Compression Evaluation of Fiberboard Containers

The fiberboard structures as shown in Figure 45 were exposed to 8 h time intervals to the prescribed climatic conditions. In general, the bottom container for each set experienced the greatest amount of deflection, as it supported the highest load. As shown in Figure 46, the deflection values of the corrugated prototypes were directly compared to the existing MRE™ solid fiberboard container.

Figure 45. MRE™ control during 8 h rain test: (a) Top, (b) Bottom

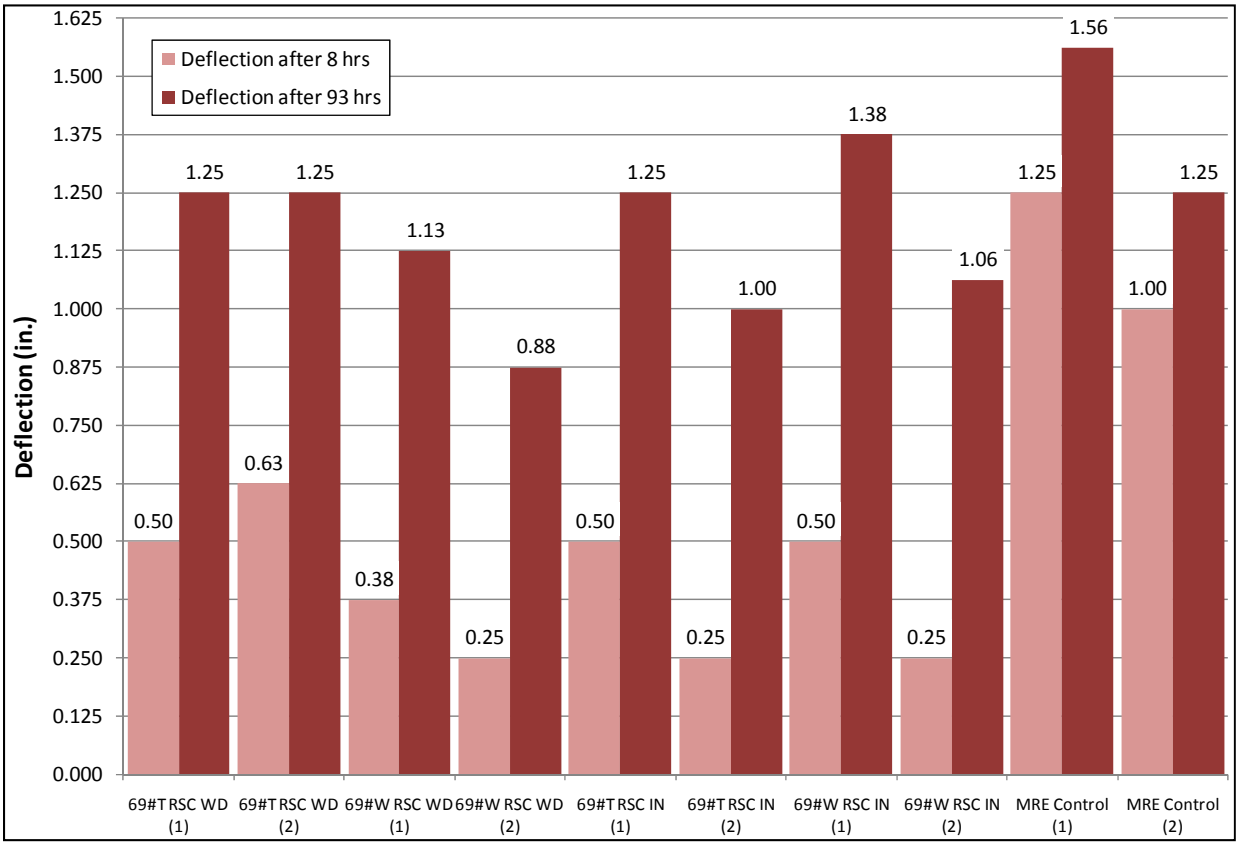

Figure 46. Total deflection of stacked column of MRE™ containers after 8 h rain exposure and 93 h recovery period (four containers per stack)

During the 8 h rain test the corrugated prototype containers exhibited lower amounts of deflection when compared to the solid fiberboard container. The coated corrugated containers exhibited deflection values which ranged from 0.25 in to 0.625 in over the 8 h period in contrast with the solid fiberboard containers which had values at 1 in and 1.25 in of deflection. However, after 93 h of recovery from the rain test the corrugated samples had comparable deflection values when compared to the existing MRE™ containers. After 93 h, the coated corrugated containers exhibited deflection values which ranged from 0.875 in to 1.375 in over the 93 h period in comparison with the solid fiberboard containers which had values at 1.25 in and 1.5625 in of deflection. Figure 47 highlights the deflection rates over the hourly time periods and also includes the final deflection of the column stack after 93 h from the onset of rain testing. The chart clearly shows that the solid fiberboard material deflects rapidly over the first 2 h of testing and then continues to deflect more gradually over the remainder of the 8 h rain test. The corrugated prototype containers gradually deflect for the first 4 h and reach a steady state for the remaining 4 h but over time deflect similarly to the solid fiberboard containers as shown in the results taken at 93 h after testing. In conclusion, results from the stack test have shown that both the corrugated and solid fiberboard containers are negatively impacted by humid or "wet" environments. Each set showed significant signs of deflection under load with bulge in the bottom container, which signals the onset of container failure. No containers failed in compression in this study but with increased levels of compression, failure would be certain under these extreme conditions. This test was a good indicator of overall container performance in adverse environments and demonstrated that the coated containers have good water resistance properties with few signs of delamination between the medium and coated liners within the combined board. To further demonstrate the performance of fiberboard containers in adverse climates, unit load testing with additional weight could also be performed to test the containers as a complete system. These loads could be tested under static load for long durations, measuring the rate of deflection over time until catastrophic failure.

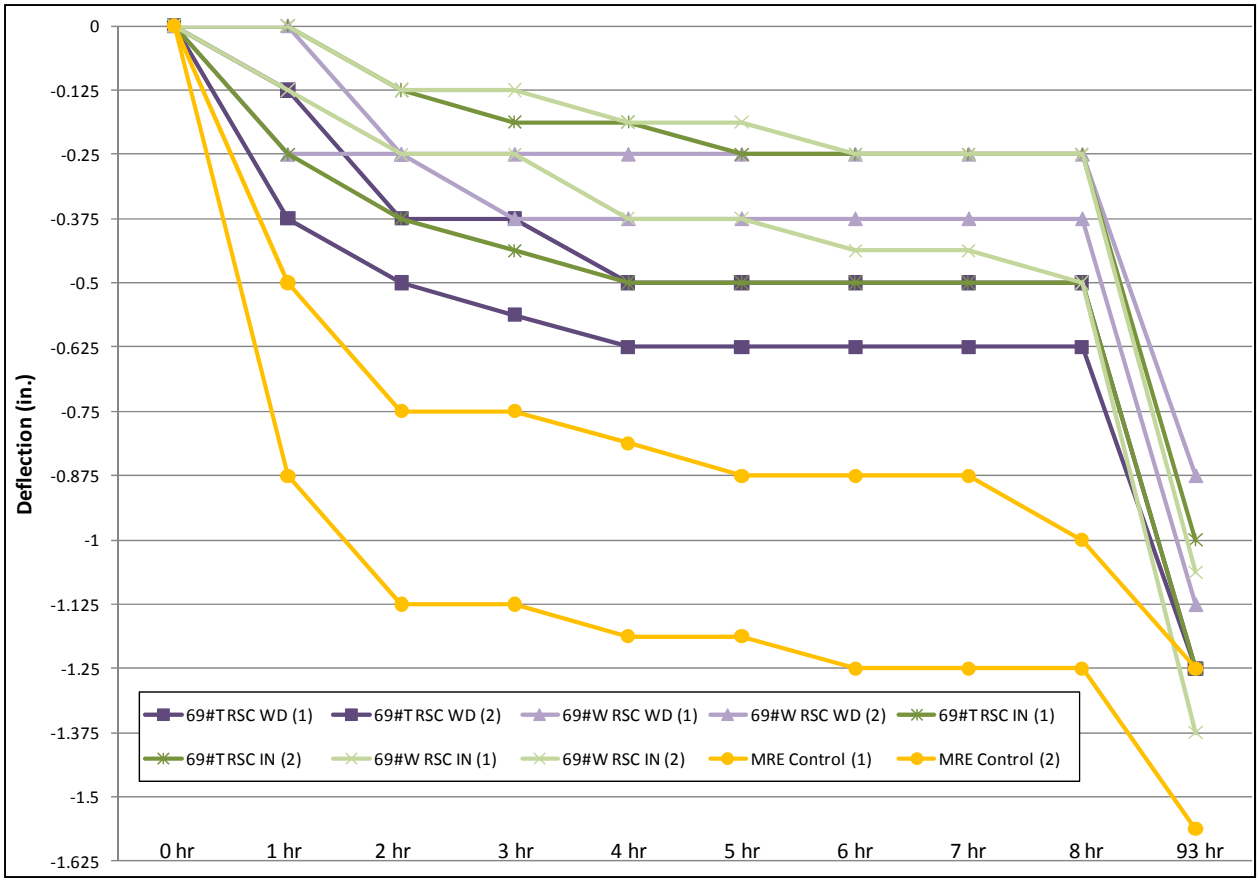

Figure 47. Deflection of stacked column of MRE™ containers during 8 h rain exposure and 93 h recovery period

During the rain study and resulting compression study, a total of 200 MRE™ ration containers and 80 UGR™ containers were exposed to a variety of environments which included: standard conditions (50% RH/23 °C), 85% RH/37.8 °C, 4 h high intensity rain and 8 h high intensity rain conditions. The ration containers were subsequently tested in compression after exposure to specified environments. Measurements of top-to-bottom compression strength and the container's load-deflection behavior were analyzed during the study and compared directly to existing ration containers. Load verses deflection plots were generated for each sample set and compared to the existing systems at each of the four environmental conditions. The chart shown in Figure 48 highlights the average compression values for each set at the four environmental conditions and directly compares the prototype values to the MRE™ results shown in the orange column.

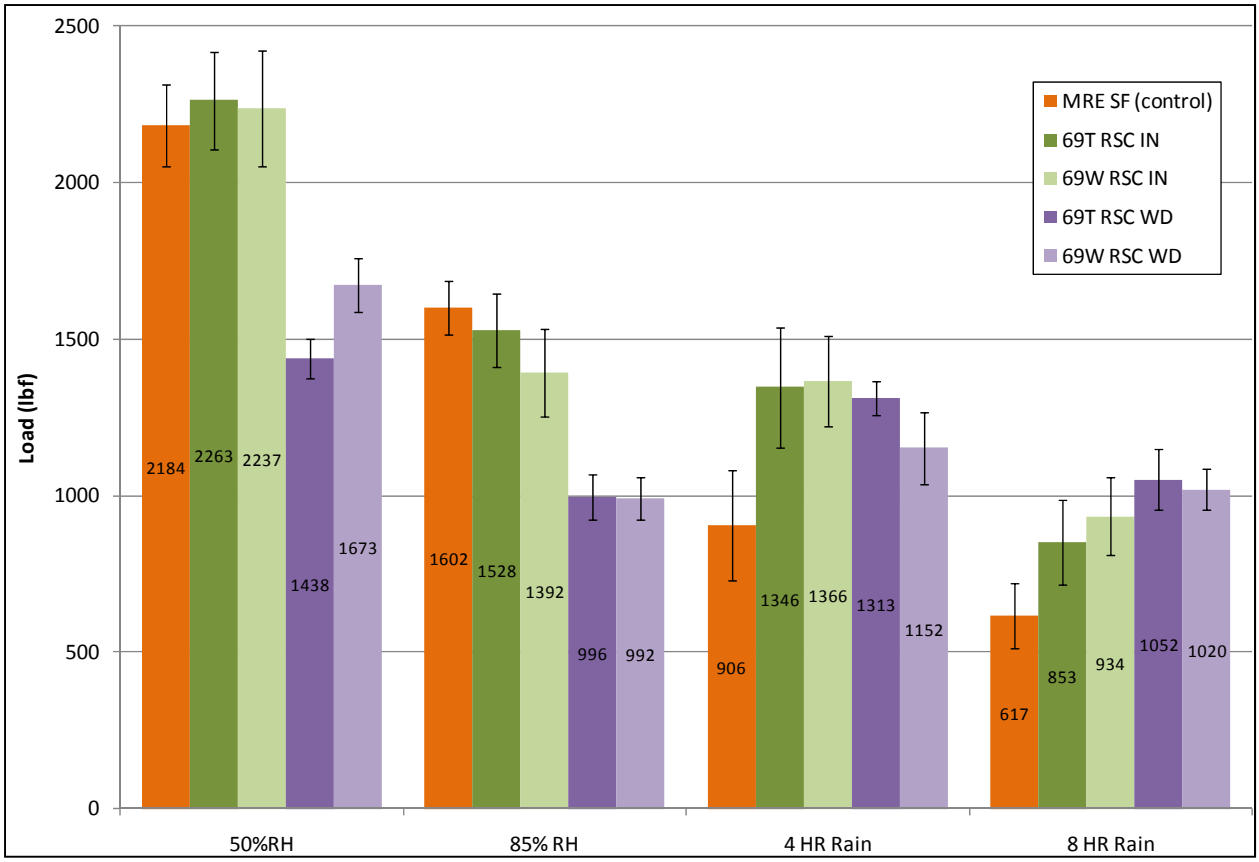

Figure 48. MRE™ compression summary of prototype and existing fiberboard containers

Samples were exposed to four distinct environmental conditions which included 50% RH/23 °C, 85% RH/37.8 °C, 4 and 8 h high intensity rain conditions. As shown in Figure 49, there is a general regression in compression strength as the containers are further exposed to humid or "wet" conditions. Results from the compression study at 50% RH and 23 °C show that each of the RSC IN containers have comparable ultimate compression values when compared to the MRE™ SF container. The Regular Slotted Container with RSC WD containers have significantly lower compression values when compared to the MRE™ SF with the control samples having a 31-52% increase in ultimate compression strength. Results from the compression study after 48 h of exposure to 85% RH and 37.8 °C conditions again show that each of the RSC IN containers have comparable ultimate compression values when compared to the MRE™ SF container. The MRE™ control samples showed a 27% reduction in compression strength between standard and high humidity conditions. In comparison, the 69T RSC IN samples shown a 32% decrease in compression and the 69W RSC IN samples averaged a 38% reduction in compression strength. The 69T RSC WD and 69W RSC WD also demonstrated similar trends with 31% and 41% respective reductions in compression strength. After exposure to four hours of high intensity rain conditions the MRE™ SF samples showed a 59% reduction in compression strength when compared to the average value at standard conditions. In comparison, the 69W RSC IN and 69T RSC IN samples experienced a 39% and 41% decrease, respectively. The 69T RSC WD and 69W RSC WD samples experienced the lowest reduction in compression strength with a respective decrease of 9% and 31%.

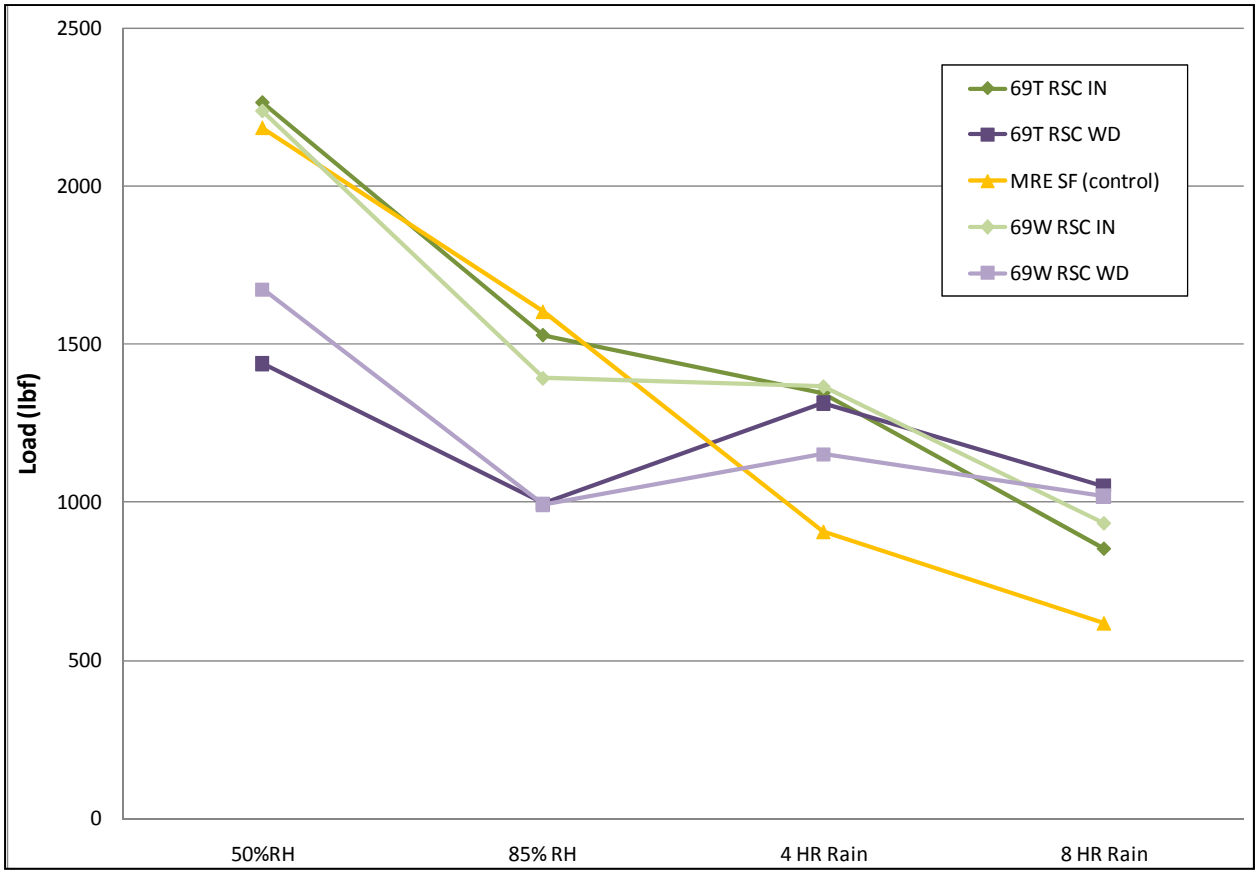

Figure 49. MRE™ compression summary of prototype and existing fiberboard containers

Samples were exposed to four distinct environmental conditions which included 50% RH/23 °C, 85% RH/37.8 °C, 4 and 8 h high intensity rain conditions. The results from the 8 h rain test showed that the MRE™ SF experienced the largest decrease with a 72% reduction in compression. In comparison, the 69W RSC IN and 69T RSC IN samples experienced a 58% and 62% decrease, respectively, and the 69T RSC WD and 69W RSC WD samples experienced the lowest decrease with a respective decrease of 27% and 39%. In general, the MRE™ SF and RSC IN containers demonstrated a general downward trend as conditions became more humid or wet. In contrast, the RSC WD containers seemed to maintain similar compression performance in each humid environment. The RSC IN design was most comparable to the MRE™ SF container as it performed comparably in standard and humid conditions and outperformed the control in each wet environment. The results from the study also showed that there is no marked difference or trend in performance between the Tallow and WAM™ coatings. The 69T RSC IN was chosen as the most ideal candidate for further development as it compared favorably to the MRE™ SF in compression and also incorporated other favorable features outside the scope of this study such as lower coating costs in comparison to the WAM™ coating and ease of technology insertion into the existing assembly/packing environment. The compression plots in Figure 49 through Figure 61 highlight each container's response to an externally applied load and illustrate failure trends within each sample set of containers.

During the rain study and resulting compression study, 80 UGR™ containers were tested at standard conditions (50% RH/23 °C), 85% RH/37.8 °C, 4 and 8 h high intensity rain conditions and were subsequently tested in compression. Measurements of top-to-bottom

compression strength and the container's load-deflection behavior were recorded and analyzed during the study and compared directly to existing UGR™ A ration containers. Figure 50 highlights the average compression values for each set at the four environmental conditions and directly compares the prototype values to the UGR™ A results shown in the blue line. As shown in the chart below, there is a general regression in compression strength as the containers are further exposed to humid or "wet" conditions. Results from the compression study at 85% RH and 37.8 °C show that each of the containers has comparable reductions in ultimate compression values when compared to standard conditions. After the 4 h rain exposure and recovery time of 48 h the samples seemed to have regained some of their initial compression strength. The UGR™ A showed no reduction in compression strength at this condition while the UGR™ WD containers showed an average of 18% decrease in compression. After the 8 h rain exposure and recovery time the UGR™ A container showed a higher regression in compression with a 43% reductionfrom the baseline values at 50% RH. The UGR™ WD containers showed similar results with a 35% reduction in compression strength. Overall, the UGR™ A container had higher levels of compression at each test mainly due to the extra liners incorporated into the design of the ration container which help support much of the load. In comparison the UGR™ WD container only has a single wall of fiberboard for support and is inherently weaker than the existing container. The design of the UGR™ WD was developed to dramatically reduce packaging weight and material at the cost of lowering compression performance. Future designs will incorporate a double walled coated container to improve the compression performance while still lowering material consumption.

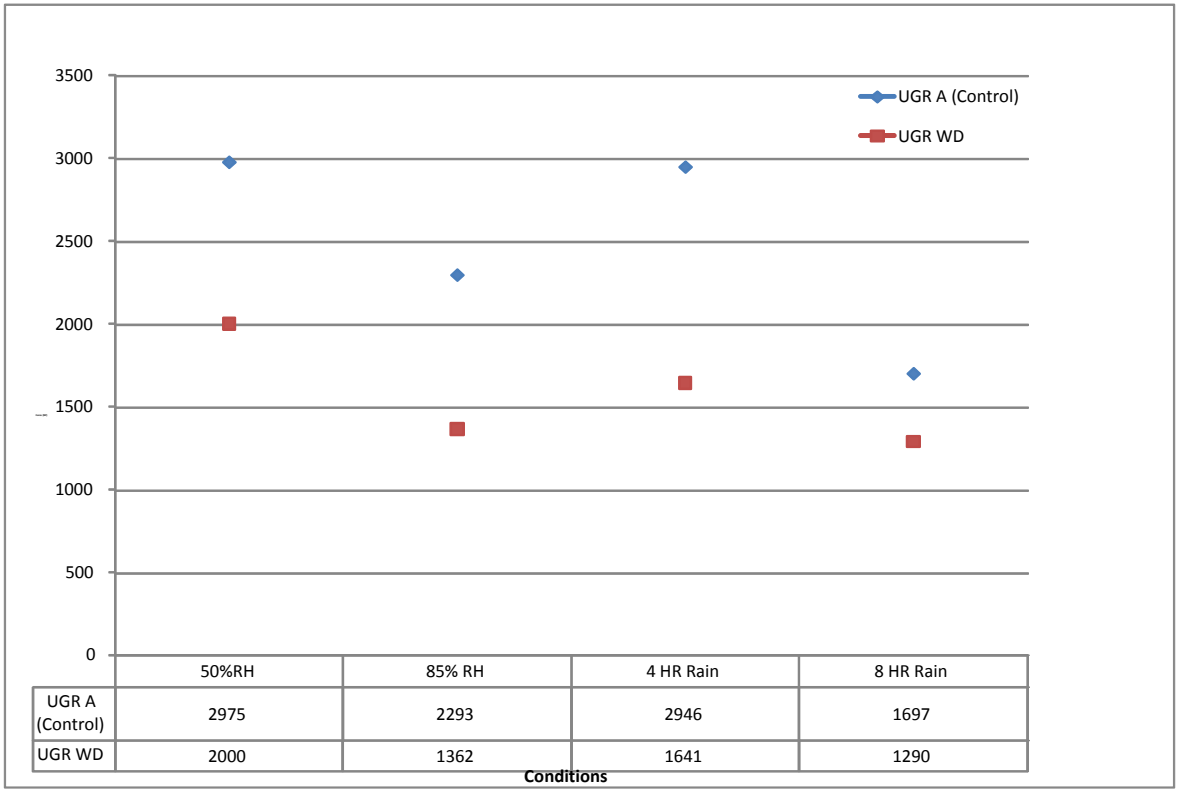

Figure 50. Compression summary of UGR™ A and UGR™ WD prototype containers, tested at 50% RH/73°F, 85% RH/100°F, 4 and 8 h high intensity rain conditions

The plots generated during compression testing highlight the response of each of the containers to an applied load and simulated environment. The red circles (A and B) shown in Figure 51 highlight the failure peaks of the UGR™ A containers. Circle A represents the area where the containers failed at standard conditions with the peaks representing the failure of the container to further support the applied load. The peak regression in circle B illustrate that the samples exposed to four hours of high intensity rain were degraded by the wet environment as seen in the downward shift in ultimate compression values and deflection at failure. The shift from area A to B shows a trend that suggests degradation of performance after exposure to humid environments and is observed in both the UGR™ A and UGR™ WD containers as shown in Figure 51 and Figure 52, respectively.

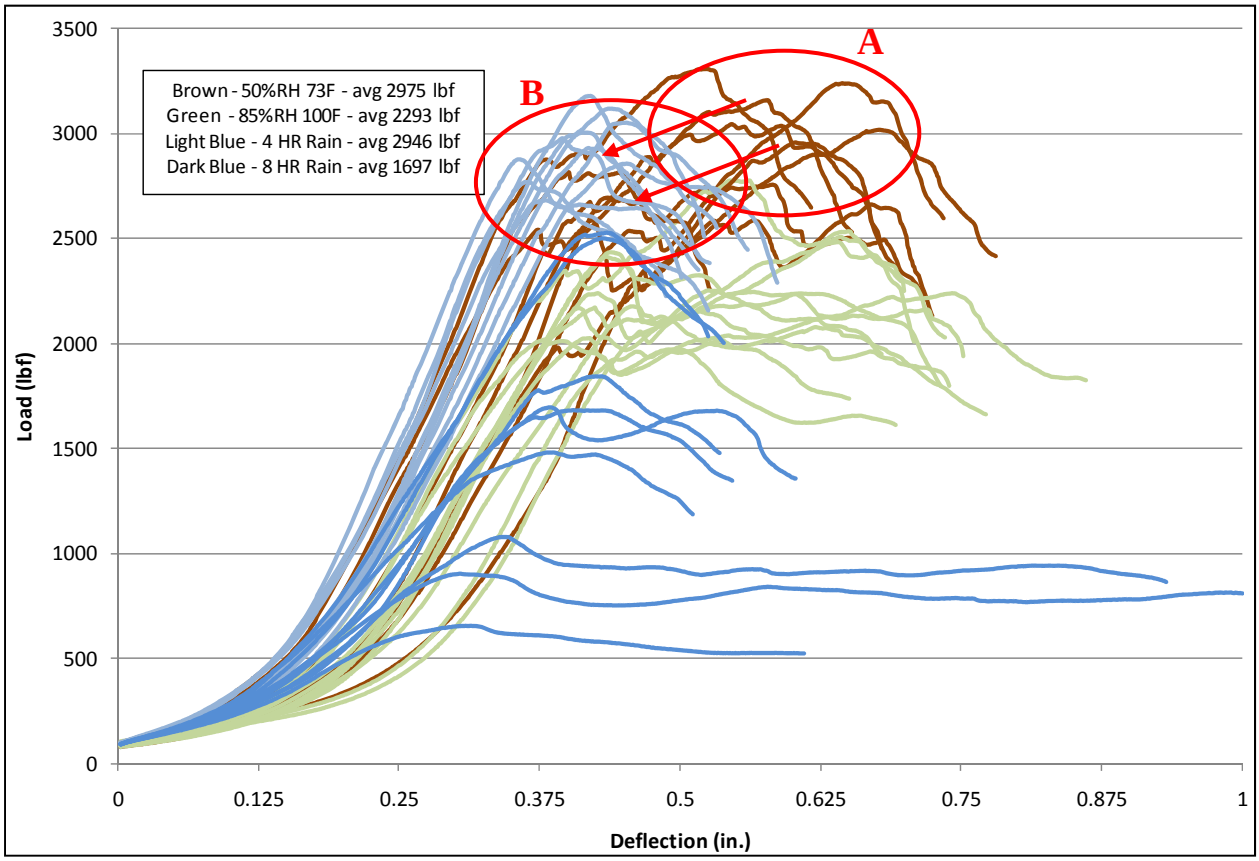

Figure 51. Compression plots of UGR™ A samples at standard conditions and compared to samples tested after 85% RH, 4 h and 8 h exposure to high intensity rain conditions

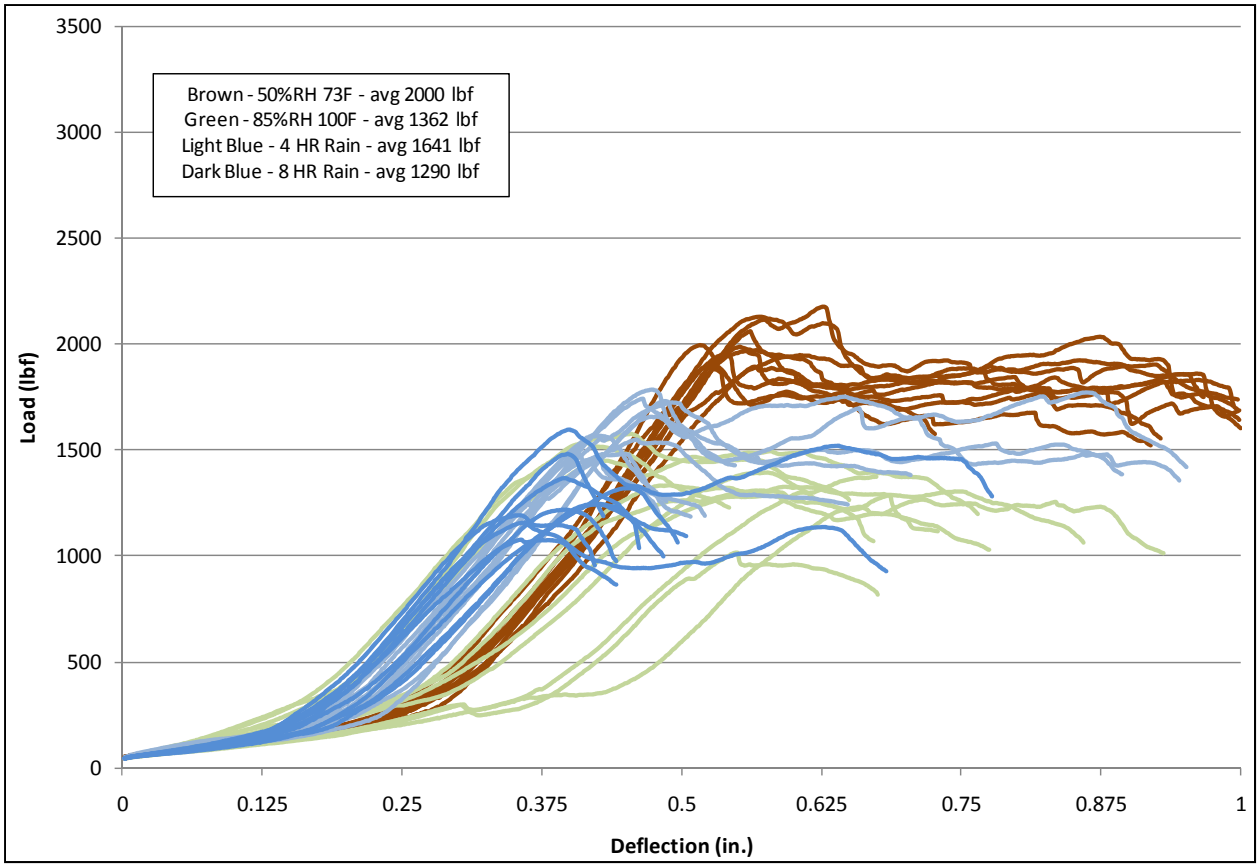

Figure 52. Compression plots of UGR™ WD samples at standard conditions and compared to samples tested after 85% RH, 4 h and 8 h exposure to high intensity rain conditions

Results from the study demonstrated that UGR™ A containers had a substantial decrease in compression resistance with increased exposure to wet conditions. Performance trends within the compression plots were also identified as shifts in ultimate compression strength and deflection at failure were observed, providing keen insight into the overall performance of the coated packaging systems under adverse climate conditions.

The plots generated during MRE™ SF compression testing, as shown in Figure 53, highlight the response of each of the containers to an applied load and simulated environment. The red circles (A and B) shown in the chart below highlight the failure peaks of the MRE™ SF containers. Circle A represents the area where the containers failed at standard conditions with the peaks representing container failure. The failure peak regression highlighted in circle B illustrates that the samples exposed to 4 h of high intensity rain were significantly degraded by the wet environment as seen in the considerable downward shift in ultimate compression values and deflection at failure. The shift from area A to B shows a trend that suggests severe degradation of performance after exposure to wet environments. Circle C highlights samples from the 8 h test which show a further degradation of performance as the shift in ultimate compression is reduced to 600 lb of resistance to the applied load.

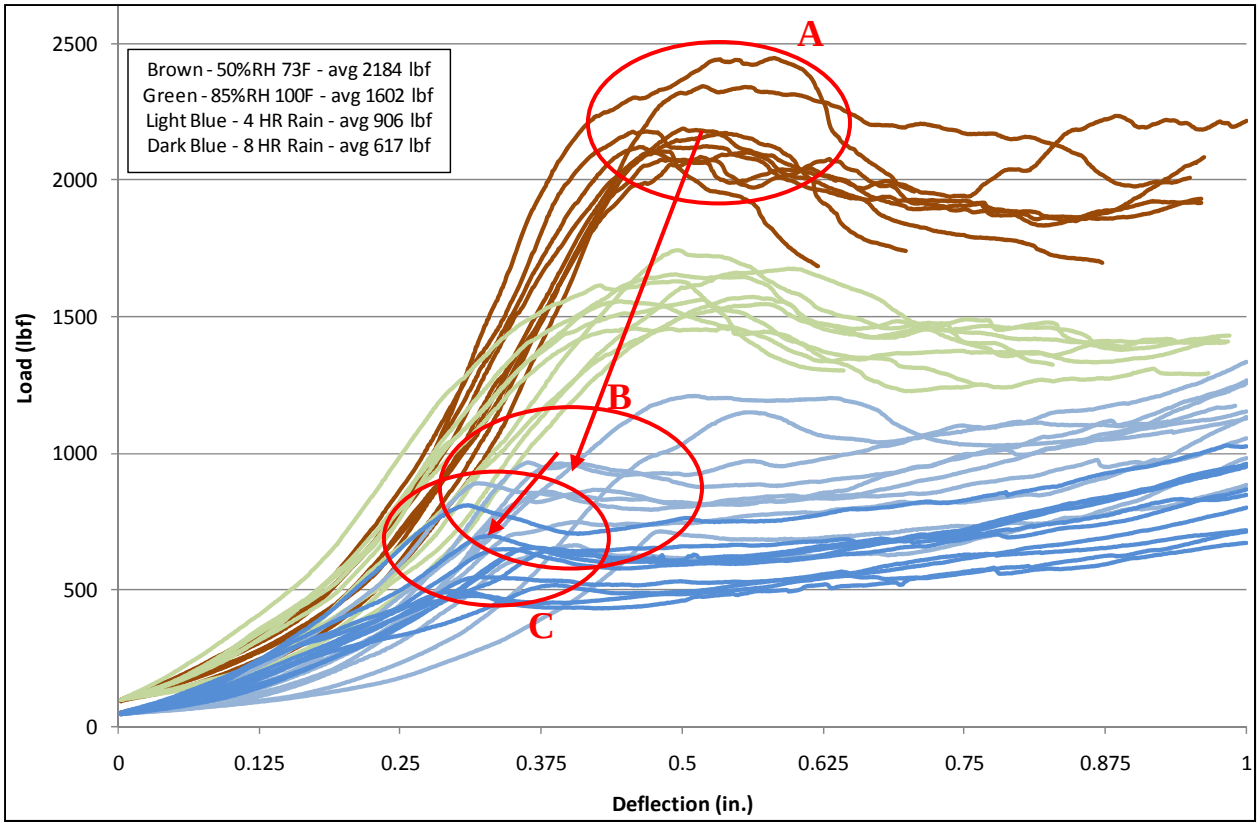

Figure 53. Compression plots of MRE™ SF samples

Results from the study demonstrated that the MRE™ SF containers had a substantial decrease in compression resistance with increased exposure to wet conditions. Performance trends within the compression plots were identified as shifts in ultimate compression strength and deflection at failure were observed, providing overall indicators of performance for the existing solid fiberboard systems under adverse climate conditions.

The plots generated during RSC IN compression testing, shown in Figure 54 and Figure 55, highlight the response of each of the containers to an applied load and simulated environment. The red circles (A and B) shown in the chart below highlight the failure peaks of the RSC IN containers. Circle A represents the area where the containers failed at standard conditions with the peaks representing container failure. The failure peak regression highlighted in circle B illustrates that the samples exposed to 85% RH and 37.8 °C were degraded by the humid environment as seen in the downward shift in ultimate compression values. The shift from area B to C shows a trend that suggests further degradation of performance after exposure to wet environments. Circle D highlights samples from the 8 h test which shows a further degradation of performance as the shift in ultimate compression is reduced to approximately 850 lb of peak resistance to the applied load.

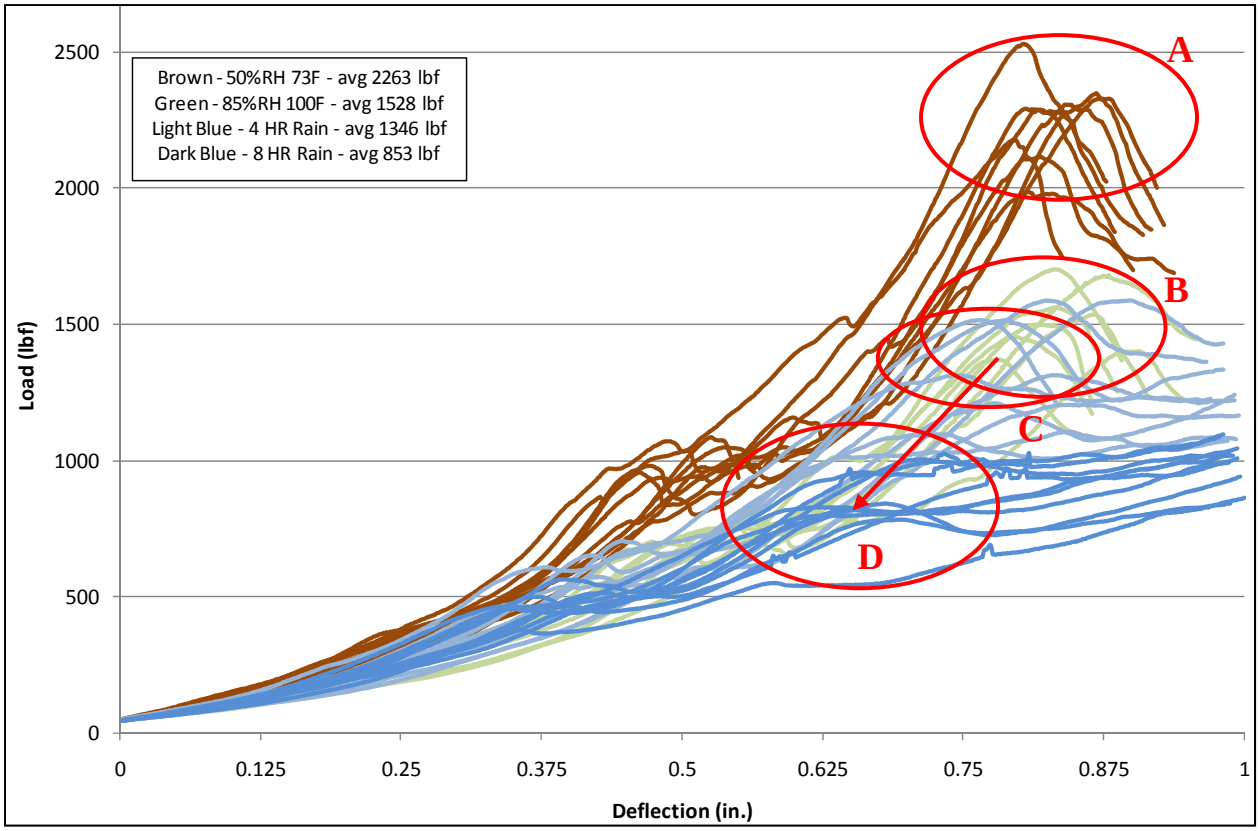

Figure 54. Compression plots of 69T RSC IN samples

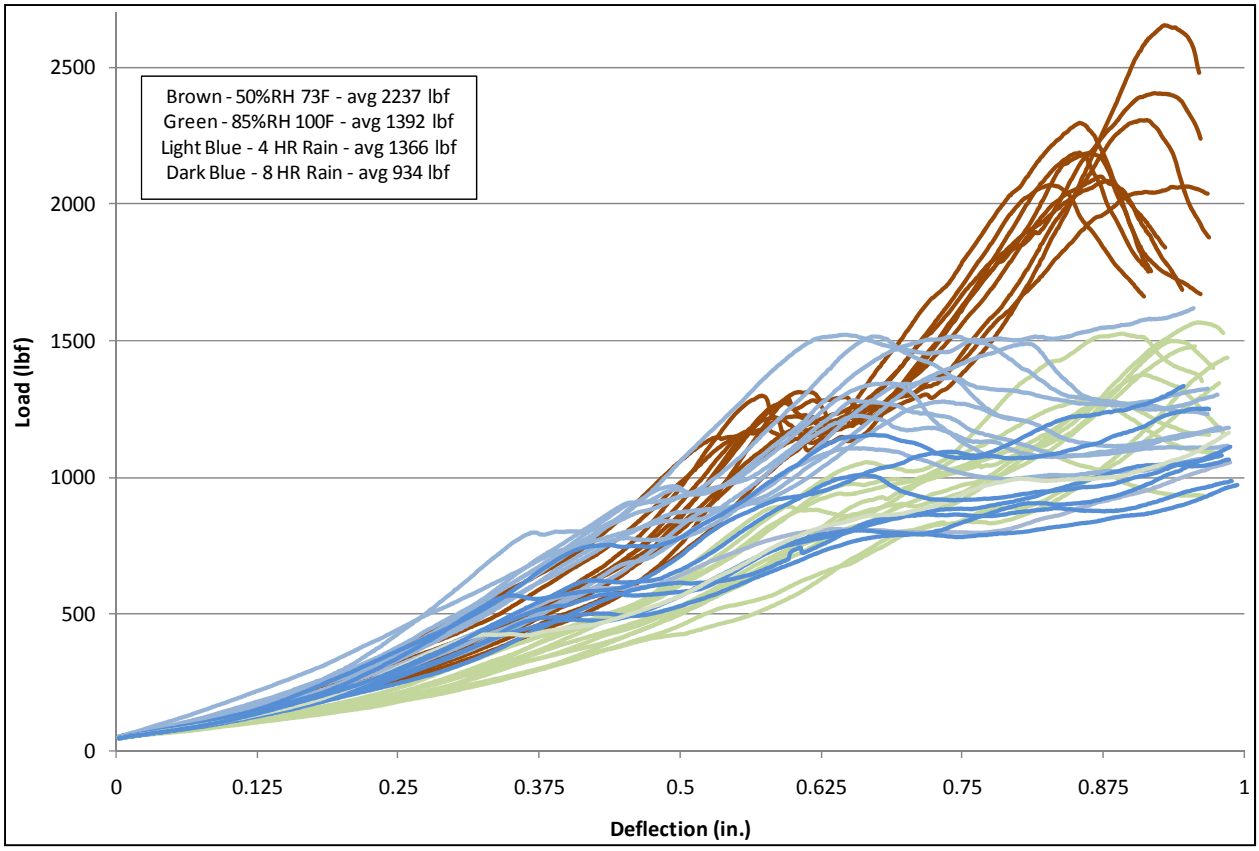

Figure 55. Compression plots of 69W RSC IN samples

Results from the study demonstrated that the RSC IN containers showed a decrease in compression resistance with increased exposure to wet conditions. Performance trends within the compression plots were identified as shifts in ultimate compression strength and deflection at failure were observed, providing overall indicators of performance for the prototype systems under adverse climate conditions.

The plots generated during RSC WD compression testing as shown in Figure 56 and Figure 57 highlight the response of each of the individual containers to an applied load and simulated environment. The red circles (A and B) shown in the chart below highlight the failure peaks of the RSC WD containers. Circle A represents the area where the containers failed at standard conditions with the peaks representing container failure. The failure peak regression highlighted in circle B illustrates that the samples exposed to 4 h of high intensity rain were degraded by the wet environment as seen in the downward shift in ultimate compression values and deflection at failure. The shift from area A to B shows a trend that suggests degradation of performance after exposure to wet environments. Line C highlights an additional increase in support after the container has failed in compression; this support is from the MRE™ ration samples. As pressure inside the containers increases, the meal bags begin to push against the walls of the containers which enhance container rigidity. Ideally the product support and onset of failure should occur at similar deflections in order to maximize the compression performance of the container. In general, product support begins after 0.75 in of deflection in the container, which will be illustrated as linear path after container failure as shown by Line C in Figure 56.

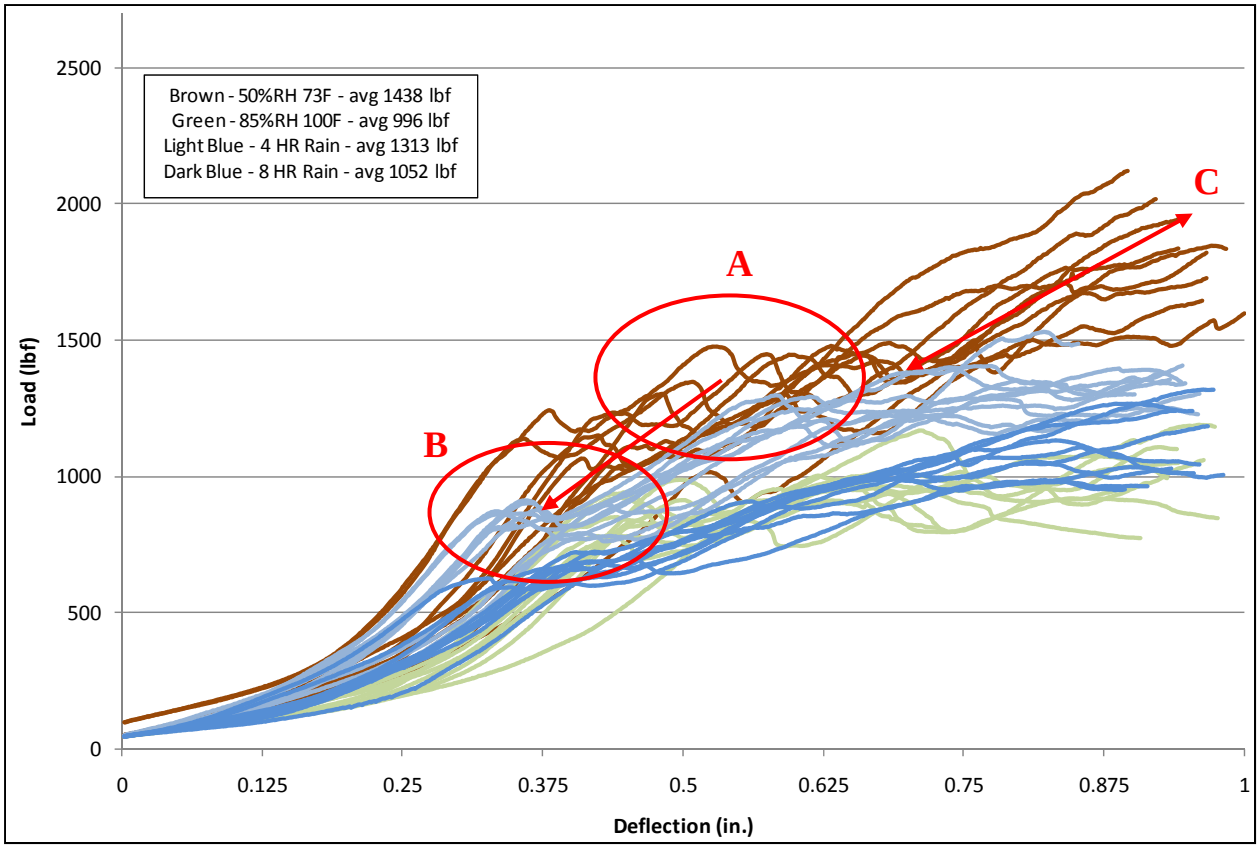

Figure 56. Compression plots of 69T RSC WD samples

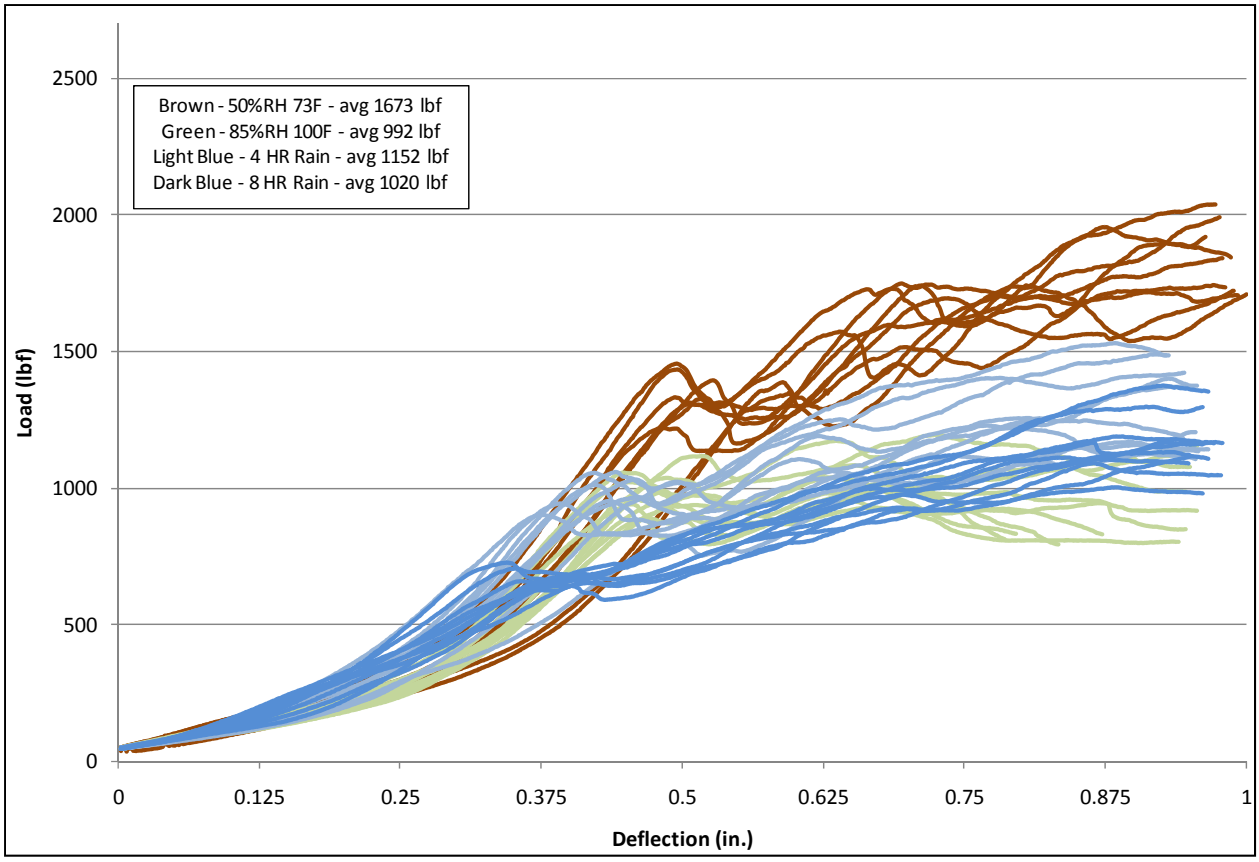

Figure 57. Compression plots of 69W RSC WD samples

Results from the study demonstrated that the RSC WD containers had a substantial decrease in compression resistance with increased exposure to wet conditions. Performance trends within the compression plots were identified as shifts in ultimate compression strength and deflection at failure were observed, providing overall indicators of performance for the existing solid fiberboard systems under adverse climate conditions.

The plots generated in Figure 58, Figure 59, Figure 60, and Figure 61 show a direct comparison between the 69T RSC IN and MRE™ SF existing solid fiberboard container. The 69T RSC IN prototype container was identified as the principle candidate as it demonstrated superior performance in comparison to the MRE™ SF control under adverse conditions. The plots generated from exposure to standard conditions and 85% RH showed that both containers performed comparably in compression. The two designs had similar compression values but also had noticeable differences in deflection at failure. At both conditions, the MRE™ SF container failed at around 0.5 in of deflection while the RSC IN prototype failed at around 0.875 in of deflection. As stated earlier, product support begins around 0.75 in and may provide the RSC IN with additional support at the onset of failure, which may help delay container failure. At wet conditions, the RSC IN showed superior performance in adverse climate environments as demonstrated in the compression plots in Figure 60 and Figure 61. Note that samples were allowed to "recover" or dry for a period of 72 h prior to compression testing. When compared to the MRE™ SF, the RSC IN container showed an average improvement in compression by approximately 50% after 4 h of exposure to high intensity rain and a 40% increase after 8 h of exposure to high intensity rain.

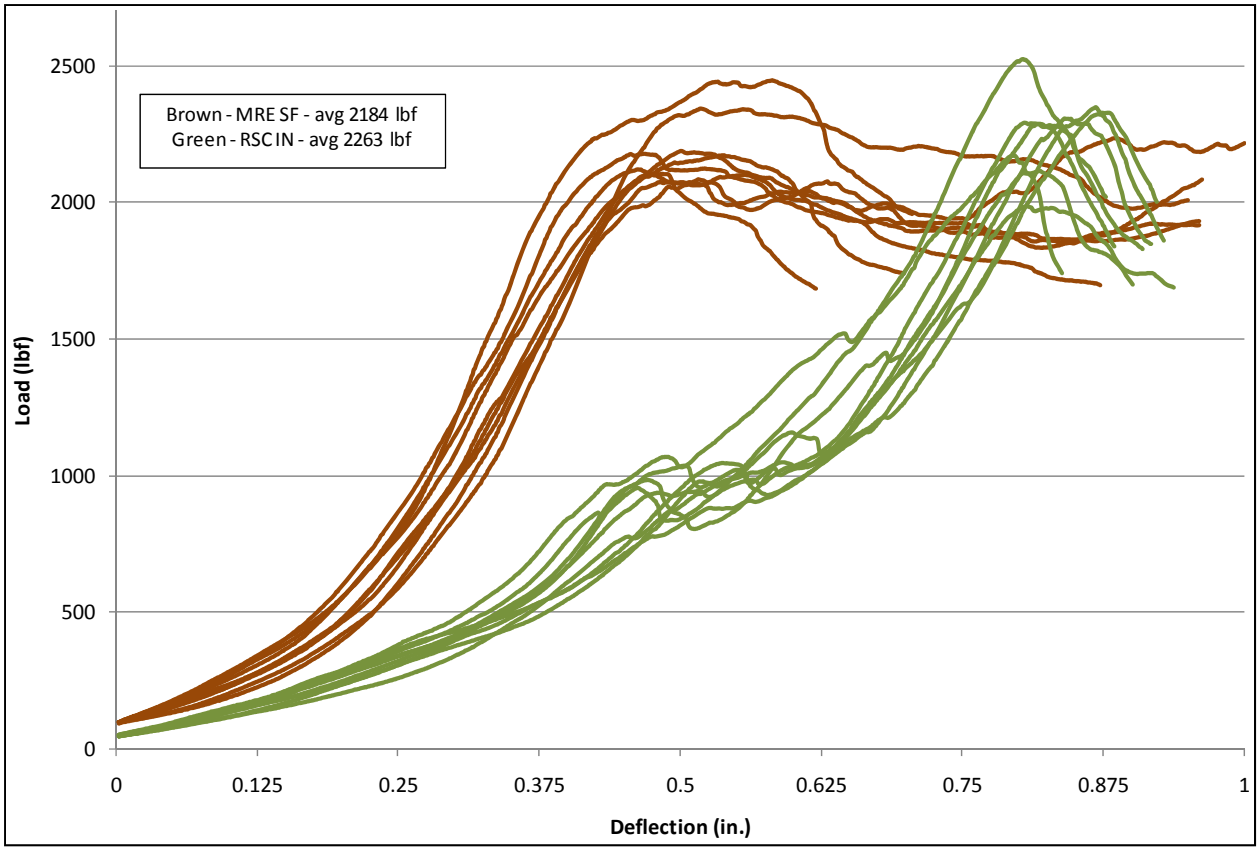

Figure 58. Compression plots of MRE™ SF and 69T RSC IN samples at standard conditions

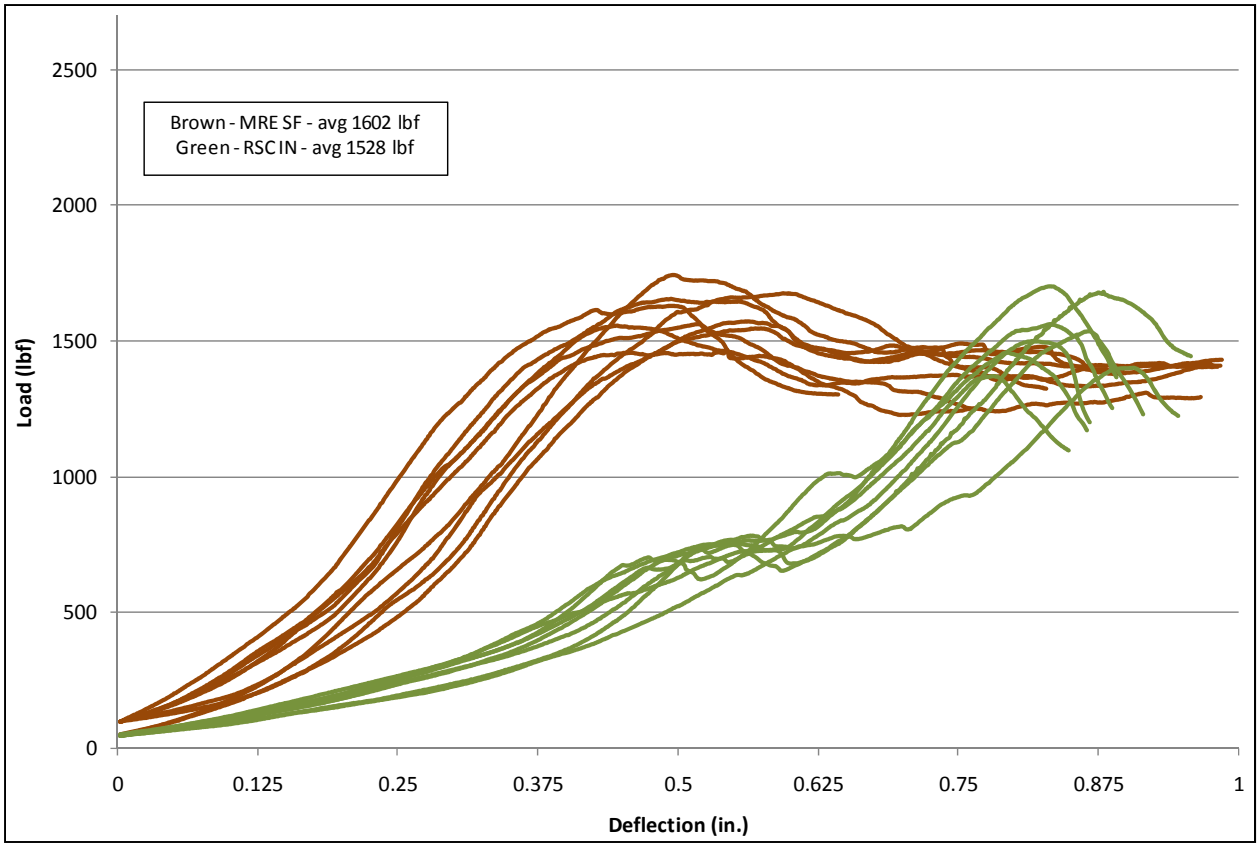

Figure 59. Compression plots of MRE™ SF and 69T RSC IN samples after exposure to 85% RH conditions for 48 h

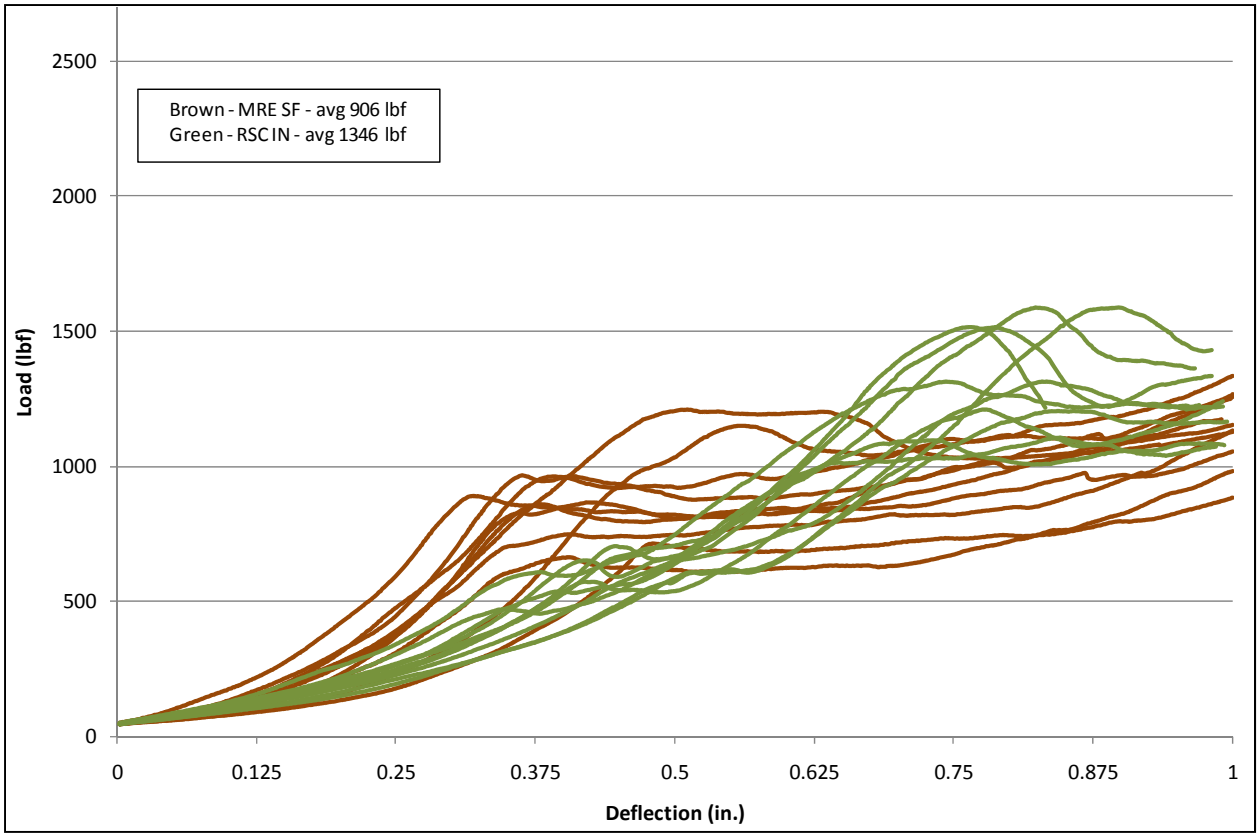

Note: Samples were allowed to "recover" or dry for a period of 72 h prior to compression.

Figure 60. Compression plots of MRE™ SF and 69T RSC IN samples after exposure to 4 h of high intensity rain conditions

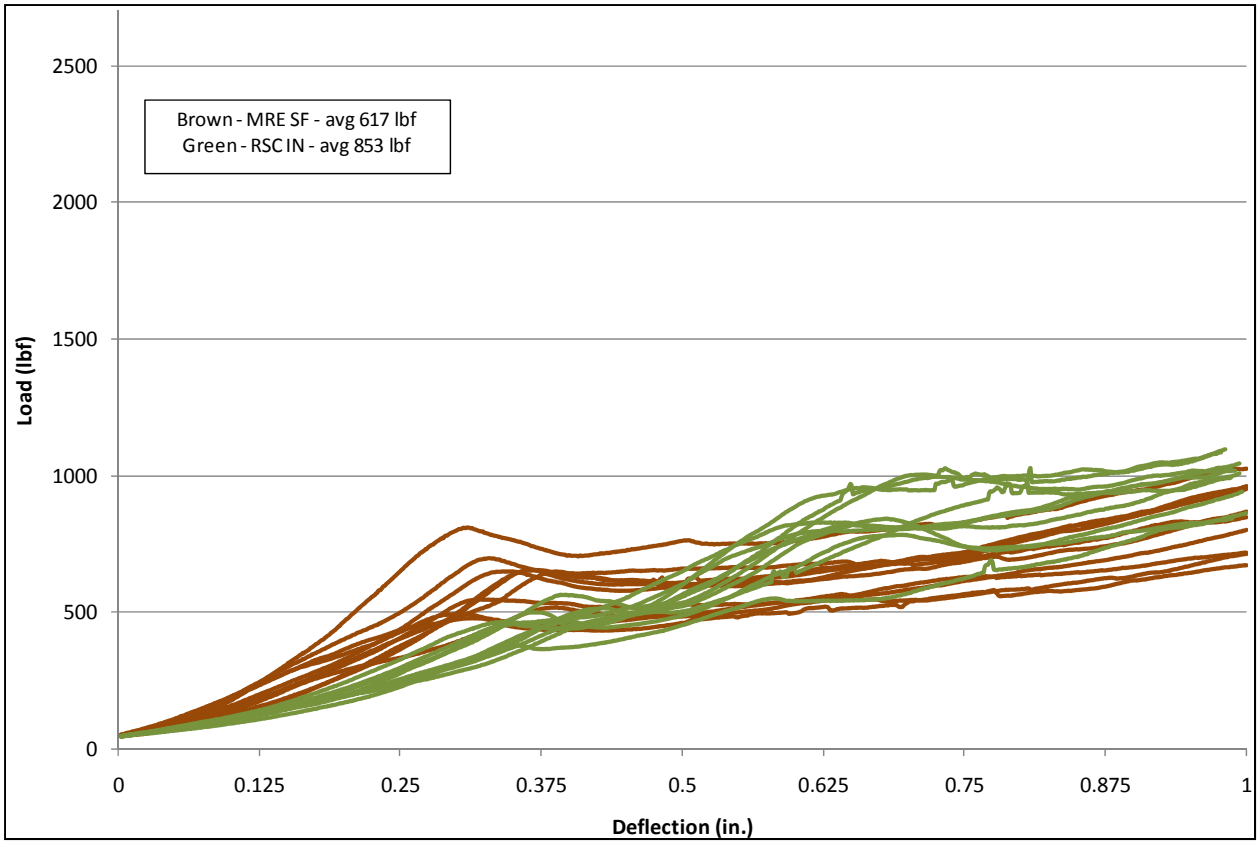

Figure 61. Compression plots of MRE™ SF and 69T RSC IN samples after exposure to 8 h of high intensity rain conditions

The development effort has created secondary packaging systems that have reduced fiber content and that utilize lightweight corrugated fiberboard instead of military grade solid fiberboard currently used in the construction of MRE™ ration packaging. The lightweight MRE™ designs show significant savings in material usage with an annual reduction of up to 870,000 to 3,300,000 pounds average reduction in packaging consumption as shown in Figure 62. The new containers also have improved functionality by incorporating water resistant coatings that are both re-pulpable and recyclable adding a new avenue of recovery for military logistics, as well as for the commercial market.

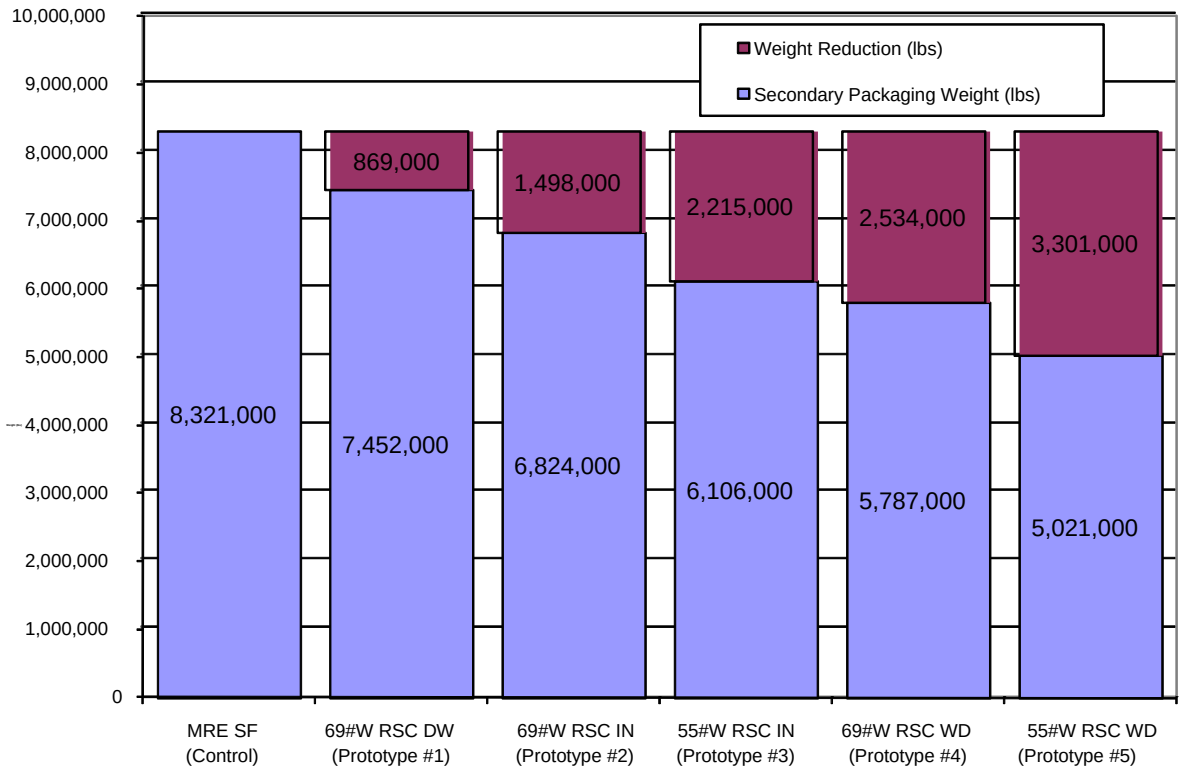

Figure 62. Annual weight reductions of the corrugated prototype containers for MRE™ rations

These results from the rain study and compression analysis highlighted important failure/performance trends within each set of containers within the compression plots and generated useful indicators of performance in adverse climates. Results from this study will directly influence further development of the prototype corrugated containers and will be used as a data baseline for additional environmental testing. Through the evaluations, an optimized container was identified as an ideal candidate for further development based on compression performance in adverse conditions and other factors outside this study such as manufacturability, coating/overall cost and ease of implementation into the existing MRE™ assembly/packing environment.

5.2.3 Results of Cold Weather Study

The majority of the corrugated samples seemed to be in fair condition. There were some signs of moisture retention which could be seen as darker areas on the container and most containers felt damp to the touch. Some of the corrugated samples had delamination on the flaps. In general, the corrugated container flaps, joints and edges seemed to be intact. The water did not penetrate into the structure and cause further degradation. The solid fiberboard current MRE™ containers also showed signs of moisture retention, and several samples had delamination of the fiber sheets due to excessive moisture.

5.2.4 Air Drop Results

The information and data shown in Table 22 reflects the samples in Table 20 with the designated Load number. The effort demonstrated that the corrugated prototype containers were

able to withstand representative hazards encountered during aerial delivery operations and showed minimal signs of damage during rigging and aerial delivery as shown in Figure 60.

Table 22. Air Drop Results

	Load 1	Load 2	Load 3	Load 4	Load 5	Load 6
Date of Drop	23-Sep	21-Sep	25-Aug	23-Sep	25-Aug	23-Sep
Lift #	5	5	2	5	2	5
Pass #	8	3	5	10	6	7
Altitude (ft)	17,500	17,500	15,000	17,500	15,000	17,500
Aircraft	C-130	C-130	C-130	C-130	C-130	C-130
Load	2K ICDS	2K ICDS	2K ICDS	2K ICDS	2K ICDS	2K ICDS
Suspended Weight (lbs)	1000	1000	1000	512	512	1000
Rigged Weight (Total)	1262	1258	1182	697	678	1177
Weight of Rigging	262	258	182	185	166	177
Height	82	78	69	60	58	69
Length	48	48	48	48	48	48
Width	48	48	48	48	48	48
Pass / Fail	pass	NA*	NA*	Pass	NA*	Pass

*Chute failed during testing making evaluation not valid. Samples will be tested at a later date.

Figure 63. Unitized load of MRE™ rations containers after delivery and final impact

5.2.5 Analysis of Variance (ANOVA)

In addition to the trends seen in the compression results, an ANOVA test was completed to identify statistically significant trends in the data for the different fiberboard prototypes. Results of the ANOVA included the sum of the squares (SS), mean square (MS), F and *P*-values

for the compression and Cobb data as a function of paper weight, type of coating and insert. Note: only *P*-values ≤0.05 were considered to be statistically significant.

A three-way completely randomized ANOVA was performed for the prototypes generated in 2008 containing the 55 and 69 lb paper, WAM™ vs. Tallow coating and width divider *vs.* insert. The compression data is displayed in Figure 64.

The compression tests were performed on each prototype after exposure to rain for 8 h and after equilibration to the control conditions of 50% RH. The sample control MRE™ SF has comparable compression results to the containers with the insert versus the width divider. Overall, as expected, both paper weights showed that the compression decreased for the samples that were exposed to the rain for 8 h. The width divider showed the lowest values for compression at 50% RH, but also showed the smallest decrease after the rain chamber exposure, especially at 69 lb paper.

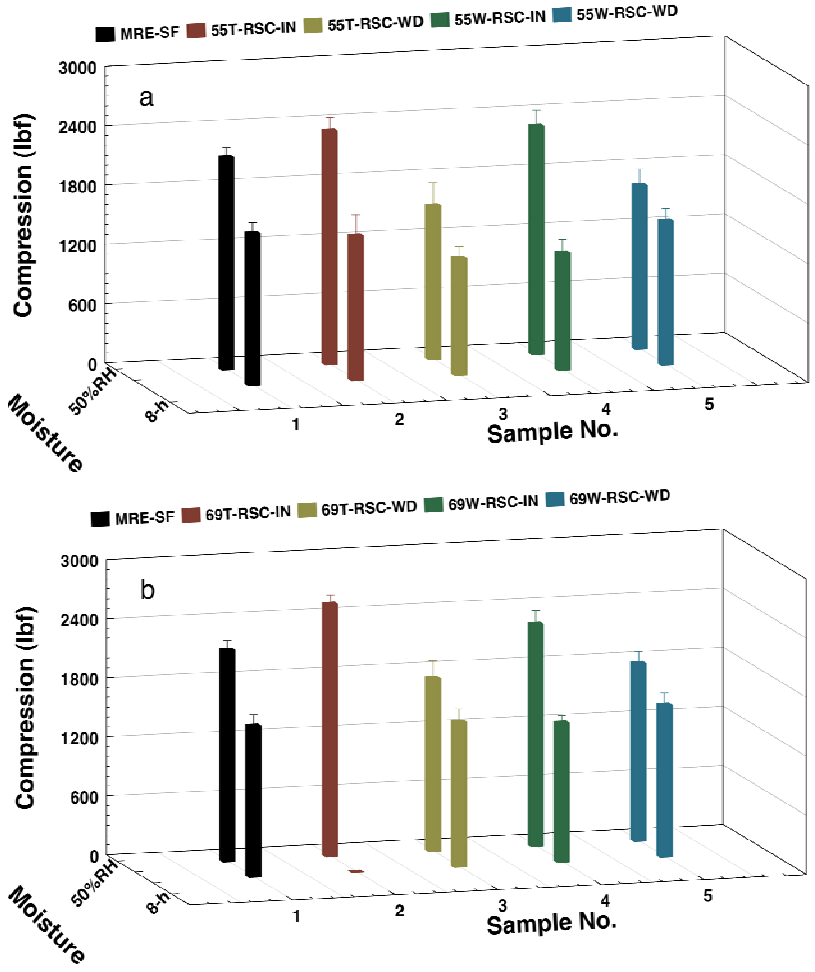

Figure 64. Effect of moisture on compression of samples:
(a) 55 lb weight paper; (b) 69 lb weight paper

The three-way ANOVA was performed with paper weight, coating, and insert as the main factors; the test variable was "relative compression" (i.e., the compression result for each test material divided by the value for the MRE™ SF standard). Relative compression was used

to account for the control, which did not vary in terms of weight, coating or insert, and so could not be included in the ANOVA. Results of the ANOVA are shown in Table 23.

Table 23. Three-way, completely randomized ANOVA showing the effect of paper weight (Pwt), coating and type of insert on relative compression of the test materials

Source	df	Type III SS	MS	F	P
Main Effects					
Pwt. (lb)	1	0.293900856	0.2939009	19.675655	0.0000 *
Coating	1	0.030363196	0.0303632	2.0327119	0.1569 ns
Insert	1	1.26580579	1.2658058	84.741361	0.0000 *
Interaction					
Pwt. (lb) X *Coating*	1	0.038227717	0.0382277	2.5592147	0.1126 ns
Pwt. (lb) X *Insert*	1	0.000724433	0.0007244	0.0484983	0.8261 ns
Coating X *Insert*	1	0.266950241	0.2669502	17.871404	0.0000 *
Pwt. (lb) X *Coating* X *Insert*	1	0.000175282	0.0001753	0.0117345	0.9139 ns
Error	107	1.5982894	0.0149373<-		
Total	114	3.264004487			
Model	7	1.665715087	0.2379593	15.93056	.0000 *

* Indicates significance at the $P \leq 0.001$ level of probability.

Note: relative compression results were averaged across all moisture conditions.

The results show that both the weight of the paper and type of insert have a significant effect on relative performance (compression), but that performance was essentially independent of coating type. More specifically, the 69 lb paper outperformed the 55 lb paper and the materials with the insert outperformed those with the width divider. Although coating type by itself had no effect on relative performance, there was a significant coating-by-insert interaction. This indicates that the effect of the coatings on the performance of the individual materials was variable.

The least significant difference (LSD) test, with $P \leq 0.05$, was used to test for (and rank) significant differences among prototypes (Table 24). This analysis was performed using both the relative and the actual results of the compression test, with both tests yielding essentially the same results. The ranked means, along with the non-significant ranges, are summarized in Table 23. The data analysis revealed that, in terms of the compression test, the Tallow-coated, 69 lb paper with insert (69T-RSC-IN) exhibited the best overall performance.

In 2009, all prototypes were prepared using the 69 lb paper and included a new design that incorporated a double wall (identified as 69W-RSC-DOW). The prototypes were evaluated after exposures at 50% RH (the control condition) and 85% RH, and after exposures to the rain for 4 h or 8 h. Results of compression tests are illustrated in Figure 65. Clearly, moisture had a significant effect, with compression values decreasing as the amount of water absorbed by the samples increased. Although the standard MRE™ SF performed well at 50% and 85% RH (Figure 65), its performance was severely compromised after exposures to rainfall for 4 h or 8 h. Indeed, at the higher moisture contents, the MRE™ SF was outperformed by the prototypes with the insert or width divider. Moreover, only the sample with the double wall (69W-RSC-DOW) performed more poorly than the MRE™ SF at the highest moisture contents.

Table 24. Ranking by mean for 2008 MRE™ prototypes

Sample ID	Relative compression	Non-significant ranges*	Actual compression (lbf)	Non-significant ranges*
69T-RSC-IN	1.19	a	2562	A
55T-RSC-IN	1.04	b	2025	B
69W-RSC-IN	1.02	bc	2017	B
MRE –SF	1.00	bc	1917	Bc
55W-RSC-IN	0.96	cd	1858	Bcd
69W-RSC-WD	0.91	de	1706	Cde
69T-RSC-WD	0.87	de	1662	De
55W-RSC-WD	0.84	e	1575	Ef
55T-RSC-WD	0.74	f	1405	F

*Means with the same letter are not significantly different ($P \leq 0.05$).

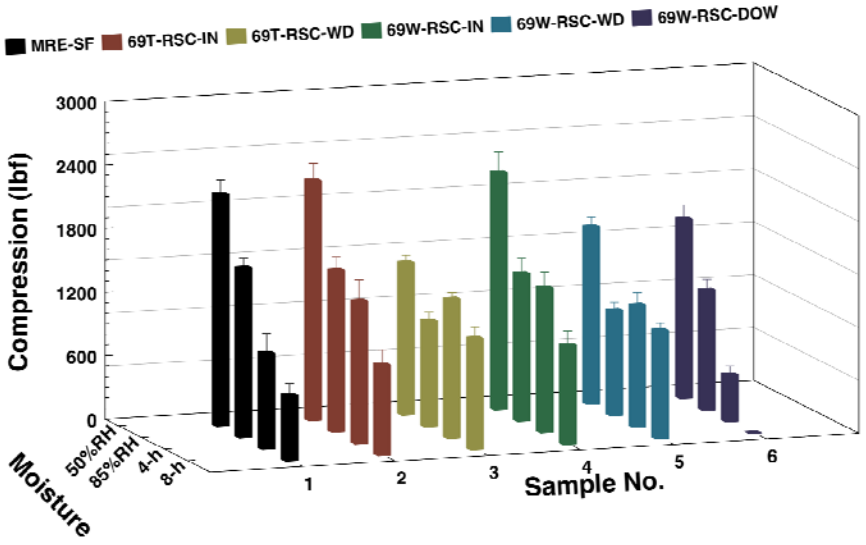

Figure 65. Effect of moisture on compression of samples composed of 69 lb weight paper

The compression data were analyzed using a two-way completely randomized ANOVA, with coating and insert type as the main factors (see Table 25). Averaged across all moisture conditions, the 2009 prototypes with the insert outperformed those with the width divider; especially under at 50% and 85% RH (see Figure 65). The LSD test, with $P \leq 0.05$, was used to test for (and rank) significant differences among prototypes (Table 26). Again, averaged across all moisture conditions, the prototypes with inserts were comparable to the MRE™ SF standard, but outperformed the prototypes with width divider and the prototype with the double wall construction.

Table 25.Two-way, completely randomized ANOVA showing the effect of paper weight (Pwt), coating and type of insert on relative compression of the test materials

Source	df	Type III SS	MS	F	P
Main Effects					
Coating	1	1776.632479	1776.632479	0.0109332	0.9169 ns
Insert	1	3119916.53	3119916.53	19.19955	0.0000 *
Interaction					
Coating X *Insert*	1	8076.119658		0.0496994	0.8239 ns
Error	150	24374919.23	162499.46		
Total	153	27511825.97			
Model	3	3136906.743	1045635.6	6.4347018	0.0004 *

* Indicates significance at the $P \leq 0.001$ level of probability.

Note: relative compression results were averaged across all moisture conditions.

Table 26. Ranking by mean for 2009 MRE™ prototypes

Sample ID	Compression (lbf)	Non-significant ranges**
69W-RSC-IN	1496	A
69T-RSC-IN	1475	A
MRE –SF	1297	Ab
69T-RSC-WD	1204	B
69W-RSC-WD	1197	B
69W-RSC-DOW	808	C

**Means with the same letter are not significantly different ($P \leq 0.05$).

The effect of moisture conditions was also examined using a two-way completely randomized ANOVA, with insert and moisture as the main effects. As expected, there were significant insert ($F = 89.79$* and moisture effects ($F = 574.73$*). However, there also was a significant insert-by-moisture interaction effect ($F = 74.53$*), indicating that the effectiveness of the different inserts varied as a function of moisture content. Indeed, the data indicate that at the highest moisture contents (i.e., following 4 and 8 h exposures in the rain) the prototypes incorporating the width divider performed as well or better than those with the insert or double wall construction.

In addition to the data analyses described above, there were also comparisons involving structural effects: (i) standard *vs* corrugated (MRE™ SF *vs* 69W-RSC-DOW) and (ii) insert *vs* corrugated (69W-RSC-IN & 69W-RSC-WD *vs* 69W-RSC-DOW). In both instances, the reference samples significantly outperformed the corrugated sample ($F = 10.15$* and $F = 17.15$*, respectively).

ANOVAs also were performed to test for significant effects of coating and insert type on the Cobb test. Whereas the type of insert had no effect on the Cobb test for either the inside or outside liner, the type of coating did affect the results for both liners. That is, the Tallow-coated prototypes outperformed the WAM™-coated materials. LSD test, with $P < 0.05$, was used to test for (and rank) significant differences among prototypes and the MRE™ SF (Table 27).

Table 27. Ranking by mean for the Cobb tests of both the outside and inside liners

Outside Liner			Inside Liner		
Sample ID	Mean	Non-significant ranges*	Sample ID	Mean	Non-significant ranges*
MRE™ SF	96.6	a	MRE™ SF	96.8	A
69T-RSC-IN	13.4	b	69T-RSC-IN	18.8	B
69T-RSC-WD	13.4	b	69T-RSC-WD	18.8	B
69W-RSC-DOW	11.2	bc	69W-RSC-IN	14.3	C
69W-RSC-IN	11.0	c	69W-RSC-WD	14.3	C
69W-RSC-WD	11.0	c	69W-RSC-DOW	11.2	D

*Means with the same letter are not significantly different ($P \leq 0.05$).

In a separate ANOVA, the DOW structure was compared to the standard MRE™ SF and the other WAM™ structures. Although the DOW structure was highly recommended by Interstate Containers, it did not perform as well as was hoped. That is, there was a significant structural effect, with performance decreasing in the order: MRE SF >> 69W-RSC-IN = 69W-RSC-WD > 69W-RSC-DOW.

6.0 Compost Studies of Fiberboard

6.1 Materials and Methods

All test materials are listed in Table 28 and were provided by the NSRDEC. All materials were used as provided—except that prior to biodegradation testing, appropriate sub-samples of each material were dried to a constant weight in a convection oven (50 °C for 12 to 18 h), cooled to room temperature in a desiccator, and stored in polyethylene Ziploc™ bags at 4 °C until needed. [Note: the various test materials were provided as they were developed; hence, the Tier I and Tier II tests were repeated as necessary over a 3 year period. Moreover, not all of the samples included in the Tier I test were evaluated in the Tier II test; i.e., based on recommendations by the NSRDEC group—and the results of the Tier I tests—the samples included in the Tier II and III tests (see Table 29) were confined to only those that exhibited the desired performance characteristics.]

6.1.1 Tier I – Polymer Mineralization Test: Aerobic biodegradation of polymeric materials under controlled composting conditions [100, 101, 102]

Unlike weight loss, which reflects structural changes in a test material (i.e., deterioration or material erosion); CO_2 evolution provides an indication of the ultimate biodegradability (i.e., mineralization) of the material. Polymer mineralization studies were conducted using a *static compost biometer system* incorporating elements of the soil biometer system of Bartha & Pramer [103] as well as features of a standard forced-air composting system [104]. In general, the test consisted of: (i) collecting and characterizing a matured compost inoculum from a full-scale commercial composting facility; (ii) exposing representative samples of the plastic bags to the compost matrix under controlled isothermal and aerobic conditions; (iii) measuring the amounts of CO_2 produced as a function of time; and (iv) assessing the degree of biodegradability of the plastics by comparing the net amount of CO_2 produced from the test materials to that produced from the positive control (e.g., cellulose powder). [Note: CO_2 production was expressed as a fraction of the measured carbon content of the test material.]

Powdered samples were prepared by grinding the test materials using a SPEX Model 6770 cryogenic mill filled with liquid nitrogen (ATS Scientific; Burlington, ON). The carbon and nitrogen content of the test and reference materials were determined using a LECO Model 2000 CNS analyzer (LECO Instruments Ltd.; Mississauga, ON). Sub-samples of the powdered materials (yielding a substrate loading of 10 ± 1 mg polymer-C g^{-1} compost) were mixed with 75 g of a matured compost (screened to pass a 2 mm sieve) at a water content of 60% water-holding capacity (WHC); placed into 1 L Pyrex glass bottles sealed with screw-top lids fitted with a gas sampling port; and incubated in a controlled environment chamber at 52 ± 2 °C. Samples of the headspace gas were withdrawn from the reactors at 12 to 120 h intervals and analyzed for CO_2 and O_2 content using a Varian Model CP-2003 micro-GC equipped with Molecular Sieve 5A and Poraplot U columns and dual micro-TCDs (thermal conductivity detectors). Each time the headspace gas was sampled, the systems were aerated by allowing the atmosphere in the bioreactors to exchange and equilibrate with atmospheric air for 5 to 10 min; at the same time, the compost was hand-mixed to ensure that anaerobic microenvironments did not develop. Daily and cumulative CO_2 production (total and net) were calculated relative to a control reactor

(unamended compost). In addition, net mineralization of the cellulose samples was monitored to ensure that the compost could support an actively degrading microbial population throughout the test exposure. All analyses were run in triplicate.

Table 28. Materials Evaluated in the Tier I Mineralization Tests[a]

Sample[b]			Sample[b]		
Name	ID	% C	Name	ID	% C
V3C corrugated board	V3C	42.17	MRE™ -SF	MRE™ -SF	42.17
V2S solid board	V2S	41.05	MRE™ -Liner	MRE™ -LN	42.05
1-12×12 w/EvCo in liners and medium (69-30-69)	EvCo-1	45.02	Fiberboard	KSU-Q	48.11
2-12×12 w/EvCo in liners and medium (35-36-35)	EvCo-2	45.97	Raw wood fiber	KSU-R	47.11
3-EvCo medium and inside liner (35-30-55)	EvCo-3	44.93	Cheese cloth	KSU-S	42.26
4-12×12 w/EvCo coating (55-36-55)	EvCo-4	48.08	Modified soy protein	KSU-T	44.60
90",36#	90/36	41.91	Chicken feather	KSU-U	48.19
36# W.S. 56"	36WS	41.09	Pulp fiber/modified soy flour (99.5:0.05 w/w) /0.6-mm	KSU-1	45.90
90" 36# Medium	90/36M	37.69	Pulp fiber (control sample)/0.6-mm	KSU-2	45.15
30#, 51 2/8"	30/51	36.21	Pulp fiber/modified soy flour (99.5:0.05 w/w) /1.2-mm	KSU-3	45.60
52# IPC	52-IPC	37.80	Pulp fiber (control sample)/1.2-mm	KSU-4	45.90
55#, 56" IPC	55/56	39.75	Wood fiber/soy protein (80:20 w/w)	KSU-5	49.80
69#, 51.06"	69/51	44.21	Medium density fiber	KSU-6	49.45
90# Liner	90-L	44.60	UGR™ A carton	UGR™ A-C	45.40
WAM™ Spectra A	WAM™-A	46.22	UGR™ A liner	UGR™ A-L	44.80
WAM™ Spectra B	WAM™-B	41.82	55ss48 liner/30 Tallow/55ss48 liner	55ss48-T	47.05
WAM™ Spectra C	WAM™-C	42.66	69ss liner/30 Tallow/69ss48 liner	69ss48-T	46.95
WAM™ Spectra D	WAM™-D	42.39	55ss48 liner/30 WAM™/55ss48 liner	55ss48-W	46.05
30# Uncoated Kraft	30-UCK	43.79	69ss liner/30 WAM™/69ss48 liner	69ss48-W	45.85
30# Kraft coated w/MBX CS06082205	30-CK	45.98	69ss liner/30 Tallow/42 liner/30 medium//69ss48 liner	69ss48/42/30	45.25
MRE™ box	MRE™ -BX	42.20	45 Kraft liner/30B Kraft/45 Kraft liner	45-K	45.15
MRE™ liner	MRE™ -LN	42.05	P2001 PHA	P2001	56.45
M1240 PHB	M1240	57.00	Uncoated paper bag (Portco)	ucPB	44.20
Cellulose powder (Positive control)[c]	Cell	44.54	Coated paper bag (Portco/mirel™)	cPB	46.80

[a] Tests were conducted in six runs over a 3 year period.

[b] Source: Dr. Jo Ann Ratto; NSRDEC, Natick, MA.

[c] Positive control; purchased from Sigma Chemical Corp., St. Louis, MO.

Table 29. Materials evaluated in the Tier II (bench-scale) and Tier III (field-scale) weight loss tests

Solid board samples[a]		Corrugated samples[a]	
Name	ID	Name	ID
Tier II Testing -		***Tier II testing***	
V2S solid board [4-L, 180-L]	V2S	V3C corrugated board [4-L, 180-L]	V3C
V2S (International Paper) [4-L, 180-L]	V2S(IP)	Corrugated internal liner from V2S pack [180-L]	IL(V2S)
MRE™ -V2S [4-L, 180-L]	MRE™ -V2S	MRE™ -Liner [4-L, 180-L]	MRE™ -LN
MRE™ -SF [4-L, 180-L]	MRE™ -SF	WAM™ Spectra D [4-L]	WAM™-D
MRE™ -SF (Temple Inland) [4-L, 180-L]	MRE-SF(TI)	1-12X12 w/EvCo in liners and medium (69-30-69) [4-L]	EvCo-1
MRE ™box [4-L]	MRE™ -BX	2-12X12 w/EvCo in liners and medium (35-36-35) [4-L]	EvCo-2
36# W.S. 56" [4-L]	36WS	3-EvCo medium and inside liner (35-30-55) [4-L]	EvCo-3
69#, 51.06" [4-L]	69/51	4-12X12 w/EvCo coating (55-36-55) [4-L]	EvCo-4
90# Liner [4-L,]	90-L	55#sg48 liner [4-L, 180-L]	55sg48
30# Uncoated Kraft [4-L]	30-UCK	72#sg48 liner [4-L, 180-L]	72sg48
30# Kraft coated w/MBX CS06082205 [4-L,]	30-CK	55ss48 liner/30 Tallow/55ss48 liner [180-L]	55ss48-T
Uncoated paper bag (Portco) [4-L]	UCPB	69ss liner/30 Tallow/69ss48 liner [180-L]	69ss48-T
Coated paper bag (Portco/Mirel) [4-L]	MCPB	55ss48 liner/30 WAM™/55ss48 liner [180-L]	55ss48-W
		69ss liner/30 WAM™/69ss48 liner [180-L]	69ss48-W
		69ss liner/30 Tallow/42 liner/30 medium//69ss48 liner [180-L]	69ss48/42/30
		45# Kraft liner/30B Kraft/45# Kraft liner [4-L]	45-K
		Tier III testing	
		MRE™ -SF (Wornick Co. Cincinnati spec ACR-M-043)	MRE™ -SF(WC)
		MRE™ -SF (International Paper, Lancaster Evansville Indiana)	MRE™ -SF(IP)
		MRE™ coated with liner	MRE™ -LN
		MRE™ meal box	MRE™ -BX
		Long corrugated strips	LCS

[a] Source: Dr. Jo Ann Ratto; NSRDEC, Natick, MA.

[4-L] Tests were conducted in bench-scale (4-L), externally heated (52±2°C) bioreactors.

[180-L] Tests were conducted in a pilot-scale (180-L), self-heated drum composter.

Biodegradation data were plotted in the form of substrate mineralization *vs*. time curves; results of the mineralization studies were interpreted using a modification of the response parameters defined by Farrell et al. (i) MAX-CO_2, defined as the percent cumulative net CO_2-C evolved during the test exposure; (ii) Lag, defined as the time required for net CO_2-C evolution to reach 10% of the MAX-CO_2; (iii) r_{pdp}, average rate of mineralization during the primary degradation phase—defined as the slope of the linear least-squares regression line plotted between the end of the lag period and start of the plateau region (i.e., the point where net mineralization = two-thirds MAX-CO_2); (iv) the relative biodegradation index (RBI), defined as the ratio of cumulative net mineralization of the test sample to cumulative net mineralization of the positive control; and (v) t_{60}, the time required for net mineralization to reach 60% ThCO_2.

6.1.2 Tier II – Rapid Screening Test: Weight loss from plastic materials exposed to a simulated municipal solid-waste (MSW) aerobic compost environment [105, 106]

The Tier II test was used to determine the biodegradability of the test material, relative to that of a standard biodegradable material, in a controlled composting environment. Testing was carried out under carefully controlled laboratory conditions to ensure reproducibility and precision. However, because test conditions are optimized, the observed biodegradability of the test material may not correlate well with that observed in an actual composting environment. Consequently, the rapid screening test is only intended to provide information regarding the inherent degradability of the test material.

Test materials were cut into 2.5 cm × 2.5 cm pieces, assigned an identification number, and (to facilitate recovery) placed in 5 cm square litter bags made from nylon-coated fiberglass screen (1.5 mm square mesh). Each sample bag was supplemented with one-half teaspoon of matured compost (screened to pass a 2 mm sieve) on each side of the film; the sample bags were then placed in 4 L bioreactors containing approximately 300 g of fresh simulated municipal solid waste (sMSW) compost, and incubated at 52 ± 2 °C and a water content of 55 ± 5% (w/w). Test exposures was considered valid if dry-weight loss from the compost matrix itself exceeded 40% (w/w) in the active bioreactors and <10% in a poisoned-control reactor.

In addition to the small isothermal (4 L/52 ± 2 °C) compost reactors, a large self-heating (180 L/variable temperature) drum composter also was used to assess the compostability of a subset of the test materials. Test materials were cut into 5 cm × 5 cm pieces, assigned an identification number, and (to facilitate recovery) placed in 7 cm square litter bags made from nylon-coated fiberglass screen (1.5 mm^2 mesh). Each sample bag was supplemented with one teaspoon of matured compost (screened to pass a 2 mm sieve) on each side of the film; the sample bags were then placed in the 180 L self-heating compost reactors containing approximately 30 kg of raw, simulated yard-waste compost, and incubated for up to 12 weeks at a water content of 55 ± 5% (w/w).

Triplicate samples of the test materials were recovered at 7–14 d intervals for a total of 6–12 weeks. [Note: on each sampling date, one replicate of each material was selected at random and removed from each of three active reactor vessels.] Each sample was carefully removed from its litter bag and cleaned; the residual material was then dried to a constant weight in a convection oven (50 °C for 12 to 18 h), cooled to room temperature in a desiccator, and weighed. Preliminary tests indicated that the paperboard and fiberboard materials generally achieved <40% weight loss after the standard 42 d test; thus, in subsequent tests the *sMSW* compost matrix was increased to 400 g and the test exposures extended to 84 d.

6.1.3 Tier III – Field Testing

Field-scale biodegradation studies are desirable and ultimately may be necessary; however, they are generally expensive, difficult to control and replicate, and are generally unsuitable for establishing biodegradation pathways. Nevertheless, if we are to ensure that laboratory-scale tests do an adequate job of predicting a material's performance in "real world" disposal environments, it is imperative that we first determine the bio-environmental degradability of these materials under conditions representative of various commercial/municipal and backyard composting systems.

Composting was carried out in a large (ca. 1.5 m × 1.85 m × 3.7 m) static windrow that was turned once every 2 weeks. Source materials for the compost included yard waste (primarily grass clippings and leaves) and a bulking agent (wood chips) (target C:N ratio = 30:1). The compost pile was monitored for oxygen content (target >10%), moisture (target = 40–60%, w:w), and temperature (target = 35–60 °C, depending on the stage of composting process) and mechanically manipulated as necessary to keep these variables within their optimal ranges. Upon completion of the composting period (i.e., 3 months of active composting), the quality of the finished compost was determined as described by the US Composting Council [107].

The compostability of the final test materials also was assessed by randomly placing pieces of the material [10 cm square; pre-dried to a constant weight in a convection oven at 50 °C, weighed and placed in 15 cm square litter bags made from nylon-coated fiberglass screen with a 1.5 mm square mesh] in the windrows. One day prior to placing the samples in the compost, 5 ± 0.5 g of matured compost was added to the litter bags on each side of the film. The bags were then tagged, placed in polyethylene Ziploc® bags, and stored in Styrofoam coolers at 4 °C until placed in the compost. To facilitate recovery, a piece of nylon fishing line was attached to each bag and to a flag placed at the surface of the windrow. Upon retrieval from the compost (at 14 d intervals), each sample was carefully removed from its litter bag and assigned a visual rating of sample disintegration; oven dried at 50 °C; and weighed.

6.1.4 Statistical Analyses

Exploratory data analysis [108] was used in the initial stage of the statistical analysis to assess the nature of the frequency distribution for each variable and to identify outliers. Outliers (measured value ≥ median value + k) were defined using a k value of 1.5 times the interquartile range and are excluded from the ANOVA, means separation, and correlation analysis. The Tier I (mineralization) test employed a one-way randomized complete block with repeated measures design (RCBD-RM) with test material as the main factor, cumulative net mineralization as the variable, and replicates as the blocks. The Tier II (weight loss) test employed a two-way randomized complete block design (RCBD) with test material and time as the main factors, weight loss as the variable, and replicates as the blocks. The Tier III (field-scale) test was intended to demonstrate (i) the compostability of test materials under field conditions and (ii) that these materials produce quality compost. Due to cost factors, this test was not replicated.

6.2 Results and Discussion

6.2.1 Tier I – Polymer Mineralization Test

Measurements of a material's net mineralization in an active (fresh) compost are hampered by high levels of CO_2 produced as a result of the decomposition of the compost matrix itself. Thus, to avoid the problems associated with high background CO_2 levels, the Tier I test employed a matured (finished) compost as the test matrix. The matured compost matrix also provided a rich source of the microorganisms needed to biodegrade the test materials as well as the inorganic nutrients needed to support these microorganisms. It should be noted, however, that because mature compost is inherently less active than fresh (active) compost, the Tier II test should be considered a "conservative" test intended only to elucidate information relating to the ultimate biodegradability (i.e., mineralization) of the test material.

6.2.1.1 Validity of the test runs

Unlike weight loss, which reflects structural changes in a material (i.e., deterioration or material erosion), CO_2 evolution provides an indication of the ultimate biodegradability (i.e., mineralization) of the material. Results for the unamended composts and positive controls (i.e., the compost amended with cellulose powder), conducted over a 3 year period, are presented in Figure 66, and the mineralization parameters summarized in Table 30. Carbon dioxide produced in the unamended systems is a result of mineralization of the native organic matter (i.e., background emissions); in the cellulose amended systems, the total CO_2 produced includes the background emissions plus the CO_2 produced during mineralization of the test material. In accordance with ASTM Standard D5338[104], the test exposures were considered valid only if net mineralization of the positive control (i.e., cellulose powder) exceeded 70% within the first 45 d of the test.

Background CO_2 production (i.e., mineralization of the compost matrix itself) ranged from about 400 to 800 mg CO_2-C during test exposures of 83 to 103 d, reflecting differences in the quality of the compost matrices over a 3 year period. Moreover, the CO_2 production curves for the compost matrix generally followed a biphasic pattern with an initial, near-linear (R^2>0.98) period of rapid CO_2 production followed by a period of declining CO_2 production ending in a plateau (defined as a 'flattening' of the curve). This pattern is fairly typical and reflects the changing degradability of the matrix as the most readily-degradable components of the compost are used up. Nevertheless, all six test runs were considered valid, with the positive control (cellulose) achieving 70% net mineralization in 25 to 40 d (the exception being the 3rd test run, which reached the 70% threshold in only 14 d).

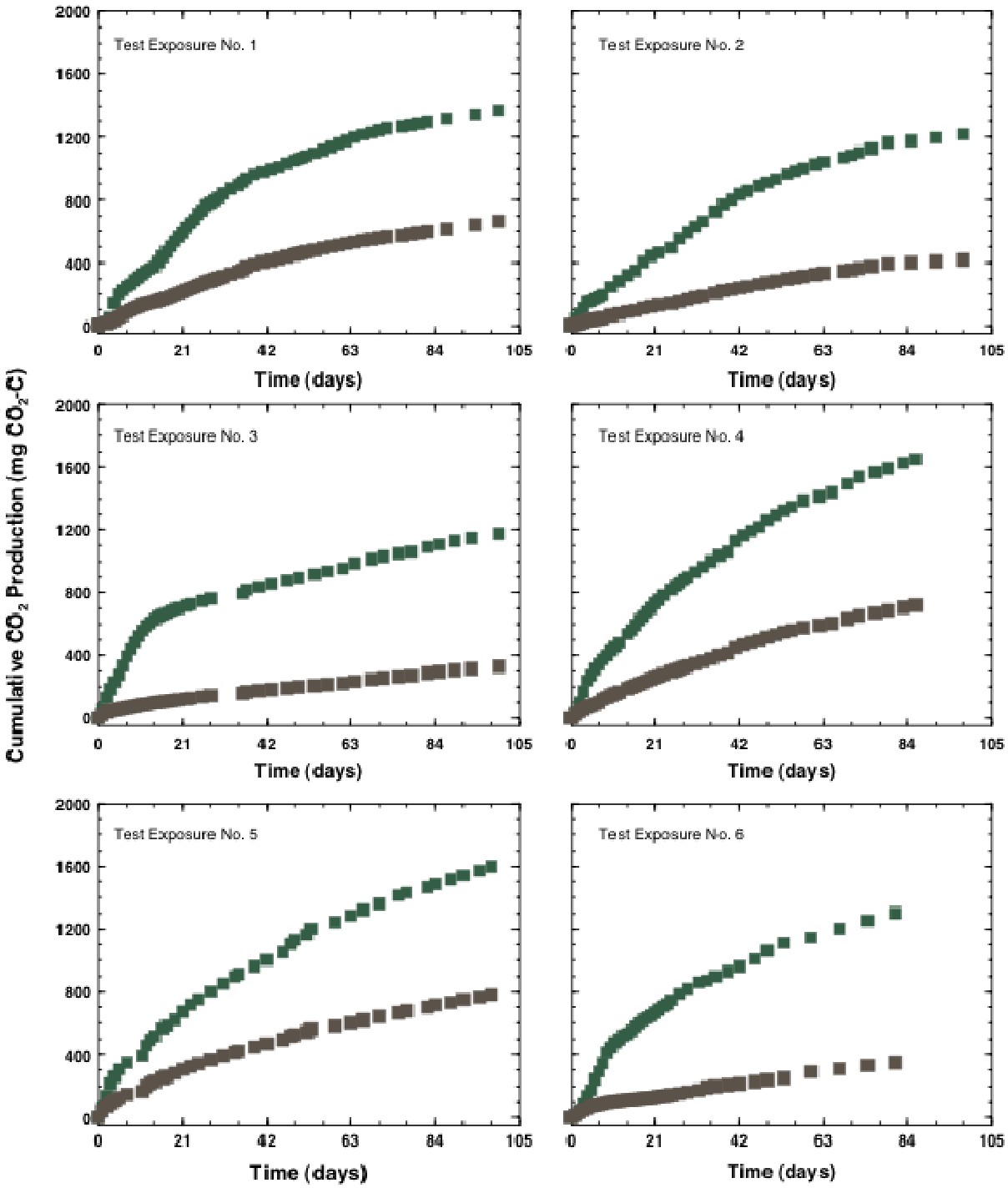

■ Unamended control

■ Cellulose-amended

Note: Because the various test materials listed in Table 28 were delivered over a 3-year period—and because of space limitations in the controlled environment cabinet—the Tier I mineralization test was repeated (n=6) as materials and space became available.

Figure 66. Carbon dioxide produced by the unamended control and cellulose-amended composts during the six test exposures

All test runs were performed with compost obtained from a commercial supplier (Early's Garden Centre; Saskatoon, SK) and were maintained at 52 ± 2 °C and 55 ± 5% WHC. In all test exposures, total net mineralization of the positive control exceeded 100%, as shown in Table 30 which is indicative of a 'priming effect' [109]. That is, the addition of a readily biodegradable substrate (in this case, cellulose powder) to a matrix with a low available-C content results in an increase in both the size and activity of the indigenous microbial population. This, in turn, results in enhanced mineralization of the native organic matter as the added substrate is depleted– yielding amounts of *net* CO_2-C that may exceed 100% of the added substrate-C. In either case, it is assumed that the *relative performance* of the test materials (i.e., relative to the positive control) is not influenced by matrix effects.

Table 30. Summary of mineralization parameters for the positive control (cellulose powder) included in each test run

Test run no.	% C	Lag[a] *(d)*	r_{PDP}[b] *(mg CO_2-C d^{-1})*	Duration[c] *(d)*	t_{70}[d] *(d)*	Net mineralization[e] *(%ThCO_2-C)*
1	44.54	3	15.8	32	31	109 ± 5
2	44.54	3	12.4	44	37	136 ± 17
3	44.54	2	41.6	12	14	122 ± 6
4	44.54	3	15.4	29	26	124 ± 7
5	44.54	2	9.3	49	39	131 ± 9
6	44.54	4	45.9	7	21	127 ± 4

[a] Time required for net mineralization to reach 10% of the Max-CO_2. Note: In those cases where the net mineralization curve did not reach a plateau, the Lag was defined as the time required for net CO_2-C evolution to reach 5% of the ThCO_2 maximum.

[b] Average rate of mineralization during the primary degradation phase: defined as the slope of the linear least-squares regression line plotted between the end of the lag period and start of the plateau region (i.e., the point where net mineralization = two-thirds MAX-CO_2).

[c] Duration of the linear phase.

[d] Time required for net mineralization to reach 70% ThCO_2.

[e] The maximum amount of CO_2-C evolved (expressed as % ThCO_2-C) during a 180 d test exposure.

To verify that the relative performance of the test materials was not significantly affected by the activity of the compost matrix, four test materials (V3C, V2S, MRE™ SF, and MRE™ Liner) were included in both the 2nd and 5th test runs. Cummulative net mineralization curves for these four materials are shown in Figure 67, and the results for those materials (as well as those plotted in Figures 68 and 69) are summarized in Table 31. Despite differences in the rate and total net mineralization, the relative performance of the test materials was not significantly affected by the differences in compost activity, which is shown in Table 31. That is, all four materials were classified as biodegradable (i.e., net mineralization ≥60% in less than 180 d)—with *RBI* values greater than 0.70. Moreover, the V3C and MRE™ SF exhibited performance characteristics that equaled or exceeded the positive control in both tests; and, in both tests, the *RBI* decreased in the order: V3C ≈ MRE™ SF > MRE™ Liner ≈ V2S.

Net mineralization curves for WAM™ (Spectra-Kote Corp.; Gettysburg, PA) and EvCo (EvCo Research, LLC; Pendergrass, GA) samples are presented in Figure 68, and the results summarized in Table 31. The WAM™ products (Figure 68a) are a series of "wax alternative materials" consisting of a water-based polymer (composition unknown) applied to paper and fiberboard packaging materials. Likewise, the EvCo products (Figure 68b) are polyester-based

coatings and adhesives based on recycled polyethylene terephthalate (PET). For the respirometry tests, samples of various weight paperboards with the WAM™ and EvCo coatings were ground to a powder to maximize the surface area and facilitate biodegradation. Whereas the WAM™ samples exhibited typical biphasic mineralization curves, the EvCo samples exhibited a more unusual, triphasic mineralization pattern. This pattern is indicative of a material consisting of two components that vary in their inherent biodegradability. In this case, one component degrades very rapidly (with an initial degradation rate of 22–28 mg C d^{-1}), while the other degrades in a manner similar to that of the positive control (cellulose), but with an r_{PDP} of 13–15 mg C d^{-1}. This was reflected in t_{60} values that were slightly greater (3–36 d) than that for the positive control (25 d). The lone exception was the EvCo-4, which exhibited slower mineralization kinetics (r_{PDP} = 10 mg C d^{-1}) and required significantly longer (t_{60} = 56 d) to reach the 60% mineralization threshold. Nevertheless, all of the EvCo™ materials were classified as biodegradable. Likewise, the WAM™ samples met the criterion for a biodegradable material, with the *A* and *B* samples exhibiting performance characteristics comparable to the positive control.

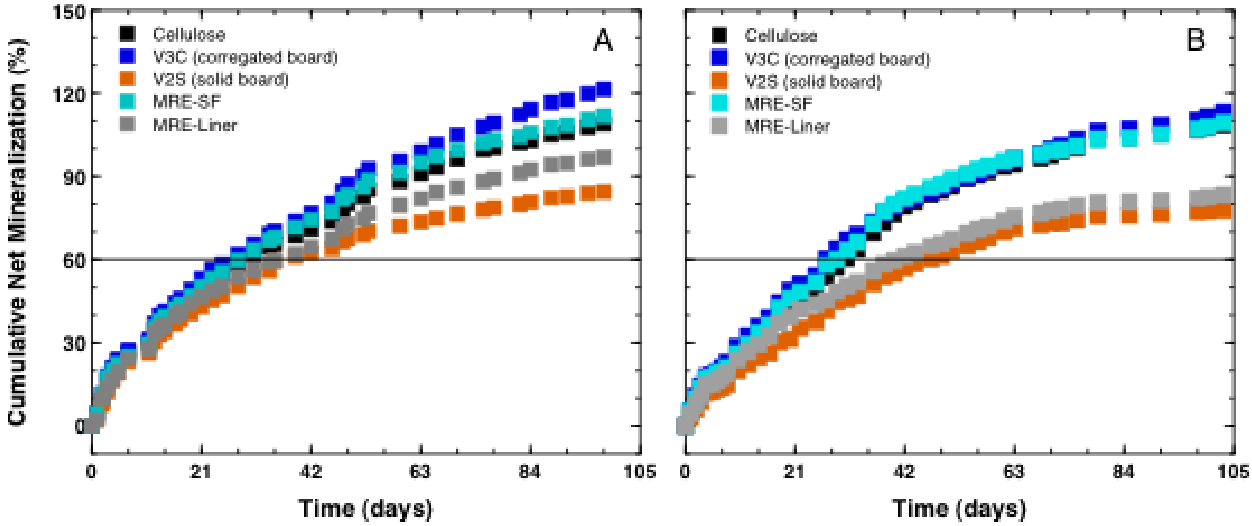

The solid black line indicates the net mineralization threshold for a "biodegradable" material.
Note: The test materials were added as a powder (10 mg C g-1 compost); bioreactors were incubated in the dark at 52±2 °C and 55±5% WHC.

Figure 67. Cumulative net mineralization (%ThCO2) of the reference samples under controlled composting conditions: (a) Test run no. 5; (b) Test run no. 2

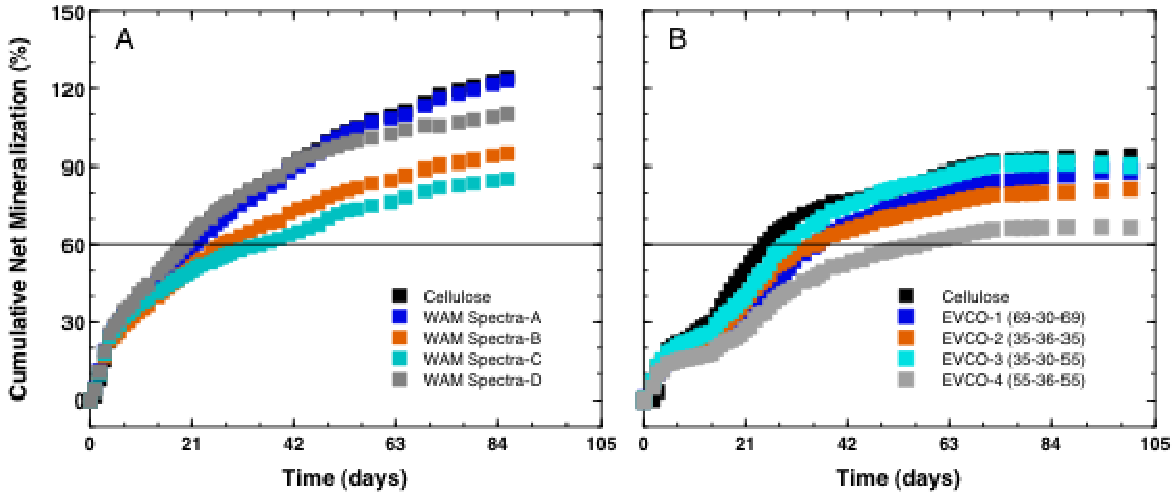

The solid black line indicates the net mineralization threshold for a "biodegradable" material.
Note: The test materials were added as a powder (10 mg C g^{-1} compost); bioreactors were incubated in the dark at 52±2 °C and 55±5% WHC.

Figure 68. Cumulative net mineralization (%$ThCO_2$) of the samples under controlled composting conditions: (a)WAM™, (b) EvCO™

Net mineralization curves for the different fiberboards are presented in Figure 69, and the results summarized in Table 31. With one notable exception, these materials exhibited performance characteristics that were comparable to, or exceeded, those of the positive controls. The 69 lb/51.06" sample was the lone exception—and was one of only five test samples that failed to meet the ASTM criterion for a biodegradable material; that is, although it achieved 60% net mineralization in 69 d (and nearly 80% after 180 d), this yielded an *RBI* value of only 0.53 (and 0.57 after 180 d). This presumably reflects a compositional difference in the test material—though what that difference is, is not clear at this time.

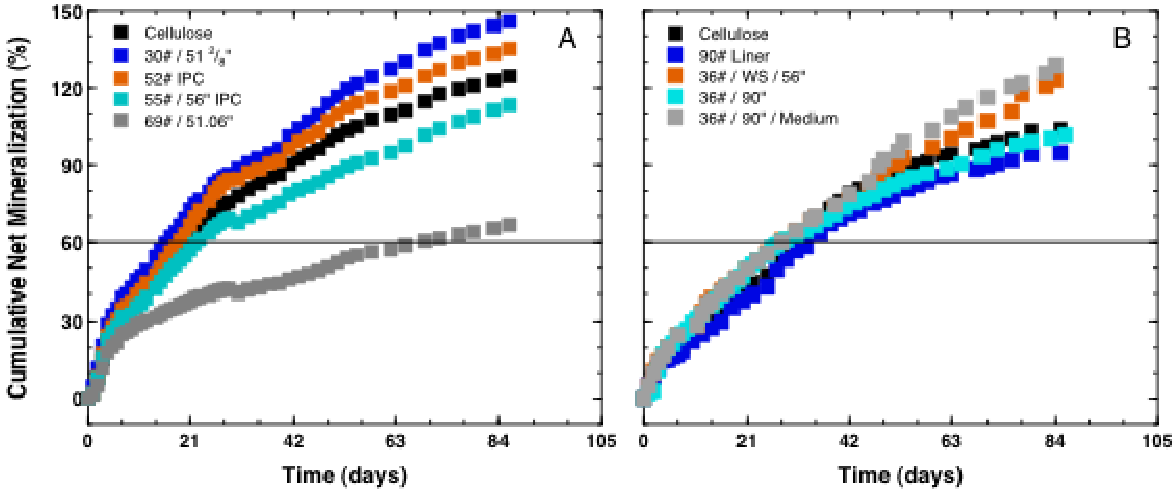

The solid black line indicates the net mineralization threshold for a "biodegradable" material.
Note: The test materials were added as a powder (10 mg C g^{-1} compost); bioreactors were incubated in the dark at 52±2 °C and 55±5% WHC.

Figure 69. Cumulative net mineralization (%$ThCO_2$) of fiberboard paper weight samples under controlled composting conditions: (a) Various paper weights compared to cellulose (b.) 36# paper formulations compared to 90# liner paper and cellulose

Table 31. Mineralization parameters of materials evaluated in the Tier I respirometry studies

Name[a]	Lag[b] (d)	r_{PDP}[c] (mg C d^{-1})	Duration[d] (d)	Max-CO_2-C[e] (%ThCO_2)	RBI[f]
V3C corrugated board [5]	2	9.7	52	147 ± 9	1.09 ± 0.03
V2S solid board [5]	2	9.3	28	91 ± 10	0.83 ± 0.04
MRE™ -SF [5]	2	9.7	46	129 ± 11	1.03 ± 0.01
MRE™ -Liner [5]	2	6.8	58	114 ± 10	0.90 ± 0.01
V3C corrugated board [2]	3	12.5	42	149 ± 13	1.04 ± 0.03
V2S solid board [2]	3	8.5	49	101 ± 17	0.73 ± 0.02
MRE™ -SF [2]	2	12.1	49	138 ± 10	1.02 ± 0.03
MRE™ -Liner [2]	2	8.3	37	81 ± 9	0.76 ± 0.06
WAM™ Spectra A [4]	2	13.2	35	122 ± 8	0.98 ± 0.02
WAM™ Spectra B [4]	2	11.2	27	94 ± 6	0.79 ± 0.02
WAM™ Spectra C [4]	2	8.7	20	85 ± 15	0.72 ± 0.03
WAM™ Spectra D [4]	2	14.6	26	110 ± 11	0.97 ± 0.05
1-12×12 w/EvCo in liners and medium (69-30-69) [1]	3	12.7	34	103 ± 9	0.70 ± 0.02
2-12×12 w/EvCo in liners and medium (35-36-35) [1]	3	13.9	24	86 ± 10	0.85 ± 0.02
3-EvCo medium and inside liner (35-30-55) [1]	3	14.6	28	95 ± 10	0.96 ± 0.02
4-12×12 w/EvCo coating (55-36-55) [1]	3	10.2	26	72 ± 9	0.70 ± 0.02
36#, 90" [4]	3	12.7	28	101 ± 5	0.81 ± 0.01
52# IPC [4]	2	17.2	28	135 ± 13	1.08 ± 0.01
55#, 56" IPC [4]	2	14.0	24	113 ± 10	0.88 ± 0.02
69#, 51.06" [4]	2	6.1	20	66 ± 6	0.53 ± 0.03
90# Liner [4]	3	11.0	47	126 ± 12	0.91 ± 0.01
36# W.S. 56" [4]	3	10.4	58	157 ± 13	1.12 ± 0.06
36# Medium90" [4]	4	10.8	72	163 ± 13	1.17 ± 0.07
30#, 51 2/8" [4]	2	17.1	26	145 ± 6	1.15 ± 0.02
55ss48 liner/30 Tallow/55ss48 liner [6]	5	7.5	19	48 ± 9	0.38 ± 0.02
55ss48 liner/30 WAM™/55ss48 liner [6]	5	14.8	18	93 ± 14	0.74 ± 0.02
45 Kraft liner/30B kraft/45 kraft liner [6]	3	14.9	16	95 ± 9	0.89 ± 0.11
69ss liner/30 Tallow/69ss48 liner [6]	5	11.0	19	84 ± 4	0.67 ± 0.01
69ss liner/30 WAM™/69ss48 liner [6]	2	11.2	14	95 ± 6	0.75 ± 0.02
69ss liner/30 Tallow/42 liner/30 medium/69ss48 liner [6]	3	11.0	20	94 ± 15	0.76 ± 0.01

[a] The number in brackets refers to the test run in which the sample was included.

[b] Time required for net mineralization to reach 10% of the Max-CO_2. Note: In those cases where the net mineralization curve did not reach a plateau, the Lag was defined as the time required for net CO_2-C evolution to reach 5% of the ThCO_2 maximum.

[c] Average rate of mineralization during the primary degradation phase: defined as the slope of the linear least-squares regression line plotted between the end of the lag period and start of the plateau region (i.e., the point where net mineralization = two-thirds MAX-CO_2).

[d] Duration of the linear phase.

[e] The maximum amount of CO_2-C evolved during a 180 day test exposure.

[f] Relative biodegradation index; defined as the ratio of cumulative net mineralization of the test sample to cumulative net mineralization of the positive control. Note: values in red indicate that the RBI is below the acceptable ASTM standard (i.e., RBI<0.60).

Net mineralization of the 55ss48, 69ss48 and Kraft composite papers is presented in Figure 70. Biodegradation of these materials was generally quite good—with five of the six samples achieving greater than 80% net mineralization after 84 d. Whereas the 69ss48-liner/30-Tallow/69ss48-liner (69ss48-T) exhibited relatively good performance characteristics (r_{PDP} = 11.0 mg C d^{-1}; t_{60} = 29-d; *RBI* = 0.67), the 55ss48-liner/30-Tallow/55ss48-liner (55ss48-T) performed quite poorly—with a relatively slow r_{PDP} (7.5 mg C d^{-1}) and one of the lowest *RBI*

values (0.38) of the 46 materials tested. Moreover, this was one of only three samples that failed to reach the 60% net mineralization threshold during the 84 d test[1]. It is worth noting that the 55ss48-T had essentially reached the plateau phase by Day 49 and that extending a linear least-squares regression line through the plateau region of the curve (i.e., from Day 49 to Day 180) predicted that total net mineralization was likely to increase by only about 4–6%. Thus, it was considered highly unlikely that total net mineralization would have exceeded the 60% threshold even if the test had not been terminated. Again, this presumably reflects a compositional difference in the 55ss48 liner and the 69ss48 liner; though the exact nature of this difference is unknown at this time.

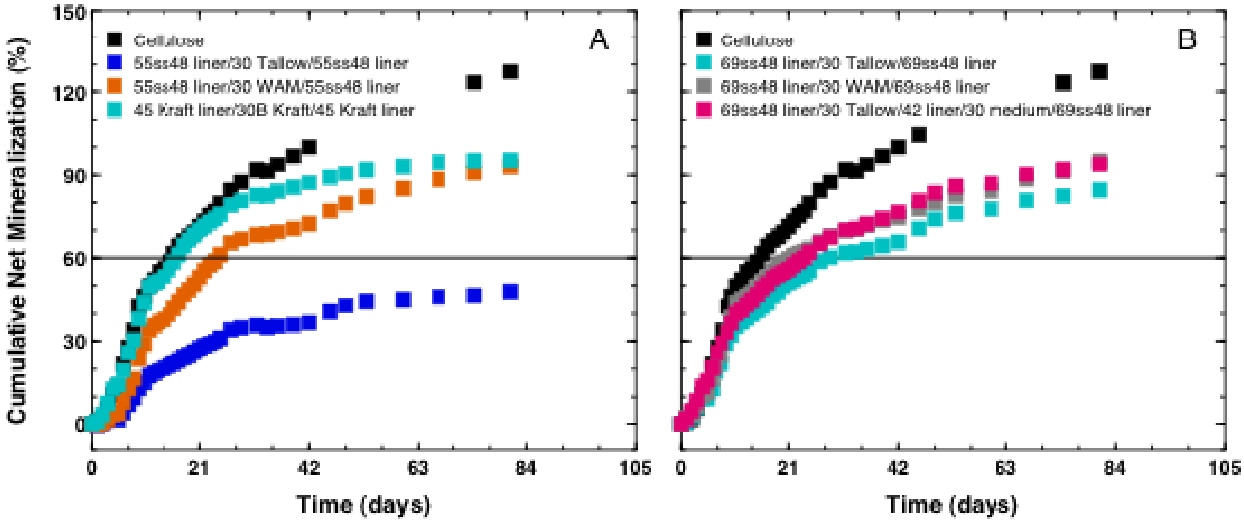

The solid black line indicates the net mineralization threshold for a "biodegradable" material.

Note: The test materials were added as a powder (10 mg C g^{-1} compost); the bioreactors were incubated in the dark at 52±2 °C and 55±5% WHC.

Figure 70. Cumulative net mineralization (%$ThCO_2$) of the samples under controlled composting conditions: (a) 55ss48 samples and Kraft paper; (b) 69ss48

Net mineralization curves for a series of fiberboards prepared (courtesy of Dr. Susan Sun) .at Kansas State University (KSU) are presented in Figure 71. The first series of fiberboards (Figure 71A) consisted of pulp fiber (KSU-2 & KSU-4), a 199:1 (w/w) pulp fiber/modified soy flour blend (KSU-1 & KSU-3), an 80:20 (w/w) wood fiber/soy protein blend (KSU-5) and a MDF (KSU-6). Sample thickness also varied, at 0.6 mm (KSU-1 & KSU-2) and 1.2 mm (KSU-3 & KSU-4). Incorporation of modified soy flour into the pulp fiber matrix resulted in slower net mineralization of the substrate (i.e., a 20–34% reduction in the r_{PDP} and a doubling of the t_{60}) and significantly reduced the relative biodegradability (*RBI*) of the pulp fiber as seen in Figure 71A and Table 32. Despite this effect, both the control and soy-modified fiberboards mineralized to a high extent (81–120% $ThCO_2$; *RBI* = 0.66–0.95) and, as such were classified as biodegradable materials.

[1] Note: this test run (No. 6) was terminated at 84-d, due to an error that resulted in the bioreactors becoming anaerobic.

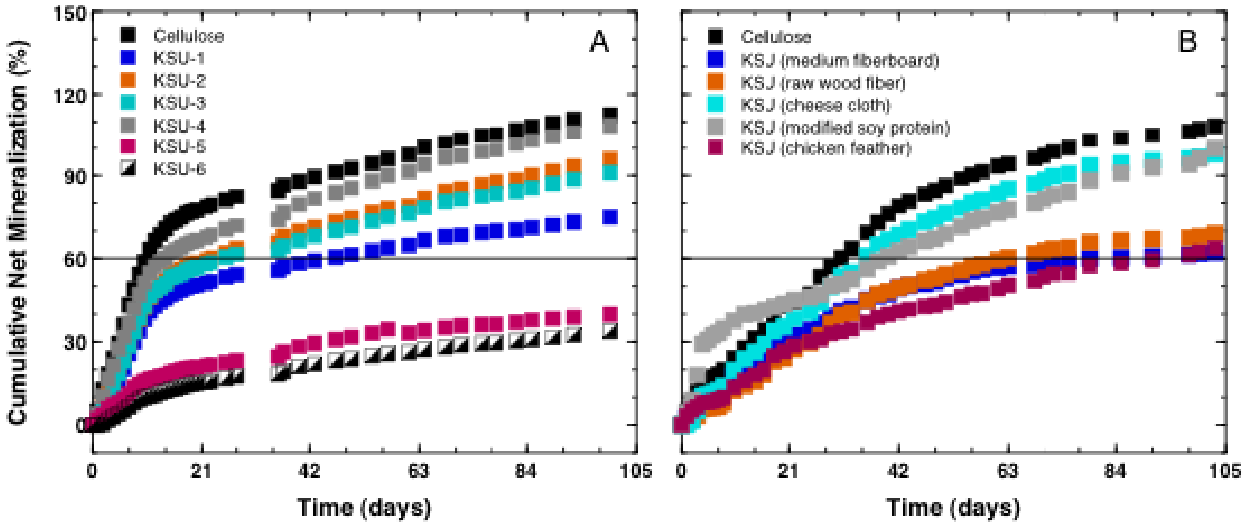

The solid black line indicates the net mineralization threshold for a "biodegradable" material.

Note: The test materials were added as a powder (10 mg C g^{-1} compost); the bioreactors were incubated in the dark at 52±2 °C and 55±5% WHC.

Figure 71. Cumulative net mineralization (%ThCO_2) of the Kansas State University samples under controlled composting conditions: (a) Fiberboards, (b) Fiberboard components

The second set of KSU samples (Figure 71b) included a composite fiberboard and the individual components of the fiberboard, including raw wood fiber, cheese cloth, modified soy protein, and chicken feathers. Whereas the mineralization characteristics of the modified soy protein and cheese cloth were comparable to those of the positive control, as shown in Figure 71b and Table 32, the raw wood fiber, chicken feathers and the composite fiberboard all exhibited much slower mineralization kinetics. Nevertheless, the individual components and the composite all achieved greater than 60% net mineralization in 5 to 12 weeks, and all but the chicken feathers yielded *RBI* values ≥0.60.

Table 32. Mineralization parameters of fiberboard and coated papers evaluated in the Tier I respirometry studies

Name[a]	Lag[b] (d)	r_{PDP}[c] (mg C d^{-1})	Duration[d] (d)	Max-CO_2-C[e] (%ThCO_2)	RBI[f]
KSU-1: Pulp fiber/modified soy flour (99.5:0.05 w/w)/0.6-mm [3]	3	2.5	85	80.9 ± 8	0.66 ± 0.01
KSU-2: Pulp fiber (control sample)/0.6-mm [3]	3	3.8	87	107.1 ± 16	0.84 ± 0.02
KSU-3: Pulp fiber/modified soy flour (99.5:0.05 w/w)/1.2-mm [3]	3	3.5	88	100.7 ± 9	0.79 ± 0.02
KSU-4: Pulp fiber (control sample)/1.2-mm [3]	2	4.4	88	119.7 ± 12	0.95 ± 0.02
KSU-5: Wood fiber/soy protein (80:20 w/w) [3]	2	2.8	45	44.9 ± 5	0.35 ± 0.02
KSU-6: Medium density fiber [3]	5	2.2	67	42.8 ± 3	0.29 ± 0.03
KSU-Q: Fiberboard [2]	3	8.7	33	79.7 ± 7	0.60 ± 0.04
KSU-R: Raw wood fiber [2]	8	8.7	44	97.8 ± 2	0.64 ± 0.02
KSU-S: Cheese cloth [2]	7	10.8	51	131.8 ± 13	0.89 ± 0.02
KSU-T: Modified soy protein [2]	3	5.2	170	150.4 ± 29	0.88 ± 0.09
KSU-U: Chicken feather [2]	4	3.6	63	74.6 ± 23	0.55 ± 0.03
P2001 PHA [6]	5	37.8	10	136.8 ± 5	1.41 ± 0.20
M1240 PHB [6]	4	36.6	12	110.1 ± 9	1.04 ± 0.16
Uncoated paper bag (Portco) [6]	4	20.1	10	128.0 ± 10	1.07 ± 0.04
Coated paper bag (Portco/mirel) [6]	5	16.5	18	106.8 ± 9	0.95 ± 0.06
30# Uncoated Kraft [2]	3	7.9	63	124.6 ± 10	0.80 ± 0.03
30# Kraft coated w/MBX CS06082205 [2]	3	8.4	51	108.2 ± 2	0.77 ± 0.01
UGR™ A carton [3]	2	2.2	94	80.6 ± 19	0.66 ± 0.01
UGR™ A liner [3]	2	2.9	95	77.3 ± 18	0.61 ± 0.02

[a] The number in brackets refers to the test run in which the sample was included.

[b] Time required for net mineralization to reach 10% of the Max-CO_2. Note: In those cases where the net mineralization curve did not reach a plateau, the Lag was defined as the time required for net CO_2-C evolution to reach 5% of the ThCO_2 maximum.

[c] Average rate of mineralization during the primary degradation phase: defined as the slope of the linear least-squares regression line plotted between the end of the lag period and start of the plateau region (i.e., the point where net mineralization = two-thirds MAX-CO_2).

[d] Duration of the linear phase.

[e] The maximum amount of CO_2-C evolved during a 180 d test exposure. Note: values in red indicate that the RBI is below the net mineralization threshold for a biodegradable material.

[f] Relative biodegradation index; defined as the ratio of cumulative net mineralization of the test sample to cumulative net mineralization of the positive control. Note: values in red indicate that the RBI is below the acceptable ASTM standard (i.e., RBI<0.60).

In addition to the various fiberboard and fiberboard components, we also examined the mineralization of a set of polymer-coated papers and their respective uncoated controls (see Figure 72 and Table 32). The first set of samples included a conventional Portco paper bag (Portco Packaging; Vancouver, WA) and a bag coated with "*Mirel*", a polyhydroxyalkanoate (P2001 PHA) manufactured by Metabolix (Cambridge, MA). The second set of samples included a 30 lb Kraft paper bag and a bag coated with a second PHA (MBX CS06082205: Metabolix; Cambridge, MA). The PHAs by themselves exhibited performance characteristics that generally exceeded those of the positive control (Figure 72A). Indeed, both PHAs reached 60% net mineralization in less than 14 d, which would classify them as *readily* biodegradable [110]. The uncoated and *Mirel*-coated Portco paper bags also exhibited performance characteristics comparable to those of the positive control. However, mineralization of the coated bag reached a plateau sooner than that of the uncoated bag and, as a result, the final RBI value for the coated bag was less than that for the uncoated bag.

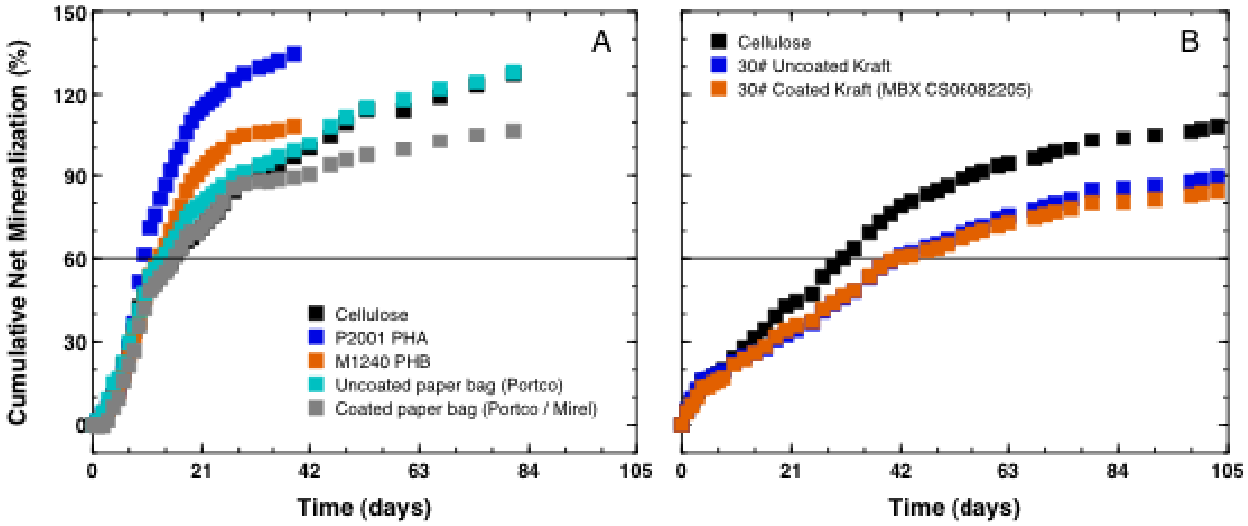

The solid black line indicates the net mineralization threshold for a "biodegradable" material.

Note: The test materials were added as a powder (10 mg C g^{-1} compost); the bioreactors were incubated in the dark at 52±2 °C and 55±5% WHC.

The P2001 PHA and M1240 PHB sample runs were terminated once net mineralization exceeded 100% and the mineralization curves entered the plateau phase.

Figure 72. Cumulative net mineralization (%ThCO_2) of polymer coatings: (a) (P2001 PHA & M1240 PHB) and the coated (Portco/Mirel & MBX-coated Kraft); (b) Uncoated (Portco & Kraft) papers under controlled composting conditions

In addition to the samples described above, we also examined the mineralization of the materials used to ship UGR™ A. Net mineralization curves for the UGR™ A carton and liner are presented in Figure 73**.** In general, mineralization of both the carton and liner were similar in that net CO_2 production proceeded relatively quickly during the first 10–12 d of the test exposure, and then entered an extended (95 d) period characterized by a slow, linear increase in net mineralization as shown in Figure 73. As a result, the t_{60} values for the carton and liner were 43 d and 66 d, respectively. Despite the relatively slow biodegradation of these materials, both yielded *RBI* values >0.60 and were thus classified as biodegradable.

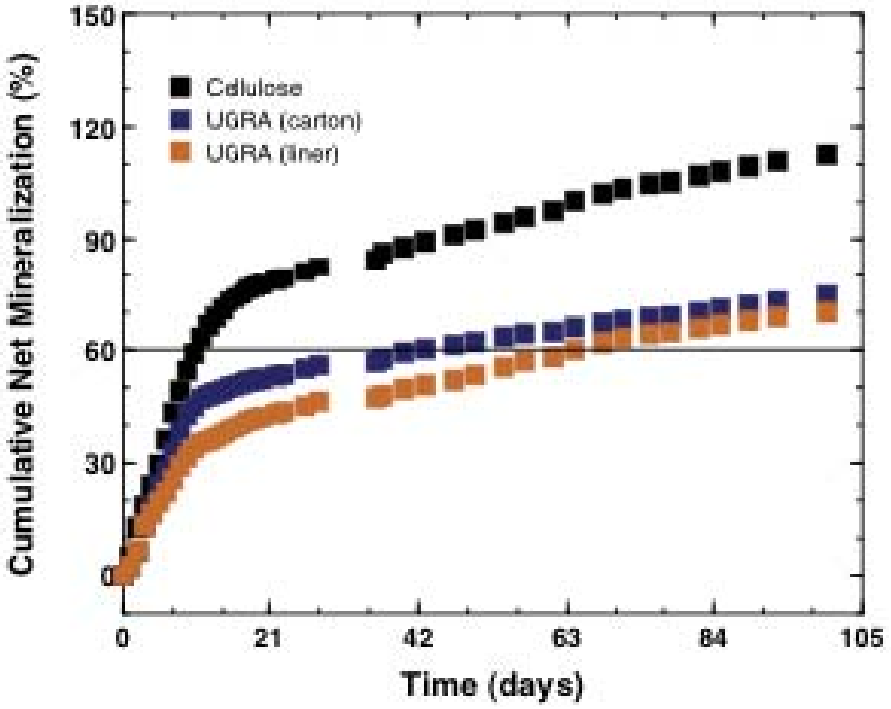

The solid black line indicates the net mineralization threshold for a "biodegradable" material. Note: The test materials were added as a powder (10 mg C g^{-1} compost); thebioreactors were incubated in the dark at 52±2 °C and 55±5% WHC.

Figure 73. Cumulative net mineralization (%ThCO_2) of the UGR™ A samples under controlled composting conditions

6.2.2 Tier II – Rapid Screening Test

The Tier II weight-loss test was used as a rapid screening test to assess the compostability of the test materials under standard, controlled conditions. Validation of the lab-scale weight loss test was made by assessing key indicators of compost activity; i.e., a reduction in weight and increase in pH of the compost matrix itself during the test exposure. Weight loss from the active bioreactors averaged about 71% (w/w) while the pH of the compost matrix increased from about 6.5 to 8.0 during the 84 d test exposures. On the other hand, compost in the poisoned-control exhibited only about 8% (w/w) weight loss and there was no significant change in pH during the test exposures; consequently, all test exposures were considered valid.

Results from the preliminary (42 d) Tier I test are presented in Figure 74. In general, the corrugated materials (V3C, MRE™ Liner & EvCo-1) tended to degrade faster, and to a greater extent, than the solid board samples (V2S, MRE™ Box and MRE™ SF). Indeed the ANOVA indicated that the overall degradation of the corrugated samples [as indicated by the time-averaged Performance Index (*PI*)] was significantly ($P \leq 0.05$) greater than that of the solid board samples (Table 33). This most likely reflects greater access to the interior surfaces of the corrugated materials; i.e., whereas the solid board materials degrade from the outer surfaces inward, the open spaces in the corrugated materials also allow them to degrade from the inside outward. Nevertheless, total (42 d) weight loss did not exceed 40% for any of the samples, which suggested that the timeframe for the Tier I test was too short. Consequently, all subsequent test exposures were increased to 84 d.

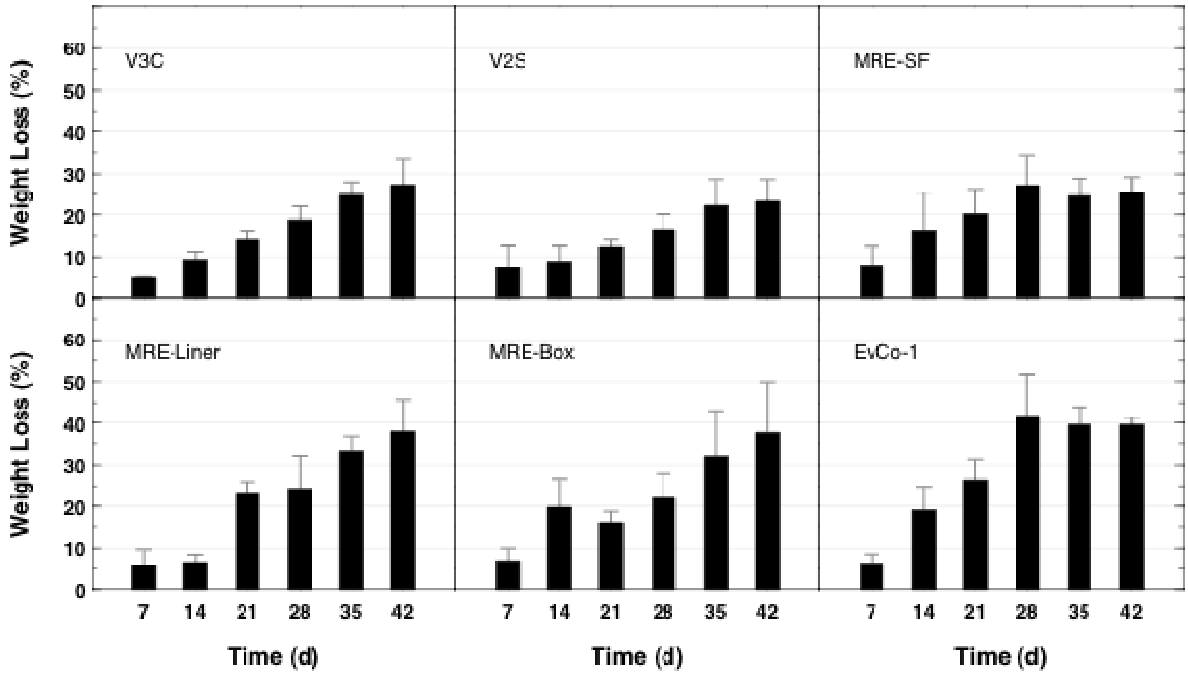

Note: The samples were placed in a continuously aerated, externally heated, 4 L bioreactor containing approximately 300 g of fresh *sMSW* compost. The bioreactors were incubated in the dark at 52±2 °C and 55±5% WHC. Test materials were added as intact (2.5 cm × 2.5 cm) pieces.

Figure 74. Tier II weight loss test—preliminary (42 d) study

Table 33. Results of the LSD test for the preliminary (42 d) weight loss and overall performance index obtained during composting in bench-scale (4 L) bioreactors

Sample ID	Weight loss (%)[a, b]	Sample ID	*PI*[a, b]
EvCo-1	39.5 a	EvCo-1	28.8 a
MRE™-LN	38.0 ab	MRE™-BX	22.4 b
MRE™-BX	37.7 ab	MRE™-LN	21.9 b
V3C	27.2 abc	MRE™-SF	20.2 b
MRE™-SF	25.2 bc	V3C	16.5 cd
V2S	23.3 c	V2S	15.1 d

[a] Within columns, values followed by the same letter are not significantly different ($P \leq 0.05$).

[b] Overall performance index = weight loss (%) averaged across time.

Extending the test exposures generally resulted in greater degradation of the test materials, though weight loss generally tended to plateau between Day 56 and Day 70 as shown in Figure 75. Degradation of the coated papers (30-CK & MCPB) was similar to that of the uncoated papers (30-UCK & UCPB), indicating that the use of a biodegradable PHA coating had no significant (F = 2.417ns) effect on degradation of the paper itself. Nevertheless, the Kraft papers (both uncoated & coated) degraded faster and to a greater extent than the Portco papers as shown in Table 34. Although the coated and uncoated Portco paper bags degraded to about the same extent (i.e., 78±2%) over the 84 d test exposure, the Mirel coating appeared to increase the rate at which the bag degraded; i.e., degradation of the Mirel-coated bag reached a maximum

after about 42 d as opposed to the uncoated bag, which required about 56 d to reach its plateau. Comparison of the three NSRDEC fiberboards [Natick-6 (36 lb WS 56”), Natick-11 (69 lb, 51.06”) and Natick-12 (90 lb Liner)] revealed a significant difference in both overall performance and total weight loss as illustrated in Figure 75 and Table 34, with the Natick-6 and Natick-12 samples degrading more rapidly, and to a slightly greater extent, than the Natick-11 sample. The rapid weight loss of the Natick-12 sample (which was the thickest of the three samples) appeared to be related to degradation of the outer layers of the fiberboard (see photographs in Appendix A)—with the core material being considerably more recalcitrant.

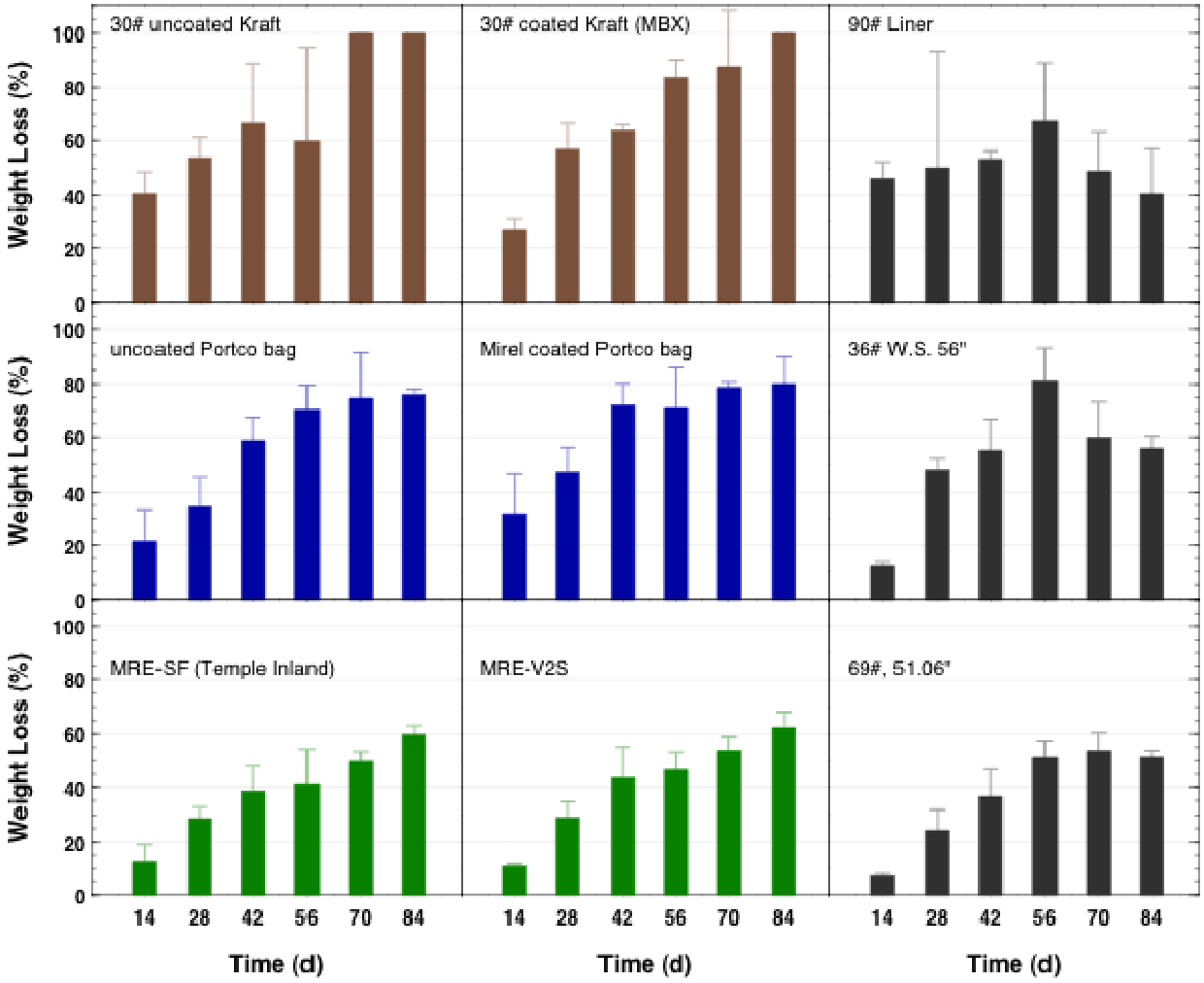

Note: The bioreactors were incubated in the dark (at 52±2 °C and 55±5% WHC) for 84 d. The test materials were added as intact (2.5 cm × 2.5 cm) pieces.

Figure 75. Weight loss from paper and solid board materials in a continuously aerated, externally heated, 4 L bioreactor containing approximately 300 g of fresh *sMSW* compost

Table 34. Results of the LSD test for the 84 d weight loss and overall performance index for paper and solid board materials

Sample ID	Weight loss (%)[a, b]	Sample ID	*PI*[a, b]
30-UCK	100 a	30-UCK	70.1 a
30-CK	100 a	30-CK	69.7 a
MCPB	80.1 b	MCPB	63.4 a
UCPB	76.1 b	UCPB	56.0 b
MRE™-V2S	62.5 c	36WS	51.9 b
MRE™-SF(TI)	59.7 c	90-L	51.1 b
36WS	55.7 c	MRE™-V2S	41.1 c
69/51	51.2 cd	MRE™-SF(TI)	38.4 c
90-L	40.4 d	69/51	37.4 c

Note: Results obtained during composting in bench-scale (4 L) bioreactors

[a] Within columns, values followed by the same letter are not significantly different ($P \leq 0.05$).

[b] Overall performance index = weight loss (%) averaged across time.

Degradation of the EvCO-1, -2, and -3 corrugated boards differed from that of most other test materials in that there was a distinct lag period. That is, despite the fact that some of the layers had begun to separate by Week 2 (see photographs in Appendix) there was little or no net weight loss from the test samples during the first 2 weeks of the test exposure (see Figure 76). On the other hand, the EvCo-4 sample exhibited significant weight loss (*ca.* 26%) after only 2 weeks in the compost. Moreover, EvCo-4 exhibited a performance index (*PI* = 57.6) and total weight loss (74.6%) that were significantly greater than those of the other EvCo products (Table 35). In terms of overall performance, however, the data suggest that the polyester-based coatings and adhesives used in the EvCo products have a minimal effect on their overall environmental performance.

Unlike the EvCo products, the water-based polymer coating in the WAM™-D did not seem to slow the initial degradation of the fiberboard (Figure 76). Indeed, during the first 2 weeks of the test exposure, weight loss by the WAM™-D was comparable to that of several of the paper and paperboard products. Somewhat surprisingly, the internal (corrugated) layer in the WAM™-D seemed to weaken and collapse during extended exposure in the compost, suggesting that degradation was occurring primarily in the internal layer. Whether this effect was related to the coating used is unknown at this time.

The 45#/30B/45# Kraft corrugated sample also exhibited very good environmental performance, with a *PI* that was among the highest recorded in the Tier II tests—comparable to (i.e., not significantly different from) those of the coated and uncoated Portco paper bags, as was shown in Table 34. Comparison of the 55#sg48m and 72#sg48m samples indicated that they degraded to the same extent and at comparable rates (see Table 35). In terms of overall performance, they were comparable to the EvCo products and V2S solid board.

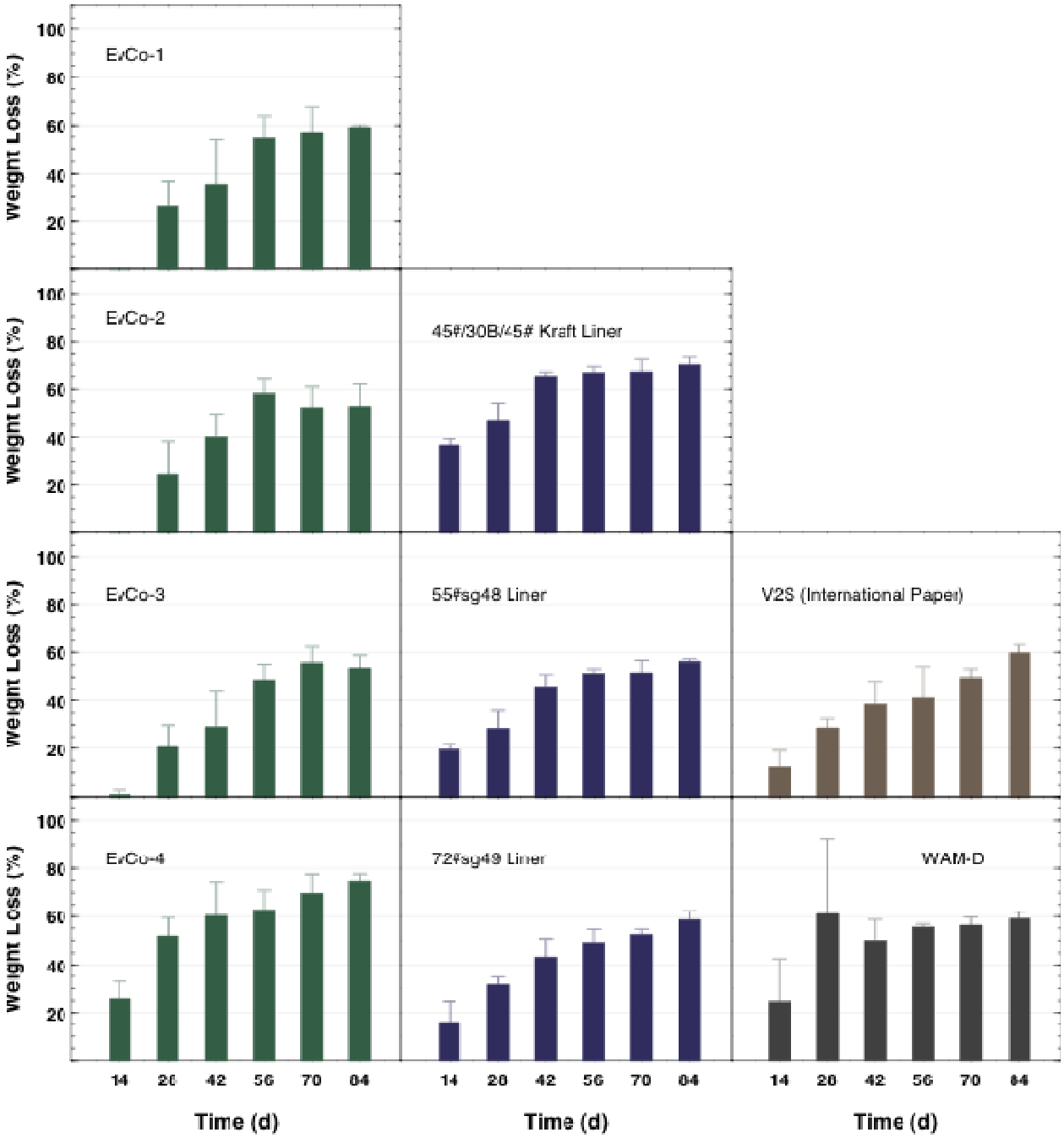

Note: The bioreactors were incubated in the dark (at 52±2 °C and 55±5% WHC) for 84 d. The test materials were added as intact (2.5 cm × 2.5 cm) pieces.

Figure 76. Weight loss from corrugated packaging materials in a continuously aerated, externally heated, 4 L bioreactor containing approximately 300 g of fresh *sMSW* compost

Table 35. Results of the LSD test for the 84 d weight loss and overall performance index for corrugated fiberboards. Results obtained during composting in bench-scale (4 L) bioreactors

Sample ID	Weight loss (%)[a, b]	Sample ID	*PI*[a, b]
EvCo-4	74.6 a	45/30B/45 Kraft	58.6 a
45/30B/45 Kraft	69.9 a	EvCo-4	57.5 a
WAM™-D	62.1 b	WAM™-D	51.1 b
EvCo-1	59.4 b	V2S(IP)	45.5 bc
72sg48	58.6 b	55sg48	42.3 c
55sg48	56.3 bc	72sg48	41.8 c
EvCo-3	52.9 bc	EvCo-1	38.2 cd
EvCo-2	53.6 bc	EvCo-2	37.9 cd
V2S(IP)	47.7 c	EvCo-3	34.8 d

[a] Within columns, values followed by the same letter are not significantly different ($P \leq 0.05$).

[b] Overall performance index = weight loss (%) averaged across time.

A series of corrugated materials incorporating Tallow or WAM™ coatings also were evaluated in the 4 L compost bioreactors. In general, the corrugated fiberboards incorporating the WAM™ coatings (55ss48-W and 69ss48-W) outperformed the comparable fiberboards incorporating the Tallow coatings (55ss48-T and 69ss48-T), though the differences were small as shown in Figure 77 and Table 36. This effect was moderated by the weight of the material used to construct the corrugated fiberboards, with the lighter weight (55ss48-W and –T) fiberboards degrading somewhat faster—and to a slightly greater extent—than the heavier weight (69ss48-W and –T) fiberboards.

Table 36. Results of the LSD test for the 84 d weight loss and overall performance index for Tallow and WAM™ coated corrugated fiberboards. Results obtained during composting in bench-scale (4 L) bioreactors

Sample ID	Weight loss (%)[a, b]	Sample ID	*PI*[a, b]
55ss48 liner/30 WAM™/55ss48 liner	68.4 a	55ss48 liner/30 WAM™/55ss48 liner	53.4 a
55ss48 liner/30 Tallow/55ss48 liner	66.5 a	55ss48 liner/30 Tallow/55ss48 liner	50.5 a
69ss48 liner/30 WAM™/69ss48 liner	65.3 a	69ss48 liner/30 WAM™/69ss48 liner	48.4 ab
69ss48 liner/30 Tallow/69ss48 liner	64.4 ab	69ss48 liner/30 Tallow/69ss48 liner	45.2 b
69ss48 liner/30 Tallow/42 liner/30 medium/69ss48 liner	63.0 b	69ss48 liner/30 Tallow/42 liner/30 medium/69ss48 liner	43.3 b

[a] Within columns, values followed by the same letter are not significantly different ($P \leq 0.05$).

[b] Overall performance index = weight loss (%) averaged across time.

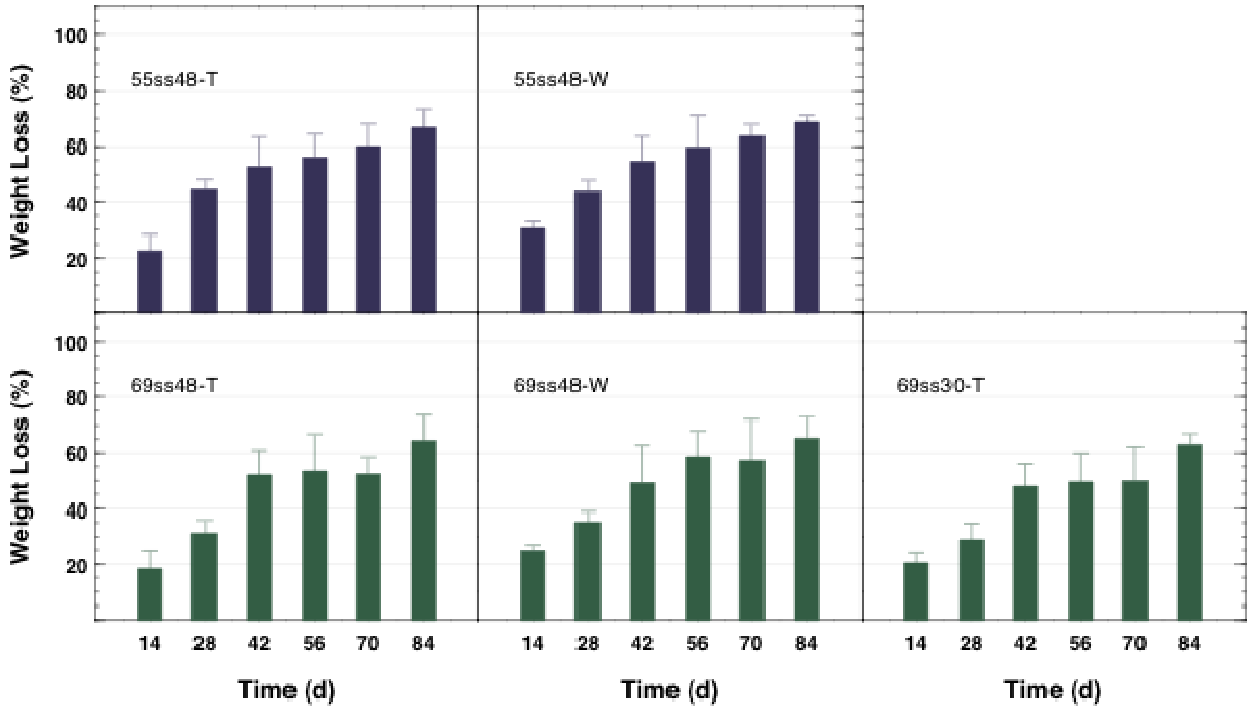

Note: The bioreactors were incubated in the dark (at 52±2°C and 55±5% WHC) for 84 d. The test materials were added as intact (2.5 cm × 2.5 cm) pieces.

Figure 77. Weight loss from Tallow and WAM™ coated corrugated fiberboards in a continuously aerated, externally heated, 4 L bioreactor containing approximately 300 g of fresh *sMSW* compost

A subset of the test samples were placed in both the 4 L bioreactor and 180 L drum composter to assess the relative performance of the two systems. These samples included both samples used in the current generation of MRE™ packaging [solid boards: V2S, V2S(IP), MRE™ V2S, MRE™ SF, and MRE™ SF(TI); corrugated boards: V3C, IL(V2S), and MRE™ LN] and several of the newer packaging materials [72sg48, 55sg48, 55ss48-W, 55ss48-T, 69ss48-W, 69ss48-T, and 69ss-30T]. In general, the test materials degraded more slowly (with *PI* values that were *ca*. 40% lower) and to a lesser extent (*ca*. 20% less weight loss) during an 84 d test exposure in the drum composter as illustrated in Figure 78 and Table 37. This reflects the more variable conditions to which the test samples were subjected in the drum composter. That is, unlike the small (4 L) bioreactors—which were maintained at a core temperature of 52±2 °C and a moisture content of 55±5%—the core temperature and moisture content of compost in the 180 L, self-heating drum composter were more difficult to maintain and varied over a fairly wide range (*ca.* 40–62 °C and 35–70%). Consequently, test materials placed in the drum composter were subjected to a more variable composting environment—generally encountering repeated cycles of high and low activity. Despite these variations in composting conditions (with the 4 L bioreactors providing a *high activity* environment and the 180 L drum composter providing a *low activity* environment), both systems yielded statistically similar results. That is, the relative performance of the test materials was only mildly affected by the composting environment.

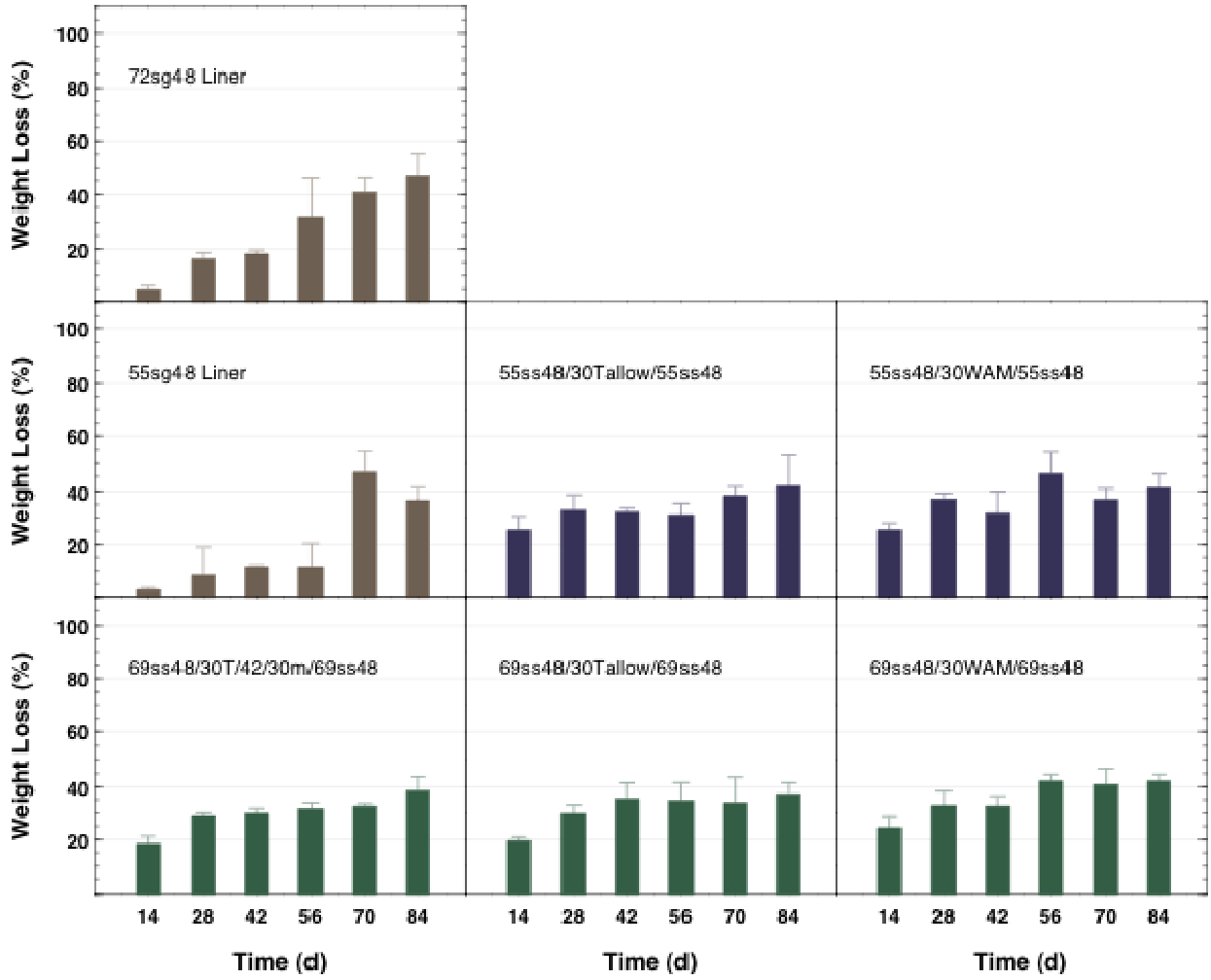

Note: The bioreactors were incubated in the dark (at 52±2 °C and 55±5% WHC) for 84 d. The test materials were added as intact (5 cm × 5 cm) pieces.

Figure 78. Weight loss from corrugated packaging materials in a continuously aerated, self-heating, 180 L drum composter containing approximately 30 kg of fresh *sMSW* compost

Table 37. Results of the LSD test for the 84 d weight loss and overall performance index for corrugated fiberboards. Results obtained during composting in the large (180 L) drum composter

Sample ID	Weight loss (%)[a, b]	Sample ID	*PI*[a, b]
72sg48	46.8 a	55ss48-W	36.4 a
69ss48-W	42.1 a	69ss48-W	35.8 a
55ss48-T	42.0 a	55ss48-T	33.6 ab
55ss48-W	41.4 a	69ss48-T	31.7 bc
69ss48/42/30	38.5 a	69ss48/42/30	30.0 c
69ss48-T	37.1 a	72sg48	25.0 d
55sg48	36.5 a	55sg48	21.1 e

[a] Within columns, values followed by the same letter are not significantly different ($P \leq 0.05$).

[b] Overall performance index = weight loss (%) averaged across time.

Surprisingly, in the drum composter, the solid board materials [V2S, V2S(IP), MRE™ V2S, MRE™ SF, and MRE™ SF(TI)] generally outperformed the corrugated fiberboards [V3C, MRE™ LN and IL(V2S)] in terms of both their overall performance and maximum achievable weight loss (see Figure 79 and Table 38). This was a reversal of what was observed during tests with the more active 4 L bioreactors. It was noted that, in many instances, the corrugated materials became compressed during exposure in the drum reactor—a result of the much greater weight of the compost matrix itself—which may have contributed to the slower degradation of these materials. However, given that the three corrugated samples were from a single test run, it is more likely that this reflects a failure of the system to maintain adequate composting conditions and thus these results should be considered as outliers.

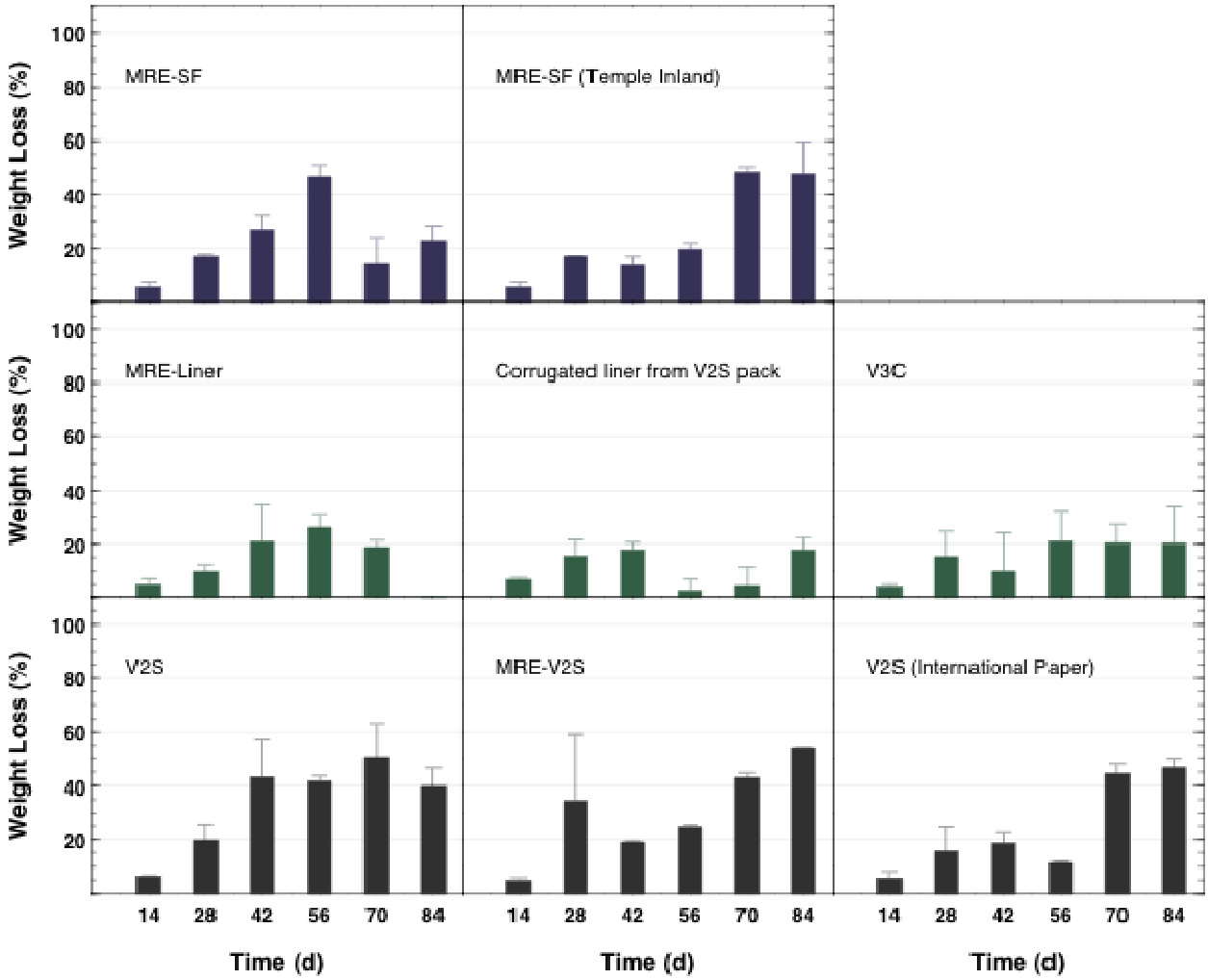

Note: The bioreactors were incubated in the dark (at 52±2 °C and 55±5% WHC) for 84 d. The test materials were added as intact (5 cm × 5 cm) pieces.

Figure 79. Weight loss from MRE™ packaging materials in a continuously aerated, self-heating, 180 L drum composter containing approximately 30 kg of fresh *sMSW* compost

Table 38. Results of the LSD test for the 84 d weight loss and overall performance index for the MRE™ packaging materials. Results obtained during composting in the large (180 L) drum composter

Sample ID	Weight loss (%)[a, b]	Sample ID	*PI*[a, b]
MRE™-V2S	54.0 a	V2S	33.5 a
MRE™-SF(TI)	47.7 a	MRE™ -V2S	29.9 ab
V2S(IP)	46.7 a	MRE™ -SF(TI)	25.3 bc
V2S	39.7 a	V2S(IP)	23.7 c
MRE™-SF	23.0 b	MRE™ -SF	22.2 c
V3C	20.2 b	V3C	15.1 d
IL(V2S)	17.8 bc	MRE™ -LN	13.4 d
MRE™-LN	6.9 c	IL(V2S)	10.8 d

[a] Within columns, values followed by the same letter are not significantly different ($P \leq 0.05$).

[b] Overall performance index = weight loss (%) averaged across time.

When results from the Tier II (weight loss) tests were grouped together (with the outliers removed) and analyzed, the following trends emerged: (i) the lightweight papers (coated and uncoated) degraded fastest and to the greatest extent—yielding about 80–100% weight loss after an 84 d test exposure; (ii) the corrugated fiberboards generally outperformed the solid board materials—presumably because of the enhanced access to internal surfaces provided by the corrugation; (iii) degradation of corrugated fiberboard with the EvCo polyester-based coatings exhibited a pronounced lag period—and, though this had a negative impact on the overall performance index (*PI*), it had little effect on total degradation of the test materials; and (iv) in general, most of the experimental materials outperformed the standard V3C (and MRE™ liner) and V2S (and MRE™ box) materials.

6.2.3 Tier III – Field Testing

Field-scale biodegradation studies are desirable and ultimately may be necessary; however, they are generally expensive, difficult to control and replicate, and are generally unsuitable for establishing biodegradation pathways. Nevertheless, some field testing is necessary to (i) verify that the laboratory-scale tests do an adequate job of predicting a material's performance under conditions representative of various commercial/municipal and backyard composting systems and (ii) ensure that these materials do not adversely affect the quality of the resulting compost.

Static windrows are the most common type of composting system in use, primarily because of low start-up and maintenance costs. In the summer of 2009, a large (ca. 1.5 m × 1.85 m × 3.7 m) static windrow was established on the campus of the University of Saskatchewan. Source materials for the windrows included yard waste (primarily grass clippings and leaves), shredded fiberboard (either currently being used or being developed for use in packing and shipping MRE™ rations), a bulking agent (wood chips) (target C:N ratio = 30:1), and MRE™ food waste (non-dairy) supplemented with food waste from the University of Saskatchewan

Food Services Division[2]. Three windrows were set-up: (i) a yard waste compost using the standard MRE™ fiberboard (MRE™ SF; YW_S); (ii) a yard waste compost using the experimental MRE™ fiberboard (69ss48/30WAM™/69ss48; YW_E), and (iii) a food waste compost using the experimental MRE™ fiberboard (69ss48/30WAM™/69ss48; FW_E). As an added feature, replicate (n = 3) samples of the standard and experimental fiberboards (along with cut-outs from the boxes and liners used to ship MRE™ rations to the University of Saskatchewan) were inserted into nylon mesh litter bags and placed in the center of the YW_E and FW_E windrows. Samples were recovered at 2 week intervals over a 3 month period, cleaned of debris, dried and weighed.

In general, the composition of the windrow (i.e., YW_E *vs.* FW_E) had no significant effect on degradation of test samples as shown in Figure 80 and Figure 81. Indeed, averaged across all samples, total degradation (measured as weight loss) increased from about 57% in the YW_E compost to 61% in the FW_E compost ($F = 2.790$ns); overall performance indices, which are shown in Table 39 for the two systems were essentially the same (40%; $F = 0.116$ns). The ANOVA also revealed that there was no significant blocking effect, indicating that where the samples were placed in the windrows had no significant effect on degradation. This latter result also suggests that composting conditions were fairly uniform throughout the center of the windrows.

Table 39. Results of the LSD test for the 84 d weight loss and overall performance index for corrugated fiberboards

Yard Waste Compost				Food Waste Compost			
Sample ID	Weight loss (%)[a, b]	Sample ID	*PI*[a, b]	Sample ID	Weight loss (%)[a, b]	Sample ID	*PI*[a, b]
LCS	64.3 a	LCS	45.1 a	MRE™ -BX	69.4 a	MRE™ -BX	46.9 a
MRE™ -LN	61.5 a	MRE™ -LN	44.3 a	MRE-SF(IP)	61.3 a	LCS	42.5 ab
MRE™ -BX	53.4 a	MRE™ -BX	40.4 ab	MRE™ -LN	57.8 a	MRE-SF(IP)	38.0 bc
MRE-SF(IP)	47.7 a	MRE-SF(IP)	36.7 bc	MRE-SF(WC)	57.7 a	MRE™ -LN	37.6 bc
MRE-SF(WC)	44.9 a	MRE-SF(WC)	34.1 c	LCS	56.4 a	MRE-SF(WC)	33.3 c

[a] Within columns, values followed by the same letter are not significantly different ($P \leq 0.05$).

[b] Overall performance index = weight loss (%) averaged across time.

Note: Results obtained during composting in bench-scale (4 L) bioreactors

[2] Left-over vegetable matter that could not be re-used in the cafeterias. [No post-consumer food waste was used in this study.]

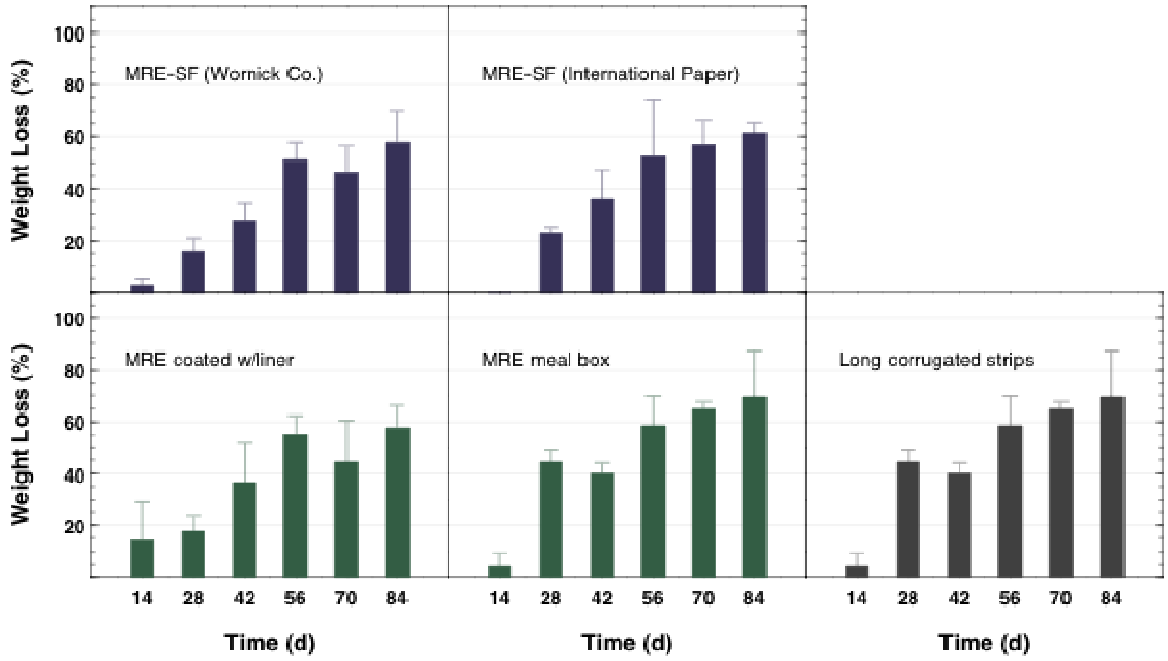

Note: The compost consisted of yard waste (grass clippings and leaves), the experimental MRE™ fiberboard (69ss48/30WAM™/69ss48), and wood chips (added as a bulking agent).

Figure 80. Weight loss from MRE™ packaging materials degraded in a pilot-scale (Tier III) yard waste static windrow compost during a 42 d test exposure

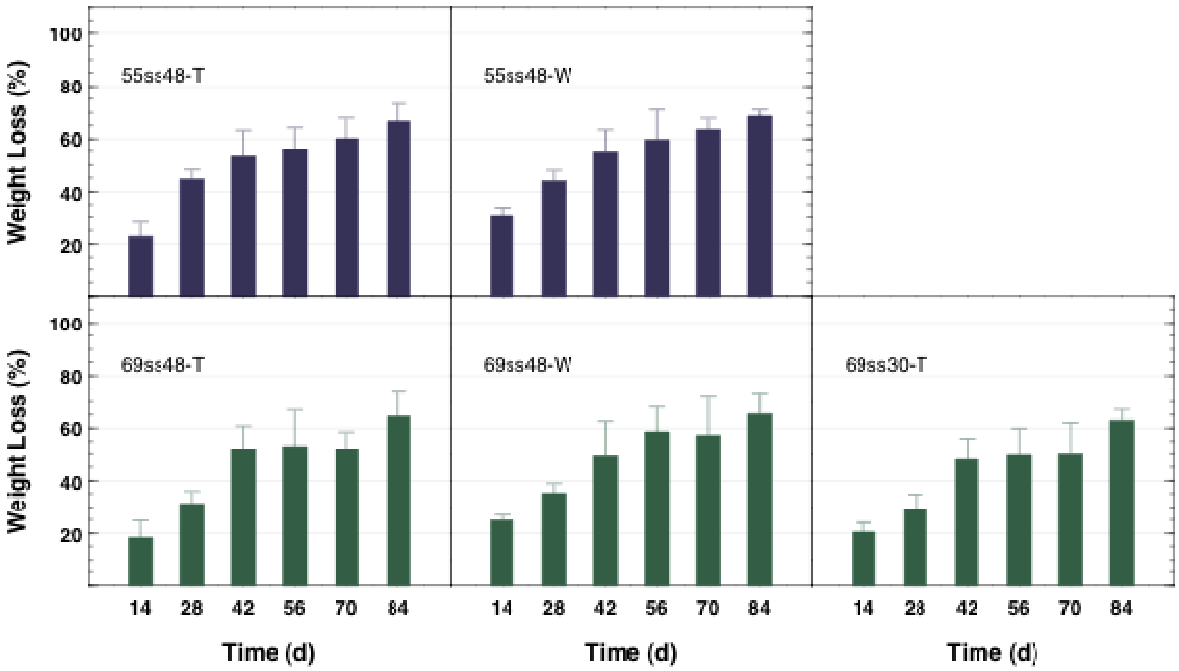

Note: The compost consisted of yard waste (grass clippings and leaves), non-dairy MRE™ food waste, the experimental MRE™ fiberboard (69ss48/30WAM™/69ss48), and wood chips (added as a bulking agent).

Figure 81. Weight loss from MRE™ packaging materials degraded in a pilot-scale (Tier III) food waste static windrow compost during a 42 d test exposure

Core temperatures in the windrows were generally adequate for composting, but were consistently higher in the food waste compost than those in the yard waste compost. In retrospect, the windrows should have been covered with a layer of straw to insulate them and maintain higher core temperatures. Nevertheless, given the cool temperatures that prevailed throughout the summer months, active composting in the windrows continued for 10–12 weeks. At the end of the active composting period, samples of the compost collected from the core of the composts were evaluated for compost quality.

In general, the chemical and physical attributes of the 14 week old composts[3], shown in Table 40, are characteristic of immature compost. This was not totally unexpected, as the size (i.e., mass) of the windrows[4] was most likely too small to sustain the high temperatures needed to obtain a more completely developed compost in the time available. Nevertheless, the quality of the two composts derived from yard wastes—which included the standard and experimental fiberboards—were not significantly different. The compost derived from the food waste (including the experimental fiberboard) had a higher nitrogen (N) content (total- and available-N), electrical conductivity (EC), and sodium (Na^+) content. These differences primarily reflect differences in the starting materials; e.g., the food waste had a significantly greater N content (5–7%) than the grass clippings and leaves (1–3%) used as yard wastes. As well, almost all of the food wastes contained added salt, which contributed to the higher Na^+ content and EC of the FW_E compost.

Table 40. Chemical and physical characteristics[a] of composts produced by windrowing yard waste (YW_S and YW_E) and food waste (FW_E)

Compost	pH	EC	Na^+ (m*M*)	TC (%)	TN (%)	C:N	NO_3-N ($\mu g\ g^{-1}$)	NH_4-N ($\mu g\ g^{-1}$)	PO_4-P ($\mu g\ g^{-1}$)	TS (%)	VS (%)	FS (%)
- - - - - - - - - Samples collected 14 weeks after the windrow was established - - - - - - - - -												
YW_S	8.6	3.6	3.4	38.6	1.58	24:1	63	29	622	23.6	69.4	30.6
YW_E	8.0	3.7	12.4	37.5	1.70	22:1	60	37	659	20.6	69.3	30.7
FEW	7.7	8.7	66.2	39.0	2.81	14:1	553	82	1500	21.8	74.0	26.0
- - - - -- - - - - Samples collected 13 months after the windrow was established - - - - - -- - - -												
YW_S	6.9	0.42	0.5	30.8	1.9	16.2	10.5	1.76	43.9	33.1	56.4	43.6
YW_E	7.0	0.64	0.8	27.8	1.8	15.4	13.6	1.94	44.9	39.3	57.8	42.2
FEW	6.8	0.68	3.4	20.7	1.7	12.2	11.6	0.90	59.1	46.5	52.3	47.7

[a] EC = electrical conductivity; TC = total carbon content; TN = total nitrogen content; NO_3-N + NH_4-N = available nitrogen; PO_4-P = available phosphorus; TS = total solids content; VS = volatile solids content; FS = fixed solids content.

After the litter bags containing the various fiberboard samples were recovered from the windrows, the compost piles were turned and allowed to continue composting for an additional

[3] Note: the windrows were approximately 2 weeks old when the test samples were added to the compost; consequently, after the 12 weeks exposure period, the "final" compost was 14 weeks old.

[4] The final size of the windrows was dictated by the amount of MRE™ food waste available. Whereas this was supplemented with a small amount of food waste from the Food Services Division of the University of Saskatchewan, a decision was made not to add too great a quantity of this material so that the compost would more accurately reflect what one could construct from disfibered MRE™s and their packaging.

10 months (total composting time = *ca*. 13 months), at which time chemical and physical characteristics of the composts were determined[5] (see Table 40). In general, there was a narrowing of the C:N ratio, especially for the food waste compost, and significant ($P \leqslant 0.05$) decreases in pH, EC, Na^+ content, available N and P, and volatile solids. These results reflect the maturation of the compost and, in the case of EC and Na^+ content, a washing out of the soluble salts—this was especially noticeable in the food waste compost. Thus, it was concluded that the composts generated from feedstocks that included the MRE™ packaging were stabilized, mature products that would have few, if any, restrictions for use in landscaping or horticultural production (gardening).

Phytotoxicity tests based on seed germination and root (radicle) elongation measurements [107, 111] were conducted on 1:2 (v/w) compost:water extracts and are shown in Table 41. In general, no phytotoxic effects were observed and though some treatment (compost) effects were identified, they were mostly stimulatory. In particular, radicle elongation was generally greater for seeds germinated in the compost extracts. This most likely reflects a beneficial effect of the nutrients (e.g., NO_3 and PO_4) present in the compost extracts. It was mildly surprising that salinity effects were not observed in the phytotoxicity test, especially with cucumber which is considered to be moderately sensitive to salts. However, it may just be that any adverse salt effect was offset by the benefits of the added nutrients. It is worth noting that a series of phytotoxicity tests using garden cress (*Lepidium sativum*) as the test plant also were conducted (data not shown). Although the cress tests indicated a moderate to severe inhibition of both seed germination and root elongation, the tests suffered from very poor germination in the controls—which indicated that seed viability itself was an issue. The cress tests were repeated three times with fresh seed, but with the same results. Consequently, only the multispecies test is reported here.

[5] Note: the windrows were left intact till spring 2011, at which time they were sampled again. Results of the 2011 analyses (data not shown) indicated that there had been only minor changes in the composition of the composts, indicating that the composts had reached full maturity by the summer 2010 sampling (see Table 41).

Table 41. Multiple plant species bioassay results for compost water extracts

Plant	Compost	Seed germination[a]		Root elongation[b]		*GI*[c]	Interpretation
		%	$\frac{MGT}{MGC}$	Mean (mm)	$\frac{MRLT}{MRLC}$		
Cucumber	YW_S	96.5	0.97	20.6	1.07	1.03	No inhibition
	YW_E	97.5	0.98	21.4	1.73	1.69	No inhibition
	FW_E	95.0	0.95	14.3	0.91	0.86	No inhibition
LSD (P ≤0.05)[d]		*4.7*	*0.05*	*4.8*	*0.32*	*0.31*	
Wheat	YW_S	62.5	1.14	20.0	1.36	1.54	No inhibition
	YW_E	62.5	1.25	19.0	2.57	3.21	No inhibition
	FW_E	60.0	1.09	15.9	1.55	1.69	No inhibition
LSD (P ≤0.05)		*11.6*	*0.22*	*4.5*	*0.43*	*0.60*	
Barley	YW_S	95.5	1.06	18.8	1.82	1.94	No inhibition
	YW_E	97.0	0.97	16.5	1.73	1.68	No inhibition
	FW_E	98.0	0.98	19.9	1.27	1.25	No inhibition
LSD (P ≤0.05)		*3.5*	*0.04*	*3.6*	*0.32*	*0.33*	

[a] Percent (%) germination calculated relative to the number of seeds in each Petri dish (20 seeds per replicate); MGT = mean germination in the control (i.e., water); MGT = mean germination in the compost extract.

[b] MRLC = mean radicle length of seeds germinated in the water control; MRLT = mean radicle length of seeds germinated in the compost extract.

[c] Zucconi's germination index [107].

[d] LSD; significant at the 5% level of probability.

Results of the field study indicate that (i) the individual test materials (i.e., the current and experimental fiberboards used for packing MRE™ rations) are compostable and (ii) a longer, more active composting environment will be required to turn these materials into usable compost. Nevertheless, the results of the field study support the results of the Tier I and II bench-scale tests that indicate the new generation of experimental solid board and corrugated fiberboards are compostable.

7.0 Conclusions

New secondary packaging prototypes have been developed for this SERDP project to incorporate sustainable features while achieving military performance. The research effort focused on replacing solid fiberboard with a more sustainable packaging system that is lightweight, recyclable and repulpable and utilizes effective structural designs that reduce material usage.

The first approach incorporated soy protein adhesives and other natural materials into a formulation to produce a fiberboard with wet strength and mechanical properties needed by the military. This research was not able to be scaled up to produce large quantities or prototype containers for the military, but was an innovative combination of materials that had water resistance and attractive mechanical properties at the laboratory scale.

The second approach studied biodegradable coated paper which did contribute to coating paper methods with optimizing adhesion and strength. This gave fundamental knowledge for understanding the properties of the paper and coated paper which are incorporated into a fiberboard container. A roll of biodegradable coated paper could ultimately be used in corrugators as one of the structures in a fiberboard container.

The third approach worked closely with Interstate Containers to design and coat corrugated fiberboard containers with an environmentally friendly coating or WAM™s. Coating formulations and fiberboard structures were optimized and trials were performed to obtain fiberboard containers to evaluate for compression strength and performance in comparison to the existing MRE™ containers. From this approach, optimized formulations, designs and containers were produced and studied.

The composting studies at Tier I, II and III testing levels showed that the corrugated fiberboard is compostable. In general, most of the experimental materials outperformed the standard V3C (and MRE™ liner) and V2S (and MRE™ box) materials. However, the controls and current solid fiberboard are indeed biodegradable.

The objectives of this SERDP project have been met in the producing the corrugated fiberboard. The corrugated structures have tremendous resource-savings potential with design and material selection as the key points of consideration during development process. For example, the optimized structure of the RSC IN demonstrated an 18% reduction in total packaging weight which generates a 700 lb reduction in total weight per full truckload. Over the course of an annual procurement cycle this weight reduction can translate into an immense savings of 1.5 million lb of packaging that no longer uses valuable natural resources during material processing, ration assembly, transportation, storage, operational use and its subsequent disposal requirements at the end of its life cycle.

Research questions that are under investigation pertain to the recycling process and how the new fiberboard will be recycled in comparison to the existing fiberboard. The biobased content and recyclable content as well as toxicity of these materials if burned must be evaluated in detail.

The proposed materials are not expected to disrupt or degrade the value of the material stream. On the contrary, they are expected to add value to the recycling process since they are made with no chemical treatments such as wet strength additives, wax coatings and water repellants. Preliminary work has been done with Western Michigan University on the repulpablity and recyclability of the new fiberboard, but a full trial would need to be performed.

The prototypes would have an expected increased recycled content as no harmful chemicals, adhesives or water resistant additives are being used in these formulations which would decrease the chances of recyclability. Since the existing MRE™ structures are primarily made from cellulose which is a biobased material, the biobased content should not fluctuate significantly. The amount of fiber will decrease in a corrugated structure versus the solid fiberboard.

NSRDEC is unaware of any harmful agents that are incorporated into the coating or fiberboard structure that would pose any discernible risks to human health or outdoor air quality. Spectra Kote Corporation and Interstate Resources would be responsible for ensuring that the fiberboard material is made from resources that are generally regard as safe for normal use and disposal. The substrates themselves do not contain any heavy metals and are approved by the FDA for food contact. The primary material used to make the packaging material is wood fiber and starch adhesives to bind the fluted medium and liners. Pyrolysis type studies can be done in the laboratory to determine emission gases that can be analyzed for chemicals known or suspected of toxicity.

Overall, this research allowed NSRDEC to explore a new fiberboard container, which has not been fully explored at NSRDEC in a long time. NSRDEC learned about the existing fiberboard container and used it as the control in this study. There are knowledge gaps within the Army on existing data on the performance tests and data of these containers and what testing needs to be done to meet military requirements.

These containers could be implemented for any DoD organization as well as for the US Army. The container structure can be applied to the US Army's UGR™ as well as any packaging application for the military. An optimized structure and design is now ready to be scaled up for a demonstration and validation program. This technology for the military will be integrated into a full evaluation of these containers as a replacement to the existing one. Studies need to be performed on the storing, handling, delivering, and maintaining of the containers and overall life cycle costs observed during manufacturing, transportation, storage, end-use and disposal.

This document reports research undertaken at the U.S. Army Natick Soldier Research, Development and Engineering Center, Natick, MA, and has been assigned No. NATICK/TR- 12/023 in a series of reports approved for publication.

This page intentionally left blank

Appendix A

Supporting Data

A.1 Manufacture of Corrugated Fiberboard

Tables A-1 and A-2 list the processing parameters recorded by Interstate Containers for the fiberboard trial. This includes temperature, time and speeds for the corrugator equipment.

The process of making corrugated fiberboard starts with three large rolls of paper. One forms the corrugated medium, and the other two form the liner boards on either side of the medium. The top board is normally called the single-face liner board, and the bottom layer is often called a double-face liner board. To make the board, the corrugated medium is softened with steam in a preconditioner and then formed into flutes by pressing it in between meshed rolls which fit together like huge gears. As the web emerges from the forming operation, it is held close to the corrugating roll while glue is placed on the tips of the flute. The glue is normally starch-based and is applied to the tips of the flutes which are then pressed against the liner board, which has also been pre-heated. The adhesive sets up quickly following which the single-faced material is moved up onto a bridge where the glue finishes the setting operation. In the next section of the machine, known as the double-backer or double-facer, a second layer of liner board is added. This layer is also pre-heated and adhesive is applied to the outside of the flutes just as before. Again, the glue setup is rapid and curing is accelerated with additional heating sections. This is followed by an unheated section which allows the board to cool to its usable form. The completed corrugated structure is then slit or cut into sheets as required for the individual application.

Table A-1. Typical Processing Parameters of Fiberboard Trial

Adhesive Parameters:
Gel Temp - 144 °F
Solids – 30%
Steinhall Viscosity – 40.0 s
Temperature @ time of Viscosity measurement - 101 °F
Harper Love Water Proof Resin – XW – 200
Addition – 91 lb
Weight per Gal. – 9.1 lb/gal

Table A-2. Corrugator parameters during fiberboard production run (January 2008)

LOWELL CORRUGATOR PARAMETERS		
1st TRIAL SET – w/55 lb Liners		
SINGLE FACER		
Liner Moisture (%)		
Front	Mid.	Back
8.7%	7.0%	7.5%
Single Face Glue Gap – 13 thou		
Pre-Heater Wrap – Full		
Corrugator Speed – Average 380 fpm		
Peak Speed – 410 fpm		
Brake Tension - 50 psi		
Liner Temp (°C) exiting Pre- heater into Corrugator – Temp taken 6-8 in from initial roll:		
Front	Mid.	Back
90	84	96
MEDIUM		
Medium Moisture (%)		
Front	Mid.	Back
5.5%	5.1%	5.5%
Pre Condition Steam – Heavy		
Medium Temp (°C) exiting Pre- conditioning roll into Corrugator – Temp taken at initial idler rolls		
Front	Mid.	Back
70	69	76
Single Face Web (Liner and Medium) Temp (°C) exiting Corrugator to Bridge – Temp taken 3 ft after Corrugator Rolls		
Front	Mid.	Back
96	106	99
DOUBLE BACKER		
Liner Moisture (%)		
Front	Mid.	Back
7.5%	8.0%	8.8%
Pre-Heater Wrap – ¾ (75%)		
Double Back Glue Gap – 18 thous		
Double Backer Liner Temp (°C) exiting Pre-Heater – 6 in after exiting pre-heater		
Front	Mid.	Back
75	81	79

A.2 Tier II Composting

The Tier II test results were used to determine the biodegradability of the test material, relative to that of a standard biodegradable material, in a controlled composting environment to ensure reproducibility and precision.

Test materials were labeled and cut into 2.5 cm^2 pieces and placed in 5 cm x 5 cm litter bags made from nylon-coated fiberglass screen (1.5 mm^2 mesh). Each sample bag was supplemented with one-half teaspoon of matured compost (screened to pass a 2 mm sieve) on each side of the film; the sample bags were then placed in 4 L bioreactors (shown in figures A-1

to A-2) containing approximately 300 g of fresh simulated municipal solid waste compost, and incubated at 52 ± 2 °C and a water content of 55 ± 5% (w/w).

In addition to the small isothermal (4 L/52 ± 2°C) compost reactors, a large self-heating (180 L/variable temperature) drum composter also was used to assess the compostability of a subset of the test materials. (Figure A-3). Test materials were cut into 5 cm × 5 cm pieces, assigned an identification number, and (to facilitate recovery) placed in 7 cm square litter bags made from nylon-coated fiberglass screen (1.5 mm square mesh). Each sample bag was supplemented with one teaspoon of matured compost (screened to pass a 2 mm sieve) on each side of the film; the sample bags were then placed in the 180 L self-heating compost reactors containing approximately 30 kg of raw, simulated yard-waste compost, and incubated for up to 12 weeks at a water content of 55 ± 5% (w/w).

Triplicate samples of the test materials were recovered at 7–14 day intervals for a total of 6–12 weeks and the resulting photographs of weight loss as a function of time are shown in Figures A-4 to A-20. Each sample was carefully removed from its litter bag and cleaned; the residual material was then dried to a constant weight in a convection oven (50 °C for 12 to 18 h), cooled to room temperature in a dessicator, and weighed.

Figure A-1. 4 L compost reactor (t=0wk; DSCN3682)

Figure A-2. 4 L compost reactor (t=2wk; DSCN3750)

Figure A-3. Bench Scale Composter

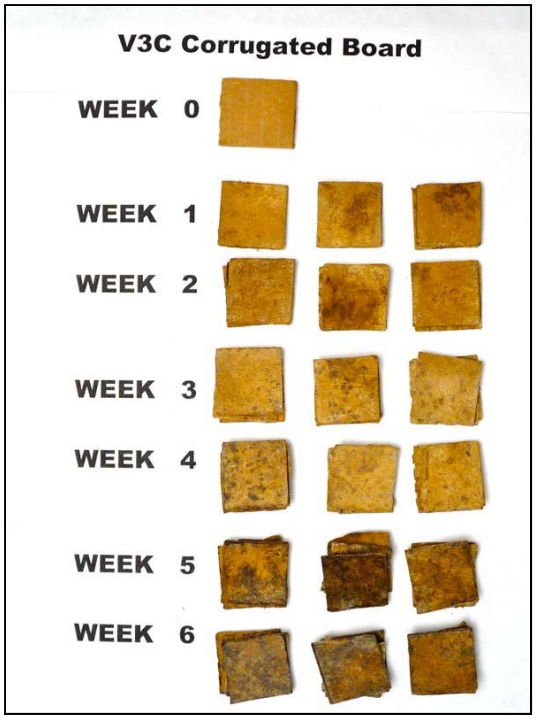

Figure A-4. V3C corrugated board (P1010253)

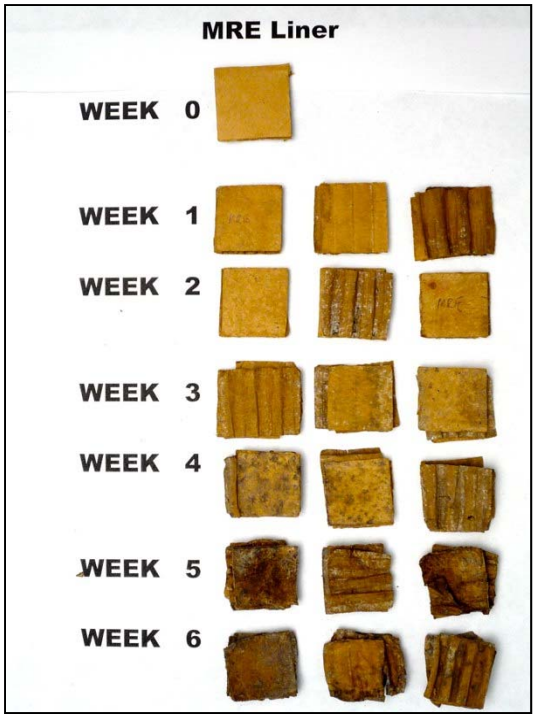

Figure A-5. MRE™ Liner (P1010262)

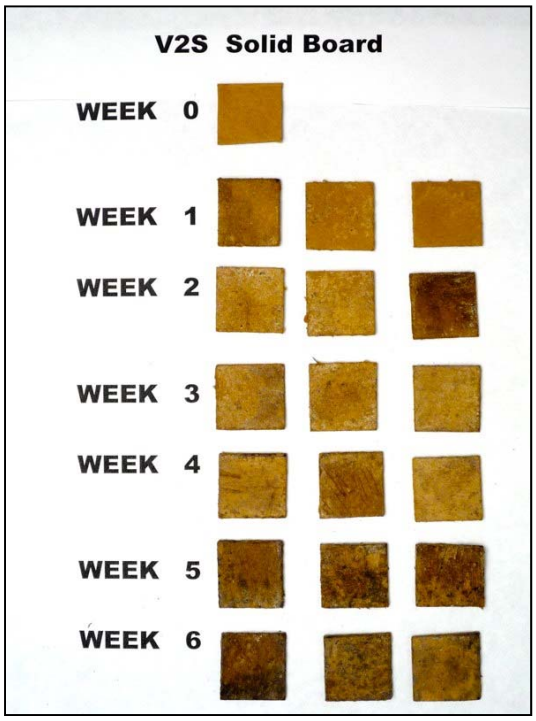

Figure A-6. V2S solid board (P1010242)

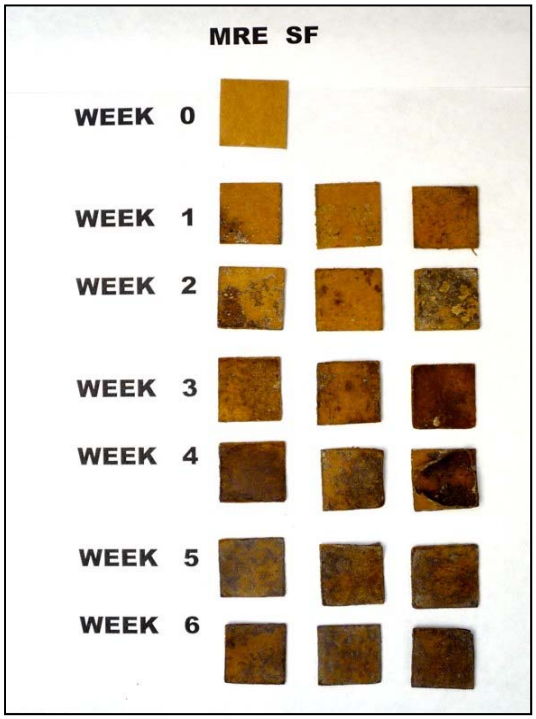

Figure A-7. MRE™ SF (P1010224)

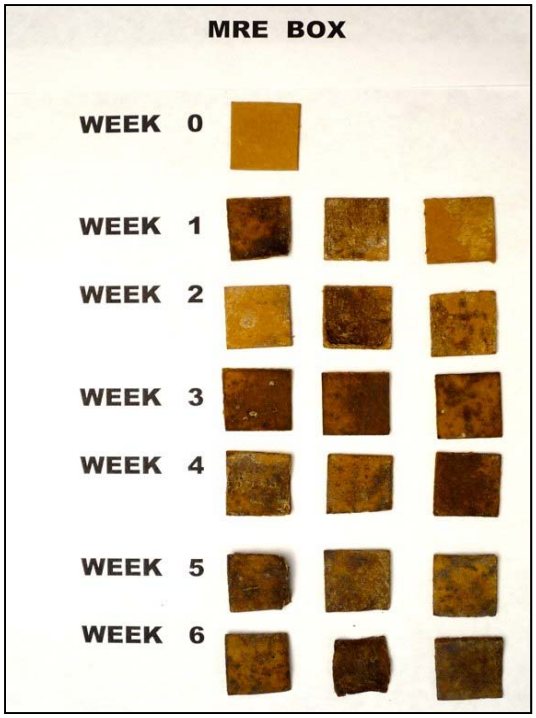

Figure A-8. MRE™ Box (P1010230)

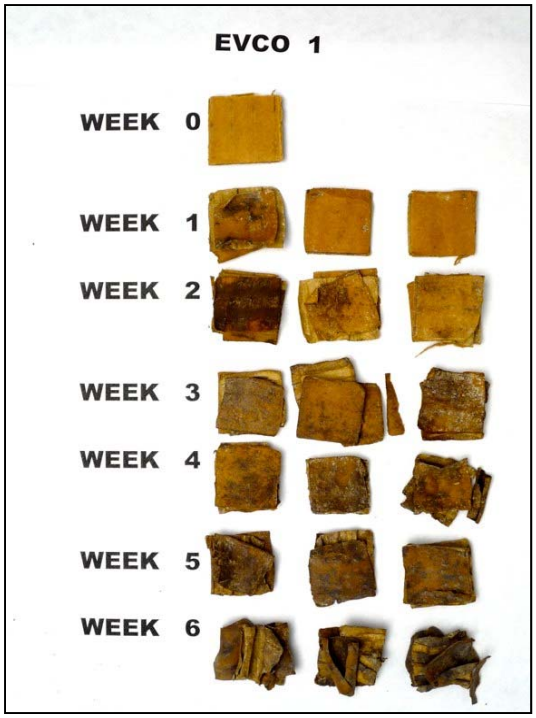

Figure A-9. EVCO 1 (P1010236)

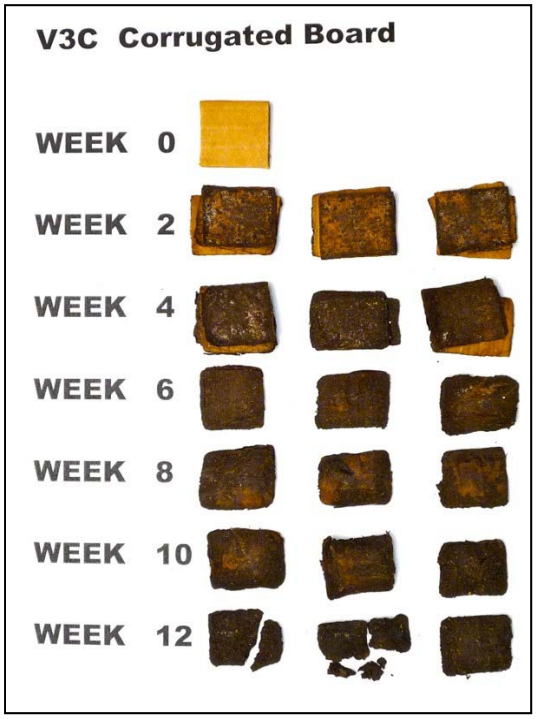

Figure A-10. V3C Corrugated Board (P1010253)

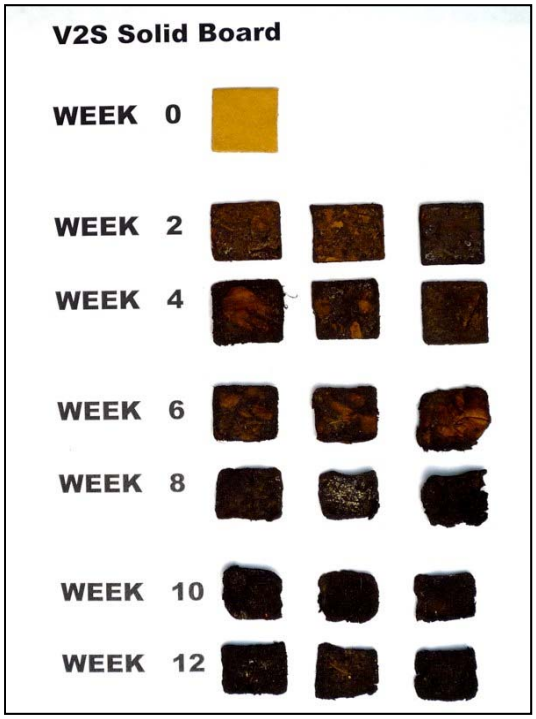

Figure A-11. V2S Solid Board (P1010012)

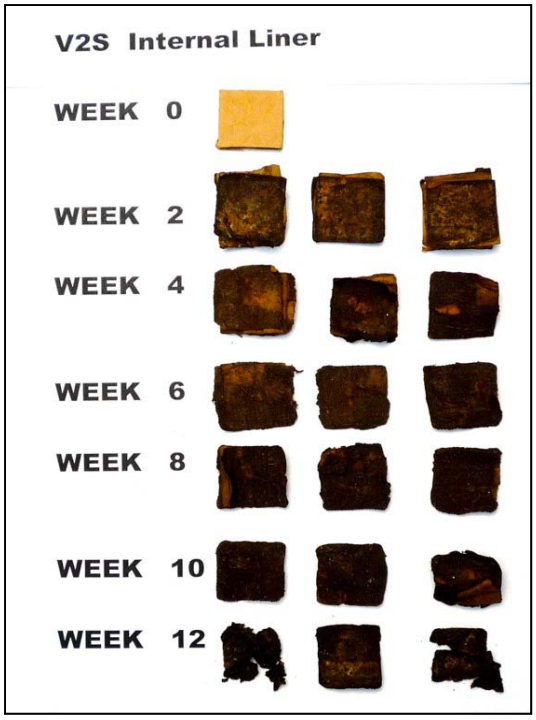

Figure A-12. V2s Internal Liner (P1000998)

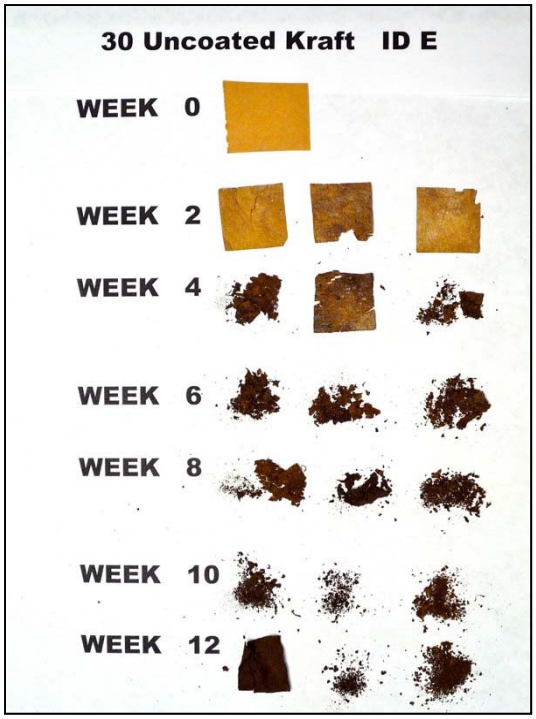

Figure A-13. 30# Uncoated Kraft ID#E (P1010171)

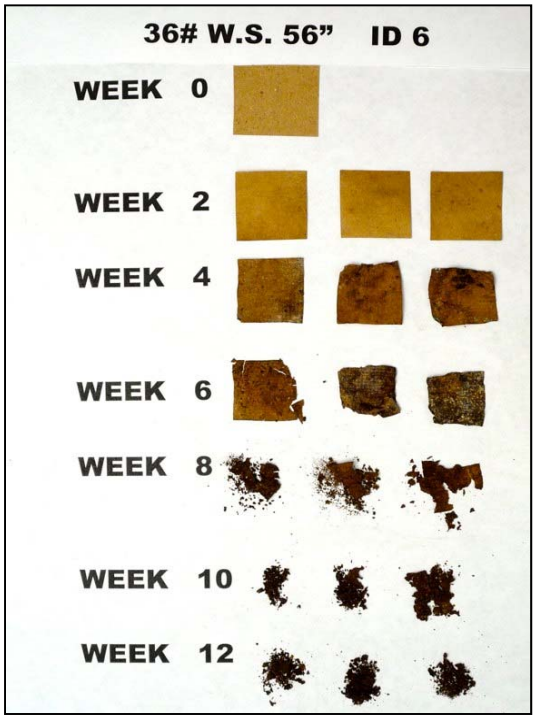

Figure A-14. 36# W.S. 56" ID 6 (P1010156)

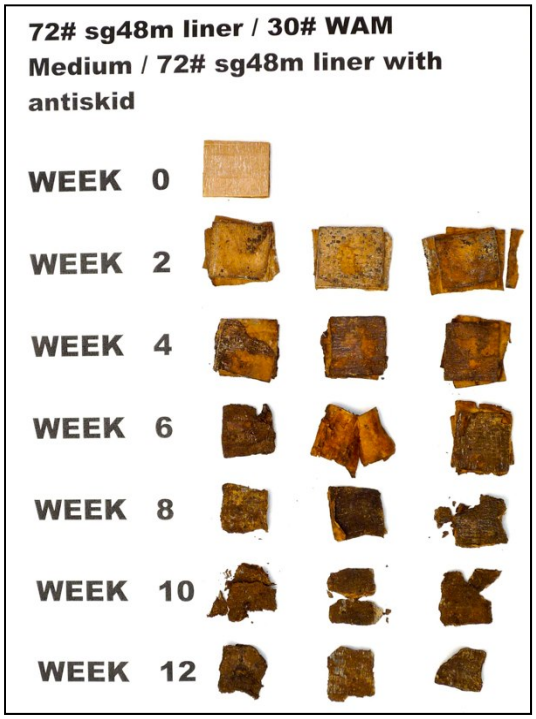

Figure A-15. 72# sg48m liner / 30#WAM™ Medium / 72#sg48m liner with antiskid; (P1000597)

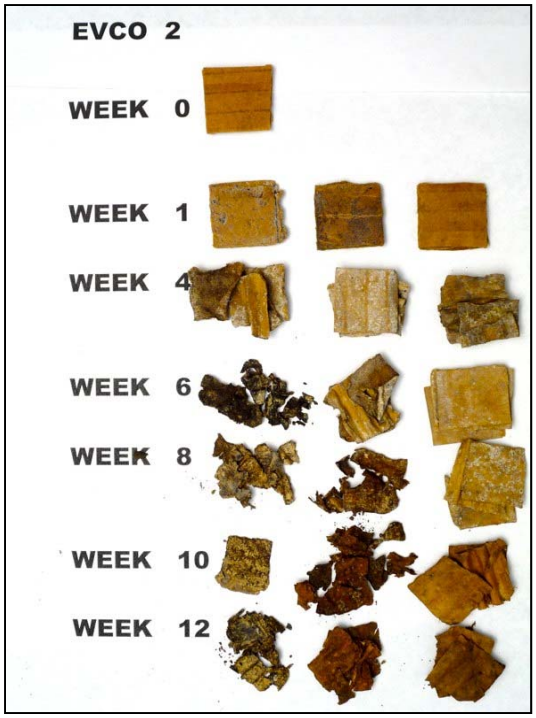

Figure A-16. EVCO 2 (P1010192)

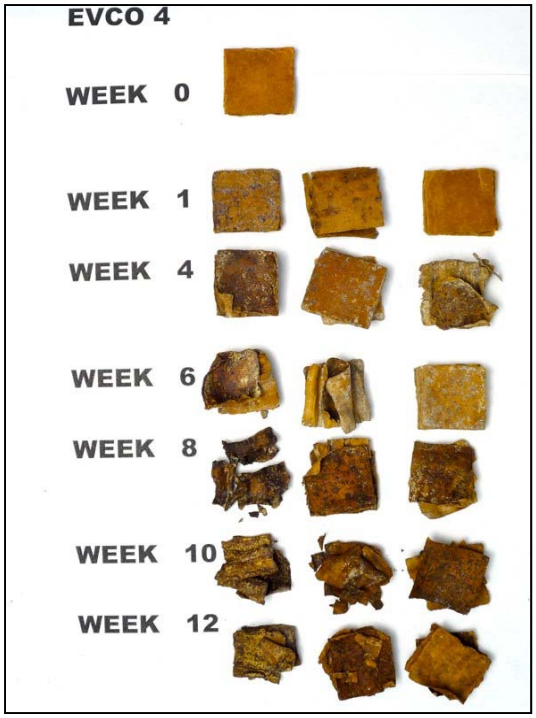

Figure A-17. EVCO 4 (P1010211)

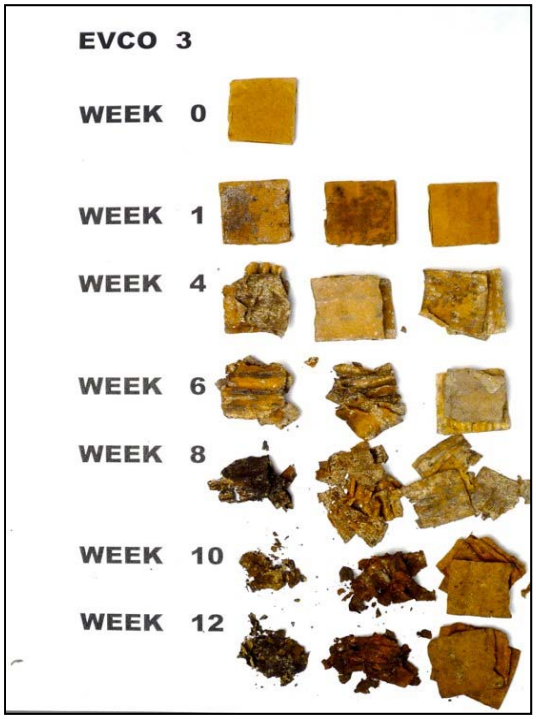

Figure A-18. EVCO 3 (P1010200)

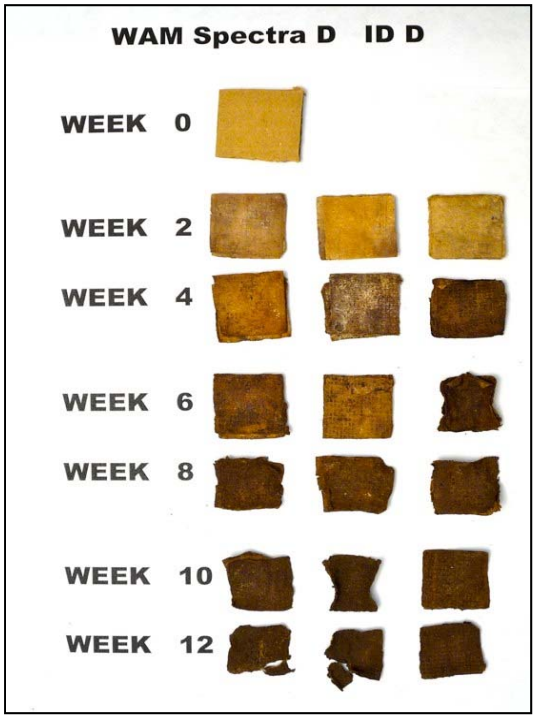

Figure A-19.WAM™ Spectra D (P1010143)

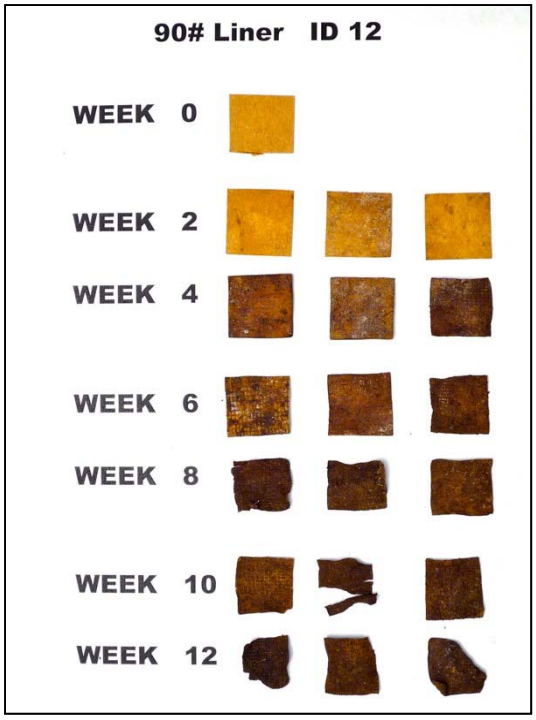

Figure A-20. 90# Liner ID#12; (P1010138)

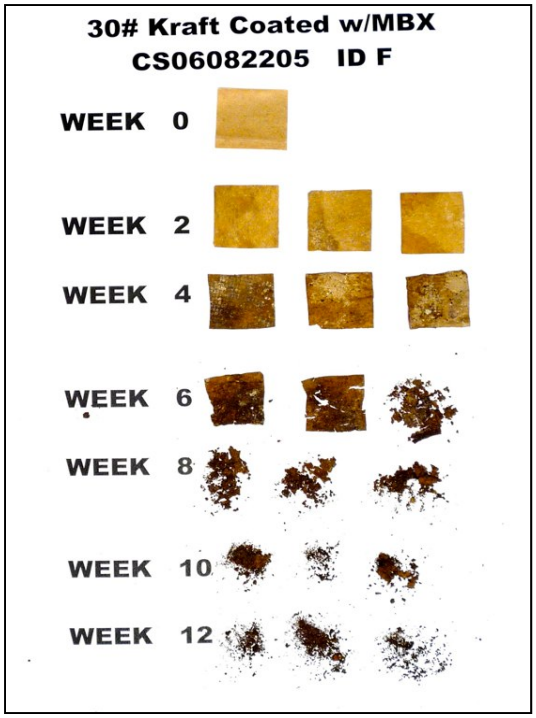

Figure A-21. 30# Kraft coated w/MBX CS06082205 ID#F; (P1010147)

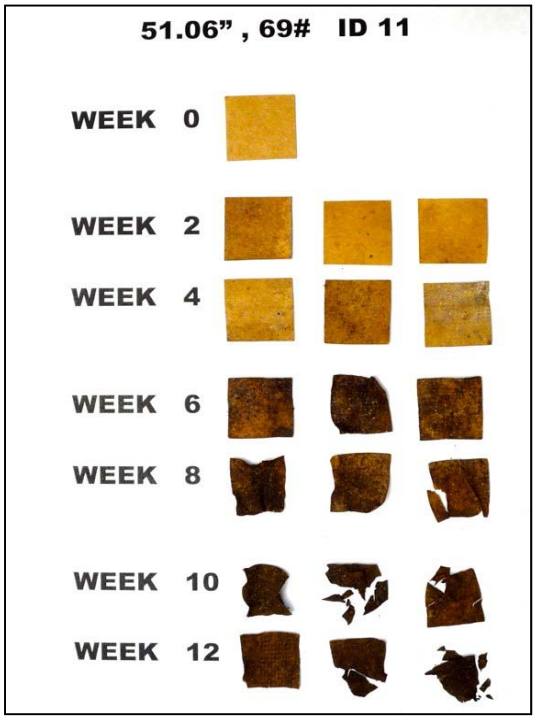

Figure A-22. 51.06, 69# (ID#11)

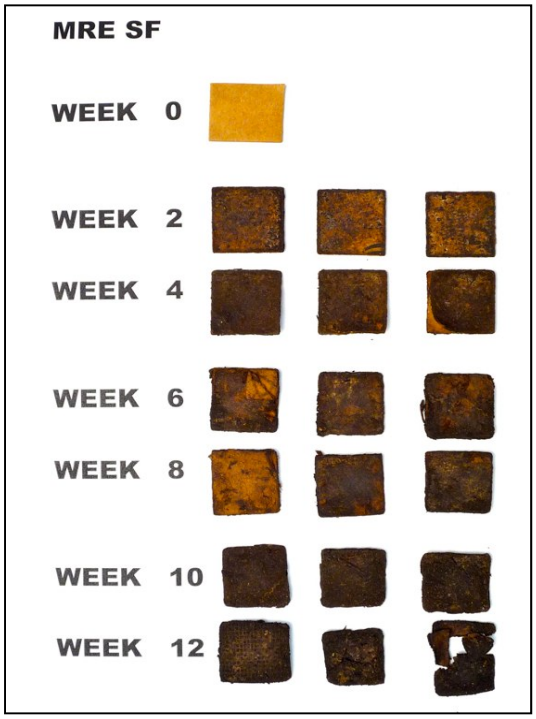

Figure A-23. MRE™ SF (P1010024)

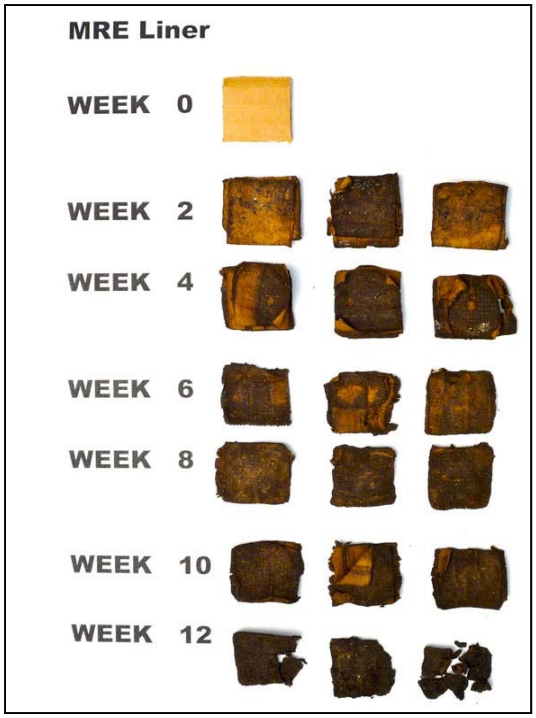

Figure A-24. MRE™ Liner (P1010006)

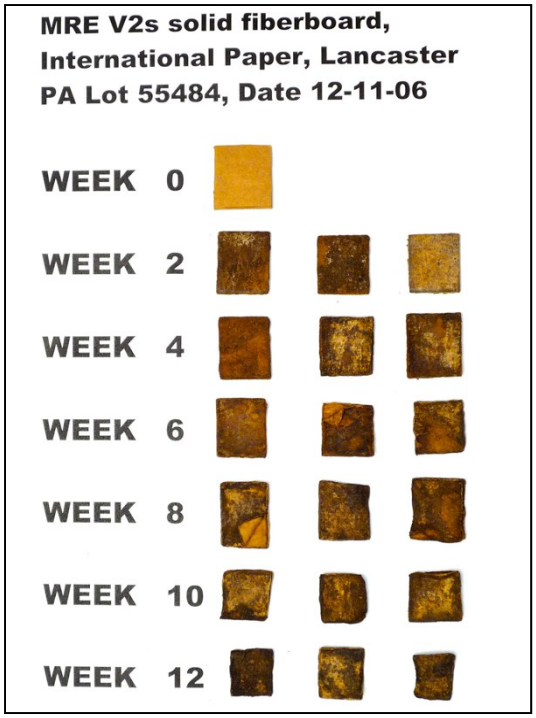

Figure A-25. MRE™ V2S solid fiberboard IP Lot #55484, 12/11/06; (P1000633)

Figure A-26. Corrugated Internal Liner taken from V2S pack; International Paper (P1000599)

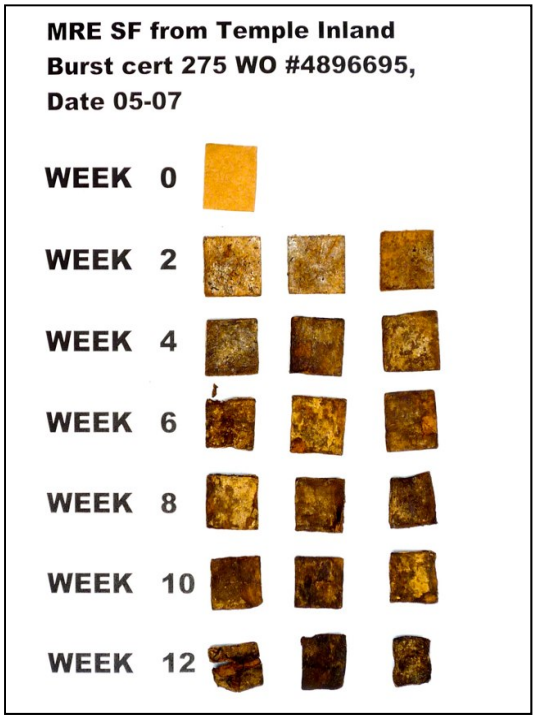

Figure A-27. MRE™ SF Temple Inland, Burst cert 275 WO#4896695 05/07; (P1000558)

A.3 Tier III Composting

The last phase of the testing program involved field trials (Tier III tests) to demonstrate the compostability of the test materials under field conditions and assess the overall quality of the final compost.

Composting was carried out in a large static windrow that was turned once every 2 weeks. Source materials for the compost included yard waste (primarily grass clippings and leaves) and a bulking agent (wood chips) (target C:N ratio = 30:1). The compost pile was monitored for oxygen content (target >10%), moisture (target = 40–60%, w:w), and temperature (target = 35–60 °C, depending on the stage of composting process) and mechanically manipulated as necessary to keep these variables within their optimal ranges. Upon completion of the composting period (i.e., 3 months of active composting), the quality of the finished compost was determined as described by the US Composting Council.

Figure A-28. Shredder being prepared for use

Figure A-30. MRE™ SF boxes being prepared for shredder

Figure A-29. Preparation of wood chips; used as bulking agent

Figure A-31. Shredded fiberboard being discharged

Figure A-32. Insertion of cardboard strips into shredder

Figure A-33. Close-up of shredded cardboard

References

1 TRADOC Pam 525-66, Military Operations, Force Operating Capabilities, January 30, 2003, Chapter 11, p. 86-92.

2 Kumar Rakesh, et al. Adhesives and plastics based on soy protein products. Industrial Crops and Products 16: 2002, 155-172

3 Liu, Yuan, Li Kaichang. Chemical Modification of soy protein for wood adhesives. Macromol. Rapid Commun. 2002, 23, 739-742.

4 A. L. Lambuth, Protein Adhesives for Wood, in: Handbook of Adhesive Technology, A. Pizzi and K. L. Mittal (Eds.). Ch. 13, pp. 259-281. Marcel Dekker, New York 1994.

5 Mo X., Sun X.S., Wang D. Thermal properties and adhesion strength of modified soybean storage proteins. J. Am. Oil. Chem. Soc. 2004, 81(4), 395-400.

6 Kalapathy U., Hettiarachchy N.S., Myers D., Hanna M.A. Modification of soy proteins and their adhesive properties on woods. J. Am. Oil. Chem. Soc. 1995, 72(5), 507-510.

7 Sun X.S, Bian K. Shear strength and water resistance of modified soy protein adhesives. J. Am. Oil. Chem. Soc. 1999, 76(8), 977-980.

8 Huang W., Sun X. S. Adhesive properties of soy proteins modified by urea and guanidine hydrochloride. J. Am. Oil. Chem. Soc. 2000b, 77(1), 101-104.

9 Huang W., Sun X.S. Adhesive properties of soy proteins modified by sodium dodecyl sulfate and sodium dodecylbenzene sulfonate. J. Am. Oil. Chem. Soc. 2000a, 77(7), 705-708.

10 Zhong Z., Sun X.S., Wang D. Isoelectric pH of polyamide-epichlorohydrin modified soy protein improved water resistance and adhesion properties. J. Appl. Polym. Sci. 2007, 103(4), 2261-2270.

11 Wang Y., Sun X.S., Wang D. Performance of soy protein adhesive enhanced by esterification. Trans. ASABE. 2006, 49(3), 713-719.

12 Lodha, P., Netravali, A.N.Characterization of Phytagel Modified Soy Protein Isolate Resin and Unidirectional Flax Yarn Reinforced “Green” Composites. Polym. Compos. 2005, 26(5): 647-659.

13 Netravali, A. “Green” Composites from Cellulose Fabrics & Soy Protein Resin. http://www.human.cornell.edu/che/fsad/research/upload/F01-CR01-A3.pdf. 2003.

14 Tanford, Charles. Protein denaturation. Adv. Protein Chem, 23:1968, 121-282.0

15 Zhong Z., Sun X.S., Fang X., Ratto J.A. Adhesion properties of soy protein with fiber fiberboard. J. Am. Oil. Chem. Soc. 2001a, 78(1), 37-41.
16 Wescott, J.M., Frihart, C. R. Competitive soybean flour/phenol- formaldehyde adhesive for oriented strandboard. In: Proceedings of the 38th International Wood Composites Symposium, Pullman, WA, Washington State University. 2004, pp 199-206.

17 Mo X., Hu J., Sun X.S., Ratto J.A. Compression and tensile strength of low-density straw-protein particleboard. Ind. Crops Prod. 2001, 14(1), 1-9.

18 Mo X., Cheng E., Wang D., Sun X.S. Physical properties of medium-density wheat straw particleboard using different adhesives. Ind. Crops Prod. 2003, 18(1), 47-53.

19 Cheng, E, Sun, X.S., Karr G. Adhesive properties of modified soybean flour in wheat straw particleboard. Composites: Part A. 2004, 35(3), 297-302.

20 Wang D., Sun X.S. Low density particleboard from wheat straw and corn pith. Ind. Crops Prod. 2002, 15(1), 43-50.

21 Kuo M., Adams D., Myers D., Curry D., Heemstra H., Smith J., Bian Y. Properties of wood agricultural fiberboard bonded with soybean-based adhesives. For. Prod. J. 1998, 48(2), 71-75.

22 Ye X., Julson J., Kuo M,, Myers D. Biocomposite hardboard from renewable biomass bonded with soybean-based adhesive. Trans. ASABE. 2005, 48(4), 1629-1635.

23 Z. W. Wicks Jr., F. N. Jones, and S. P. Pappas, In Encyclopedia of Polymer Science and Technology, Edited Z. W. Wicks Jr., Wiley-Interscience, New York (1999), Vol. 1, pp. 670-739.

24 Levit, M. R.; Farrell, R. E.; Gross, R. A.; McCarthy, S. P. Biodegradable composites and laminated paper. Polymers, Laminations & Coatings Conference, Boston, Sept. 8-12, 1996, 2 p.545-551

25 Iwasaki, Yoshio; Teranishi, Masayoshi; Abe, Shingo. Biodegradable paper-plastic laminate for food packaging material. Japanese Patent No. 2003291296, 2003.

26 Kuusipalo, Jurkka; Nevalainen, Kimmo; Penttinen, Tapani. Compostable coated paper or paperboard, its manufacture and use for package products. EU Patent No. 2000001530, 2000.

27 Niizeki, Koichi; Okutani, Masahiro; Kamio, Katsuhisa. Aqueous biodegradable polymer dispersions for paper coatings with good water and oil resistance, and high gloss and mechanical strength. Japanese Patent No. 2003-296038, 2004.

28 Abe, Shingo; Itakura, Minoru. Biodegradable food packaging paper. Japanese Patent No. 2003001764, 2003.

29 Okutani, Masahiro; Kamio, Katsuhisa; Hosoda, Kazuo; Moriya, Masafumi. Water-based dispersions of biodegradable resins and their composites with sheets. Japanese Patent No. 2002121288, 2002.
30 Minowa, Toshiyuki. Paper having a biodegradable plastic layer and manufacturing methods. Japanese Patent No. 2001303478, 2001.

31 Kamio, Katsuhisa; Okutani, Masahiro; Kuroda, Iwao; Hosoda, Kazuo; Kamata, Yukio. Aqueous dispersions of biodegradable resins and biodegradable composite materials. Japanese Patent No. 2001011294, 2001.

32 Vaha-Nissi, Mika; Lahti, Johanna; Savolainen, Antti; Rissa, Kati; Lepisto, Toivo. New water based barrier coatings for paper and paperboard. Appita Annual Conference Proceedings, 2000, 54th(2), p. 581-590.

33 Kawashima, Masatake; Hosoda, Kazuo; Moriya, Masafumi. Biodegradble lactic acid polymer-based emulsions for water-resistant coatings of paper bags. Japanese Patent No. 10101911, 1998.

34 Takagi, Masatoshi; Minazu, Hiroshi; Ajioka, Masanobu; Yamaguchi, Teruhiro. Manufacture of decomposable composites including cellulosic materials. Japanese Patent No. 08027280, 1996.

35 Gruber, Patrick R.; Kolstad, Jeffrey J.; Ryan, Christopher M.; Hall, Eric S.; Eichen, Conn Robin S. Paper having a melt-stable lactide polymer coating and process for manufacture. Cont.-in-part of US Patent No. 5,338,822, 1995.

36 Putkisto, Kaisa; Maijala, Juha; Gron, Johan; Rigdahl, Mikael. Polymer coating of paper using dry surface treatment - coating structure and performance. TAPPI European PLACE Conference, 9th, Rome, Italy, May 12-14, 2003, p. 881-900.

37 Sakai, Shigekazu; Fujita, Toshiyasu. Environment-friendly coating compositions for paper. Japanese Patent No. 2004059812, 2004.

38 Haasmaa, Kristiina; Paronen, Timo Petteri; Urtti, Arto Olavi; Peltonen, Soili; Heikkila, Maija Elina; Vuorenpaa, Jani. Solventless hydrophobic biodegradable polymer dispersions, their manufacture and uses. EU Patent No. 9749762, 1997.

39 Yoshihara, Kazuo; Kawamura, Shunichi; Kobayashi, Takako; Hakamada, Yoshinori; Tanaka, Hidenori. Biodegradable natural fiber-based printing paper with good water resistance. Japanese Patent No. 2003220680, 2003.

40 Kaminaga, Junichi; Matsuo, Ryukichi; Yamawaki, Kentaro; Kato, Yumiko. Gas-barrier paper laminates and their containers with good recyclability. Japanese Patent No. 2003103692, 2003.

41 Yamawaki, Kentaro; Matsuo, Ryukichi; Kaminaga, Junichi; Kato, Yumiko; Kakemura, Toshiaki. Paper sheet coated or impregnated with biodegradable resin for manufacture of gas-barrier containers. Japanese Patent No. 2003013391, 2003.

42 Holy, Norman L. Compostable, degradable plastic compositions and monofilament, shaped article or film articles. EU Patent No. 2001074555, 2001.

43 Lee, Peter F.; Cornelius, Elizabeth C.; Potnis, Prasad S.; Cleveland, Christopher S.; Knauf, Gary H. Biodegradable paper-based agricultural substrate. EU Patent No. 2001060143, 2001.

44 Zhu, Wanqiang. Biodegradable reinforced paper-plastic composite packaging film. Chinese Patent No. 1273173, 2000.

45 Vaha-Nissi, Mika; Lahti, Johanna; Savolainen, Antti; Rissa, Kati; Lepisto, Toivo. New water-based barrier coatings for paper and paperboard. Appita Journal 2001, 54(2), p.106-115.

46 Ioelovich, Michael; Figovsky, Oleg. Hydrophobic biodegradable cellulose-containing composite materials with good resistance to water. EU Patent No. 2001021881, 2001.

47 Fringant, C.; Rinaudo, M.; Gontard, N.; Guilbert, S.; Derradji, H. A biodegradable starch-based coating to waterproof hydrophilic materials. Starch/Staerke, 1998, 50(7), p.292-296.

48 Nakamura, Ayako. Biodegradable laminates manufactured by extrusion coating of blended polymers. Japanese Patent No. 10006445, 1998.

49 Kim, Sung-ho; Hwang, Bong-ik; Kim, Tae-sik. Biodegradable coated paper manufacture. German Patent No. DE 19541681, 1996.

50 Lauzier, Christian A.; Monasterios, Clevys J.; Saracovan, Ilie; Marchessault, R. H.; Ramsay, Bruce A. Film formation and paper coating with poly(β-hydroxyalkanoate), a biodegradable latex. Tappi Journal 1993, 76(5), p. 71-77.

51 Doi, Yukio; Ishioka, Ryoji; Okino, Yoshiro; Imaizumi, Mitsuhiro. Process for producing aqueous dispersion of biodegradable polyester. EU Patent No. 2001096449, 2001.

52 Asrar, Jawed; Pierre, Jean R.; D'Haene, Pol. Manufacture of biodegradable polyhydroxyalkanoate coatings having good heat sealing properties and moisture resistance, EU Patent no. 9904948, 1999.

53 Pawde, S.M., Deshmukh, A.R., and Kalim, J. Studies on surface properties of polymeric coated paper material. J of Appl Polym Sci 101, 4167 (2006). of Appl Polym Sci 101, 4167 (2006).

54 Cai, Z and Kim, J. Characterization and electromechanical performance of cellulose–chitosan blend electro-active paper, Impregnation of kraft paper with cassava-starch acetate - analysis of

the tensile strength, water absorption and water vapor permeability. Smart Mater. Struct. 17, 035028 (8pp) (2008)

55 Larotonda, F.D.S., Matsui, K.S., Paes, S.S., and Laurindo, J.B. Impregnation of kraft paper with cassava-starch acetate - analysis of the tensile strength, water absorption and water vapor permeability. Starch/Stärke, 55,504 (2003).

56 Despond,S., Espuche, E., Cartier, N., Domard, A. Barrier properties of paper-chitosan and paper-chitosan-carnauba wax films. J. of Appl. Polym. Sci. 98, 704 (2005).

57 Anderson, A.J. and Dawes, E.A. Occurrence, metabolism, metabolic role, and industrial uses of bacterial polyhydroxyalkanoates. Microbiological Reviews 54, 4, 450 (1990).

58 Andersson, C. New ways to enhance the functionality of paperboard by surface treatment - a review. Packag. Technol. Sci. DOI: 10.1002/pts.823 (2008).

59 Petersen, K., Nielsen,P.V., and Bertelsen, G. Potential of biobased materials for food packaging. Trends Food Sci. Technol. 10, 52 (1999).

60 Weber, C.J. (ed.). Biobased Packaging Materials for the Food Industry – Status and Perspectives. The Royal Veterinary and Agricultural University: Frederiksberg, Denmark, (2000).

61 Barber, J. Industrial Bioprocessing 28, 10, 7 (2006).

62 Lim, H.A., Raku, T., and Tokiwa, Y. A new method for the evaluation of biodegradable plastic using coated cellulose paper. Macromol. Biosci. 4, 875 (2004).

63 Kuusipalo, J. PHB/V in Extrusion Coating of Paper and Paperboard: Part I: Study of Functional Properties J of Polymers and the Environment 8, 1, 39 (2000).

64 Kuusipalo, J. of Polymers and the Environment 8, 2, 49 (2000).

65 Krook, M.S. Hedenqvist, A.C. Albertsson. Barrier and mechanical properties of pulp fiber/polymer laminates and blends. Polym. Eng. Sci., 40, 1, 143 (2000).

66 Fibre Box Association. Fibre Box Handbook, 22nd Edition, Elk Grove Village, IL. 2005, pp. 3.12-3.14

67 Diana Twede and Susan E. M. Selke. Cartons, crates and corrugated board: handbook of paper and wood packaging technology. DEStech Publications. 2005, pp. 472-476.

68 Staley, B.F. and Barlaz, M.A., "Composition of Municipal Solid Waste in the United States and Implications for Carbon Sequestration and Methane Yield," *Journal of Environmental Engineering.* 2009, 135 (10), pp. 901-909.

69 Anonymous, “Shrinking a landfill”, Annenberg Media, [On-line; verified 18 December 2009] Available at: http://www.learner.org/interactives/garbage/landfill/paper.phtml.

70 Bost, J., Stouter, S., Lee, J. Engineer, “Composting Solid Waste in Military Contingency Operations” October-December, 2005, 34-35.

71 Tuomela, M., Vikman, M., Hatakka, A., and Itävaara, M., “Biodegradation of lignin in a compost environment: A review,” Bioresource Technology 72, pp. 169–183, 2000.

72 American Society for Testing and Materials (ASTM), D6002 Standard Guide for Assessing the Compostability of Environmentally Degradable Plastics," ASTM International, West Conshohocken, PA, 2002, DOI: 10.1520/D6200-96(2002), www.astm.org.

73 ASTM Standard D6400-04, Standard Specification for Compostable Plastics ASTM International, West Conshohocken, PA, 2004, DOI: 10.1520/D6400-04, www.astm.org.

74 ASTM Standard D1037-99, Standard Test Methods for Evaluating Properties of Wood-Base Fiber and Particle Panel Materials Specification for Concrete Aggregates," ASTM International, West Conshohocken, PA, 2003, DOI: 10.1520/D1037-99, www.astm.org.

75 Mo X., Sun X.S., Wang Y. Effects of molding temperature and pressure on properties of soy protein polymers. J. Appl. Polym. Sci. 1999, 73(13), 2595-2602.

76 Technical Association of the Pulp and Paper Industry. Bursting strength of corrugated and solid fiberboard, T 810 om-06, TAPPI, Norcross, GA. 2006.

77 Ganev, S., Cloutier, A., Beauregard, R., Gendron, G. Linear expansion and thickness swell of MDF as a function of penal density and sorption state. Wood Fiber Sci. 2005, 37(2), 327-336.

78 Zhong Z., Sun X.S., Fang X., Ratto J.A. Adhesion strength of sodium dodecyl sulfate - modified soy protein to fiberboard. J. Adhes. Sci. Technol. 2001b, 15(12), 1417-27.

79 Composite Panel Association. American National Standard – Medium density fiberboard (MDF) for interior applications, ANSI A208.2-2002. Composite Panel Association, MD.

80 Chronakis, Ioannis S. Network formation and viscoelastic properties of commercial soy protein dispersions: Effect of heat treatment, pH and calcium ions. Food Research International (1996), 29(2), 123-134

81 Lambuth A.L.: Protein adhesives for wood. In: Handbook of adhesive technology, 2nd ed. Eds. Pizzi, A., Mittal, K.L. Marcel Dekker, New York. 2003, pp. 459
82 Qian, L. Zhu, J. Zhang, R.B. Whitehouse, J. of Appl. Polym. Sci.: Part B: Polym. Phys., 45, 1654 (2007).

83 Luo, K. Xu, G.Q. Chen, J Study of miscibility, crystallization, mechanical properties, and thermal stability of blends of poly(3-hydroxybutyrate) and poly(3-hydroxybutyrate-co-4-hydroxybutyrate). J.of Appl Polym Sci 105, 3402 (2007).

84 Xu, B. H. Guo, R. Yang, Q. Wu, G.Q. Chen, Z.M. ZhangIn situ FTIR study on melting and crystallization of polyhydroxyalkanoates. Polym. 43, 6893 (2002).

85 Soares, N.M.P.S. Ricardo, S. Jones, F. Heatley, High temperature thermal degradation of cellulose in air studied using FTIR and 1H and 13C solid-state NMR. Europe. Polym J. 37, 737 (2001).

86 Kunioka, A. Tamaki, Y. Doi, Crystalline and thermal properties of bacterial copolyesters: poly(3-hydroxybutyrate-co-3-hydroxyvalerate) and poly(3-hydroxybutyrate-co-4-hydroxybutyrate) Macromolecules 22, 694 (1989).

87. Galego, C. Rozsa, R. Sánchez, J. Fung, A. Vásquez, J.S. Tomas, Characterization and application of poly(*β*-hydroxyalkanoates) family as composite biomaterials Polym Testing 19, 485 (2000).

88 Cong, S. Zhang, R. Xu, W. Lu, D. Yu, The influence of 4HB content on the properties of poly(3-hydroxylbutyrate-co-4-hydroxylbutyrate) based on melt molded sheets,J. of Appl. Polym. Sci. 109, 1962 (2008).

89 Hsu, J.C., Penner, M.H., Nutr, J., 119, 872 (1989).

90 Kang, T.J. and Kim, C. Impact Energy Absorption Mechanism of Largely Deformable Composites with Different Reinforcing Structures. Fibers and Polymers, 1, 45(2000).

91 Spectra-Kote Corporation. Spectra-Guard (3001 and 3003) factsheets, Gettysburg, PA. 2009.

92 ASTM Standard ASTM D 5118/D 5118M, Standard Practice for Fabrication of Fiberboard Shipping Boxes ASTM International, West Conshohocken, PA, 2004, DOI: 10.1520/D5118/D,5118M, www.astm.org.

93 ASTM D 4727/D 4727M Standard Specification for Corrugated and Solid Fiberboard Sheet Stock ASTM International, West Conshohocken, PA, 2004, DOI: 10.1520/ D 4727/D 4727M, www.astm.org.

94 Assembly Requirements: *Meal, Ready-to-Eat (MRE.)* Assembly Requirements (ACR-M-029) 03 October 08 Natick Soldier Research, Development and Engineering Center. 2008.

95 Technical Association of the Pulp and Paper Industry. Water absorptiveness of sized (non-bibulous) paper, paperboard, and corrugated fiberboard (Cobb test), T 441 om-04, TAPPI, Norcross, GA. 2004.

96 Technical Association of the Pulp and Paper Industry. Standard Conditioning and Testing Atmospheres for Paper, Pulp Handsheets, and Related Products, T 402 sp-03, TAPPI, Norcross, GA. 2003.

97 American Society for Testing and Materials (ASTM). Standard Test Method for Water Resistance of Shipping Containers by Spray Method, D 951-04, (Reapproved 2004), ASTM, West Conshohocken, PA. 2004.

98 American Society for Testing and Materials (ASTM). Standard test methods for Determining Compressive Resistance of Shipping Containers, Components, and Unit Loads, D 642-00 (Reapproved 2005), ASTM, West Conshohocken, PA. 2005.

99 Technical Association of the Pulp and Paper Industry (TAPPI) Compression Test of Fiberboard Shipping Containers, T 804 om-06, TAPPI, Norcross, GA. 2006.

100 American Society for Testing and Materials, "Standard Test Method for Determining Aerobic Biodegradation of Plastic Materials Under Controlled Composting Conditions," ASTM, West Conshoscken, PA, Vol. 08-03, Standard D5338, 2003.

101 American Society for Testing and Materials, "Standard Test Method for Determining Aerobic Biodegradation in Soil of Plastic Materials or Residual Plastic Materials After Composting," ASTM, West Conshocken, PA, Vol. 08-03, Standard D5988, 2003.

102 Pramer, D. and Bartha R., "Preparation and processing of soil samples for biodegradation studies," *Environmental Letters* **2**, pp. 217–224, 1972.

103 Bartha R. and Pramer, D., "Features of a flask for measuring the persistence and biological effects of persticides," *Soil Science* 100, pp. 68-70, 1965.

104 ASTM D5338-11 Standard Test Method for Determining Aerobic Biodegradation of Plastic Materials Under Controlled Composting Conditions. ASTM International, West Conshohocken, PA, 2011, DOI: 10.1520/D5338-11, www.astm.org.

105 Farrell, R.E., Adamczyk, T.J., Broe, D.C., Lee, J.S., Briggs, B.L., Gross, R.A., McCarthy, S.P. and Goodwin, S., "Biodegradable bags comparative performance study: A multi-tiered approach to evaluating the compostability of plastic materials," in *Biopolymers from Polysaccharides and Agroprotein, ACS Symposium Series 786* edited by Gross, R.A. and C. Scholz, American Chemical Society, Washington, pp. 337-375, 2001.

106 ASTM D6300, Standard Test Method for Determining Weight Loss From Plastic Materials Exposed to Simulated Municipal Solid-Waste (MSW) Aerobic Compost Environment," ASTM International, West Conshocken, PA, 2011, DOI: 10.1520/ D6003-03.

107 Leege, P.B. and W.H. Thompson (eds.), "Test Methods for the Examination of Composting and Compost," The US Composting Council, Bethesda, MD, 1997.

108 Tukey, J.W. "Exploratory data analysis," Addison-Wesley, Reading, MA, 1977.

109 Sharabi, N.E. and Bartha, R., "Testing some assumptions about biodegradability in soil as measured by carbon dioxide evolution," *Applied Environmental Microbiology* 59, pp. 1201-1205, 1993.

110 US Environmental Protection Agency, "Fate, Transport and Transformation Test Guidelines OPPTS 835.3110 Ready Biodegradability," US EPA 712-C-98-088, Washington, DC, January 1988.

111 Erikson, C., Harrass, M.C., Osborne, C.M., Sayre, P.G., and Zeeman, M., "Environmental Assessment Technical Handbook PB87-175345," US Food and Drug Administration, Washington, DC, 1987.

Acronyms

AMET	Advanced Materials Engineering Team
ANOVA	Analysis of Variance
ASTM	American Society for Testing and Materials
ATR	Attenuated Total Reflectance
BBF	Bio-based Fiberboard
BI	Burst Index
CAM	Contact Angle Meter
CFD	Combat Feeding Directorate
CI	Crystallinity Index
C-N	Carbon to Nitrogen
DMA	Dynamic Mechanical Analysis
DOW	Double Wall
DSC	Differential Scanning Calorimetry
EC	Electrical Conductivity
ESEM	Environmental Scanning Electron Microscopy
FDA	Food and Drug Administration
FPM	Feet per minute
FTIR	Fourier Transform Infrared Spectroscopy
HCL	Hydrochloric Acid
IB	Internal Bonding Strength
ICDS	Intermediate Container Delivery System
ID	Identification
IMC	Initial Moisture Content
IPC	International Paper Company
KN	Kilonewton
Lbf	Pound Force
LE	Linear Expansion
LSD	Least Significant Difference
MDF	Medium Density Fiberboard
MOR	Modulus of Rupture
MOE	Modulus of Elasticity
MRE™	Meal, Ready-to-Eat™
MRE™ SF	Meal, Ready-to-Eat™ Solid Fiberboard
NSRDEC	Natick Soldier Research, Development and Engineering Center
OCC	Old Corrugated Containers
PET	Polyethylene terephthalate
PHA	Polyhydroxyalkanoate
PHB	Polyhdroxybutyrate
PI	Performance Index
PLA	Polylactic Acid

PT	Press Time
PTT	Press Time and Temperature
P(3HB-co-4HB)	Poly(3-hydroxybutyrate-co-4hydroxybutyrate)
P(3HB-co-#HV)	Poly(3-hydroxybutyrate-co-3-hydroxyvalerate)
RBI	Relative Biodegradation Index
RCBD	Randomized Complete Block Design
RCBD-RM	Randomized Complete Block with Repeated Measures Design
RH	Relative Humidity
RSC	Regular Slotted Container
RSC IN	Regular Slotted Container with Insert
RSC WD	Regular Slotted Container with Integral Width Divider
RSM	Response Surface Methodology
SDS	Sodium Dodecyl Sulfate
SEM	Scanning Electron Microscopy
sg48m	Spectra-Guard 48 for Military Applications
s*MSW*	Simulated Municipal Solid Waste
SPA	Soy Protein-based Adhesives
SPI	Soy Protein Isolates
TAPPI	Technical Association of the Pulp and Paper Industry
TCD	Thermal Conductor Detector
TGA	Thermogravimetric Analysis
Thou	One Thousand of an Inch
TS	Thickness Swell
TSH	Tensile Strength
UGR™ A	Unitized Group Ration – A Version
UGR™ WD	Unitized Group Ration with Integral Width Divider
UN	United Nations
WA	Water Absorption
WAM™	Wax Alternative Medium
WAXD	Wide Angle X-Ray Diffraction
W-MOE	Wet Modulus of Elasticity
W-MOR	Wet Modulus of Rupture
W-TSH	Wet Tensile Strength

Glossary
Fiberboard Terminology

Double Back Liner	Second paper substrate to be attached to the medium (outside of box/printed side)
Inline treated	Coatings that are applied to either the liner or medium during the corrugation process
Medium	Fluted material initially applied to the single face liner
Offline treated	Liner board is coated prior to the corrugation process at another location and then shipped to corrugating facility.
Recyclable	Used paper, including in-plant and post-consumer waste paper and paperboard which is capable of being processed into new paper or paperboard
Repulpable	To test material that can undergo the operation of re-wetting and fiberizing for subsequent sheet formation
Single Face Liner	The first paper substrate used in the corrugated board manufacturing process that is attached to the medium (inside of box)